Impact des forçages physiques sur la dynamique des éléments biogéochimiques en mer Méditerranée : approche couplée observations in situ et réseaux de neurones

Marine Fourrier

Sorbonne Université

École doctorale des sciences de l'environnement d'Île de France (ED129)

Unité de recherche Laboratoire d'Océanographie de Villefranche

Thèse présentée par **Marine Fourrier**

Soutenue le **22 novembre 2021**

En vue de l'obtention du grade de docteur de Sorbonne Université

Discipline **Océan Atmosphère, Climat et Observations Spatiales**

Spécialité **Océanographie**

Impact des forçages physiques sur la dynamique des éléments biogéochimiques en mer Méditerranée

Approche couplée observations *in situ* et réseaux de neurones

Thèse dirigée par Laurent Coppola directeur
Fabrizio D'Ortenzio co-directeur

Composition du jury

Rapporteures	Virginie Thierry	chargée de recherche HDR au LOPS
	Karina Von Schuckmann	chargée de recherche HDR à Mercator Ocean
Examinateurs	Rodolphe Lemée	professeur à Sorbonne Université
	Björn Fiedler	chargé de recherche à GEOMAR
	Patrick Raimbault	directeur de recherche à Aix-Marseille Université
	Maurizio Ribera d'Alcalà	professeur à la Stazione Zoologica Anton Dohrn
Directeurs de thèse	Laurent Coppola	physicien adjoint CNAP
	Fabrizio D'Ortenzio	directeur de recherche au CNRS

Mots clés : réseaux de neurones, mer Méditerranée, nutriments, système des carbonates, oxygène dissous, flotteurs Argo

Keywords: neural networks, Mediterranean sea, nutrients, carbonate system, dissolved oxygen, Argo floats

Cette thèse a été préparée au

Laboratoire d'Océanographie de Villefranche
Sorbonne Université
181 chemin du Lazaret
06230 Villefranche-sur-Mer
France

Site https://lov.imev-mer.fr/web/

Remerciements

Merci à mes directeurs de thèse Laurent et Fabrizio de m'avoir accompagnée du stage de master (master 1 pour Laurent) jusqu'à l'aboutissement de cette thèse. Merci également pour toutes les conférences et campagnes en mer auxquelles j'ai pu participer ainsi que l'expérience d'enseignement pour laquelle vous (et l'équipe pédagogique de Villefranche) m'avez fait confiance. Ces expériences ont été parmi les plus enrichissantes que j'ai eu l'occasion de vivre et m'ont beaucoup fait grandir.

Merci aux membres du jury de thèse, Rodolphe, Karina, Virginie, Patrick, Maurizio et Björn d'avoir accepté d'évaluer les travaux issus de ma thèse, et tout particulièrement Karina et Virginie qui ont accepté d'être rapportrices de mon manuscrit.

Merci à Guillaume, Thibaut et Caroline d'avoir accepté de me suivre dans mon comité de thèse et pour les échanges enrichissants et pertinents que nous avons pu avoir à cette occasion. Merci d'ailleurs à Caroline de m'avoir prise en stage de master 1 il y a maintenant quelques années et de m'avoir fait collaborer avec Laurent, sans laquelle je ne serais jamais arrivée au LOV en thèse.

Merci au LOV et à toutes ses équipes, des directeurs aux personnels administratifs, sans compter les membres de toutes les équipes pour les échanges au fil des années. Une pensée toute particulière pour OMTAB et toutes les personnes (LOV comme IMEV ;)) que j'ai eu le plaisir de côtoyer.

Merci à la mezzateam (Flavien, Loulou, Marin et Jie) pour ces années passées à vos côtés, et merci d'avoir supporté mes décorations de Noël.

Une pensée toute particulière pour M. Stanek et Mme Tirseni, mes enseignants au lycée, qui m'ont transmis le goût de la science, de la recherche et m'ont encouragé à aller à l'université.

Merci à C. Ridame et D. Cardinal qui m'ont permis dès la L3 de découvrir le monde de la biogéochimie que je n'ai quitté depuis.

Enfin merci à tous les ami · es qui m'ont suivi de près ou de loin, et soutenue au cours de ces dernières années à Villefranche. Félix depuis ta Bretagne éloignée, les potes de Time for the Planet pour leurs bonnes ondes et la convection qu'on peut changer le monde et surtout toute la team Nice-Villefranche (Alice, Juju, Loulou, Louis, Laëti (et la famille de passage), Nico, Marie, Solène, Lucas, Florian, Raph) pour ces apéros, ces beaux week-ends de dépaysement (Fitou <3) et les amitiés associées.

Flo, merci d'avoir supporté tous mes craquages et de ne jamais m'avoir laissé baisser les bras. À bientôt en Belgique.

Laëti et Alice, vous êtes parmi les plus belles rencontres que j'ai pu faire au cours de cette thèse, je ne peux pas mettre les mots dessus, merci pour tout.

Enfin, merci à mes parents et à ma soeur pour leur soutien au cours de cette expérience. Clem, merci pour tous nos échanges dans mes moments de doute, tes relectures, tes conseils avisés et toute ton aide Overleaf. PS : un jour tu m'expliqueras ce qui, dans ma galère intense, t'as donné envie de toi aussi faire une thèse !

Activités scientifiques durant la thèse

Enseignement

- 2019 - 2021 Chargée de Mission d'Enseignement au LOV. 64h/an.
  Cours, TDs, TPs, de la L2 au M2. Taxonomie, écotoxicologie, plateformes-autonomes d'observation de l'océan, introduction au plancton et à l'océanographie, Ocean Data View, récoltes d'échantillons et encadrement de sorties en mer.
- 2019 Vacataire en écoles d'été au LOV. 18h.

Campagnes océanographiques

- PERLE 2, Février-Mars 2019 (30 jours, N/O Pourquoi Pas ?).
  Prélèvement et analyse d'échantillons d'oxygène (titration Winkler) et de pH (spectrophotométrie). Prélèvement de DIC. Mise à l'eau de flotteurs Argo et BGC-Argo.
- MOOSE-GE 2019, Juin 2019 (12 jours, N/O La Thalassa).
  Mise à l'eau de bathysondes, prélèvement et analyse d'échantillons d'oxygène (titration Winkler), de pH (spectrophotométrie), de fluorescence et de nutriments. Prélèvement de DIC. Mise à l'eau de flotteurs Argo et BGC-Argo.
- PERLE 3, Mars 2020 (10 jours, N/O Pourquoi Pas ?).
  Prélèvement et analyse d'échantillons d'oxygène (titration Winkler) et de pH (spectrophotométrie). Prélèvement de DIC.

Colloques scientifiques

- EGU General Assembly, Vienne, Autriche, Avril 2019 (poster).
- Journée des doctorants ED129, Paris, France, Juin 2019 (poster).
- 7th Euro-Argo Science Meeting, Athènes, Grèce, Octobre 2019 (poster).
- virtual EGU General Assembly 2020, en ligne, Mai 2020 (poster).
- webinaire FORMAL, en ligne, Juin 2020 (présentation).
- Med2020, en ligne, Novembre 2020 (poster).
- 9th MONGOOS workshop, en ligne, Novembre 2020 (présentation orale).
- ASLO Aquatic Sciences Meeting, en ligne, Juin 2021 (présentation orale).
- EVOLECO, La Rochelle, France, Novembre 2021 (présentation orale). *Prix du meilleur oral doctorant.*

Médiation scientifique

- 2018, Collège Jules Romain.
  Intervention auprès d'élèves de 5ème autour du projet « Adopt a Float », dans le programme de SVT. Chlorophylle, flotteurs, photosynthèse et couleur de l'eau.

— 2019, Ecole Saint-Antoine.
Intervention auprès d'élèves de CM2 autour du projet « MEDITES ». Propriétés de l'eau de mer et observations robotisées.
— 2019, IMEV, Fête de la Science, 2 jours de présentations grand public.
Campagnes océanographiques et observations robotisées des océans. Quiz sonores des sons de l'océan pour enfants.
— 2019, Sophia Antipolis, Fête de la Science, 2 jours de présentations grand public.
Campagnes océanographiques et observations robotisées des océans.
— Présentations ponctuelles des flotteurs et des moyens d'observation robotisés des océans auprès de stagiaires de 3ème.

Impact des forçages physiques sur la dynamique des éléments biogéochimiques en mer Méditerranée
Approche couplée observations *in situ* et réseaux de neurones

Résumé

La mer Méditerranée est caractérisée par une circulation rapide des masses d'eau, des concentrations faibles en nutriments avec un fort gradient d'oligotrophie, et une acidification plus rapide que pour l'océan global. Les Eaux Levantines Intermédiaires (LIW) reliant les deux bassins sont marquées par un minimum d'oxygène (O_2). Les variabilités du contenu en O_2, des nutriments et du carbone inorganique restent méconnues du fait de leur faible densité d'observation. Le développement et la validation d'une méthode neuronale CANYON-MED, spécifiquement conçue pour la Méditerranée, ont permis de dériver nutriments (nitrates, phosphates, silicates) et variables du système des carbonates (alcalinité totale, carbone total et pH) à partir de variables systématiquement mesurées (pression, température, salinité et O_2, position spatio-temporelle). La dynamique du minimum d'O2 dans la LIW face à la variabilité des processus de ventilation des eaux intermédiaires en Méditerranée nord-occidentale a été étudiée sur la période 2012-2020. L'application de CANYON-MED a permis la description des tendances en nutriments et carbonates dans cette zone, face au phénomène intermittent de convection profonde. L'importance de la convection sur la ventilation des masses d'eau, et sur les tendances des nutriments et d'acidification sont mises en évidence, dans un contexte de stratification accrue par le changement climatique. Enfin, la ventilation de la LIW a été explorée dans sa zone de formation (le bassin Levantin) à l'aide de flotteurs Argo sur la période 2018-2019, nuançant l'injection d'O_2 dans le patch de mélange.

Mots clés : réseaux de neurones, mer Méditerranée, nutriments, système des carbonates, oxygène dissous, flotteurs Argo

Abstract

The Mediterranean Sea is characterized by rapid circulation of its water masses, low nutrient concentrations with a strong oligotrophy gradient, and a more rapid acidification than the global ocean. The Levantine Intermediate Waters (LIW) that connect the two basins are marked by a minimum of oxygen (O_2). Variability in O_2 content, nutrients, and inorganic carbon remain poorly understood given their low density of observation. The development and validation of a neural method CANYON-MED, specifically designed for the Mediterranean Sea, allowed to derive nutrients (nitrates, phosphates, silicates) and carbonate system variables (total alkalinity, total carbon and pH) from systematically measured variables (pressure, temperature, salinity and oxygen, position in time and space). The dynamics of the O_2 minimum in the LIW in the face of variability in intermediate water ventilation processes in the northwestern Mediterranean was studied over the period 2012-2020. The application of CANYON-MED allowed the description of nutrients and carbonate trends in this area, in response to the intermittent deep convection phenomenon. The importance of convection on the ventilation of water masses, as well as on nutrient and acidification trends are thus highlighted, in a context of increased stratification by climate change. Finally, the ventilation of the LIW has been explored in its formation area (Levantine basin) using Argo floats over the period 2018-2019, nuancing the injection of O_2 in the mixing patch.

Keywords: neural networks, Mediterranean sea, nutrients, carbonate system, dissolved oxygen, Argo floats

Laboratoire d'Océanographie
de Villefranche
Sorbonne Université – 181 chemin du Lazaret – 06230 Villefranche-sur-Mer – France

Table des matières

Liste des tableaux

Table des figures

Liste des équations

Chapitre 1

La mer Méditerranée

Sommaire du présent chapitre

Une mer semi-fermée La région Méditerranéenne a de nombreuses caractéristiques morphologiques, géographiques, historiques et sociétales qui en font un lieu privilégié de l'étude des impacts du climat sur l'environnement marin. En particulier, on réfère souvent la Méditerranée à un « océan miniature », où se retrouvent en jeu de nombreux processus de la circulation globale (circulation thermohaline, apports atmosphériques, présence de régions aux caractéristiques distinctes : biorégions) mais à une échelle de temps et d'espace plus restreinte. Sa taille réduite et la facilité d'accès à son environnement hauturier en font un laboratoire d'étude idéal pour l'étude de ces nombreux phénomènes. En particulier, la Méditerranée est un « hotspot » du changement climatique (Giorgi 2006 ; Diffenbaugh et al. 2007), fortement soumise aux impacts anthropiques. De plus, de part sa taille restreinte (0.3% du volume de l'océan global), la

circulation générale des masses d'eau en Méditerranée est dix fois plus rapide que dans l'océan global et des changements y sont ainsi déjà visibles. Elle est reliée à l'océan global (figure 1.1) par des échanges au travers du détroit de Gibraltar et est donc influencée par, et influence, les masses d'eau Atlantique qui rejoignent la circulation thermohaline globale.

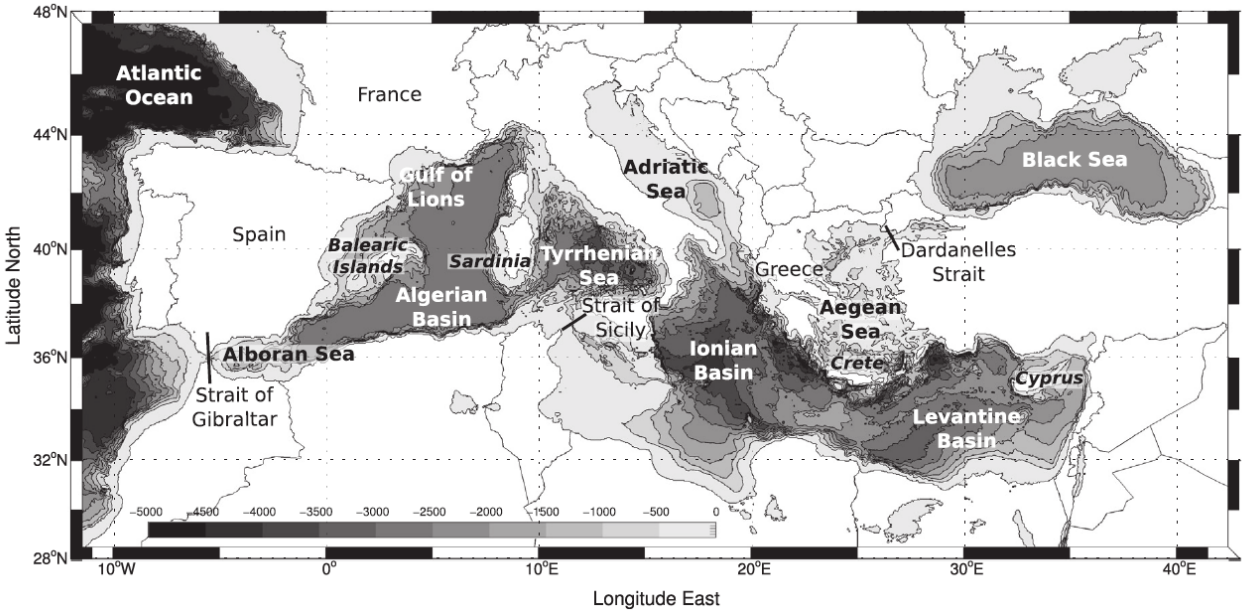

FIGURE 1.1 – Bathymétrie de la mer Méditerranée. Les noms des principaux bassins et îles de la Méditerranée sont indiqués. D'après HOUPERT et al. (2015).

1.1 Masses d'eau caractéristiques

Les trois masses d'eau principales de la mer Méditerranée sont présentées en figure 1.2 :

1. Les eaux d'origine Atlantique (Modified Atlantic Water, MAW), trouvées en surface avec une épaisseur de la surface à entre 50 et 200 mètres et caractérisées par une salinité de 36.2 près de Gibraltar à leur entrée et de 38.6 dans le bassin Levantin après avoir subi de l'évaporation le long de leur parcours (SCHROEDER et al. 2012). La circulation des MAW est globalement cyclonique (sens anti-horaire dans l'hémisphère Nord) à l'échelle des différents bassins, à l'exception de la circulation en mer Ionienne, caractérisée par une oscillation entre phase de circulation cyclonique et anticyclonique (GAČIĆ et al. 2010).
2. Les masses d'eau intermédiaires formées par mélange vertical lors de périodes hivernales : les eaux levantines intermédiaires (Levantine Intermediate Waters, LIW) formées dans le bassin Levantin, situées en moyenne entre 300 et 800 m et caractérisées par des températures autour de 13.5 °C et des salinités vers 38.6 (ZAVATARIELLI et MELLOR 1995). Leur signature est détectable par leur maximum en sub-surface de température

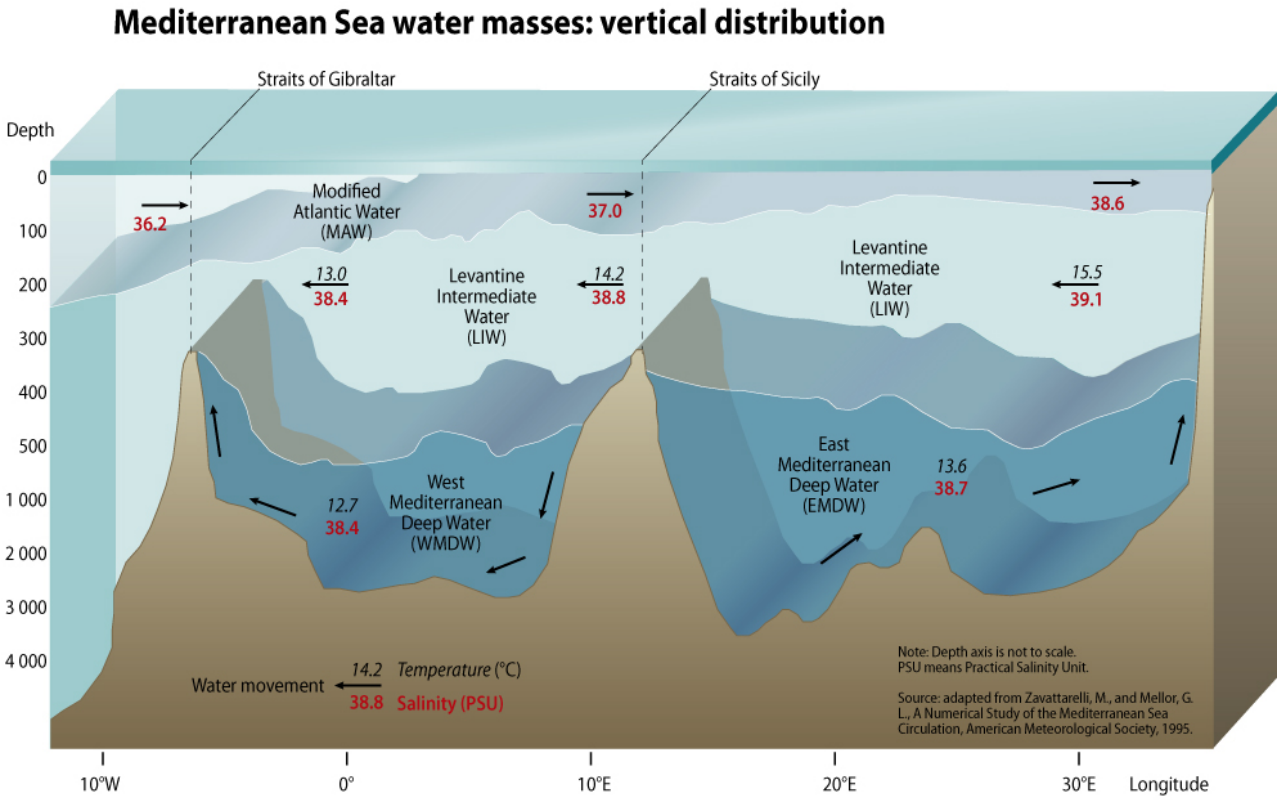

FIGURE 1.2 – Schéma simplifié de la circulation en 3 couches en Méditerranée le long d'une radiale détroit de Gibraltar - bassin Levantin. Les principales masses d'eau méditerranéennes et leurs caractéristiques en température et salinité sont présentées. Adapté de ZAVATARIELLI et MELLOR (1995).

et de salinité aux caractéristiques fortes dans le bassin Oriental et atténuées dans le bassin Occidental. Ces eaux chargées en sel et en chaleur ont un rôle crucial pour la circulation thermohaline méditerranéenne (GRIGNON et al. 2010 ; SPARNOCCHIA et al. 1994 ; LACOMBE et al. 1985). Ces eaux intermédiaires suivent globalement le trajet cyclonique décrit par les masses d'eau de surface (figure 1.3 B). Le long de leur trajet depuis leur lieu de formation dans le bassin Levantin, leurs caractéristiques évoluent, cependant elles gardent l'appellation de LIW en référence à leur site de formation principal à l'est de la Méditerranée (LASCARATOS et al. 1999). En Méditerranée Occidentale, la LIW est également caractérisée par un minimum d'oxygène dissous (O_2) reflétant l'absence de contact avec l'atmosphère depuis leur formation (COPPOLA et al. 2018).

3. Les eaux profondes méditerranéennes trouvées sous 1000 m et formées dans des zones spécifiques des bassins occidental (Golfe du Lion) et oriental (mers Adriatique et Égée) (figure 1.3 C). L'eau profonde est méditerranéenne (Eastern Mediterranean Deep Water, EMDW) est principalement formée en mer Adriatique sous l'effet de la Bora et en mer Égée sous l'effet des vents Étésiens (cf. parties 1.3.3 Formation d'eau dense en

mer Méditerranée Orientale et 1.3.2 Formation d'eau dense en mer Adriatique et en mer Égée) (Bergamasco et Malanotte-Rizzoli 2010 ; Klein et al. 1999). L'eau profonde ouest méditerranéenne (Western Mediterranean Deep Waters, WMDW) est formée dans la partie nord-occidentale, dans le Golfe du Lion, sous l'effet du Mistral et de la Tramontane (cf. partie 1.3.1 Formation d'eau dense en mer Méditerranée Nord-Occidentale) (Schroeder et al. 2008b).

1.2 Circulation

La figure 1.3 schématise les circulations principales (cyclonique), secondaires et interannuelles impliquant les masses d'eau présentées en partie 1.1 Masses d'eau caractéristiques à différentes profondeurs en Méditerranée.

La circulation générale de surface en mer Méditerranée est fortement contrainte par les vents (Pinardi et Navarra 1993) et la bathymétrie complexe de cette mer semi-fermée (figure 1.1, Testor et al. 2005). En raison de son climat, la Méditerranée est un bassin de concentration, c'est-à-dire qu'elle perd plus d'eau par évaporation qu'elle n'en reçoit par les précipitations et les fleuves (Bethoux et al. 1999). Sans l'apport de l'océan via le détroit de Gibraltar (débit entrant de 1 million de m^3 d'eau par seconde), le niveau de la Méditerranée baisserait de 0.5 à 1 m par an. En moyenne, il faut 100 ans entre le moment où l'eau entre en surface par Gibraltar et y ressort, en profondeur, transformée lors des convections (Durrieu de Madron et al. 2011).

La circulation thermohaline en mer Méditerranée est caractérisée par une circulation composée de 3 cellules :

1. Une cellule de retournement ouverte et peu profonde où la MAW entrent au niveau de Gibraltar, se propagent en surface vers l'est puis plongent sous forme de LIW en Méditerranée Orientale. La LIW se propage alors jusqu'à Gibraltar à des profondeurs intermédiaires (Pinardi et al. 2019).
2. Une cellule profonde de retournement dans le bassin Occidental, dont le moteur est la formation d'eaux profondes WMDW dans le Golfe du Lion(Pinardi et al. 2019).
3. Une cellule profonde de retournement dans le bassin Oriental caractérisée comme une cellule thermohaline fermée(Pinardi et al. 2019). Son moteur est traditionnellement situé en mer Adriatique (considérée comme la source principale) mais des modifications transitoires peuvent modifier le comportement de cette cellule(Bergamasco et Malanotte-Rizzoli 2010). La mer Égée devient alors contributrice même si elle reste majoritairement une source d'eaux intermédiaires (cf. partie 1.4.1 Eastern Mediterranean Transient).

La circulation méditerranéenne est aussi marquée par la présence de structures permanentes à l'échelle des bassins et sur différentes profondeurs (figure 1.3). Dans la partie nord du bassin

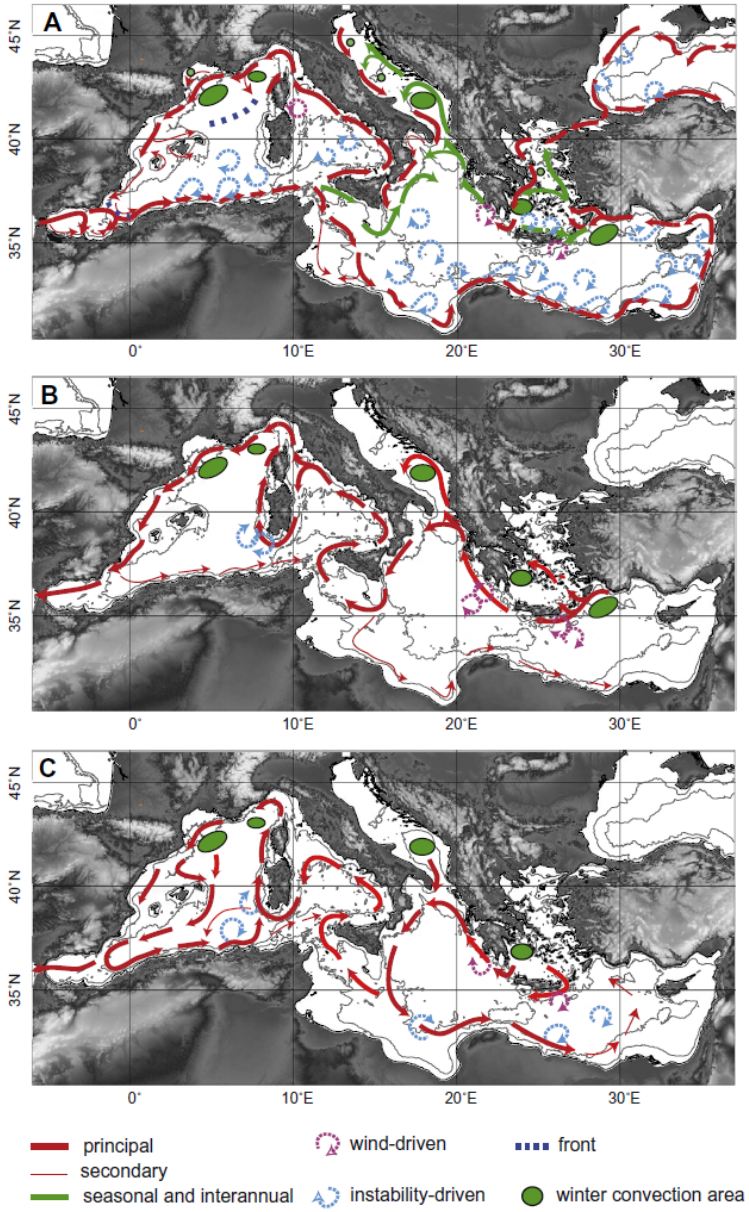

FIGURE 1.3 – Circulation en mer Méditerranée (A) des eaux de surface, (B) des eaux intermédiaires et (C) des eaux de fond. Ces masses d'eaux sont décrites dans la figure 1.2. Les isolignes représentent les isobathes 1000 m et 2000 m. Les circulations principale et secondaire (en termes de volume) sont représentées par des flèches rouges (épaisses et fines respectivement). Les flèches vertes décrivent les circulations interannuelles et saisonnières. Les flèches circulaires bleues et rouges montrent les circulations cycloniques/anticycloniques issues du vent ou des instabilités respectivement. Les cercles verts représentent les zones de convection hivernale et le tiret pointillé indique le front. Tiré de DURRIEU DE MADRON et al. (2011).

occidental, la circulation est connue comme étant cyclonique et le courant Nord (courant de bord intense) constitue une branche de cette circulation (MILLOT 1999). La circulation en mer Adriatique est caractérisée par deux gyres cycloniques (gyre Nord et gyre Sud) et en mer

d'Alboran, deux gyres anticycloniques sont présents à l'entrée de la Méditerranée (Poulain et al. 2012). À ces structures permanentes de grande taille s'ajoutent des phénomènes de mésoéchelle (environ 100 km) et submésoéchelle (environ 10 km) tels que les tourbillons et les fronts (Millot 1999). En particulier, le long des côtes algériennes, la MAW forme de nombreux tourbillons causés par des instabilités dont certains durent plusieurs années (Puillat et al. 2002). Dans le bassin Levantin, des structures cycloniques (gyre de Rhodes) et anticycloniques (gyre de Ierapetra) quasi-permanentes sont également présentes (Hamad et al. 2005 ; Rio et al. 2007 ; Estournel et al. 2021).

1.3 Processus de formation d'eau dense

La circulation thermohaline est issue des différences de densité de l'eau de mer, due aux variations de leur température et salinité (Pinardi et al. 2019). Dans certaines régions et à des saison précises, sous l'effet d'interactions avec l'atmosphère, les eaux de surface peuvent perdre en chaleur, se densifier et ainsi plonger à des profondeurs intermédiaires voire jusqu'au fond (Testor et al. 2018 ; Marshall et Schott 1999 ; Sur et al. 1993). Plus précisément, sous l'action de vents froids et secs, la couche de mélange (Mixed Layer, ML) s'approfondit sous l'effet combiné de l'évaporation et du refroidissement des eaux générant des instabilités verticales (Boyer Montégut 2004 ; D'Ortenzio et Prieur 2012). La profondeur maximale atteinte par la couche de mélange varie fortement dans le temps et dans l'espace (Lavigne 2013). En mer Méditerranée, les phénomènes de convection hivernale et par conséquent de formation d'eau dense ont lieu dans 3 zones principales : la Méditerranée Nord-Occidentale, l'Adriatique et la Méditerranée Orientale (Durrieu de Madron et al. 2011).

1.3.1 Formation d'eau dense en mer Méditerranée Nord-Occidentale

En Méditerranée nord-occidentale, la présence de masses d'eau de caractéristiques thermodynamiques différentes, ainsi que la circulation régionale cyclonique induisant une stabilité verticale réduite, font de cette région une zone de formation d'eau dense. Le phénomène de convection dans le Golfe du Lion est un phénomène intermittent (Somot et al. 2006) qui varie en intensité et en volume d'eaux nouvellement formées de façon inter-annuelle. Marshall et Schott (1999) ont conceptualisé le phénomène de convection profonde en trois étapes : préconditionnement, mélange vertical et restratification.

Préconditionnement La circulation cyclonique de la Méditerranée Nord-Occidentale entraîne un « doming » des isopycnes entraînant ainsi une remontée d'eau intermédiaire plus proche de la surface et plus facilement affectée par des pertes de chaleur localisées. De plus, la LIW complète ce préconditionnement : lorsque celle-ci remonte, elle entraîne l'augmentation de la

salinité et donc de la densité des eaux de surface qui se refroidissent avec les vents froids et secs. C'est ainsi le déclenchement du mélange vertical (MEDOC GROUP 1970).

Mélange vertical Le préconditionnement et les forçages atmosphériques varient selon les années, ce qui explique la variabilité (en terme de timing et de surface concernée) du phénomène de convection profonde dans la zone. Dans les zones soumises au préconditionnement et sous l'effet des vents froids et secs, la stabilité de la colonne d'eau est affaiblie, permettant l'apparition de cellules convectives (ou panaches, <1 km de diamètre) sur l'ensemble de la colonne d'eau. Cette phase de mélange vertical intense produit un volume important d'eaux formées et renouvelle les couches profondes. La forme du patch convectif ainsi que la profondeur maximale atteinte par la convection varient selon les épisodes convectifs. Elle est hétérogène et génère de nombreuses structures de mésoéchelle (Frajka-Williams et al. 2014) et de sub-mésoéchelle (Marshall et Schott 1999).

Restratification Dès que le refroidissement à l'interface air-mer s'arrête et que l'eau est à nouveau chauffée par l'atmosphère, les eaux de surface de la zone mélangée se restratifient (au début du printemps), tandis que les eaux denses nouvellement formées plongent et se répandent en profondeur. Elles deviennent ainsi séparées des interactions avec l'atmosphère. Les échanges latéraux reprennent le dessus avec une advection de ces eaux nouvellement formées.

Ces différentes phases se chevauchent dans le temps et le préconditionnement ainsi que la dispersion des eaux formées joue un rôle important dans le préconditionnement de l'année suivante. Le golfe du Lion, où la convection peut atteindre le fond (> 2000 m) certaines années (Houpert 2013), est classifié parmi les zones de convection les plus profondes et les plus connues au monde (Marshall et Schott 1999).

Testor et al. (2018), grâce à un effort intense d'observation multi-plateformes dans le Golfe du Lion pendant l'hiver 2012-2013, ont pu revoir et compléter la description du phénomène de convection en océan ouvert de Marshall et Schott (1999) (figure 1.4). Les trois phases décrites précédemment se chevauchent et interagissent. Le diagramme du haut montre un premier événement de mélange, avec des panaches n'atteignant pas encore le fond, du « cascading » près de la côte et de fortes instabilités près du bord de la zone de mélange. Des tourbillons cohérents de sub-mésoéchelle (Submesoscale Coherent Vortices, SCV) se forment, exportant les eaux nouvellement formées à différentes profondeurs intermédiaires (Bosse et al. 2015). Suite à un mélange additionnel, la couche de mélange peut atteindre le fond de l'océan et des SCVs se forment, également attachés au fond de l'océan, contribuant ainsi à la propagation des WMDW nouvellement formées.

Par ailleurs, il a été observé dans le passé que la convection peut s'étendre à la mer Ligure à l'est du Golfe du Lion (Coppola et al. 2017 ; Smith et al. 2008), mais ce phénomène reste toutefois principalement localisé dans la zone du Golfe du Lion où les conditions océaniques

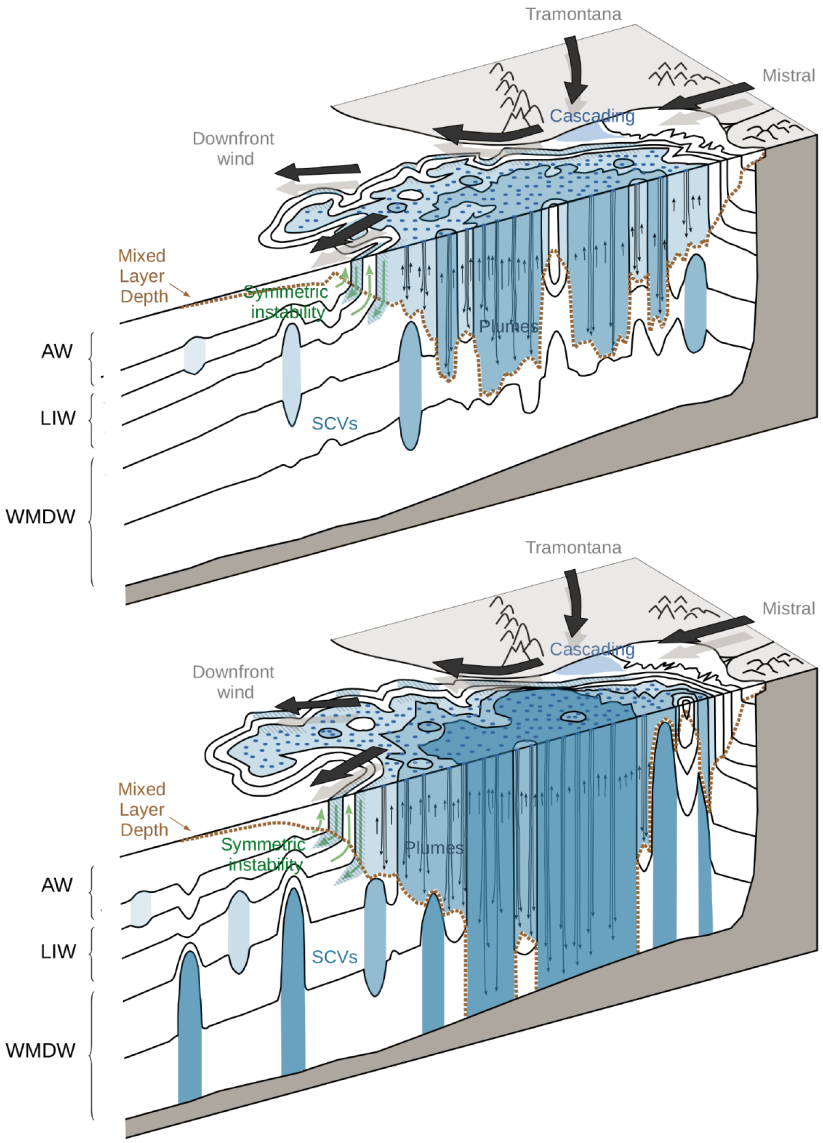

FIGURE 1.4 – Représentation schématique de l'évolution de la zone de convection pendant la phase de mélange intense sur une période de 1-2 semaines. La stratification sous-jacente est représentée par les isopycnes sélectionnés (lignes noires) et les flèches noires représentent les vents. Le volume d'eau qui vient d'être mélangé par convection est coloré selon les classes de densité potentielle (densité ramenée à la pression de surface). AW : Eaux Atlantiques (Atlantic Waters). Tiré de TESTOR et al. (2018).

sont les plus favorables au mélange profond. En plus du phénomène de convection profonde qui forme des eaux profondes au large, vers la côte le phénomène de « cascading » d'eaux denses en provenance du plateau peut avoir lieu occasionnellement sur le plateau du Golfe du Lion ou en mer Adriatique (DURRIEU DE MADRON et al. 2005 ; IVANOV et al. 2004). En effet, le cascading d'eau de plateau dense peut se produire dans des régions peu profondes (100 m) séparées de l'océan profond par une pente abrupte (DURRIEU DE MADRON et al. 2005 ; IVANOV et al. 2004),

situation qui décrit bien le plateau du Golfe du Lion. Le plateau du Golfe du Lion est séparé de l'océan profond par plusieurs canyons qui agissent comme des couloirs naturels pour les eaux denses (Durrieu de Madron et al. 2005 ; Font et al. 2007 ; Canals et al. 2006). Le phénomène de cascading a été décrit en détail par Shapiro et al. (2003).

Les deux processus de formation d'eaux profondes peuvent se produire simultanément ou séparément, et les eaux profondes formées par les deux interagissent et se trouvent à leurs profondeurs de flottabilité neutre respectives, entraînant un chevauchement parfois complexe de ces masses d'eau nouvellement formées aux propriétés (température et salinité) différentes. Ce chevauchement est bien visible sur les diagrammes θ-S de propriétés des masses d'eau (décrits en détail en partie 1.4.2 Western Mediterranean Transition). Le cascading est intermittent (n'a pas lieu tous les ans) et se produit à une fréquence moindre que le phénomène de convection profonde, variant en intensité selon les années (J. P. Béthoux et al. 2002).

1.3.2 Formation d'eau dense en mer Adriatique et en mer Égée

Sous l'influence du vent Bora, les eaux relativement chaudes et salées, riches en LIW qui rentrent dans l'Adriatique par l'est et les eaux froides et peu profondes du nord de l'Adriatique se mélangent (Bergamasco et Malanotte-Rizzoli 2010). La LIW contribue ainsi à la formation de l'eau profonde Adriatique (Adriatic Deep Water, ADW) qui alimente l'EMDW. Dans les années 90, la zone de formation d'eau dense de l'EMDW a changé du sud de l'Adriatique à la mer de Crête, phénomène appelé Eastern Mediterranean Transient (EMT) (Klein et al. 1999) (voir détails en partie 1.4.1 Eastern Mediterranean Transient).

En 1997, le gyre Nord-ionien est passé d'anticyclonique à cyclonique (Manca et al. 2002). Ce phénomène décennal d'alternance entre un mode cyclonique et anticyclonique (figure 1.5) a été nommé le BIOS : Adriatic-Ionian Bimodal Oscillating System (Gačić et al. 2010). Les variations entre le mode cyclonique et anticyclonique impliquent des trajets de masses d'eau différents, ainsi que des impacts sur les nutriments et la distribution des espèces (Civitarese et al. 2010).

La mer Égée est également considérée comme une zone de convection et une source d'eaux crétoises intermédiaires (Cretan Intermediate Water, CIW) dont les caractéristiques varient de manière interannuelle selon la profondeur maximale de mélange atteinte (Velaoras et al. 2013 ; Theocharis et al. 1993), et étant parfois plus dense que la LIW (Theocharis et al. 1999b). De plus, les eaux profondes de la mer Égée sont constituées d'eaux profondes crétoises (Cretan Deep Water, CDW) issues de l'EMT (Theocharis et al. 1999a ; Velaoras et al. 2018). L'EMDW est composée d'un mélange d'eau profonde formée en mer Égée pendant l'EMT et d'ADW formée en mer Adriatique après l'EMT (Roether et al. 2007).

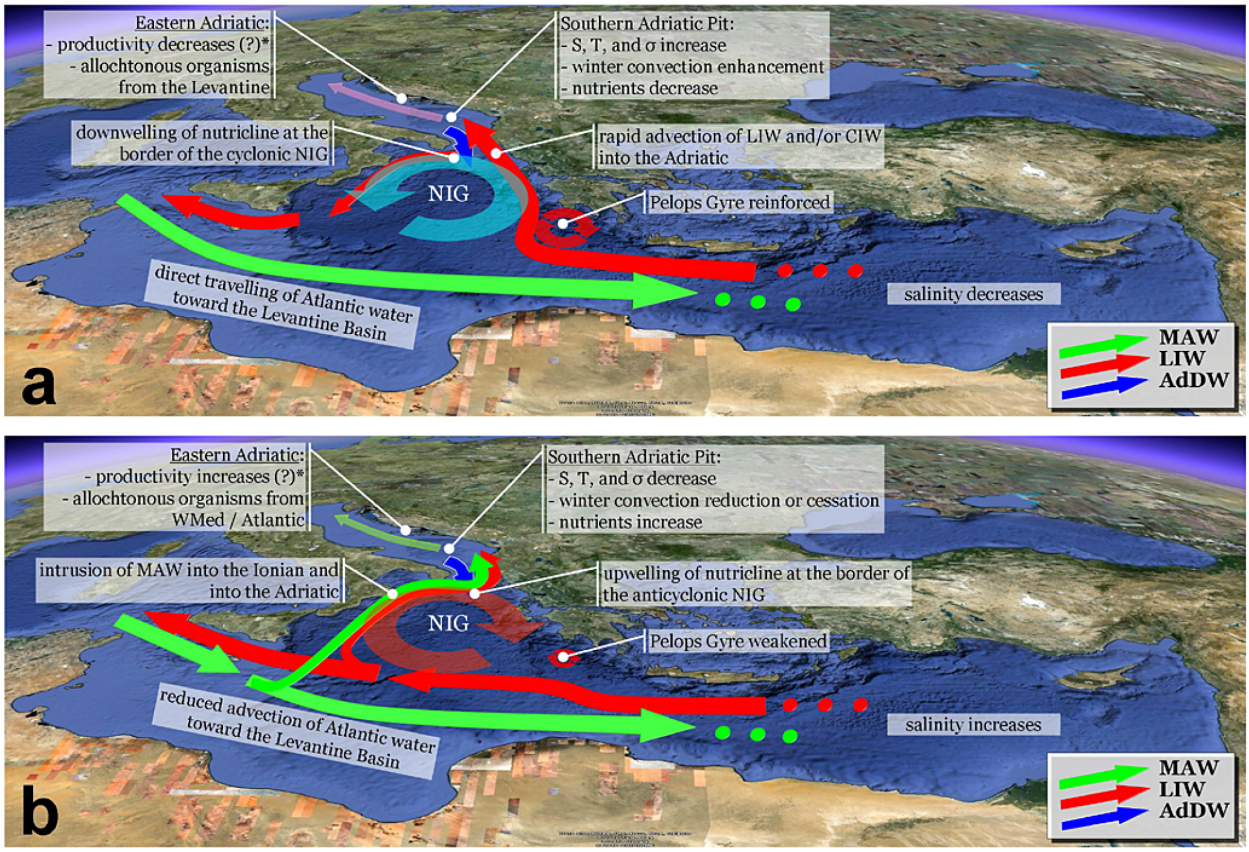

FIGURE 1.5 – Représentation schématique des caractéristiques principales du BIOS et de ses conséquences dans la zone. a. NIG cyclonique, B. NIG anti-cyclonique. Acronymes : MAW, Modified Atlantic Water, LIW, Levantine Intermediate Water, AdDW Adriatic Deep Water, NIG North Ionian Gyre. Tiré de CIVITARESE et al. (2010).

1.3.3 Formation d'eau dense en mer Méditerranée Orientale

Dans le bassin Levantin, la MAW chaude et salée en raison des faibles apports d'eau douce par les précipitations ou les fleuves (LASCARATOS et NITTIS 1998) se refroidit en surface et s'évapore sous l'effet des vents Étésiens. Ce refroidissement est le moteur de mélanges verticaux importants qui peuvent atteindre 500 à 1000 m (LASCARATOS et al. 1993). Ces mélanges sont ainsi à l'origine de la LIW assez chaude et très salée formée par une convection intermédiaire. Certaines années, la convection peut donner lieu à la formation d'eau Levantine profonde (Levantine Deep Water, LDW) (SUR et al. 1993). La LIW formée dans le bassin Levantin se propage dans le bassin Oriental et une partie entre en mer Adriatique où elle contribue à la formation d'eau dense (ROBINSON et al. 2010). Elle se mélange avec les CIW dans le bassin oriental avant de rejoindre la Méditerranée occidentale via le détroit de Sicile. Une autre partie rejoint la mer Tyrrhénienne puis le bassin Nord-Occidental. La LIW représente un réservoir de chaleur et de sel à des profondeurs intermédiaires, jouant ainsi un rôle crucial pour la circulation thermohaline globale de la mer Méditerranée (GRIGNON et al. 2010). Elle a une signature

caractéristique dans le bassin oriental (salinité de 39 et température potentielle de 15°C), et ces caractéristiques s'atténuent le long du trajet vers le bassin occidental (salinité de 38.6 et température potentielle de 13.5°C) (Zavatarelli et Mellor 1995). De plus, en Méditerranée occidentale, la LIW est caractérisée par un minimum d'O_2, reflétant son absence de contact avec l'atmosphère depuis sa formation et la dégradation bactérienne de la matière organique. Au niveau du détroit de Gibraltar, on retrouve la LIW qui représente une partie des eaux qui vont s'exporter vers l'Atlantique (H. L. Bryden et al. 1994 ; Gascard et Richez 1985).

1.4 Modifications transitoires de la circulation

1.4.1 Eastern Mediterranean Transient

L'Eastern Mediterranean Transient (EMT) s'est produit en mer Égée de 1988 à 1995 et est considérée comme la plus importante perturbation de circulation et de propriétés des masses d'eau en Méditerranée depuis les années 1950, quand les mesures instrumentales sont devenues systématiques. Différentes mécanismes sont considérés qui pourraient expliquer ce phénomène : une modification des vents, cruciaux pour la circulation des masses d'eau (Samuel et al. 1999) ; une augmentation de la salinité due à une réduction multi-décennale des apports fluviaux (Boscolo et H. Bryden 2001) et des apports de la mer Noire (Zervakis et al. 2000) ; une perte de chaleur très importante durant les hivers rudes au début des années 1990 (Tsimplis et al. 2006) ; une réduction des précipitations entre 1989 et 1993 (Theocharis et al. 1999a) ; l'impact du BIOS (Gačić et al. 2010) (voir partie 1.3.2 Formation d'eau dense en mer Adriatique et en mer Égée). Le moteur de la cellule thermohaline fermée de l'Adriatique s'est alors déplacé vers le sud de la mer Égée (sous-bassin crétois) (Bergamasco et Malanotte-Rizzoli 2010). Les eaux profondes formées en mer Égée, moins froides et plus salées, plus denses que les eaux profondes présentes dans le bassin oriental et habituellement formées en Adriatique ont provoqué un changement brutal de la composition des EMDW. Un retour à la situation de circulation précédente, pré-EMT (avant 1987), avec une dominance des eaux profondes issues de l'Adriatique, a eu lieu en 1997 (Borzelli et al. 2009). Ce retour est associé à un renversement complet de la circulation des eaux ioniennes superficielles d'un mode anticyclonique à un autre cyclonique, plutôt issu de tourbillons barocliniques (Gačić et al. 2010 ; Bergamasco et Malanotte-Rizzoli 2010). La propagation du signal de l'EMT vers l'ouest s'est manifesté au niveau de la LIW. En effet, la LIW est devenue plus salée et plus chaude au cours des années 2000, probablement par un effet couplé de l'EMT et d'une accumulation de chaleur dans les eaux intermédiaires en raison de l'absence de convection profonde engendrée par la succession d'hivers doux en Méditerranée Nord-Occidentale (Herrmann et al. 2010). Puis, lors des deux hivers très froids de 2005 et 2006, un évènement massif de production d'eaux profondes aux caractéristiques exceptionnellement chaudes et salées a eu lieu enfouissant en profondeur

l'accumulation de chaleur et de sel de la LIW (Herrmann et al. 2010). Les conséquences de ce phénomène perdurent de nos jours en Méditerranée Occidentale, en mer Tyrrhénienne et en mer Ligure (Schroeder et al. 2008b) avec des impacts importants sur les caractéristiques physico-chimiques des masses d'eau, en particulier la distribution verticale et spatiale du carbone anthropique (Touratier et Goyet 2011) ainsi qu'une modification générale de la distribution des principaux traceurs biogéochimiques (O_2, nutriments, etc., Schroeder et al. 2012).

1.4.2 Western Mediterranean Transition

Un réchauffement et une salinisation de l'ensemble de la colonne d'eau ont également été observés en Méditerranée occidentale, comparables à l'EMT, aussi bien en termes d'intensité que de conséquences observées (Schroeder et al. 2008a) : la Western Mediterranean Transition WMT.

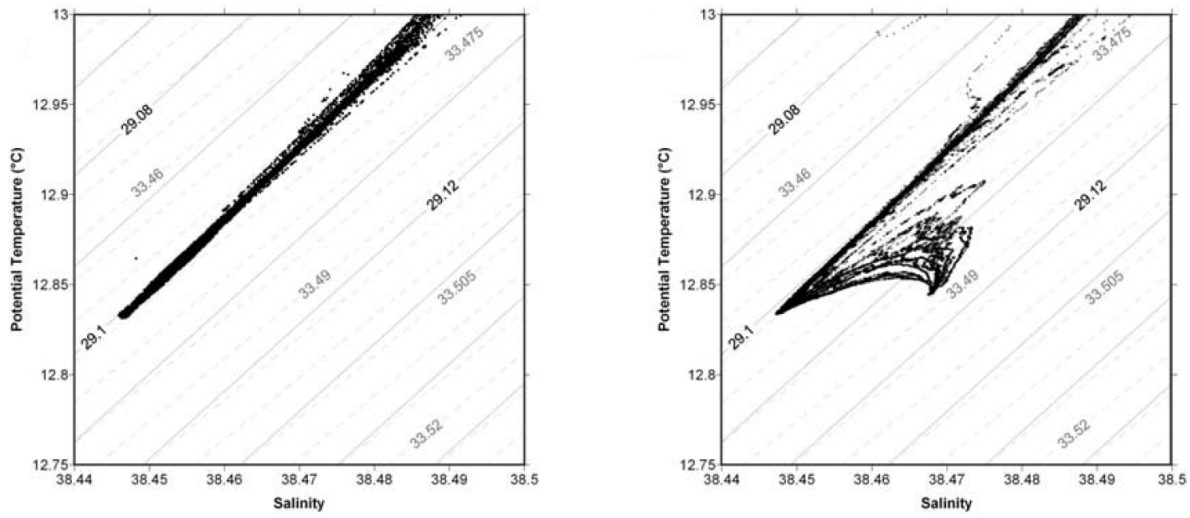

Figure 1.6 – Diagrammes θ-S des masses d'eau en octobre 2004 (gauche), et en octobre 2006 (droite) dans le bassin occidental. Tiré de Schroeder et al. (2008a).

Pendant l'hiver 2005, un évènement de convection profonde particulièrement intense a été observé dans le Golfe du Lion (López-Jurado et al. 2005 ; Font et al. 2007). La zone convective a été beaucoup plus étendue, jusque dans le sous-bassin Catalan, au Nord des Baléares (Smith et al. 2008). La WMDW alors formée est caractérisée par des température et salinité significativement plus élevées que précédemment, avec une signature très reconnaissable qualifiée de « queue de scorpion » sur les diagrammes θ-S (figure 1.6). L'origine de la WMT aurait deux explications. Tout d'abord, l'hiver 2005 a été particulièrement froid et sec et a entraîné de fortes évaporations et pertes de chaleur et donc de flottabilité en surface (López-Jurado et al. 2005 ; Font et al. 2007 ; Schroeder et al. 2010 ; Herrmann et al. 2010). Ces conditions atmosphériques ont certainement joué un rôle dans l'intensité de l'évènement de convection

profonde de l'hiver 2005. De plus, la forte évaporation des eaux de surface a pu engendrer une augmentation de la salinité de surface, ce qui pourrait en partie expliquer la salinité élevée de la WMDW produite cet hiver. Deuxièmement, les conséquences de l'EMT ont pu contribuer aussi bien en influant sur les caractéristiques des masses d'eau (plus chaudes et plus salées) arrivant de la Méditerranée Orientale en Méditerranée Nord-Occidentale que sur la stratification verticale des masses d'eau, ce qui a pu avoir un impact sur l'étendue de la convection profonde. Lors de l'hiver 2006, la convection a de nouveau été plus étendue, englobant également la mer Ligure (Smith et al. 2008) et la WMDW alors formée a été similaire à celle de l'hiver précédent. Ces eaux se sont alors dispersées et les caractéristiques de la nouvelle WMDW ont été observées le long des côtes algériennes jusqu'à la mer d'Alboran (Schroeder et al. 2008b) dès l'été 2005.

Dans le bassin Nord-Occidental, ce chevauchement de masses d'eau profondes aux caractéristiques différentes semble s'estomper pour tendre à revenir à une masse d'eau homogène. Depuis 2014 (et jusqu'au mélange de 2018), la LIW devient progressivement plus chaude et plus salée comme au début des années 1990 (Margirier et al. 2020). L'augmentation de salinité dans les eaux intermédiaires et profondes reste une conséquence marquée de ce WMT.

1.5 Biogéochimie de la mer Méditerranée

Oxygénation en Méditerranée Comparée à l'océan global, la Méditerranée a des eaux profondes plus oxygénées, en partie issu des épisodes de ventilation intense lors du mélange hivernal dans les zones de formation d'eau dense (Schneider et al. 2014). La LIW est caractérisée par un minimum d'O_2 (Coppola et al. 2018). Ce minimum est la conséquence d'un apport de matière organique par les zones productives supérieures alimentant ainsi la respiration bactérienne et engendrant la consommation d'O_2 et d'une stratification verticale des eaux de surface qui empêche la diffusion de l'O_2 depuis les couches de surfaces en contact avec l'atmosphère et bien oxygénées. De plus, la LIW est formée dans le bassin Oriental (cf. partie 1.3.3 Formation d'eau dense en mer Méditerranée Orientale) puis isolée de la surface, sa teneur en O_2 diminue donc le long de son trajet à cause d'un arrêt des échanges air-mer. Une augmentation de la stratification verticale des masses d'eau aurait entre autres pour conséquence une diminution globale de l'O_2 dans l'océan selon les modèles climatiques (Oschlies et al. 2008 ; Oschlies 2021). En l'absence de ventilation issue de la convection, il est probable que l'O_2 diminue dans cette couche intermédiaire. Coppola et al. (2018) ont par exemple estimé qu'il faudrait 25 ans pour atteindre l'hypoxie ($O_2 < 60$ μmol kg^{-1}) dans un site en Méditerranée nord-occidentale (DYFAMED, détails en partie 2.2.2 Mouillages LION et DYFAMED) selon les tendances estimées et si aucune ventilation intense du minimum d'O_2 n'a lieu.

Dynamique des nutriments en Méditerranée Les sels nutritifs tels que les nitrates, phosphates et silicates sont utilisés par les espèces de phytoplancton lors de la transformation du CO_2 dissous dans l'eau de mer en carbone organique et en utilisant l'énergie lumineuse lors de la photosynthèse. La disponibilité des nutriments est déterminante pour la productivité biologique et pour la séquestration de carbone sous-jacente. Les nutriments en Méditerranée peuvent être d'origine naturelle, atmosphérique (dépôt de poussières sahariennes), ou anthropique (apports par les fleuves, sauf pour les silicates qui n'ont aucune source anthropique) (O. P. Pasqueron de Fommervault 2015). Leur distribution est très marquée sur la verticale. Les eaux de surface sont appauvries en nutriments qui sont consommés par le phytoplancton. Au contraire, les eaux profondes sont riches en nutriments. Enfin, les masses d'eau intermédiaires présentent souvent des concentrations plus élevées issues de la forte reminéralisation de la matière organique par les bactéries dans cette couche.

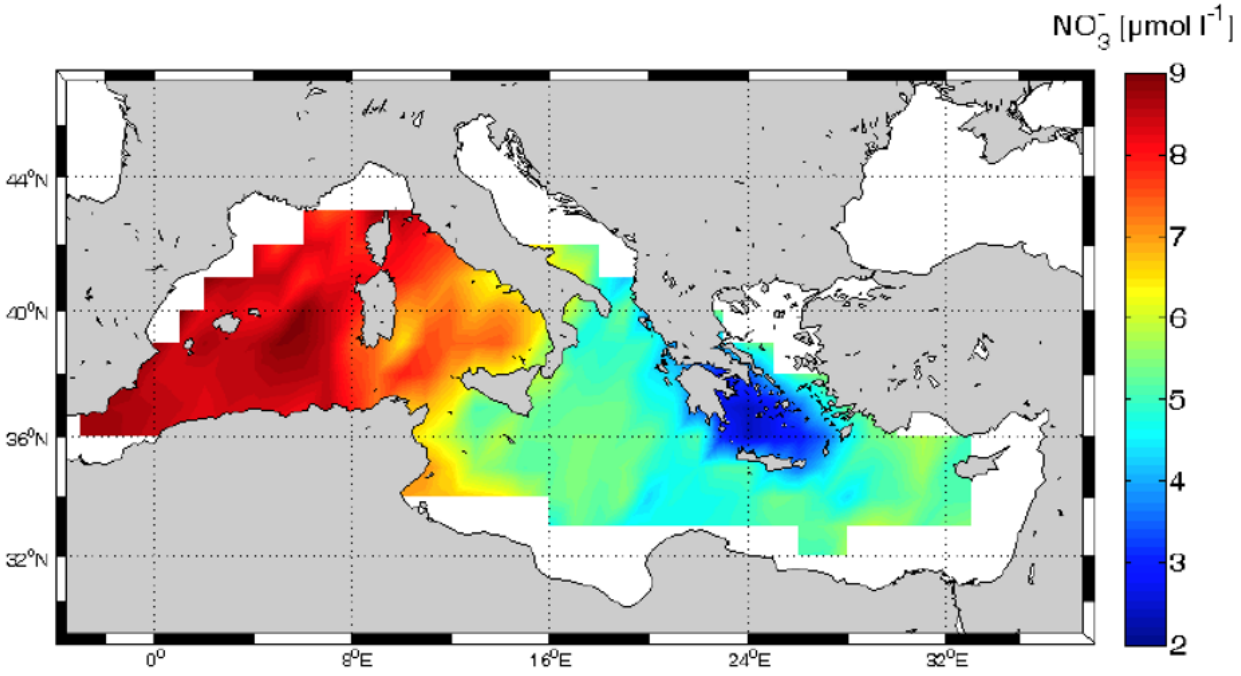

Figure 1.7 – Carte de la distribution des nitrates en profondeur (valeurs moyennées sous 800 m) montrant le gradient ouest-est. Les données issues de campagnes en mer entre 1961 et 2010 sont interpolées à l'aide d'une méthode cubique à base de triangles. Adapté de O. Pasqueron de Fommervault et al. (2015a).

La mer Méditerranée présente un gradient d'oligotrophie (limitation en nutriments) d'ouest en est (figure 1.7, Pujo-Pay et al. 2011) principalement causé par la circulation anti-estuarienne au niveau du détroit de Gibraltar (J. Béthoux et al. 1998). Ce gradient d'oligotrophie est caractérisé par une diminution des concentrations en nitrates et phosphates ainsi qu'un approfondissement des nutriclines (Moutin et Raimbault 2002 ; Pujo-Pay et al. 2011). Les nutriclines sont des zones de forts gradients des concentrations en nutriments qui séparent verticalement les zones

appauvries des zones les plus riches. Leur position détermine l'accessibilité des nutriments par le phytoplancton. En Méditerranée, le macro-nutriment limitant est le phosphore, comme mis en évidence par des rapports N/P dans les eaux profondes (rapport entre la concentration en nitrates et phosphates) supérieurs au rapport de Redfield ($C : N : P$ 106 : 16 : 1, Redfield 1934). En effet, en Méditerranée ce rapport varie de 22 au fond du bassin ouest (J. P. Béthoux et al. 2002) à 27 à l'est (Ribera d'Alcalà et al. 2003).

Suite à des régulations sur l'utilisation de phosphore (e.g. lessives, apports fluviaux, agriculture), les apports globaux de nutriments ont évolué dans les dernières décennies (Ludwig et al. 2009), dans des proportions variables influençant directement les rapports entre ces éléments nutritifs.

La convection verticale hivernale renouvelle les nutriments dans les couches de surface, et la quantité d'eau profonde formée détermine la disponibilité en nutriments dans la couche euphotique qui influence alors directement la production primaire (Mayot et al. 2017). La remontée de sels nutritifs en surface à disposition du phytoplancton est en partie contrôlée par l'intensité de la convection (O. Pasqueron de Fommervault et al. 2015b). En effet, la remontée de nutriments en surface est possible lorsque la MLD est supérieure à la profondeur des nutriclines et spécifiquement de la nitracline et de la phosphacline. La réponse des nutriments à la dynamique de la couche de mélange et au mélange vertical reste cependant nuancée : dans une certaine mesure, des profondeurs de couche de mélange plus élevées conduisent à une injection plus importante des nutriments dans les eaux de surface. Cependant, Heimbürger et al. (2013) a suggéré qu'une succession d'approfondissements de la couche de mélange, même de moindre ampleur, peut permettre un plus fort enrichissement en nutriments en surface qu'un unique approfondissement.

Principes de la chimie des carbonates

Le carbone est stocké sous forme organique ou sous forme de dioxyde de carbone dans trois réservoirs principaux : l'atmosphère, les continents et l'océan (Zeebe et Wolf-Gladrow 2001). Ce dernier représente le plus large réservoir de carbone, il contient plus de 95% du CO_2 total (Zeebe et Wolf-Gladrow 2001). Le cycle actuel du carbone implique fortement l'océan dans lequel le CO_2 atmosphérique est absorbé par l'eau de mer, avec un équilibre chimique entre les différentes espèces du système des carbonates régi par les lois de la thermodynamique. Plus précisément, le système des carbonates est un système « acide-base » issu de la dissolution du CO_2 et de minéraux carbonatés dans l'eau (figure 1.8). L'ajout d'un acide ou d'une base à une solution aqueuse contenant des espèces carbonatées donne lieu à des modifications du pH et des changements dans les concentrations de toutes les espèces qui constituent le système. Les gaz atmosphériques se dissolvent dans l'eau de mer et sont distribués à toutes les profondeurs par les courants et les autres processus thermodynamiques.

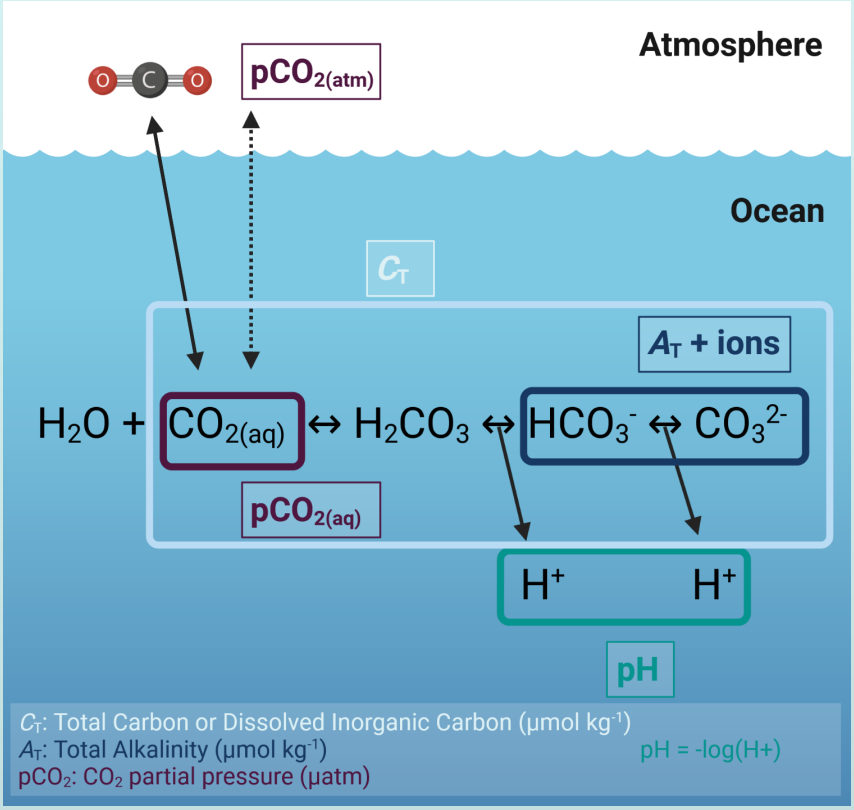

Figure 1.8 – Système des carbonates avec la dissolution du CO_2, A_T, C_T, et pH.

Dans l'eau de mer, le CO_2 se trouve, essentiellement, sous 3 formes inorganiques (figure 1.8) : CO_2 aqueux ($CO_2(aq)$), ions bicarbonates (HCO_3^-), et ions carbonates (CO_3^{2-}). Le CO_2 se dissocie dans l'eau de mer par réactions successives dont les constantes d'équilibre dépendent de facteurs environnementaux comme la température, la pression et la salinité.

Dans l'eau de mer, ces trois formes sont en équilibre permanent. On définit alors le carbone inorganique total ou C_T comme la somme suivante :

$$C_T = [CO_2(aq)] + [HCO_3^-] + [CO_3^{2-}] \tag{1.1}$$

Les ions bicarbonates constituent la forme principale de C_T (>85%), suivi des ions carbonates puis du dioxyde de carbone et de l'acide carbonique (H_2CO_3). Dans l'océan global, le C_T varie de 1850 à 2300 μmol kg^{-1} (Bégovic 2001). Le C_T est souvent le plus faible en surface dans les eaux appauvries par la photosynthèse et le plus élevé dans les eaux intermédiaires où la décomposition de la matière organique libère du carbone.
Dans l'eau de mer, le pH est gouverné essentiellement par le système des carbonates. Le pH diminue lors de la dissolution du CO_2 atmosphérique dans l'eau de mer ou lors de la reminéralisation de la matière organique qui engendrent une formation d'ions provoquant une diminution du pH. Le pH mesure ainsi l'activité des protons en solution :

$$pH = -log(H_3O^+) \tag{1.2}$$

Le pH est une mesure logarithmique, ainsi une baisse de 1 unité de pH signifie une augmentation par un facteur de 10 de la concentration des ions hydrogène. Dans la pratique, la mesure du pH dépend des solutions étalons de référence choisies. Dans les travaux de cette thèse, le pH utilisé est le pH_T ou pH sur l'échelle totale (qui prend en compte les protons associés aux sulfates, (Dickson 1993). Ce choix a été fait pour être comparable à des études ultérieures. L'acidification des océans correspond à la diminution du pH par dissolution de CO_2 atmosphérique dans l'eau de mer. Le pH global des océans a diminué de 0.017 à 0.027 unité de pH par décennie depuis la fin des années 1980 (Bindoff et al. 2019) et continue de diminuer avec l'augmentation des émissions anthropiques de CO_2 (figure 1.9).
range of 0.017–0.027 pH units per decade since the late 1980s

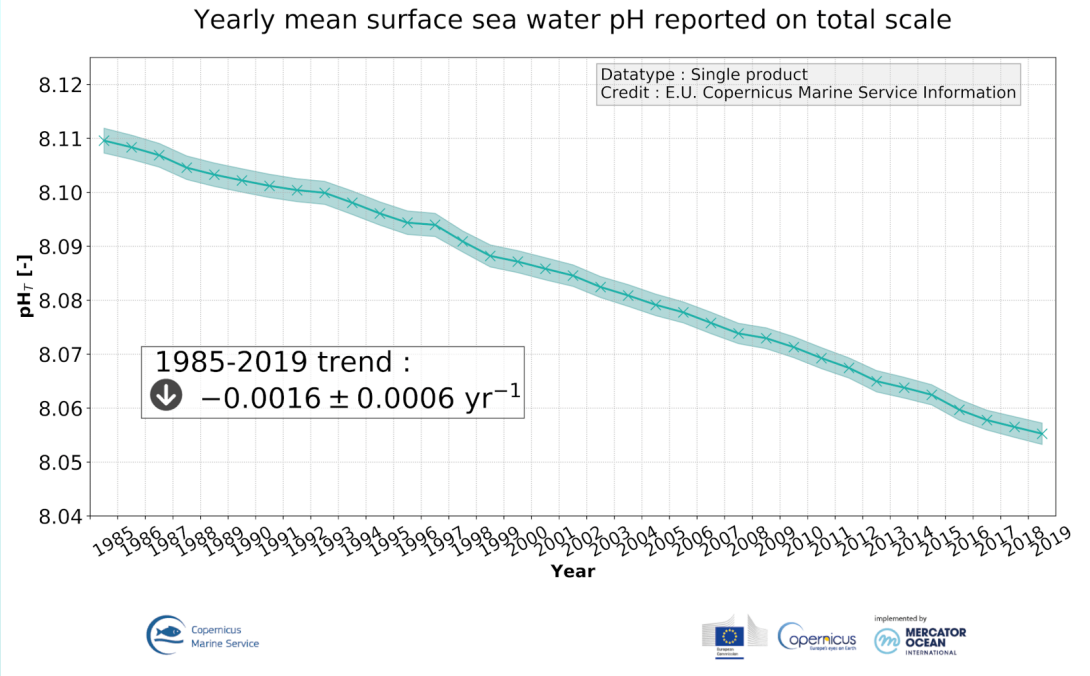

FIGURE 1.9 – Série chronologique de la moyenne annuelle du pH de l'eau de mer de surface au niveau mondial sur la période 1985-2019 en utilisant une méthodologie de reconstruction. La tendance ± sa variation sont calculées comme la moyenne et l'écart type des différences entre deux estimations consécutives. Tiré de Copernicus Marine Service

La dernière variable du système des carbonates est l'alcalinité totale (A_T) qui correspond au nombre de moles d'ions hydrogène équivalent à l'excès des accepteurs de protons (bases formées par des acides faibles) sur les donneurs de protons (acides) dans un kilogramme de l'échantillon (DICKSON et GOYET 1994) :

$$\begin{aligned} A_T = &[HCO_3^-] + 2[CO_3^{2-}] + [B(OH)_4] + [OH^-] + [HPO_4^{2-}] + 2[PO_4^{3-}] \\ &+ [SiO(OH)_3^-] + [NH_3] + [HS\_] - [H^+]F - [HSO_4^-] - [HF] \\ &- [H_3PO_4] + [bases_{mineures} - acides_{mineurs}] \end{aligned} \tag{1.3}$$

La distribution de l'A_T dans l'océan ouvert est principalement fonction de la salinité et des facteurs physiques qui la régulent : les mouvements des masses d'eau, les phénomènes de mélange, l'évaporation ou encore les précipitations (BROECKER et PENG 1982). Ainsi de nombreuses relations empiriques existent pour dériver l'A_T depuis la salinité d'une masse d'eau.

En connaissant la valeur de deux des quatre variables du système des carbonates : A_T, C_T, pH et CO_2, il est possible de recalculer les deux autres facilement, par exemple à l'aide de CO2SYS (LEWIS et WALLACE 1998 ; HEUVEN et al. 2011). CO2SYS est une

famille de logiciels qui calculent les équilibres chimiques pour les variables du carbone inorganique aquatique.

Système des carbonates en mer Méditerranée La dynamique du système des carbonates en Méditerranée dépend des apports par les continents et par les échanges avec l'océan Atlantique, la mer Noire et la mer Rouge. Ces apports peuvent être causés par le lessivage et l'érosion naturels des sols mais aussi par des apports atmosphériques ou encore par des rejets liés aux activités humaines. L'A_T en Méditerranée est élevée (2560-2620 μmol kg^{-1}) avec des concentrations plus élevées dans le bassin oriental (Álvarez et al. 2014). A l'inverse, le C_T (2270-2330 μmol kg^{-1}) présente des concentrations plus élevées dans le bassin occidental (Álvarez et al. 2014). De plus, des études ont montré que la mer Méditerranée se comporte comme un léger puits de CO_2 (moyenne sur 1998-2004, D'Ortenzio et al. 2008), avec un bassin occidental majoritairement « puits » et un bassin oriental majoritairement « source » de CO_2 (D'Ortenzio et al. 2008). La modification du pH de la mer Méditerranée a été estimé à une diminution de 0.05 à 0.14 depuis l'ère préindustrielle pour les eaux de surface (Touratier et Goyet 2009) signifiant ainsi une acidification plus rapide que pour l'océan global. De plus cette acidification est présente dans l'ensemble de la colonne d'eau à cause du mélange vertical (Coppola et al. 2020a).

Les événements comme l'EMT (cf. partie 1.4.1 Eastern Mediterranean Transient) et le WMT (cf. partie 1.4.2 Western Mediterranean Transition) ont de fortes conséquences biogéochimiques, en particulier sur le système des carbonates en Méditerranée. En effet, la Méditerranée a la capacité de séquestrer de grandes quantités de CO_2 anthropique (C_{ANT}) grâce à l'A_T et aux températures élevées sur la colonne d'eau (Álvarez et al. 2014). Cependant, les effets des changements récents de circulation sur la séquestration du C_{ANT} restent peu connus (Malanotte-Rizzoli et al. 2014).

1.6 Objectifs de la thèse

Dans le contexte d'une mer Méditerranée fortement soumise aux pressions anthropiques comme les changements globaux, les pollutions, le tourisme ou encore la sur-pêche, il est crucial d'affiner notre compréhension de ce système pour mieux appréhender les évolutions futures. Les températures des eaux de surface vont augmenter de 1 à 4°C d'ici 2100 selon les scénarios considérés, accompagnées de modifications des apports nutritifs et d'une acidification accrue, tous ces phénomènes impactant les communautés phytoplanctoniques et les réseaux trophiques (Cramer et al. p. d. ; Cherif et al. p. d.).

En combinant les méthodes classiques d'acquisition de données océanographiques de qualité (campagnes océanographiques) avec les nouvelles plateformes équipées de capteurs biogéochi-

miques ces dernières années (flotteurs-profileurs, planeurs, mouillages), nous pouvons obtenir une meilleure compréhension de cet environnement. Dans ce contexte, cette thèse se concentre en particulier sur la dynamique de l'O_2, les nutriments et le système des carbonates dans toute la colonne d'eau.

En effet, la dynamique de ces variables biogéochimiques est fortement influencée par le processus de convection hivernal, comme présenté en partie 1 La mer Méditerranée. Par ailleurs de nombreuses plateformes d'observation de l'océan sont présentes en Méditerranée mais leurs mesures sont restreintes à un faible nombre de variables biogéochimiques. Dans ce contexte, les

principales questions scientifiques traitées au cours de cette thèse sont les suivantes :

— Peut-on améliorer notre caractérisation de la distribution spatio-temporelle des concentrations en nutriments, O_2 et carbonates en combinant les observations *in situ* et de nouvelles méthodes de machine learning ?
— Quel est l'impact de la formation d'eau dense, en Méditerranée nord-occidentale, sur l'O_2, sur les nutriments et sur les variables du système des carbonates ?

Suite à ces travaux en Méditerranée nord-occidentale, et pour tirer profit des campagnes PERLE ayant eu lieu dans le bassin Levantin et auxquelles j'ai participé, une étude préliminaire sur la dynamique de l'O_2 dans cette zone de mélange hivernal a été entreprise.

Après une introduction générale sur la Méditerranée en partie 1 La mer Méditerranée, les différents moyens d'observations de l'océan sont présentées en partie 2 Mesures océanographiques. Les méthodes neuronales et les jeux de données utilisés sont présentés en partie 3 Méthodologie. La partie 4 Méthode CANYON-MED présente la méthode neuronale CANYON-MED développée au cours de cette thèse pour tirer profit des mesures systématiques de température, salinité et O_2 pour dériver nutriments et variables du système des carbonates en mer Méditerranée (objectif 2). Une attention particulière sera portée en partie 5 Convection et biogéochimie en Méditerranée nord-occidentale sur la Méditerranée nord-occidentale et sur l'impact des évènements de mélange hivernaux sur la dynamique des éléments biogéochimiques dans un contexte d'augmentation de la stratification (objectif 1). La partie 6 Ventilation dans le bassin Levantin abordera la ventilation de la LIW au niveau de sa zone de formation, masse d'eau qui se répand dans l'ensemble de la Méditerranée et a donc des conséquences à l'échelle du bassin. Enfin, les conclusions de cette thèse ainsi qu'une remise en perspective seront présentées en partie 7 Conclusions et perspectives.

Chapitre 2

Mesures océanographiques en mer Méditerranée

Sommaire du présent chapitre

L'étude de l'océan nécessite l'utilisation de nombreuses plateformes complémentaires. Les techniques de mesure océanographiques ont grandement évolué avec les développements technologiques. De nos jours, l'océan est étudié via des mesures *in situ* effectuées depuis des navires océanographiques, via des plateformes autonomes (ou semi-autonomes) déployées dans les océans ou encore via des techniques d'observation de l'océan depuis l'espace, parmi d'autres. Chaque moyen d'observation ne couvre qu'une partie du continuum d'échelles spatio-temporelles des processus physiques océaniques (figure 2.1).

2.1 Plateformes d'observation

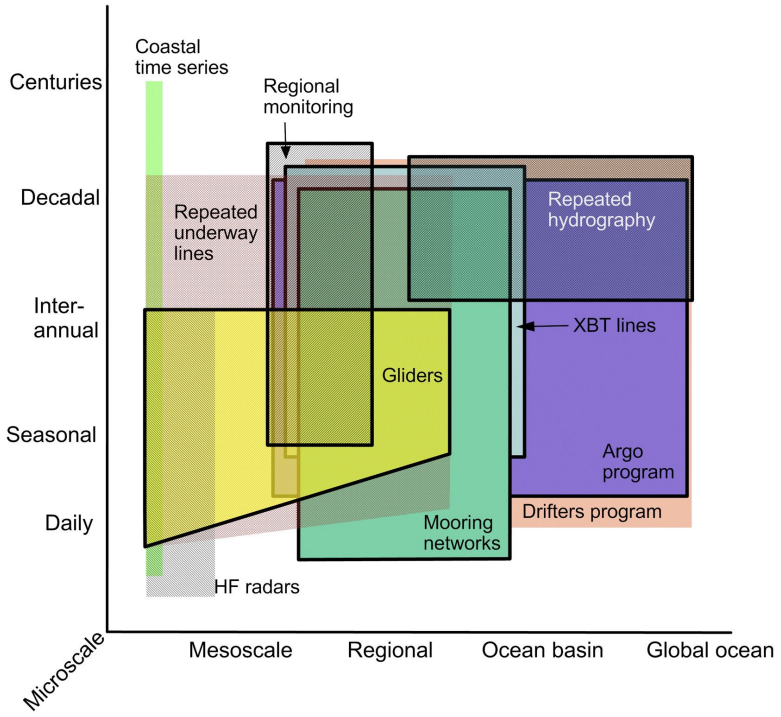

FIGURE 2.1 – Couverture spatio-temporelle de différents types de moyens d'observation de l'océan. Les échelles de temps sont représentées en ordonnée et les échelles d'espace en abscisse. Les systèmes qui acquièrent des profils verticaux sont entourés en noir. Tiré de LIBLIK et al. 2016.

2.1.1 Campagnes en mer : mensuelles, annuelles, épisodiques

Des navires océanographiques sont largement utilisés pour faire des mesures *in situ* et des prélèvements d'eau pour analyse en laboratoire embarqué ou à terre. Les bathysondes, rosettes couplées à des CTDs (Conductivity, Temperature, Depth) permettent de faire, en continu le long de la colonne d'eau, des mesures de température, salinité, pression, oxygène dissous (O_2) et fluorescence accompagnées de prélèvements d'eau *in situ* à des profondeurs d'intérêt, via les bouteilles Niskin fixées sur la rosette. Ainsi, ces instruments permettent une acquisition des paramètres physiques et biogéochimiques de la colonne d'eau à différentes positions géographiques. Cet échantillonnage est restreint à la fois dans le temps et dans l'espace, et permet d'obtenir des mesures de certaines variables biogéochimiques, mais avec une faible résolution. Par exemple, les mesures de nutriments effectuées à bord ne fournissent qu'une vision instantanée des masses d'eau et ne permettent pas une résolution des dynamiques saisonnières ou interannuelles ou des variations spatiales. Ainsi bien que fournissant des mesures *in situ* de référence, les données de campagne en mer nécessitent d'être complétées avec d'autres

plateformes d'observation du milieu océanique. De plus, les capteurs peuvent dériver au cours du temps, il est donc essentiel d'utiliser certaines données *in situ* de référence pour corriger ces données acquises, et ainsi obtenir une précision satisfaisante. Ainsi, l'O_2 de la CTD est corrigée à partir des analyses Winkler réalisées sur les échantillons prélevés et la fluorescence de la chlorophylle a est corrigée via des mesures HPLC (High Performance Liquid Chromatography) ou des mesures de fluorescence de la chlorophylle.

2.1.2 Mouillages fixes

Les mouillages fixes sont constitués d'un câble vertical ancré aux fonds océaniques qui reste droit grâce à des structures flottantes fixées le long. Ces mouillages sont équipés de nombreux capteurs autonomes et permettent l'acquisition haute fréquence de certaines variables. Ces capteurs peuvent être fixés à différentes profondeurs (selon leur position sur le câble quand le mouillage est mis à l'eau). Les variables les plus fréquemment mesurées par les mouillages sont la température, la salinité, la pression mais aussi les courants, l'export vertical de particules (via des pièges à particules) ou encore des variables biogéochimiques. Certaines lignes de mouillages sont également reliées à une bouée de surface qui va mesurer les variables météorologiques ainsi que des variables en subsurface à la même position géographique. Les lignes de mouillage et leurs capteurs sont déployées, récupérées et entretenues à l'aide de navires océanographiques. La plupart des mouillages ne transmettent pas leurs données en temps réel, ils sont donc récupérés systématiquement à fréquence régulière pour récolter les données et permettre l'entretien du mouillage et des capteurs. Les capteurs sont sensibles aux facteurs environnementaux et peuvent dériver au cours du temps et il n'existe pas à l'heure actuelle de moyen de connaître l'état de ceux-ci. Ainsi, les mouillages permettent d'effectuer des mesures à haute fréquence sur l'ensemble de la colonne d'eau (selon la position des capteurs) et ils ont l'avantage de pouvoir embarquer des capteurs nécessitant beaucoup d'énergie. La localisation en point fixe permet également des visites régulières et donc l'obtention de mesures de référence à côté du mouillage afin de corriger les mesures issues des capteurs. Cependant, la résolution spatiale des mouillages fixes est souvent restreinte, ce pourquoi les mouillages sont souvent organisés en réseau de mouillages fixes. Au niveau européen ces mouillages sont gérés par EMSO (Dañobeitia et al. 2020) et au niveau global par OceanSites.

2.1.3 Flotteurs-profileurs Argo

Dans les années 2000 a été lancé le programme Argo (Roemmich et al. 2019) dédié à l'observation des propriétés physiques des océans. Les flotteurs profileurs sont des plateformes autonomes lagrangiennes qui dérivent au grès des courants. Elles contrôlent leur flottabilité en modifiant leur volume grâce à un système de vessie hydraulique, permettant au flotteur de

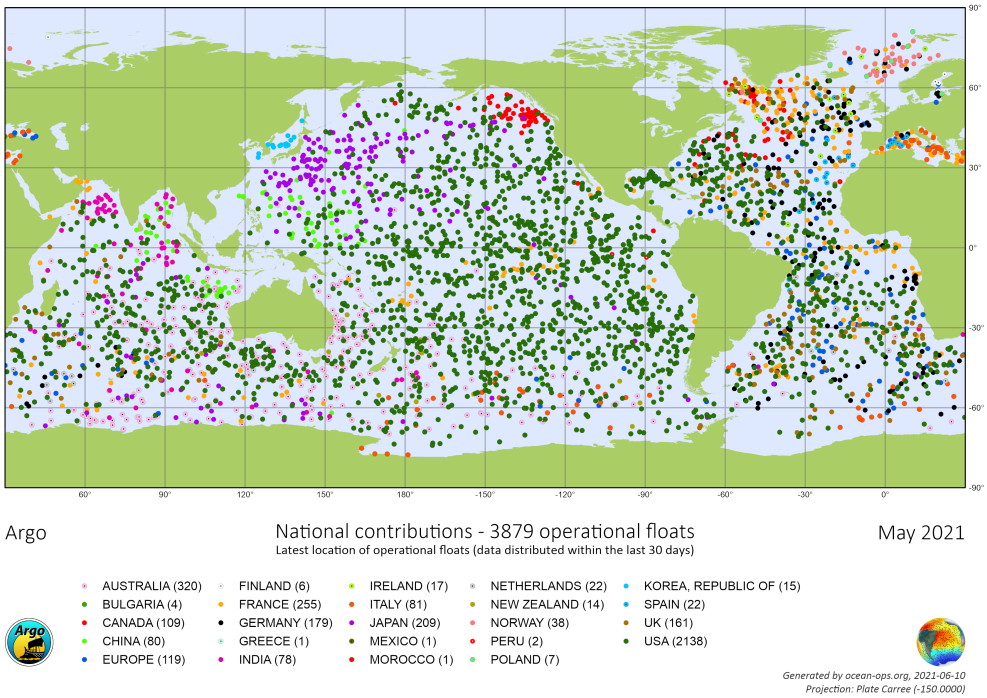

FIGURE 2.2 – Flotteurs profileurs Argo, un effort international. Carte des déploiements par pays. Tiré de Ocean-Ops.

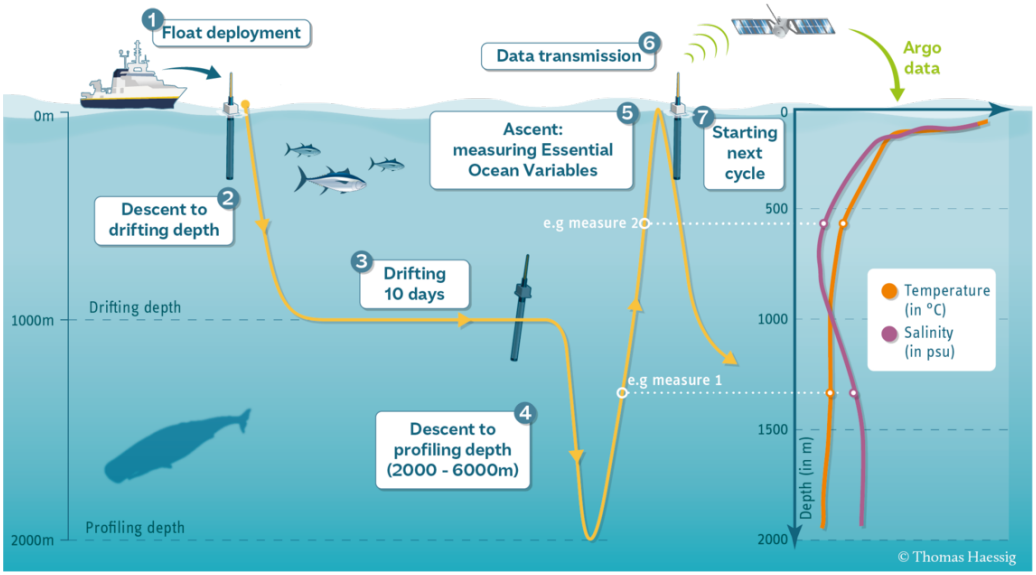

FIGURE 2.3 – Cycle de vie d'un flotteur profileur Argo. ©Thomas Haessig.

se déplacer verticalement sur la colonne d'eau à bas coût énergétique. Durant cette phase de mouvement vertical (et notamment lors de l'ascension), les capteurs du flotteurs sont activés et acquièrent des données, ce qui permet d'obtenir de profils verticaux. Le programme Argo est un programme international (figure 2.2) comprenant un réseau mondial de presque 4000 flotteurs profileurs actifs de nos jours. Les flotteurs profileurs sont le plus souvent déployés depuis des

navires océanographiques ou des navires d'opportunité. Les flotteurs fonctionnent selon des cycles (figure 2.3) : depuis la surface, le flotteur plonge à une profondeur dite « de parking » vers 1000 mètres où il dérive au grès des courants pendant 10 jours (selon ses paramètres de cycles). Au bout de ces 10 jours, le flotteur descend à 2000 m puis il remonte lentement jusqu'à la surface tout en mesurant de nombreuses variables lors de sa remontée. Une fois en surface, les données sont transmises par satellite à des centres de données à terre (Data Assembly Center, DAC). Le flotteur replonge ensuite et entame un nouveau cycle de mesures, et ce jusqu'à ce que sa batterie se vide au bout de plusieurs années ou que le flotteur soit récupéré dans certains cas.

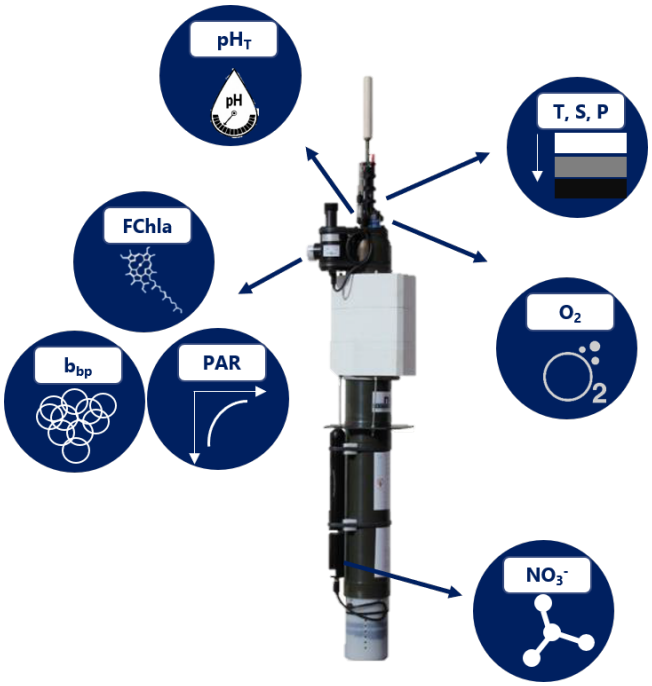

FIGURE 2.4 – Flotteur Argo et ses capteurs. T : température, S : salinité, P : pression, FChla : fluorescence de la chlorophylle a, PAR : Photosynthetically active radiation, b_{bp} : coefficient de rétrodiffusion particulaire, NO_3^-, O_2 : Oxygène dissous.

A l'origine, les flotteurs profileurs étaient équipés uniquement de capteurs CTD, mais au vu du succès du programme Argo et des développements technologiques (notamment la miniaturisation des capteurs), le programme BGC-Argo (pour BioGeoChemical-Argo) a officiellement vu le jour en 2016 (ROEMMICH et al. 2019 ; CLAUSTRE et al. 2020) après des premiers déploiements de flotteurs équipés de capteurs d'O_2 dans les années 2006-2007 (GRUBER et al. 2007). Ainsi, sur cette nouvelle génération de flotteurs profileurs peuvent être implémentés (figure 2.4) des capteurs d'oxygène dissous (O_2, KÖRTZINGER et al. 2004), de concentration en nitrates (NO_3^-, RISER et JOHNSON 2008), de différentes mesures bio-optiques (fluorescence de la chlorophylle, coefficient de rétrodiffusion particulaire, coefficient d'atténuation, fluorescence de la matière organique dissoute colorée, CLAUSTRE et al. 2009), de radiométrie (éclairement dans la colonne d'eau et lumière disponible pour la photosynthèse, XING et al. 2014), ou encore de mesure de

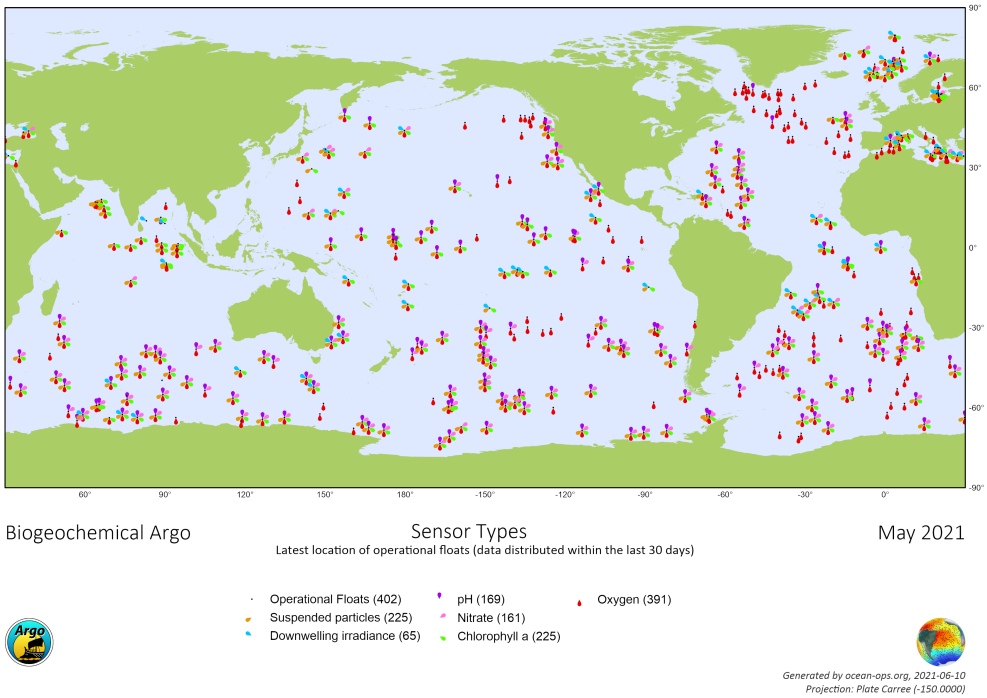

FIGURE 2.5 – Carte des flotteurs profileurs BGC-Argo en fonction des variables mesurées. Tiré de Ocean-Ops.

pH (JOHNSON et al. 2016). De nos jours, environ 400 flotteurs équipés de capteurs d'O_2 (figure 2.5) sont déployés, l'objectif étant d'atteindre un réseau de 1000 flotteurs BGC-Argo, qui aurait la résolution nécessaire pour améliorer considérablement notre compréhension des processus biogéochimiques à l'échelle mondiale.

Les flotteurs profileurs permettent de couvrir de larges échelles de temps (phénomènes journaliers, saisonniers à pluriannuels) et d'espace (de la méso-échelle à l'échelle d'un bassin) complétant ainsi les dispositifs plus classiques d'échantillonnage du milieu marin principalement basés sur les campagnes à bord de navires océanographiques. Cependant, il est important de rappeler que les flotteurs-profileurs Argo évoluent simultanément dans le temps et dans l'espace ; il est donc difficile de séparer ces deux composantes lors de l'exploitation de leur données.

2.1.4 Planeurs sous-marins

Les planeurs sous-marins ou « gliders » (Stommel 1989) sont des plateformes autonomes de mesure qui explorent l'océan mais dont la trajectoire reste pilotable. Ces planeurs se déplacent par un système de vessie hydraulique qui change leur volume. Cependant, au contraire des flotteurs profileurs Argo, leurs ailettes permettent de transformer une partie du déplacement vertical en déplacement horizontal (TESTOR et al. 2010). Ils sont programmés pour aller d'un point A à un point B en effectuant des montées et descentes en dent de scie (comme sur la figure 2.6), effectuant

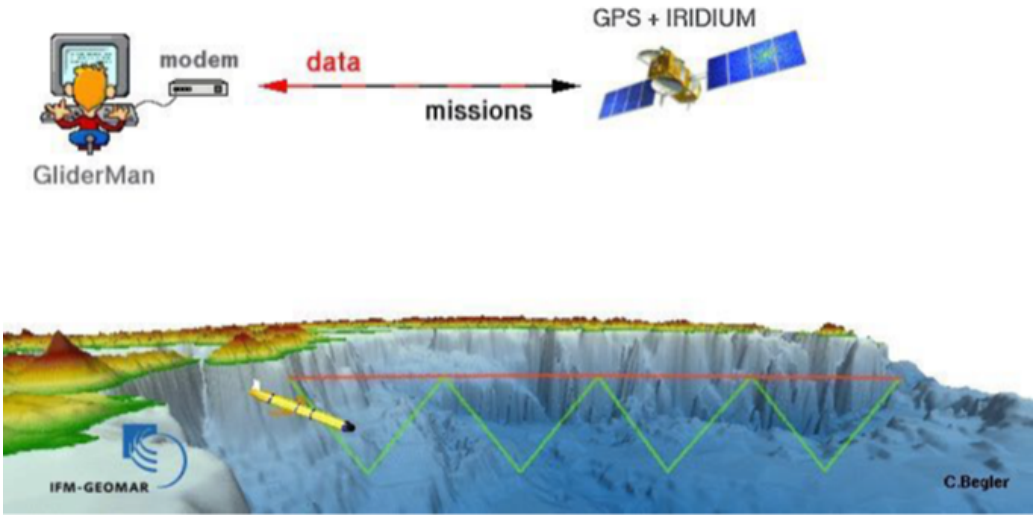

FIGURE 2.6 – Principe de fonctionnement d'un planeur sous-marin, d'après IFM-GEOMAR.

des mesures lors des montées et des descentes le long de leur trajectoire. Ils sont habituellement équipés d'une CTD mais aussi de capteurs d'O_2, de fluorescence. À chaque remontée en surface, les planeurs peuvent estimer un courant moyen intégré sur toute la colonne d'eau en comparant les positions de sortie théorique et réelle. De plus, en surface une communication par Iridium permet un échange d'information à deux sens : le planeur transmet les données dégradées (basse résolution) et récupère les paramètres de mission. Ainsi, au contraire des flotteurs profileurs, les planeurs ont une batterie plus faible et ne sont pas faits pour être laissés en mer mais sont récupérés pour obtenir leurs données (en haute résolution, données centimétriques), les recharger et les redéployer. Les planeurs sous-marins sont ainsi un moyen d'étude des océans complémentaire aux plateformes décrites précédemment qui permettent l'étude de phénomènes précis par leur pilotabilité (par exemple la description en mer Méditerranée de structures de submésoéchelle (BOSSE 2016) ou l'étude de fronts comme le Courant Nord (NIEWIADOMSKA et al. 2008). Ils permettent également d'augmenter la couverture spatiale des autres plateformes avec notamment l'étude des processus côte-large. Les planeurs sont gérés par OceanGliders et rattachés au GOOS (Global Ocean Observing System, MOLTMANN et al. 2019 ; TESTOR et al. 2019).

2.1.5 Observations satellitaires

Un autre moyen d'observation de l'océan est le satellite qui a la particularité de couvrir une grande partie du globe et de transmettre les données en temps quasi réel. Les satellites permettent également un suivi long-terme de certaines variables à l'échelle globale. Les satellites en océanographie fournissent de nombreux types d'informations telles que les vents, le niveau de la mer (différence entre la hauteur de l'eau et l'ellipsoïde de référence prenant en compte le géoïde

et les courants océaniques), la température de surface (obtenue par mesure infrarouge ou par radiométrie) et les paramètres de couleur de l'eau. Dans les dernières années, le développement de satellites géostationnaires qui restent au-dessus d'une zone donnée au cours du temps permettraient de s'affranchir de cet effet des nuages et d'obtenir des données à plus haute fréquence, permettant ainsi l'investigation de cycles diurnes par exemple. Au cours de cette thèse ont été utilisées des données calibrées récupérées du Copernicus Marine Service.

2.1.6 Le réseau MOOSE

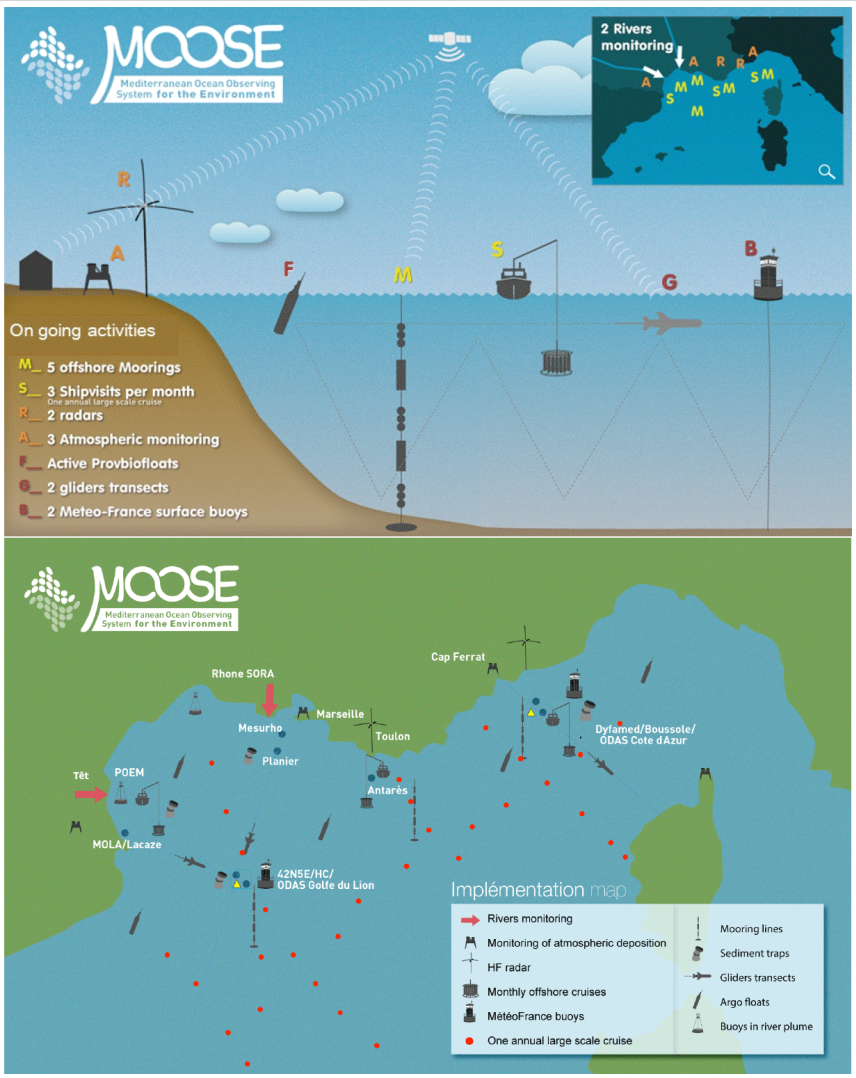

FIGURE 2.7 – Réseau MOOSE. Présentation des plateformes le long d'une coupe côté-large et positionnement géographique des plateformes. Tiré du site MOOSE.

Le réseau MOOSE (Mediterranean Ocean Observing System for the Environment) est un réseau d'observation multi-disciplinaire régional et intégré mis en place en 2010, et qui a

pour objectif d'étudier l'environnement en Méditerranée nord-occidentale face aux pressions anthropiques et au changement climatique. Plus précisément, le réseau MOOSE a pour objectif d'observer la variabilité dans l'espace et dans le temps des processus qui interagissent entre la côte et le large, et entre l'océan et l'atmosphère. Il a été construit comme un système d'observation multi-disciplinaire et intégré pour répondre à la demande scientifique et sociétale (Coppola et al. 2019). Le réseau MOOSE a été conçu pour surveiller les variabilités saisonnières ou interannuelles, ainsi que l'impact des événements extrêmes qui contrôlent les flux physiques et biogéochimiques et la biodiversité marine. Il permet un suivi long-terme et un traitement de cinq grandes questions scientifiques que sont la circulation de mésoéchelle, les cycles biogéochimiques et l'acidification, les communautés biologiques et la biodiversité, les apports fluviaux, et les dépôts atmosphériques. Ce réseau intégré est composé de mouillages, radars, bouées de surface, campagnes en mer (mensuelles et annuelles), flotteurs Argo et planeurs, ainsi que de mesures atmosphériques (figure 2.7).

2.2 Données en Méditerranée

Dans cette partie sont présentés les différents jeux de données utilisés au cours de cette thèse.

2.2.1 Campagnes en mer

En Méditerranée, le nombre de données biogéochimiques (O_2, nutriments, carbonates) est croissant ; cependant, l'effort d'échantillonage est assez disparate entre les bassins : la Méditerranée nord-occidentale est la zone la mieux échantillonnée, là où la rive sud et le bassin oriental (notamment le bassin Levantin) manquent encore cruellement d'observations (figure 2.8). Des campagnes internationales telles que GO-SHIP (tous les 10 ans) et Med-SHIP (tous les 5 ans, Schroeder et al. 2015), des campagnes nationales répétées (RADMED et MOOSE-GE) et des sorties mensuelles hauturières (MOLA, ANTARES, E1M3A et DYFAMED, série temporelle la plus ancienne en Méditerranée initiée en 1991 (JGOFS, J.-C. Marty et al. 2002)) y permettent l'acquisition de variables biogéochimiques. Plusieurs efforts pour compiler les mesures effectuées durant ces nombreuses campagnes en mer en un jeu de données homogène et de qualité sont en cours comme SOCAT (ciblé sur les variables du système des carbonates), GLODAP et CARIMED, un jeu de données qualifiées de variables biogéochimiques en Méditerranée.

2.2.2 Mouillages LION et DYFAMED

Deux mouillages précis seront utilisés au cours de ces travaux. Les mouillages LION et DYFAMED situés en Méditerranée nord-occidentale (figure 2.7) fournissent des données à haute fréquence à un endroit fixe avec une résolution verticale assez faible. Ces deux mouillages, inclus

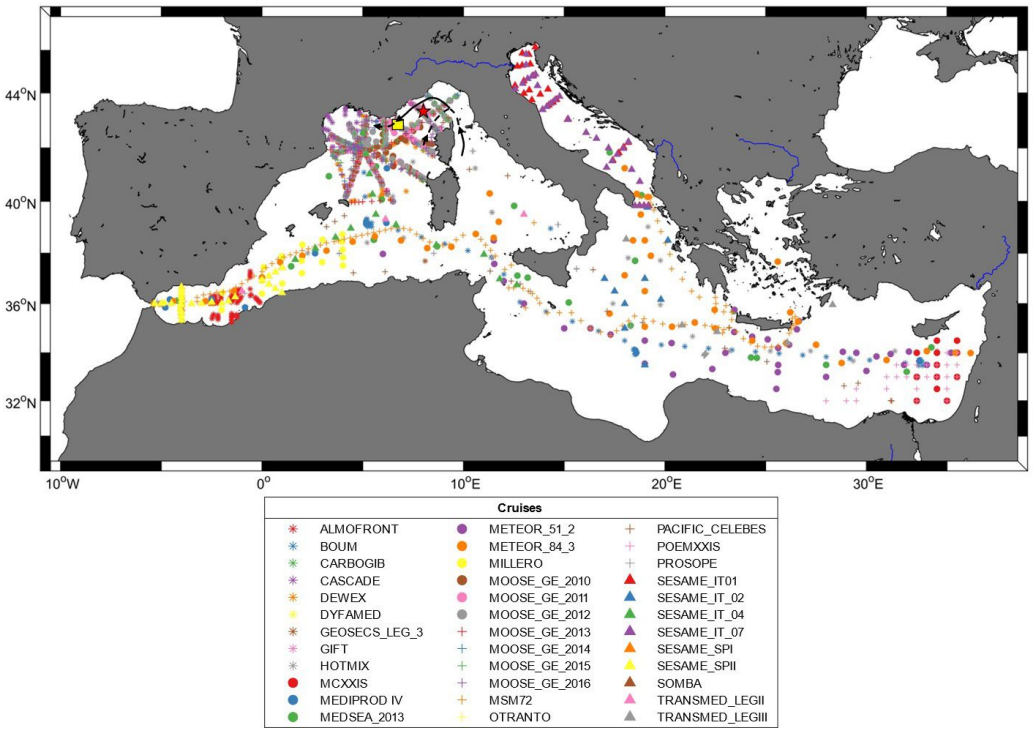

FIGURE 2.8 – Carte des campagnes en mer mesurant des variables biogéochimiques (T, S, O_2, ainsi que nutriments (nitrates, phosphates, silicates) et/ou variables du système des carbonates (A_T, C_T, pH_T) entre 1981 et 2018) utilisées au cours de cette thèse. Tiré de FOURRIER et al. (2020).

dans le réseau MOOSE (détails en partie 2.1.6 Le réseau MOOSE), sont localisés à 42°N, 5°E pour LION et 43.42°N, 7.87°E pour DYFAMED. Ils sont équipées de capteurs CTDs (avec ou sans capteur d'O_2), de courantomètres, de pièges à particules et de capteurs de température uniquement (figure 2.9). Les capteurs sont calibrés avant et après déploiement avec la CTD à bord du navire océanographique pour les variables physiques. Pour l'O_2, une intercomparaison des capteurs a lieu le jour de la maintenance et les capteurs sont révisés tous les deux ans. À cela s'ajoute une post-correction grâce aux sorties mensuelles et annuelles à la position des mouillages. En raison des conditions environnementales et du trafic maritime et halieutique, ces deux lignes de mouillages sont immergées et s'arrêtent plusieurs dizaines de mètres sous la surface. Les CTDs équipées de capteurs d'O_2 sont situées dans les eaux intermédiaires (350 m environ) et en profondeur (2000 m environ) pour les deux mouillages, donnant ainsi une vision partielle de la colonne d'eau. Cependant, le choix de ces profondeurs permet d'étudier finement la dynamique de l'O_2 dans les eaux intermédiaires (LIW) et dans les eaux profondes (WMDW) au cours du temps et en réponse aux évènements physiques et climatiques dans cette zone.

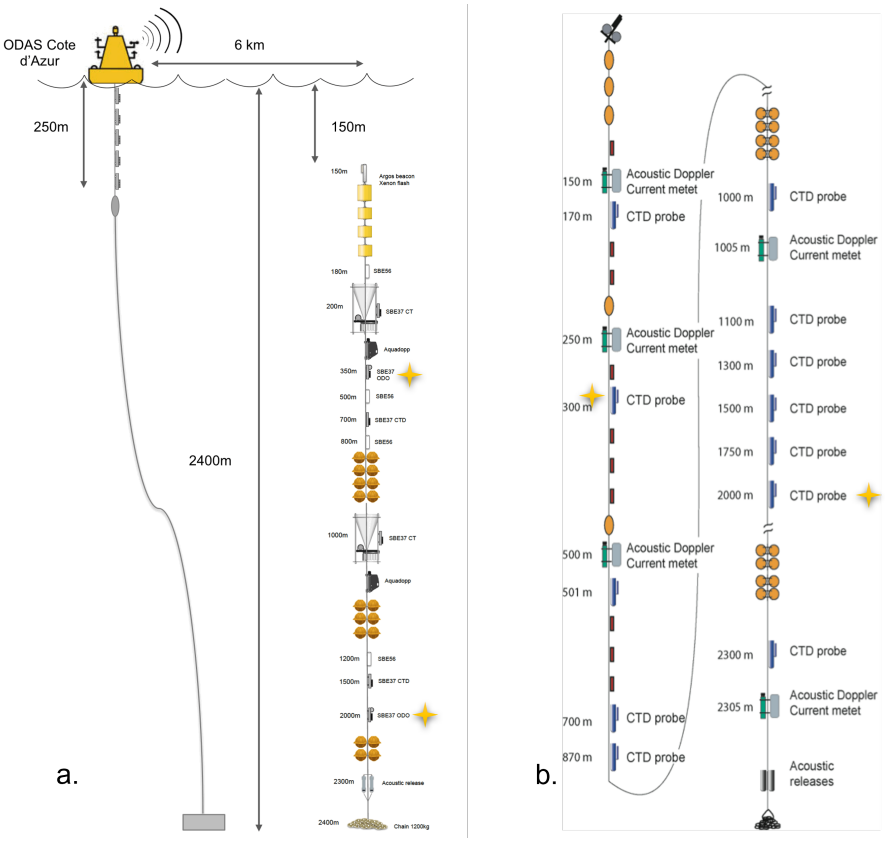

FIGURE 2.9 – Profondeurs et description des capteurs des mouillages a. DYFAMED et b. LION. Les positions des mouillages DYFAMED et LION sont visibles sur la figure 2.7 Les étoiles jaunes représentent les capteurs mesurant l'O_2. Adapté de Fixed point Open Ocean Observatory network (FixO3).

2.2.3 Flotteurs-profileurs Argo

Plusieurs programmes ont permis un ensemencement de la Méditerranée en flotteurs-profileurs équipés de capteurs d'O_2 depuis 2012 et notamment dans le bassin nord-occidental (figure 2.10). La France est un grand contributeur de données Argo-O_2 au travers de programmes comme MISTRAL, DEWEX, NAOS (Equipex 2010-2020), Med-Argo, MOOXY (LEFE-GMMC 2014, 2016, 2017, 2019), etc. et contribue ainsi à la densité élevée de flotteurs en Méditerranée. En Méditerranée, la couverture des flotteurs a évolué de 3 flotteurs Argo équipés d'O_2 et 1 flotteur BGC-Argo en 2012 à 37 et 17 respectivement en 2020. Concernant les mesures O_2 effectuées par les flotteurs Argo, les mesures dans l'air et les protocoles de calibration des optodes (capteur optique utilisé pour la mesure de l'O_2 sur les plateformes autonomes) ont permis une nette amélioration de la qualité et de la précision de ces données (BITTIG et al. 2018 ; BITTIG et KÖRTZINGER 2015). Celles-ci peuvent maintenant atteindre des précisions de 1-1,5 μmol kg^{-1} proches de celles réalisées *in situ* par la méthode Winkler. Au cours de cette thèse, nous utiliserons uniquement des flotteurs qui ont à minima un capteur d'O_2 issues du Data Assembly Center (DAC) Coriolis qui centralise les données de flotteurs de Méditerranée. Au cours de

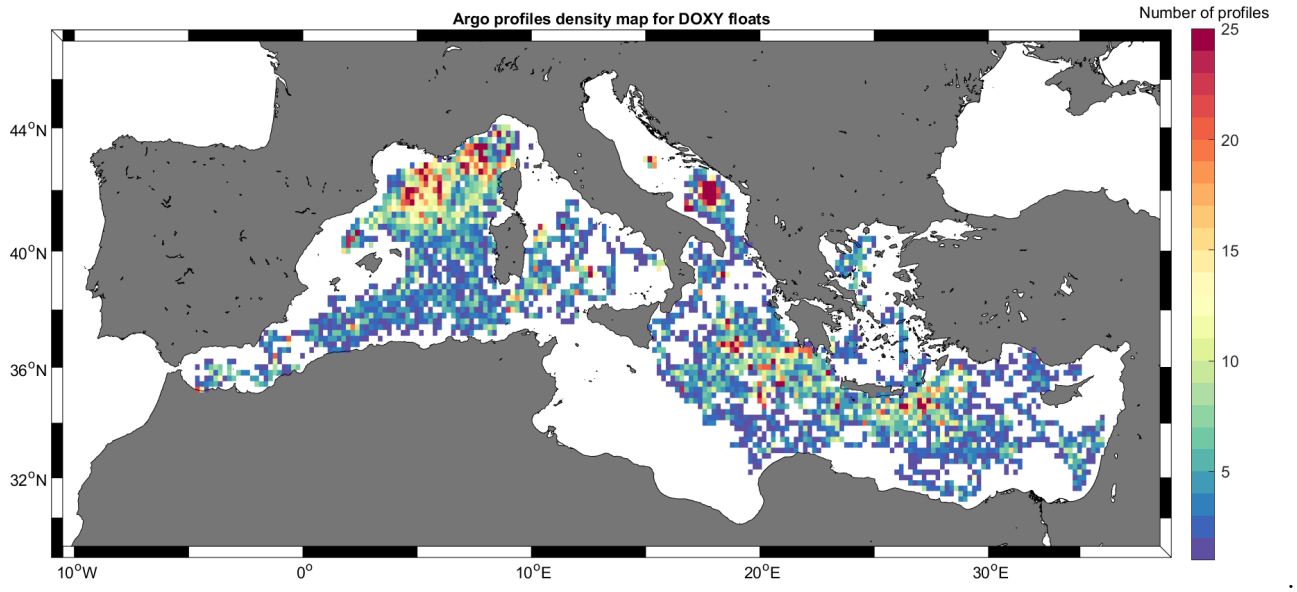

FIGURE 2.10 – Carte de densité des profils des flotteurs profileurs Argo équipés de capteur d'O_2 en Méditerranée.

ma thèse, j'ai pu contribuer à la correction des données d'O_2 sur les flotteurs Argo pour la Méditerranée (cf. partie 3.1.2 Contrôle qualité des données d'O_2 de flotteurs BGC-Argo).

2.2.4 Planeurs

En Méditerranée, les planeurs sont majoritairement déployés au niveau des Baléares par le SOCIB (Espagne), en Méditerranée Nord-Occidentale dans le cadre du réseau MOOSE ou en Adriatique. Ces déploiements sont qualifiés de lignes d'endurance le long desquelles les planeurs sont déployés de manière répétée pour suivre l'évolution des variables océaniques (figure 2.11). Dans cette thèse, les données issues d'un planeur équipé d'un capteur d'O_2 ont été utilisées. Spécifiquement il s'agit des radiales T00_23 et T00_26 dont les données ont été corrigées par BOSSE et al. (2017). Ces radiales ont eu lieu en janvier-février 2013 et en juin-juillet 2013 et correspondent à 615 et 655 profils respectivement.

2.2.5 Sorties de modèles

De nombreux modèles décrivant la circulation et les variables biogéochimiques existent en Méditerranée. Parmi eux, le modèle couplé SYMPHONIE-Eco3MS (modèle couplé circulation-biogéochimique, figure 2.12) comprend des modules de variables biogéochimiques prédites par la méthode neuronale développée au cours de cette thèse. Le modèle Eco3MS est un modèle biogéochimique multi-nutriments et multi-éléments qui décrit l'évolution temporelle de 35 variables d'état et permet de décrire la dynamique du plancton pélagique (ULSES et al. 2016). Il est forcé en « offline » par le modèle de circulation océanique SYMPHONIE (MARSALEIX et al. 2008).

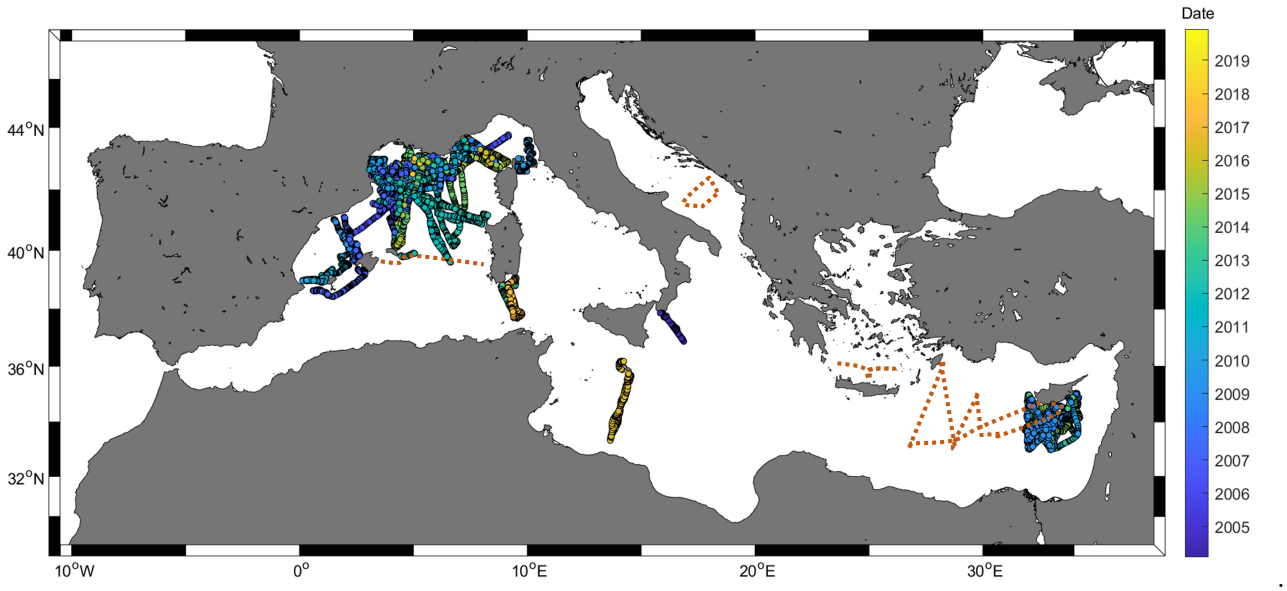

FIGURE 2.11 – Carte des profils des planeurs équipés de capteur d'O_2 en fonction des années en Méditerranée (données Everyone's Gliding Observatories (EGO)) et tracés des lignes d'endurance manquantes (tiretés oranges).

Le domaine du modèle couplé s'étend sur le bassin occidental. La modélisation couplée a été validée par ESTOURNEL et al. (2016) pour la température, la salinité et la couche de mélange, et par KESSOURI (2015) pour les nutriments inorganiques et la chlorophylle. Un module d'O_2 y a été ajouté et a été validé dans ULSES et al. (2021) (cf. Annexe 2 : Oxygen budget of the north-western Mediterranean deep-convection region).

Des comparaisons de variables du système des carbonates sont en cours en Méditerranée nord-occidentale au site DYFAMED entre des données *in situ* de campagnes, des sorties de ce modèle couplé et des sorties de la méthode neuronale développée au cours de cette thèse (détails en partie 4 Méthode CANYON-MED) (figure 2.13), afin de valider les modèles ou pour leur phase d'assimilation.

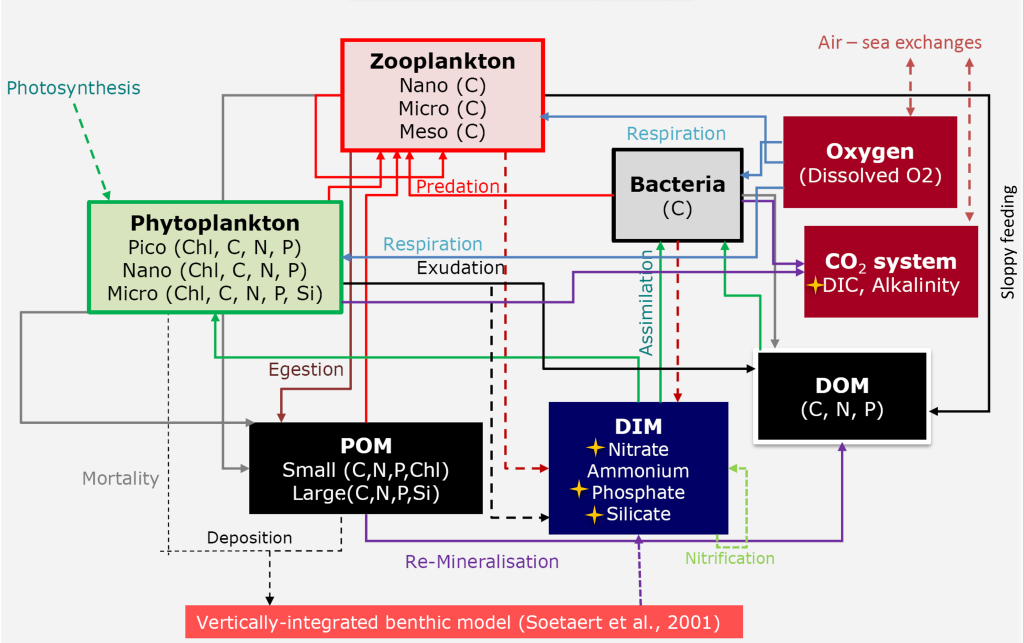

FIGURE 2.12 – Représentation schématique du modèle Eco3MS. Les étoiles jaunes correspondent aux données virtuelles générées par CANYON-MED qui peuvent servir de comparaison.

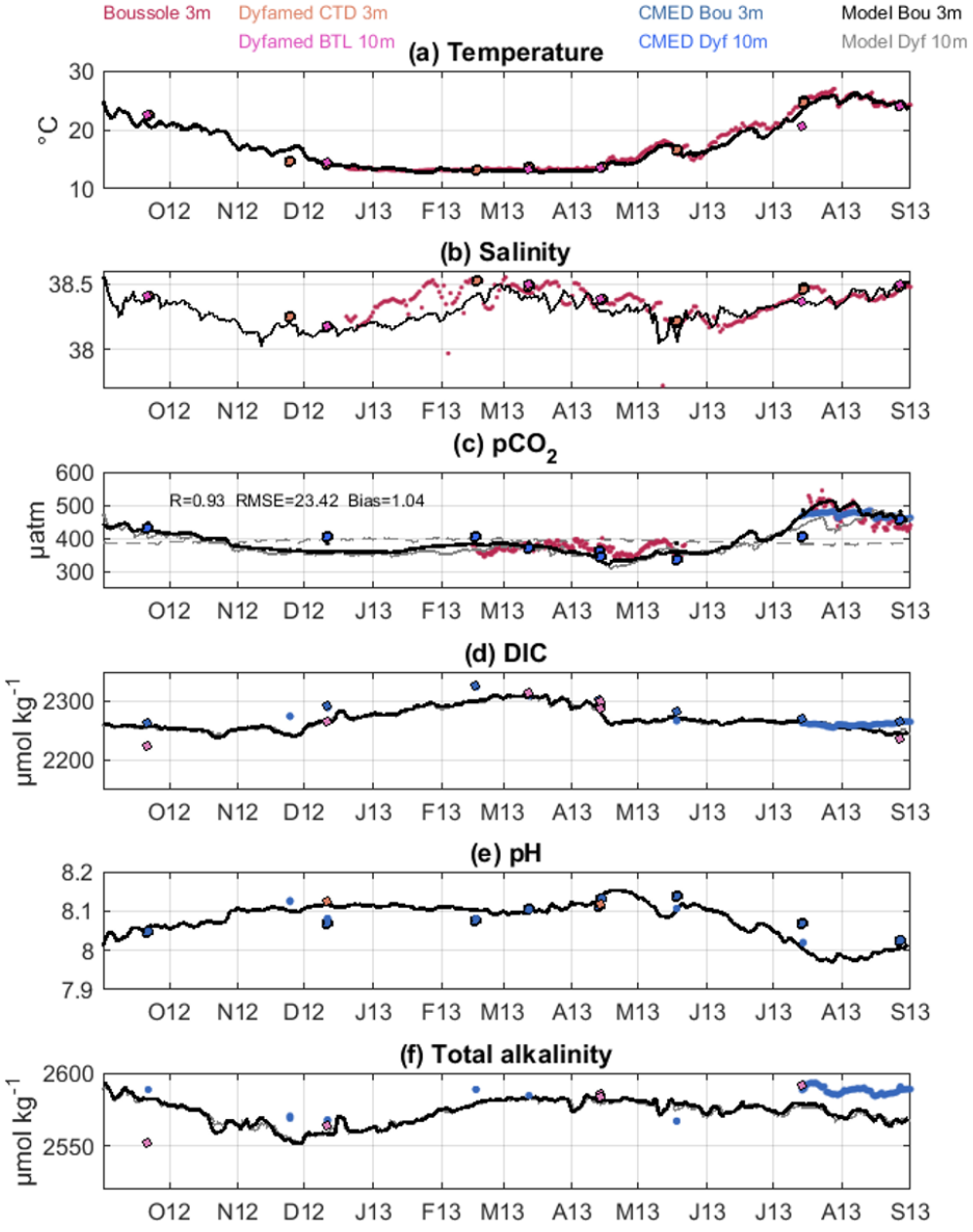

FIGURE 2.13 – Séries temporelle sur la période Octobre 2012-Septembre 2013 à DYFAMED de a. température, b. salinité, c. pCO_2, d. C_T, e. pH, f. A_T. Comparaison des données *in situ* (DYFAMED à 3 m, DYFAMED à 10 m, et BOUSSOLE à 3 m en orange, rose et rouge respectivement), des données virtuelles générées par CANYON-MED (à 3 et 10 m en bleu foncé et bleu clair) (détails en partie 4 Méthode CANYON-MED) et des données du modèle SYMPHONIE-Eco3MS (à 3 et 10 m en noir et gris). Adapté de (KESSOURI 2015).

Chapitre 3

Méthodologie

Sommaire du présent chapitre

3.1 Contrôle qualité des données

3.1.1 Contrôle qualité des données de campagnes en mer

Les données de campagnes en mer utilisées au cours de cette thèse ont été présentées en partie 2.2.1 Campagnes en mer. Les données étant issues de campagnes d'époques et de laboratoires variés, les méthodes analytiques et les unités varient beaucoup (exemple de l'O_2 exprimé en ml l^{-1}, μmol l^{-1}, μmol kg^{-1}, ...). Pour chaque campagne en mer, différents contrôles qualité ont été effectués. Tout d'abord les données ont été homogénéisées en terme d'unités de mesure afin de rendre le jeu de données cohérent. Puis un premier critère a été appliqué avec un « range test » (test de gamme vérifiant si la donnée est comprise dans un intervalle possible pour la variable) pour chaque variable, pour exclure les valeurs aberrantes et impossibles (par exemple des salinités inférieures à 35 sont aberrantes en Méditerranée). Des contrôles visuels plus poussés ont ensuite eu lieu afin de retirer les profils ou les mesures qui rentraient dans la gamme de valeur de la variable mais semblaient incohérents pour la région/saison par rapport

aux autres données ainsi qu'à la bibliographie (figure 3.1). Par exemple, des valeurs anormales de nutriments ont pu être observées à l'hiver 2006, mais ces valeurs n'ont pas été exclues car elles sont probablement la conséquence du mélange intense qu'il y a eu à cette période. Ces contrôles ont eu lieu par campagne puis inter-campagne.

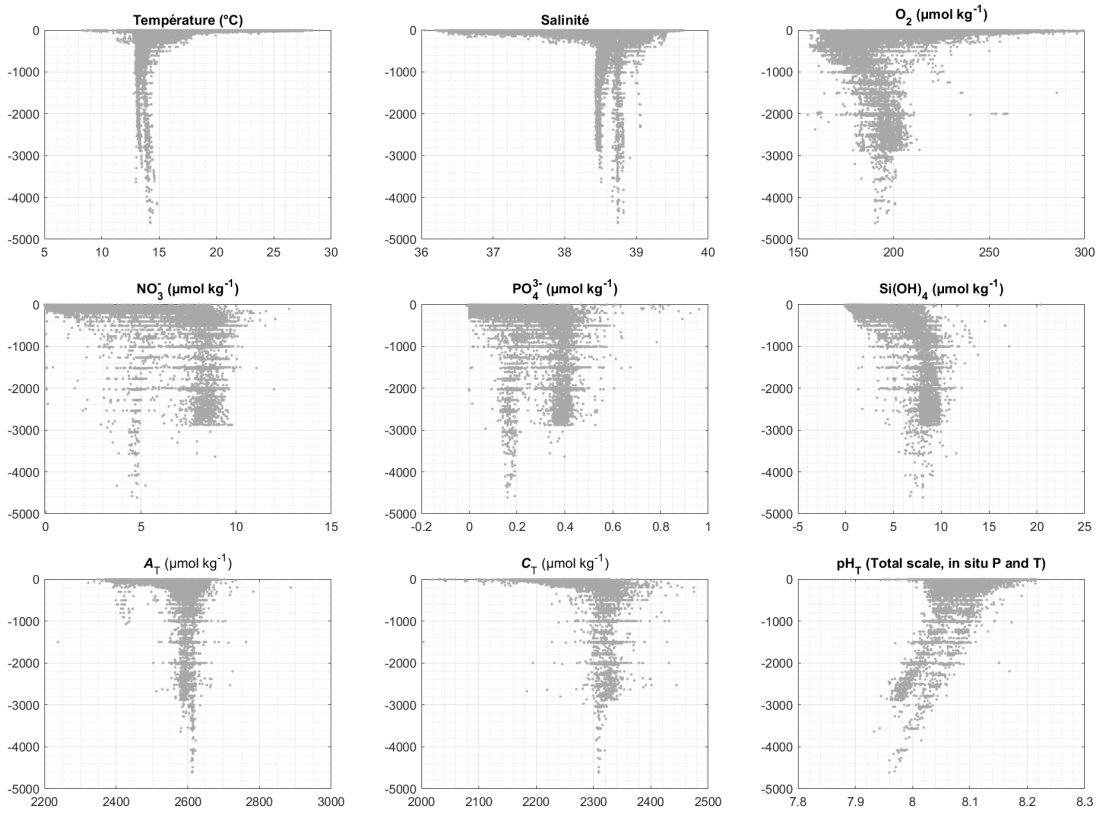

FIGURE 3.1 – Données issues de campagnes en mer utilisées au cours de cette thèse. a. Température, b. Salinité, c. O_2, d. NO_3^-, e. PO_4^{3-}, f. $Si(OH)_4$, g. A_T, h. C_T et i. pH_T.

3.1.2 Contrôle qualité des données d'O_2 de flotteurs BGC-Argo

Les données brutes envoyées par les flotteurs lors de leurs sorties en surface sont communiquées par satellite à des centres de données (Data Assembly Center, DAC) pour décodage et mise en forme. Une étape de contrôle qualité est nécessaire avant leur distribution pour les scientifiques. Les variables sont ajustées de différentes manières : soit a posteriori par un expert de la variable (données en Delayed Mode), soit en quasi temps réel (24h) via des coefficients d'ajustement calculés à un temps donné et propagés sur la vie du flotteur.

L'O_2 est le premier paramètre biogéochimique mesuré par les flotteurs BGC-Argo en termes

de volume de données (plus de 95% des flotteurs BGC-Argo mesurent l'O_2). Lorsque les données passent par les DACs, des filtres sont appliqués pour qualifier (associer un code qualité) les valeurs aberrantes (Thierry et al. 2018). Cependant, il est également nécessaire de corriger la mesure dès le déploiement et les dérives qui peuvent apparaître au cours de la vie du flotteur. La dérive et le gain peuvent être issus de la calibration des capteurs ou d'anomalies propres aux instruments (Bittig et al. 2018 ; Bittig et al. 2019). Plusieurs méthodes de correction existent selon le type de capteur, sa position (dans ou hors de l'eau quand le flotteur est en surface), la méthode de calibration, et la présence ou non de dérive dans le temps.

Les données de flotteurs utilisées au cours de cette thèse sont majoritairement des données en « Delayed Mode » et sont toutes issues du DAC coriolis (qui gère ces flotteurs déployés en Méditerranée). Pour passer des données d'O_2 en Delayed Mode, plusieurs méthodes existent selon l'O_2 mesuré par le flotteur et permettent de calculer les coefficients de correction que sont le gain et éventuellement la dérive (Thierry et al. 2018) :

1. Le flotteur effectue des mesures d'O_2 dans l'air quand il est en surface (le capteur d'O_2 est surélevé et dépasse nettement de l'eau). L'O_2 est alors converti en pO2 (pression partielle d'O_2 en saturation) et comparé à la climatologie NCEP à l'aide des outils SAGE-O2 (S. B. Argo 2021) ou LOCODOX (*LOCODOX* 2020) pour calculer les coefficients de correction selon la méthode de Bittig et Körtzinger (2015). Les coefficients sont alors appliqués et les mesures reconverties en O_2 en μmol kg^{-1}. La précision obtenue est de l'ordre de 2 mbar.
2. Le flotteur n'effectue pas de mesures dans l'air en surface. Il est alors nécessaire de prendre les mesures d'O_2 en subsurface et de les comparer à une référence. Dans notre cas, la référence en Méditerranée est la climatologie du World Ocean Atlas (WOA, Boyer et al. 2018) qui est une climatologie mondiale présentant des trous dans sa couverture spatiale en Méditerranée. Ainsi l'O_2 est converti en PPOX (pression partielle d'O_2) et l'ensemble des valeurs de subsurface sont comparées à la climatologie de référence pour calculer les coefficients de correction selon la méthode de Takeshita et al. (2013). Les coefficients sont alors appliqués et les mesures reconverties en O_2 en μmol kg^{-1}. La précision obtenue avec ce type de correction est de l'ordre de 4-6 mbar.
3. Cependant, il arrive que les mesures présentes dans le WOA soient trop éloignées spatialement ou temporellement des profils du flotteur et ainsi ne permettent pas la correction de l'O_2. Dans ce cas là, les mesures Winkler effectuées à bord du navire à la position du flotteur et converties en PPOX sont utilisées pour obtenir les coefficients de correction. Les coefficients sont alors appliqués et les mesures reconverties en O_2 en μmol kg^{-1}. Ceci présente plusieurs inconvénients : la correction a alors lieu avec un seul profil de référence à un moment donné et ce profil peut ne pas correspondre exactement à la position ni au temps du premier profil du flotteur. En effet, un flotteur dérive souvent en

surface pendant plus de 24h avant de plonger et d'effectuer son premier profil. A noter que les mesures Winkler au déploiement servent habituellement à valider la correction effectuée par les autres méthodes évoquées précédemment mais sont utilisées dans ce cas car aucun autre moyen de correction n'est possible. La précision maximale que l'on peut obtenir avec ce type de correction est de l'ordre de 4-6 mbar et peut aller jusqu'à 10 μmol kg^{-1}.

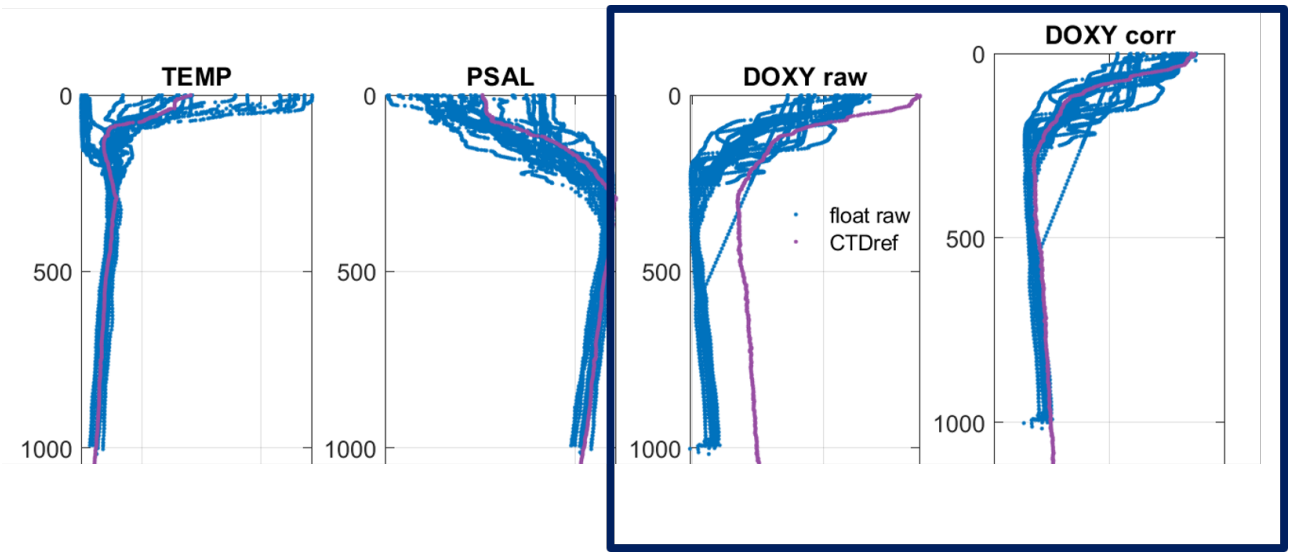

FIGURE 3.2 – Profils du flotteur 6901032 (bleu) et de la CTD de référence (violet). (a) Température, (b) salinité, (c) O_2 brut et (d) O_2 corrigé. L'O_2 corrigé est cohérent avec le profil de la CTD de référence.

De plus en plus de flotteurs sont équipés de capteurs d'O_2 qui permettent l'acquisition de mesures dans l'air, et ainsi obtiennent de meilleurs précisions lors des corrections d'O_2. Cependant, pour des flotteurs plus anciens, le paragraphe précédent montre que les corrections peuvent être compliquées et que de nombreuses méthodes et données sont utilisées pour tenter de corriger les données d'O_2 pour les rendre exploitables.

Au cours de ma thèse, j'ai participé au passage en Delayed Mode de la majorité des flotteurs équipés de capteur d'O_2 en Méditerranée en procédant au calcul des coefficients d'ajustement selon les cas de figures présentés précédemment (environ 80 flotteurs). Ces coefficients ont été transmis au DAC Coriolis pour validation par les responsables de chaque flotteur et implémentation.

Voici des exemples concrets des corrections obtenues par les différentes méthodes présentées précédemment.

Dans ce premier exemple, le flotteur n'effectue pas de mesures dans l'air et la climatologie n'a pas de mesures suffisamment proches du point de déploiement du flotteur pour pouvoir procéder à une correction. Cependant, une CTD de référence dont l'O_2 a été corrigé avec les mesures Winkler a été effectuée proche (dans le temps et l'espace) du déploiement du flotteur.

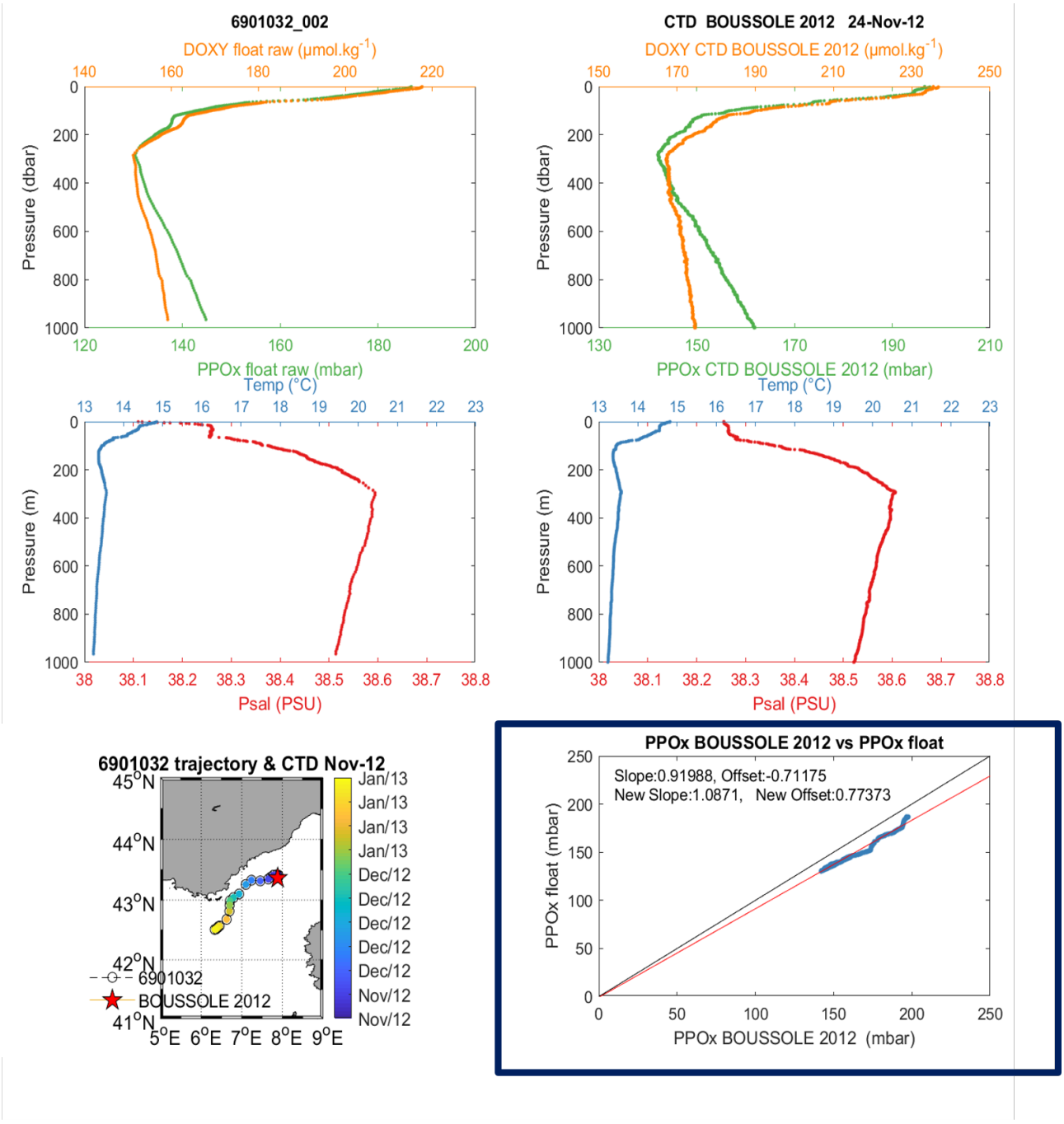

FIGURE 3.3 – Correction avec CTD de référence du flotteur 6901032. (a) O_2 et PPOX bruts du flotteur au deuxième profil, (b) O_2 et PPOX de la CTD de référence, (c) température et salinité du flotteur au deuxième profil, (d) température et salinité de la CTD de référence, (e) position du flotteur au cours du temps et position de la CTD de référence, (f) régression et coefficients entre la PPOX du flotteur et du profil de référence.

Ainsi, après avoir écarté le premier profil du flotteur qui est souvent de mauvaise qualité, le flotteur étant été hors de l'eau pendant longtemps avant son déploiement, une comparaison des profils de température, salinité et O_2 est effectué entre le second profil du flotteur et la

CTD de référence (figure 3.3). Cette comparaison permet de s'assurer que la structure verticale des masses d'eau est similaire et que les données sont comparables avant de procéder au calcul des coefficients de correction. Les coefficients sont obtenus par régression entre la PPOX du flotteur sur l'ensemble de la colonne d'eau et la PPOX du profil de référence. Ces coefficients sont ensuite appliqués en PPOX puis a lieu une reconversion en O_2 (en μmol kg^{-1}). Ainsi, l'O_2 brut du flotteur présentait un décalage de presque 20 μmol kg^{-1} (figure 3.2) et après correction les profils de référence et du flotteurs se superposent et le décalage a disparu sur l'ensemble de la colonne d'eau.

Dans ce second exemple, le flotteur n'effectue pas de mesure dnas l'air mais la climatologie présente des données à la localisation de déploiment du flotteur. L'O_2 est converti en PPOX. En inspectant visuellement la série temporelle de la PPOX du flotteur en subsurface, il apparait une dérive au cours du temps (figure 3.4a). Cette dérive est calculée puis corrigée sur le flotteur (figure 3.4b). Le ratio entre la PPOX de subsurface du flotteur corrigé de la dérive et la climatologie colocalisée est calculé sur la série temporelle du ratio (figure3.4c). On obtient finalement le coefficient de pente du ratio avec lequel la PPOX du flotteur sera corrigé. Enfin cette PPOX sera reconvertie en O_2 (en μmol kg^{-1}).

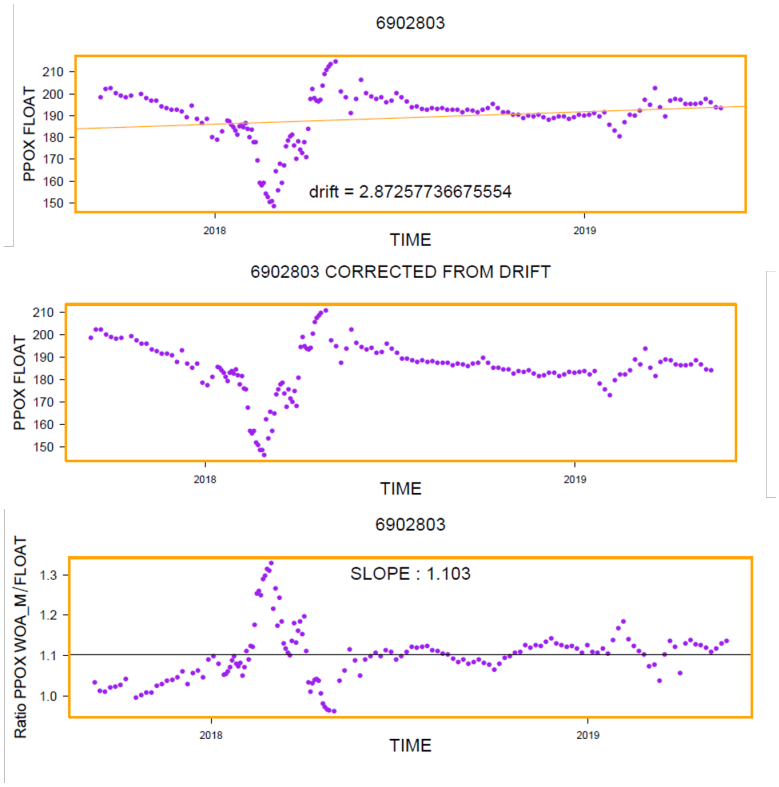

FIGURE 3.4 – Correction du flotteur 6902803 avec une climatologie de référence : le World Ocean Atlas (WOA). (a) PPOX du flotteur en subsurface au cours du temps permettant d'identifier une dérive, (b) PPOX du flotteur en subsurface corrigé de la dérive, (c) ratio entre la PPOX de subsurface du flotteur et le WOA colocalisé au cours du temps, permettant d'obtenir la pente (gain).

3.2 Méthodes neuronales

Les plateformes de mesures présentées précédemment permettent l'acquisition de large jeux de données. Afin de répondre aux problématiques présentées en partie 1.6, le choix de méthodologie a porté sur les méthodes neuronales, utilisées de plus en plus dans les sciences environnementales et en océanographie ces dernières années.

3.2.1 Définitions et historique

Bien qu'existant en théorie depuis les années 1950, (Rosenblatt 1958 ; Rosenblatt 1960) la mise en place computationnelle concrète des Réseaux de Neurones Artificiels (ANN) n'a eu lieu qu'à partir des années 1990. Ces ANN sont utilisés en sciences environnementales pour prédire des variables clés et trouver des relations à partir de jeux de données écologiques, ayant souvent des distributions spatio-temporellement complexes (non linéaires) et bruitées (Lek et Guégan 1999). Les ANNs ont ainsi ont été appliqués à différentes thématiques en écologie comme les notions de dynamique des poissons et de connectivité, de production phytoplanctonique (Scardi p. d.), d'effet de serre, de « remote sensing » atmosphérique et océanique (**haupt_neural_2009**), ... Les réseaux de neurones sont en effet des fonctions approximatrices qui permettent de modéliser des jeux de données variés (Marzban 2009), notamment ceux complexes et bruités. Ce sont donc des outils adaptés pour dériver des variables à partir de paramètres définis, notamment quand les relations sous-jacentes exactes sont difficilement formalisables ou inconnues, comme présenté en partie 1.6 Objectifs de la thèse. En océanographie spécifiquement, le potentiel des réseaux de neurones a été largement éprouvé, notamment pour dériver des variables climatiques (Landschützer et al. 2016), biogéochimiques (pCO_2, Telszewski et al. 2009, ou du système des carbonates (Broullón et al. 2019 ; Broullón et al. 2020 ; Landschützer et al. 2020)).

Ainsi, un ANN est un ensemble de processeurs élémentaires, les neurones, largement connectés les uns aux autres et capables d'échanger des informations par le biais des connexions par lesquelles ils sont reliés. Ces connexions sont directionnelles et à chaque connexion est associé un réel, appelé « poids » de la connexion. L'information est transmise d'un neurone à un autre, pondérée du poids. Les ANNs sont des méthodes approximatrices adaptées à de nombreux jeux de données (Marzban 2009). Un des principaux avantages de ces méthodes est leur capacité à reconnaître et exploiter des relations non prédéfinies dans les données (contrairement aux techniques de régressions) et qui ne nécessitent pas d'être explicitées par des équations. Cela les rend particulièrement adaptées à la cartographie des relations non linéaires et empiriques, à condition que des données soient suffisamment disponibles pour « entraîner » le réseau de neurones (Lefevre et al. 2005).

Dans cette thèse, le type de réseaux de neurones utilisé est le MLP ou Perceptron Multi-Couche.

3.2.2 Les MLPs

Parmi les différents types d'ANNs existants, les Perceptrons Multicouches (MLP : Multi-Layered Perceptrons) utilisant un algorithme de rétropropagation ont été choisis pour leurs propriétés d'approximateurs universels de n'importe quelle fonction continue et dérivable (Hornik et al. 1989). Utilisés dans 70% des études avec des ANNs (Oña et Garrido 2014 ; Gedeon et al. 1995), ils seront utilisés au cours de cette thèse pour modéliser une relation permettant de prédire, à partir des variables océanographiques essentielles (température, salinité, pression, O_2), les nutriments (NO_3^-, PO_4^{3-}, $Si(OH)_4$) et les variables du système des carbonates (A_T, C_T, pH_T). Les MLPs sont des ANNs organisés en plusieurs couches (couches d'entrée, cachée(s) et de sortie) contenant plusieurs neurones. Lors du développement du réseau de neurones, la topologie est choisie par l'utilisateur afin d'être la plus adaptée au problème choisi. La topologie d'un réseau de neurones correspond au nombre de couches cachées et au nombre de neurones sur chacune de ces couches (avec n_j, le nombre de neurones de la première couche cachée et n_i, le nombre de neurones de la deuxième couche cachée, figure 3.5). Chaque noeud du réseau (noeud d'entrée, neurone caché, noeud de sortie) est relié aux noeuds de la couche précédente/suivante grâce à un poids. Ces poids sont réajustés de manière itérative lors de la phase d'entraînement du MLP.

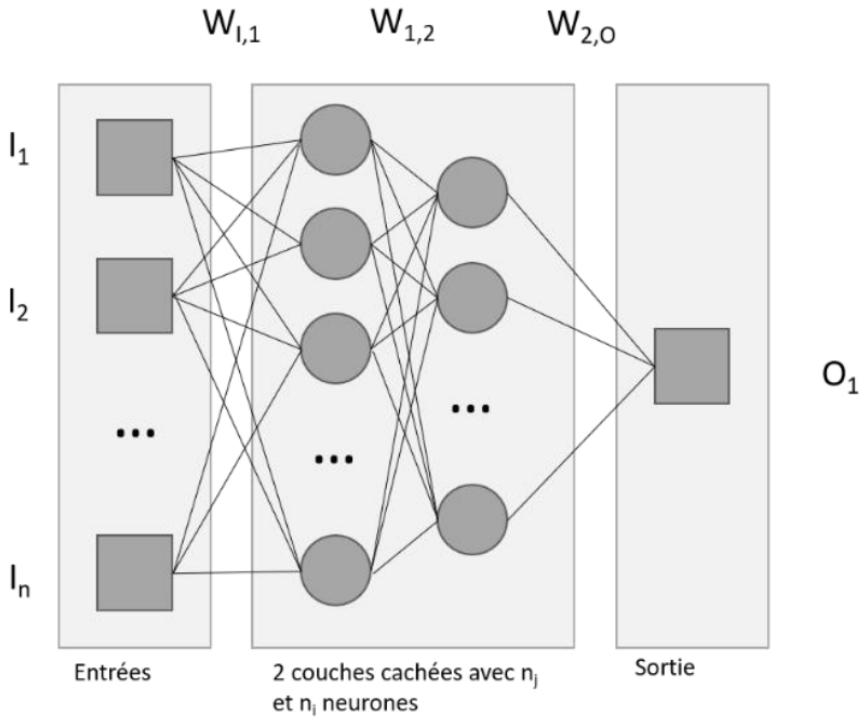

Figure 3.5 – Représentation schématique de l'architecture d'un MLP à 2 couches cachées. Chaque segment reliant les différents neurones est défini par un poids w.

Plus précisément, les poids sont réajustés de manière itérative en minimisant une fonction

de coût, définie ici comme l'erreur quadratique moyenne. L'erreur $e_i(t)$ du neurone i au temps t est définie comme $e_i(t) = c_i(t) - a_i(t)$ avec $c_i(t)$, la valeur de sortie ciblée et $a_i(t)$ la valeur de sortie actuelle. Cette erreur est réduite en minimisant la fonction de coût F :

$$F(e(t)) = \sum_{i=1}^{N} e_i^2(t) \tag{3.1}$$

avec N le nombre de neurones de sortie du réseau. La minimisation est effectuée via la technique de régularisation Bayésienne (Bishop 1995).

Il existe deux grandes phases dans la création d'un MLP : 1) la phase d'apprentissage et de validation et 2) la phase de test. Les données utilisées pour développer le réseau de neurones sont ainsi séparées en deux sous-jeux, de manière aléatoire, le jeu de la phase de test étant un sous-ensemble représentatif de la diversité des valeurs prises par les variables. La première phase utilise la majorité des données de la base de données initiale lors de la conception du réseau de neurones. Les données restantes sont utilisées lors de la deuxième phase qui teste l'efficacité du MLP. Cette phase de test détermine la capacité de généralisation du réseau de neurones (Bishop 1995). Cette séparation est souvent faite selon les proportions 80%-20%.

Architecture Les MLPs développés dans le cadre de cette thèse sont composés de quatre couches : une couche d'entrée, deux couches cachées et une couche de sortie (figure 3.5). Chaque neurone est connecté à ceux des couches suivantes. Le transfert de l'information au travers du MLP se fait de manière unidirectionnelle et de la façon suivante :

$$O = f(W^{2,O} * f(W^{1,2} * f(W^{I,1} * I))) \tag{3.2}$$

où I et O représentent respectivement les données d'entrée et de sortie du MLP, et $W^{I,1}$, $W^{1,2}$, $W^{2,O}$ représentent les matrices de poids des connections entre la couche d'entrée et la première couche cachée, la première et la deuxième couche cachée, et entre la deuxième couche cachée et la couche de sortie, respectivement (figure 3.5). f est une fonction sigmoïde telle que :

$$f(x) = A * \frac{exp^{\alpha x} - 1}{exp^{\alpha x} + 1} \tag{3.3}$$

où A et α sont deux constantes fixées respectivement à 4/3 et 1,7159 afin de garantir un comportement quasi-linéaire entre -1 et 1 (Jamet 2004).

L'architecture ou « topologie » optimale d'un réseau de neurones (nombre d'entrées, de sorties, nombre de couches cachées et de neurones dans chaque couche cachée) dépend de la complexité

des relations entre les entrées et les sorties. Après avoir testé plusieurs configurations différentes par un processus d'essais et d'erreurs, les topologies des réseaux de neurones produisant les meilleurs résultats (minimisant l'erreur sans montrer de sur-apprentissage et avec de bonnes capacités de généralisation) ont été déterminées avec 2 couches cachées, contenant entre 15 et 50 neurones pour la première couche, et entre 8 et 30 pour la deuxième.

Pré-traitement des données Les données d'entrée du MLP représentent différents types de paramètres/variables, avec donc des ordres de grandeurs différents. Ceci est aussi le cas pour les variables de sortie du MLP. Afin que le MLP prenne en compte toutes les entrées de manière similaire et pour éviter des saturations des MLPs, il est nécessaire qu'elles aient le même poids numérique, et qu'elles soient donc dans le même ordre de grandeur. Ainsi, les variables A et α ont été définies afin que le domaine $[-1;1]$ de la fonction ait un comportement linéaire. Par conséquent et pour éviter la saturation, les entrées et les sorties du MLP ($x_{i,j}$) sont centré-réduites selon :

$$X = \frac{2}{3} * \frac{x - \bar{x}}{\sigma} \tag{3.4}$$

où $x_{i,j}$, $x_{\bar{i},j}$ et $\sigma_{i,j}$ sont respectivement, la $\text{j}_{\text{ème}}$ dimension de la $\text{i}_{\text{ème}}$ donnée, la moyenne de la $\text{j}_{\text{ème}}$ dimension et l'écart-type de la $\text{j}_{\text{ème}}$ dimension. Le facteur 2/3 permet de ramener au moins 80% des données dans la gamme $[-1;1]$ (Jamet et al. 2012).

Phase d'apprentissage et validation L'apprentissage permet de déterminer les poids du réseau de neurones à l'aide d'un processus itératif tel que :

$$W_{i,j}(t+1) = W_{i,j}(t) + \delta W_{i,j}(t) \tag{3.5}$$

où $W_{i,j}(t+1)$ représente le poids reliant le neurone j au neurone i à l'itération $t+1$. Ce poids dépend du poids à la précédente itération $W_{i,j}(t)$. L'initialisation des poids au début de l'entraînement est aléatoire (entre -1 et 1). La modification des poids au cours de l'apprentissage a lieu via une fonction de coût au travers du terme $\delta W_{i,j}(t)$. L'apprentissage consiste à minimiser cette fonction de coût, dans notre cas à l'aide d'une méthode de régularisation bayésienne (Bishop 1995). Cette méthode minimise le sur-apprentissage en tenant compte de la qualité de l'ajustement ainsi que de l'architecture du réseau de neurones. L'algorithme d'entraînement utilisé est précisément une méthode d'apprentissage itérative supervisée mettant à jour les poids selon l'optimisation de Levenberg-Marquardt (Linares-Rodriguez et al. 2013). Cet algorithme a été choisi car il est mieux adapté à l'ajustement de fonctions et ne nécessite pas de temps ni de

puissances de calcul excessifs, tout en généralisant de manière appropriée (Beale et al. p. d.). Pour éviter de tomber sur un minimum local, une combinaison linéaire de poids et d'erreurs quadratiques a été minimisée par descente de gradient, et de multiples initialisations avec des poids aléatoires ont été effectuées. Ensuite, pour déterminer la combinaison appropriée de poids et d'erreurs, la régularisation bayésienne a été utilisée. Cela a permis la généralisation du réseau de neurones par l'optimisation de la combinaison linéaire des poids et des erreurs (MacKay 1992b ; MacKay 1992a ; Foresee et Hagan 1997 ; Hagan et al. 2014). L'apprentissage et la validation sont simultanées : en effet, pendant la phase d'apprentissage (également appelée « entraînement »), une validation croisée (Bishop 1995) a lieu. Cette validation croisée permet de tester la robustesse des résultats obtenus sur la base de données indépendantes. L'erreur calculée, durant la phase d'apprentissage, entre les valeurs du jeu de validation et celles obtenues par le MLP renseigne sur la validité du réseau. Il faut arrêter l'apprentissage du réseau de neurones avant que l'erreur de validation n'augmente (figure 3.6), cette augmentation signifiant que le MLP devient mauvais en généralisation et qu'un « sur-apprentissage » commence. Si un sur-apprentissage a lieu, cela entraîne une dégradation de la performance du MLP qui n'est plus capable de généraliser, puisqu'il n'a alors pas appris la relation sous-jacente aux données mais juste une relation qui lui permet de retrouver avec précision les données d'apprentissage (figure 3.7).

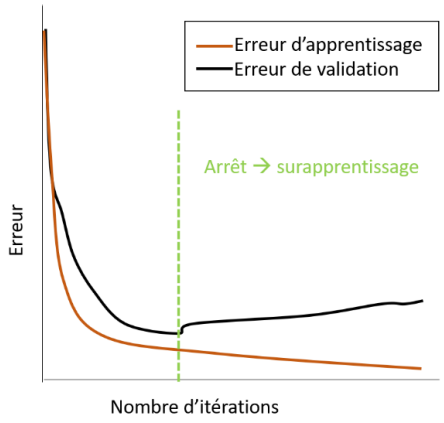

Figure 3.6 – Illustration de la validation croisée : arrêt du réseau de neurones avant que l'erreur de validation n'augmente.

Ce sur-apprentissage peut avoir lieu quand l'arrêt de l'apprentissage n'est pas fait assez tôt ou lorsque la topologie du réseau devient trop complexe par rapport au problème à résoudre. Un ANN avec trop peu de neurones sera sous-ajusté : par manque de neurones, il ne trouvera pas la relation sous-jacente aux données (3.7 a). Par opposition, un ANN ayant trop de neurones sera sur-ajusté : il va « inventer » des relations lui permettant de retrouver toutes les valeurs (figure 3.7 c).

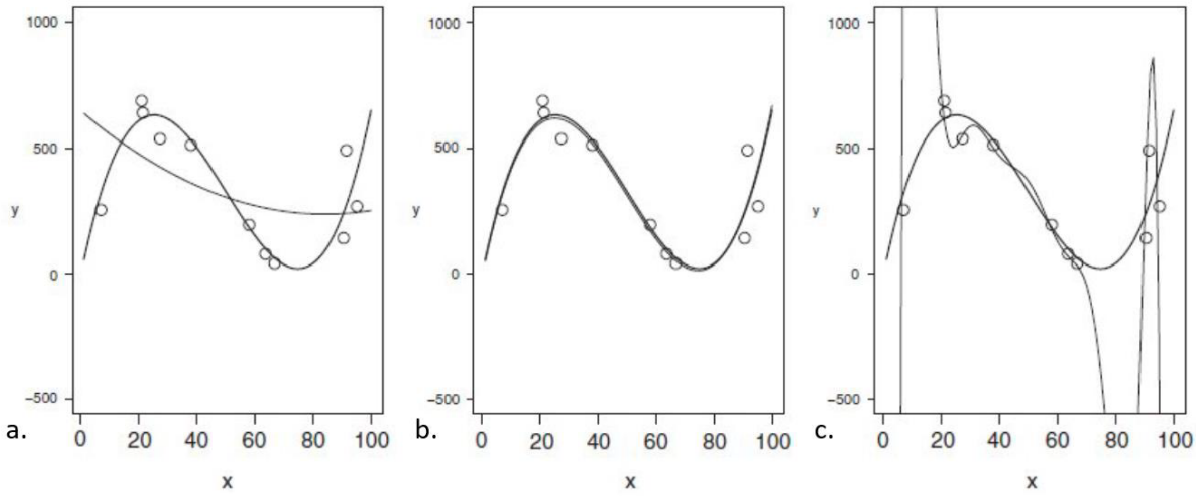

FIGURE 3.7 – Exemples de (A) sous-ajustement, (B) bon ajustement et (C) sur-ajustement avec y la variable à expliquer et x la variable explicative. La vraie relation entre x et y est : $y = 0.01x^3 - 1.5x^2 + 56.5x + 0.01$. Tiré de MARZBAN (2009).

Phase de test Lors de cette phase, les poids (W) obtenus lors de l'apprentissage et de la validation sont figés, et utilisés pour générer des valeurs de sortie prédites. Pour comparer les valeurs prédites à partir du MLP (Y) aux valeurs observées (X), un modèle linéaire est choisi : $Y = aX + b$, le coefficient de détermination (R^2) ainsi que la pente du modèle linéaire sont extraits. Le R^2 informe sur la corrélation entre les valeurs prédites et observées et la pente du modèle linéaire renseigne sur le biais entre ces valeurs. De plus, l'erreur-type (RMSE : Root Mean Squared Error) et l'erreur absolue moyenne (MAE : Mean Absolute Error) sont utilisées pour évaluer respectivement l'erreur et la précision de chaque MLP :

$$MAE = \frac{1}{N}\sum_{i=1}^{N}|Y_i - X_i| \tag{3.6}$$

$$RMSE = \sqrt{\frac{1}{N}\sum_{i=1}^{N}(Y_i - X_i)^2} \tag{3.7}$$

Limitations Une limitation importante des ANNs est leur incapacité à extrapoler sur des valeurs d'entrée n'étant pas comprises ou peu représentées dans la base de données d'entraînement. Les erreurs sont donc d'autant plus élevées que les valeurs d'entrée s'éloignent de celles présentes dans la base d'entraînement. De plus, les ANNs ne peuvent prédire des résultats meilleurs que les données avec lesquelles ils ont été entraînés, ce qui inclut leur bruit inhérent (VEGA et al. 2009). Ainsi, des valeurs observées lors d'évènements exceptionnels et donc anormales pour

l'ANN seront difficiles à reproduire.

3.2.3 Ensembles de réseaux de neurones

Sharkey (1999) a montré que la robustesse et la fiabilité des ANNs peuvent souvent être significativement améliorées en combinant plusieurs ANNs en un ensemble d'ANNs. La construction d'un tel ensemble se fait en deux étapes : la construction des réseaux individuels, et la combinaison des ANNs les plus performants pour produire une sortie unique (Linares-Rodriguez et al. 2013). Ainsi, pour chaque variable, plusieurs réseaux de neurones à 2 couches cachées (avec n_j et n_i neurones) ont été créés et entraînés. L'initialisation des poids et la division des sets d'entraînement et de test ont été faites de manière aléatoire. Chaque topologie a été développée et entraînée 10 fois (10 initialisations des poids par topologie). Pour chaque variable de sortie des réseaux de neurones, 10 réseaux ont été sélectionnés pour créer un ensemble de 10 MLPs produisant une sortie unique. Pour ce faire, pour chaque variable, les 50 meilleures topologies et itérations, ont tout d'abord été sélectionnées sur leurs critères statistiques (R_2, pente, MAE, RMSE), ainsi que sur leurs capacités de généralisation (statistiques issues de la validation indépendante). Puis sur ses 50 topologies, les 10 meilleures ont été sélectionnées en portant une attention particulière à leur capacité à gérer des valeurs proches de 0 (proches de la limite de détection pour les nutriments), à reproduire les différences caractéristiques entre les deux bassins méditerranéens (gradient longitudinal d'oligotrophie, différence de valeurs profondes). Ainsi, la sortie finale de l'ensemble de réseaux de neurones pour chaque variable correspond à la moyenne des sorties de ces 10 meilleurs réseaux (seulement ceux dont la valeur prédite est inférieure à un écart type par rapport à la moyenne)

La Toolbox « Neural Network » de Matlab, et précisément l'algorithme « trainbr » ont été choisis pour l'implémentation des ANNs.

Chapitre 4

Approche nouvelle pour prédire les nutriments et le système des carbonates en Méditerranée, régionalisation CANYON-MED

Sommaire du présent chapitre

4.1 Contexte

Ces dernières décennies, plusieurs modifications rapides ont été observées au niveau des processus physiques et biogéochimiques en Méditerranée (Tanhua et al. 2013 ; Malanotte-Rizzoli et al. 2014 ; Schroeder et al. 2016), bien que partiellement masquées par des évènements épisodiques et une forte variabilité régionale. Du point de vue biogéochimique, la Méditerranée est particulière pour ses concentrations élevées en O_2 (Schneider et al. 2014 ; Coppola et al. 2017), son minimum d'O_2 dans les eaux intermédiaires (LIW) (cf. partie 1.5 Oxygénation en Méditerranée). Le manque de données ne permet pas de contraindre correctement la saisonnalité des nutriments, notamment face aux sources externes dépendantes des activités humaines. Concernant le cycle du carbone, la Méditerranée possède des A_T, C_T et C_{ANT} particulièrement élevées dans les eaux profondes, comparé à l'océan global (Schneider

et al. 2010 ; Álvarez et al. 2014) (cf. partie 1.5 Système des carbonates en mer Méditerranée). Cependant, la variabilité du carbone inorganique reste méconnue, compte tenu de la faible densité d'observations sur le système des carbonates à l'heure actuelle. Ainsi la dynamique de ces éléments biogéochimiques clefs, fortement impactés par les processus océaniques physiques qui prédominent en Méditerranée, est mal connue compte tenu du manque de données biogéochimiques *in situ* et de qualité.

Face à ce manque crucial d'observations *in situ* en Méditerranée, des programmes et des systèmes d'observation intégrés se sont mis en place, principalement dans le bassin ouest depuis 2010 (MISTRALS, SOCIB, RADMED, RITMARE, MOOSE, MED-SHIP, NAOS), contribuant ainsi à augmenter la densité des mesures physiques et biogéochimiques. Dans ce contexte, le développement et la mise en oeuvre de plateformes autonomes instrumentées (planeurs sous-marins, flotteurs profileurs, mouillages) laissent espérer, à moyen terme, de densifier les mesures de certaines variables biogéochimiques. Néanmoins, les mesures réalisées par ces plateformes autonomes ne sont pas exhaustives (il n'existe pas de capteurs pour toutes les variables). Parallèlement à cette intensification des acquisitions de données en Méditerranée, techniques dérivées du « machine learning » permettent d'estimer, avec une précision connue, un certain nombre de variables biogéochimiques. Ainsi les fonctions de transfert développées à partir du réseau de neurones CANYON (pour « Carbonate system and Nutrients concentration from hYdrological properties and Oxygen using a Neural network ») permettent, à partir de mesures facilement réalisables par des plateformes autonomes (température, salinité, oxygène dissous) de prédire avec une précision connue des variables importantes mais qui ne sont pas mesurables de manière autonome (ex. silicates, phosphates, pCO_2, pH) (Sauzède et al. 2017). La méthode CANYON a été développée pour l'océan global (grâce à la base de données GLODAPv2, Olsen et al. 2016) et n'est pas adaptée au spécificités de la mer Méditerranée (salinité élevée, fort gradient d'oligotrophie, circulation rapide, forte séquestration du CO_2, etc.).

Ce chapitre vise à présenter la méthode neuronale CANYON-MED, régionalisation de la méthode CANYON développée spécifiquement à la mer Méditerranée. Ainsi CANYON-MED est modifiée pour prendre en compte les spécificités de la Méditerranée et s'appuie sur une densité de données biogéochimiques *in situ* de qualité qui couvrent un domaine spatio-temporel plus étendu que les « plus rares » données GLODAPv2 en Méditerranée (figure 4.1). Une base de données de mesures *in situ* a été spécifiquement assemblée pour constituer un nouveau jeu de données de qualité utilisé pour l'entraînement des réseaux de neurones. Plus précisément, des ensembles de réseaux de neurones ont été entraînés et leurs résultats sont comparés à ceux des architectures de réseau de neurone unique. Les réseaux optimisés CANYON-MED sont validés avec un jeu de données indépendant et comparés aux méthodes existantes pour prédire les nutriments et le système des carbonates en Méditerranée.

Suite à la publication, un corrigendum a été publié afin de rectifier des erreurs de méthodologie

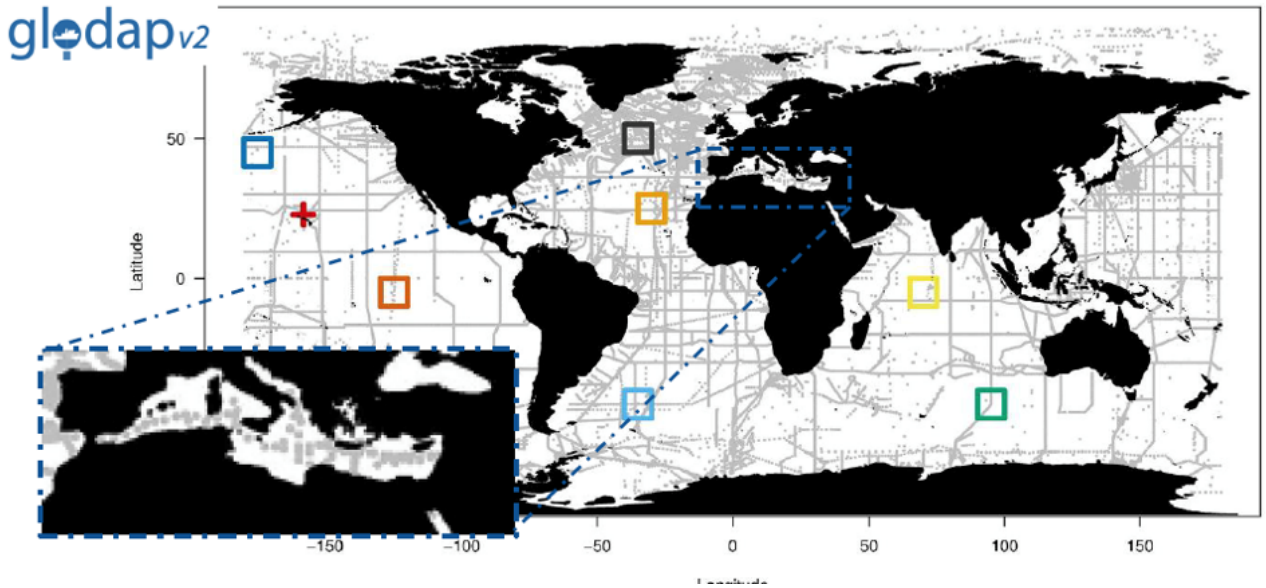

FIGURE 4.1 – Carte des données de la base GLODAPv2 et zoom sur les quelques valeurs en Méditerranée.

dans la version publiée. Celui-ci a légèrement modifié les statistiques de la méthode CANYON-MED qui sont celles présentées au long de ce manuscrit.

4.2 Résumé de l'étude

Une régionalisation à l'échelle de la mer Méditerranée d'une méthode de réseaux de neurones est développée. Cette méthode est appelée CANYON-MED pour "CArbonate system and Nutrients concentration from hYdrological properties and Oxygen using a Neural network in the MEDiterranean Sea". Elle permet l'estimation de nutriments et de variables du système des carbonates en Méditerranée à partir de variables systématiquement mesurées que sont pression, température, salinité et O_2, ainsi que la position dans le temps et dans l'espace. Six ensemble de réseaux de neurones sont développés, un par variable prédite : trois pour les macronutriments (nitrates (NO_3^-), phosphates (PO_4^{3-}), et silicates ($Si(OH)_4$) et trois variables du système des carbonates (pH sur l'échelle totale (pH_T), alcalinité totale (A_T), et Carbone Inorganique Dissous ou Carbone Total (C_T). A l'aide d'une base de données « bouteilles » de référence qualifiées en mer Méditerranée, représentative des spécificités de cette mer semi-fermée, les réseaux de neurones sont entraînés. Plus précisément, pour chaque variable, les réseaux de neurones ont été entraînés sur 80% des données choisies aléatoirement et validés sur les 20% restants. CANYON-MED prédit les variables avec une bonne précision (RMSE) : 0.73 μmol kg^{-1} pour NO_3^-, 0.045 μmol kg^{-1} pour PO_4^{3-} et 0.70 μmol kg^{-1} pour $Si(OH)_4$, 0.016 unités pour le pH_T, 11 μmol kg^{-1} pour A_T et 10 μmol kg^{-1} pour C_T.

Une seconde validation effectuée sur le jeu de données indépendant de la série temporelle

ANTARES confirme l'application de la méthode en mer Méditerranée. Après comparaison avec d'autres méthodes de prédiction des nutriments et des variables du système des carbonates en Méditerranée, CANYON-MED ressort comme la méthode la plus robuste, basée sur les paramètres d'entrée mentionnés précédemment. L'application de CANYON-MED sur des données de systèmes d'observation en Méditerranée, allant du réseau intégré de flotteurs-profileurs BGC-Argo, des mouillages eulériens ou encore de planeurs sous-marins qui mesurent des propriétés hydrologiques ainsi que l'O_2, pourrait avoir un large spectre d'applications. Ainsi en plus de la prédiction de nutriments et de variables du système des carbonates, CANYON-MED peut être utilisé pour du contrôle qualité de données, pour combler les trous dans les séries temporelles, ou encore pour de l'assimilation de données biogéochimiques et/ou l'initialisation et la validation de modèles biogéochimiques régionaux qui manquent encore cruellement de données.

Les codes en R et en Matlab sont disponibles dans un répertoire en ligne :
Github CANYON-MED

4.3 Papier publié dans *Frontiers in Marine Science*

frontiers in Marine Science

ORIGINAL RESEARCH
published: 06 August 2020
doi: 10.3389/fmars.2020.00620

A Regional Neural Network Approach to Estimate Water-Column Nutrient Concentrations and Carbonate System Variables in the Mediterranean Sea: CANYON-MED

Marine Fourrier[1], Laurent Coppola[1,2], Hervé Claustre[1], Fabrizio D'Ortenzio[1], Raphaëlle Sauzède[2] and Jean-Pierre Gattuso[1,3]*

[1] Sorbonne Université, CNRS, Laboratoire d'Océanographie de Villefranche, Villefranche-sur-Mer, France, [2] Sorbonne Université, CNRS, Institut de la Mer de Villefranche, Villefranche-sur-Mer, France, [3] Institute for Sustainable Development and International Relations, Sciences Po, Paris, France

OPEN ACCESS

Edited by:
Ananda Pascual, Mediterranean Institute for Advanced Studies (IMEDEA), Spain

Reviewed by:
Ming Fang, Changchun University of Science and Technology, China
Manuel Lopez Radcenco, UMR 8617 Institut d'Astrophysique Spatiale (IAS), France

***Correspondence:**
Marine Fourrier
marine.fourrier@obs-vlfr.fr

Specialty section:
This article was submitted to Ocean Observation, a section of the journal Frontiers in Marine Science

Received: *10 March 2020*
Accepted: *07 July 2020*
Published: *06 August 2020*

Citation:
Fourrier M, Coppola L, Claustre H, D'Ortenzio F, Sauzède R and Gattuso J-P (2020) A Regional Neural Network Approach to Estimate Water-Column Nutrient Concentrations and Carbonate System Variables in the Mediterranean Sea: CANYON-MED. Front. Mar. Sci. 7:620. doi: 10.3389/fmars.2020.00620

A regional neural network-based method, "CANYON-MED" is developed to estimate nutrients and carbonate system variables specifically in the Mediterranean Sea over the water column from pressure, temperature, salinity, and oxygen together with geolocation and date of sampling. Six neural network ensembles were developed, one for each variable (i.e., three macronutrients: nitrates (NO_3^-), phosphates (PO_4^{3-}) and silicates ($SiOH_4$), and three carbonate system variables: pH on the total scale (pH_T), total alkalinity (A_T), and dissolved inorganic carbon or total carbon (C_T), trained using a specific quality-controlled dataset of reference "bottle" data in the Mediterranean Sea. This dataset is representative of the peculiar conditions of this semi-enclosed sea, as opposed to the global ocean. For each variable, the neural networks were trained on 80% of the data chosen randomly and validated using the remaining 20%. CANYON-MED retrieved the variables with good accuracies (Root Mean Squared Error): 0.73 $\mu mol.kg^{-1}$ for NO_3^-, 0.045 $\mu mol.kg^{-1}$ for PO_4^{3-} and 0.70 $\mu mol.kg^{-1}$ for $Si(OH)_4$, 0.016 units for pH_T, 11 $\mu mol.kg^{-1}$ for A_T and 10 $\mu mol.kg^{-1}$ for C_T. A second validation on the ANTARES independent time series confirmed the method's applicability in the Mediterranean Sea. After comparison to other existing methods to estimate nutrients and carbonate system variables, CANYON-MED stood out as the most robust, using the aforementioned inputs. The application of CANYON-MED on the Mediterranean Sea data from autonomous observing systems (integrated network of Biogeochemical-Argo floats, Eulerian moorings and ocean gliders measuring hydrological properties together with oxygen concentration) could have a wide range of applications. These include data quality control or filling gaps in time series, as well as biogeochemical data assimilation and/or the initialization and validation of regional biogeochemical models still lacking crucial reference data. Matlab and R code are available at https://github.com/MarineFou/CANYON-MED/.

Keywords: nutrients, carbonate system, Mediterranean Sea, neural network, CANYON

INTRODUCTION

The global ocean currently absorbs around 25% of anthropogenic carbon dioxide (CO_2) from the atmosphere, therefore playing a crucial role in buffering the effects of climate change (Le Quéré et al., 2018). This role is likely to be modified by ocean warming and acidification, having complex impacts on marine ecosystems and organisms (Gattuso and Hansson, 2011). To better understand the underlying processes and anticipate changes, a large number of variables have to be observed in order to gain a more accurate overall picture. In this context, the "Framework for Ocean Observing" (FOO, Lindstrom et al., 2012) was designed to coordinate the ocean observing community's efforts and maintain a sustained Global Ocean Observing System (GOOS) (Tanhua et al., 2019). This framework is organized around Essential Ocean Variables (EOVs; GOOS, 2018), chosen to balance the feasibility of their measurement with their societal and scientific relevances. The sustained measurement of key EOVs helps fill the gaps in our understanding of the ocean.

Historically, measurements have come from oceanographic cruises and from continuous measurements at fixed stations (buoys and moorings) (Chai et al., 2020). However, the low spatial and temporal resolutions of these sampling platforms have resulted in chronic under-sampling of biogeochemical variables, creating "observational gaps" (Tanhua et al., 2019; Weller et al., 2019; Chai et al., 2020). Today, technological advances (miniaturization of sensors, automation of measurements) have made it possible to develop a network of autonomous platforms such as profiling floats (Riser et al., 2016; Roemmich et al., 2019; Claustre et al., 2020) and ocean gliders (Testor et al., 2019). These platforms provide measurements of physical and biogeochemical variables at much higher spatial and temporal resolutions in regions or seasons otherwise difficult to access. These active autonomous networks have thus contributed to the progressive densification of databases of key variables at global scale (Abram et al., 2019). Some variables are presently almost systematically measured regardless of the acquisition platform, for instance physical data (temperature, salinity, pressure) and dissolved oxygen concentration (O_2). However, measurements from these autonomous platforms remain limited to a small type of biogeochemical variables, owing to the high cost of some sensors and technological limitations (Bittig et al., 2019; Chai et al., 2020).

Machine learning methods represent a promising way to fill these "observational gaps". They have the potential to predict, from variables systematically measured by autonomous platforms, variables still difficult to measure accurately and cost-effectively with these platforms (e.g., Gregor et al., 2019). Transfer functions such as multiple linear regressions (e.g., Velo et al., 2013; Carter et al., 2018) have therefore been developed to estimate biogeochemical variables. Neural network methods, known to be universal substitutes for any differentiable and continuous function (Hornik et al., 1989), have been also applied to complex data sets in oceanography (e.g., estimation of the variability of the global ocean carbon sink (Landschützer et al., 2014), detection of phytoplankton groups in open ocean waters (Ben Mustapha et al., 2014).

O_2 is a key EOV in oceanography (GOOS, 2018). It is widely and increasingly measured on autonomous platforms, with measurement accuracies close to those obtained by Winkler titration of discrete samples (Bittig and Körtzinger, 2015). The O_2 concentration results from the balance between exchanges at the ocean-atmosphere interface, mixing and ventilation (Körtzinger et al., 2004; Piron et al., 2016, 2017; Coppola et al., 2018), solubility (dependent on temperature and salinity), and biological processes such as primary production and respiration (Robinson, 2019). Furthermore, O_2 is linked to nutrients and inorganic carbon via Redfield's stoichiometric ratios (Redfield, 1934). Therefore, based on the role of O_2 in remineralization and carbon fixation, Sauzède et al. (2017) have developed neural network-based methods to retrieve carbon and nutrient variables in the global ocean. They use O_2, temperature, salinity, pressure, longitude and latitude, day of the year and year as input variables to predict the concentrations of three macronutrients [nitrates (NO_3^-), phosphates (PO_4^{3-}), silicates ($SiOH_4$)] as well as carbonate system variables [total alkalinity (A_T), total dissolved inorganic carbon (C_T), pH on the total scale (pH_T), and CO_2 partial pressure (pCO_2)]. This method referred to as CANYON for "CArbonate system and Nutrients concentration from hYdrological properties and Oxygen using a Neural network" predicts these key oceanographic variables, which cannot be measured independently or with sufficient accuracy, with much improved temporal and spatial resolution (Chai et al., 2020). This method as well as its subsequent improvement, CANYON-B (Bittig et al., 2018), were trained on high-quality data collected over the past thirty years (the GLODAPv2 for Global Ocean Data Analysis Project version 2 database; Olsen et al., 2016). One of its potential applications is to generate virtual carbon and nutrients estimates from the large amount of data acquired by the Biogeochemical-Argo float array (BGC-Argo; Johnson and Claustre, 2016; Claustre et al., 2020).

The Mediterranean Sea is a semi-enclosed marginal sea characterized by high salinities and a rapid overturning circulation, rendering it capable of absorbing more CO_2 than adjacent oceanic regions (Schneider et al., 2010; Lee et al., 2011; Touratier and Goyet, 2011; Álvarez et al., 2014). Machine learning methods produce better results when trained on datasets representative of the considered case study. Therefore, both CANYON and CANYON-B approaches may underperform in this specific oceanic region making a regionalization of this approach highly desirable. Furthermore, the Mediterranean Sea is also a low nutrient concentration basin (McGill, 1966; Krom et al., 1991) with an eastward-increasing oligotrophy gradient. Nutrients are particularly important as tracers of biological cycles, biomass production, and natural and anthropogenic inputs (Béthoux, 1989; Béthoux et al., 1992). Through its rapid response to external conditions relative to other oceans (Crispi et al., 2001), the Mediterranean Sea is considered as a good indicator of global shorter-scale ocean processes and is therefore defined as a "hot spot" for climate change (Giorgi, 2006; Diffenbaugh et al., 2007). This "miniature ocean" (Millot and Taupier-Letage, 2005) is particularly relevant for the study of biogeochemical cycles because of its molar ratios of nutrients very distinct from those of other oceanic regions

(Ribera d'Alcalà et al., 2003; Krom et al., 2005; Pujo-Pay et al., 2011; Pasqueron de Fommervault et al., 2015). Additionally, the high amount of data from BGC-Argo floats and observing programs (e.g., MOOSE, NAOS) emphasize the need for a regionalized approach, specific to the Mediterranean Sea, to fully take advantage of these observing systems and platforms (Tintoré et al., 2019).

In this paper, we present the regional downscaling of the CANYON method for the Mediterranean Sea, CANYON-MED. A database of *in situ* measurements has been specifically assembled to constitute a new quality-controlled dataset used to train the regional neural networks. Neural network ensembles were trained and their results are compared to single neural network architectures. The resulting optimized CANYON-MED networks are validated with an independent dataset and compared to existing methods available for nutrients and carbonate system variables prediction in the Mediterranean Sea.

MATERIALS AND METHODS

Available Datasets

Training and Validation Datasets

The CARIMED (CARbon in the MEDiterranean Sea) data synthesis initiative (Sanleón-Bartolomé et al., 2017) aims to produce a consistent quality-controlled database for carbon relevant variables from hydrographic cruises covering the whole water column and the different basins of the Mediterranean Sea. As the validation of CARIMED data is still in progress, we performed secondary quality control through visual inspection of the profiles and by comparison with literature values, to remove outliers. After applying similar quality control, the data from ten other cruises were added to the database (i.e., CARBOGIB, CASCADE, DEWEX, GIFT, MOOSE_GE 2011, MOOSE_GE 2013, MOOSE_GE 2015, PACIFIC-CELEBES, SOMBA, MSM72; **Table 1**). The spatial coverage of the complete dataset is shown in **Figure 1**.

The DYFAMED site (Coppola et al., 2019a) is located in the Ligurian Sea (43°25′N, 7°52′E, water depth of 2350 m; red star in **Figure 1**). It is surrounded by the permanent geostrophic Ligurian frontal jet flow caused by the Northern Current's cyclonic circulation, separating the sampling area from coastal inputs by a density gradient (Millot, 1999; Niewiadomska et al., 2008). Monthly cruises are performed over the whole water column since 1991 and included in the MOOSE network since 2010 (Marty et al., 2002; Coppola et al., 2019b). This is the longest open sea time series in the Mediterranean Sea in terms of O_2, nutrients and carbonate system measurements that led to a homogeneous and calibrated data set with well-described seasonality of these variables (Copin-Montégut and Bégovic, 2002; Marty et al., 2002; Pasqueron de Fommervault et al., 2015; Coppola et al., 2018).

The dataset gathered for this study (**Table 1**) therefore includes 35 oceanic cruises and a time series, from 1976 to 2018 with samples from the surface to 4600 m depth of core variables such as O_2, temperature, salinity as well as macronutrients [nitrates: NO_3^-, phosphates: PO_4^{3-}, silicates: $Si(OH)_4$] and carbonate system variables (total alkalinity: A_T, total carbon or dissolved inorganic carbon: C_T, and pH on the total scale: pH_T). When A_T and C_T were available, pH_T was calculated using CO2SYS-MATLAB (Lewis et al., 1998; van Heuven et al., 2011). This dataset is openly accessible (Fourrier, 2020). Thermodynamic calculations within the carbonate system used the carbonic acid dissociation constants of Mehrbach et al. (1973) as refit by Dickson and Millero (1987), the dissociation constant for bisulfate of Dickson (1990) and Uppström (1974) for the ratio of total boron to salinity. These constants were used to ensure consistency with pH_T units in some of the data sets compiled.

Independent Validation Dataset

The ANTARES site is located in the Ligurian Sea (42°48′N, 06° 05′E, water depth of 2500 m; yellow square in **Figure 1**). It is visited monthly since 2010 and integrated into the MOOSE network (Lefevre, 2010). This time series extends from 2009 to 2018 for ancillary data, O_2, nutrients, and from 2009 to 2017 for A_T and C_T. pH_T was computed as described in section "Training and Validation Datasets." However, O_2 measurements are lacking prior to 2011, restricting the use of the data in this study to the period 2011–2018.

For the whole dataset and after quality control, the distribution of observations per year and month (**Figure 2**) demonstrates the systematic under-representation of winter months (which are quite exclusively sampled thanks to the DYFAMED time series), as well as the difference in coverage according to year and variable of interest, such as the lower number of C_T and pH_T data.

Neural Network Development

Artificial Neural Networks (ANNs) are approximate functions adapted to any dataset (Marzban, 2009). One of the main advantages of these methods is their ability to recognize and exploit relationships in data that are not predefined (unlike regression techniques) and do not need to be made explicit by equations (Marzban, 2009). This makes them particularly suitable for mapping non-linear relationships, provided that data are sufficiently available to "train" the neural network (Lefevre et al., 2005). Similarly to Sauzède et al. (2017) and Bittig et al. (2018) for CANYON and CANYON-B, respectively, an iterative statistical learning-based method, and more specifically an ANN was developed to predict carbon and nutrient variables.

Separate the learning data into a training dataset for training the machine learning method and a validation dataset used to assess the performance of the trained method is a common practice. It ensures that the model can produce reliable estimates outside the range of learning data (generalization capabilities) (Bishop, 1995). In the present paper, the dataset was randomly split according to the proportions of 80% and 20% for training and validation sets, respectively. Additionally, an external dataset was also used to further validate the ANNs.

Multi-Layered Perceptron

Among the different types of ANNs available, Multi-Layered Perceptron (MLP; Rumelhart et al., 1986; Bishop, 1995) using a backpropagation algorithm (Bishop, 1995; Hagan et al., 2014) has been chosen for its properties as universal approximator

TABLE 1 | List of cruises, principal investigators, references (when available), and the number of data for each variable of interest [NO_3^-, PO_4^{3-}, $Si(OH)_4$, A_T, C_T, pH_T] in our database.

Cruise	Number of measurements						Leader	References
	NO_3^-	PO_4^{3-}	$Si(OH)_4$	A_T	C_T	pH_T		
ALMOFRONT	807	843	909	425	0	427	L. Prieur	Prieur (1991)
BOUM	0	957	620	576	567	561	T. Moutin	Moutin (2008)
CARBOGIB	25	25	25	25	20	25	E. Huertas	Huertas (2007a,b,c,d,e)
CASCADE	219	220	220	210	210	210	X. Durieu de Madron	Durrieu De MadronXavier, 2011
DEWEX	1074	1076	1076	291	297	297	P. Testor, P. Conan	Testor (2013), Conan (2013)
DYFAMED	1370	1361	1474	1112	1124	1026	L. Coppola	Coppola et al. (2019a)
GEOSECS_LEG_3	31	31	31	22	22	22	AE. Brainbridge	Environmental Sciences Division (1988)
GIFT	15	15	14	15	12	15	E. Huertas	Huertas (2007f,g)
HOTMIX	0	315	320	311	104	316	J. Arístegui	–
MCXXIS	73	191	199	211	0	0	–	http://isramar.ocean.org.il/perseus_data/CruiseInfo.aspx?criuseid=1385 http://isramar.ocean.org.il/perseus_data/CruiseInfo.aspx?criuseid=1435 http://isramar.ocean.org.il/perseus_data/CruiseInfo.aspx?criuseid=1436
MEDIPROD IV	0	157	161	90	90	90	H.J. Minas and B. Coste	Minas (1981)
MEDSEA_2013	328	332	332	328	328	324	P. Ziveri	Ziveri and Grelaud (2015), Goyet et al. (2015)
METEOR_51_2	0	655	662	231	232	228	W. Roether	Schneider et al. (2013)
METEOR_84_3	540	569	573	544	557	573	T. Tanhua	Tanhua et al. (2013)
MILLERO	0	0	0	0	0	0	F.J. Millero	–
MOOSE_GE_2010	0	329	325	79	79	79	P. Testor	Testor et al. (2010)
MOOSE_GE_2011	343	358	362	94	94	90	P. Testor	Testor et al. (2011)
MOOSE_GE_2012	763	773	780	142	168	139	P. Testor	Testor et al. (2012)
MOOSE_GE_2013	621	583	626	124	124	110	P. Testor	Testor et al. (2013)
MOOSE_GE_2014	771	675	912	147	143	140	P. Testor	Testor et al. (2014)
MOOSE_GE_2015	661	606	742	147	147	147	P. Testor	Testor et al. (2015)
MOOSE_GE_2016	1004	948	1012	162	153	153	L. Coppola	Coppola (2016)
MSM72	797	749	819	713	343	855	D. Hainbucher	–
OTRANTO	0	86	87	0	0	0	E. Krasakopoulou	Krasakopoulou and Souvermezoglou (2013)
PACIFIC_CELEBES	0	0	0	22	22	22	D. Hydes	Hydes et al. (2011)
POEMXXIS	0	0	107	221	0	0	–	http://isramar.ocean.org.il/perseus_data/CruiseInfo.aspx?criuseid=1653 http://isramar.ocean.org.il/perseus_data/CruiseInfo.aspx?criuseid=1585
PROSOPE	252	231	197	185	0	209	H. Claustre	Claustre (1999)
SESAME_IT01	0	204	214	214	0	214	G. Catalano	–
SEASAME_IT02	0	149	151	160	0	160	M. Azzaro	–
SESAME_IT04	0	139	169	152	158	152	C. Santinelli	http://isramar.ocean.org.il/perseus_data/CruiseInfo.aspx?criuseid=5188 http://isramar.ocean.org.il/perseus_data/CruiseInfo.aspx?criuseid=5148
SESAME_IT07	205	204	206	164	0	167	G. Catalano	http://isramar.ocean.org.il/PERSEUS_Data/CruiseInfo.aspx?criuseid=5503
SESAME_SPI	205	205	205	205	0	204	G. Navarro	http://isramar.ocean.org.il/PERSEUS_Data/CruiseInfo.aspx?criuseid=5451
SESAME_SPII	273	274	273	274	0	271	G. Navarro	http://isramar.ocean.org.il/PERSEUS_Data/CruiseInfo.aspx?criuseid=5450
SOMBA	0	0	0	184	184	172	L. Mortier	Mortier et al. (2014)
TRANSMED_LEGII	78	78	78	44	0	45	M. Azzaro	–
TRANSMED_LEG_III	97	91	99	92	0	94	S. Fonda	–

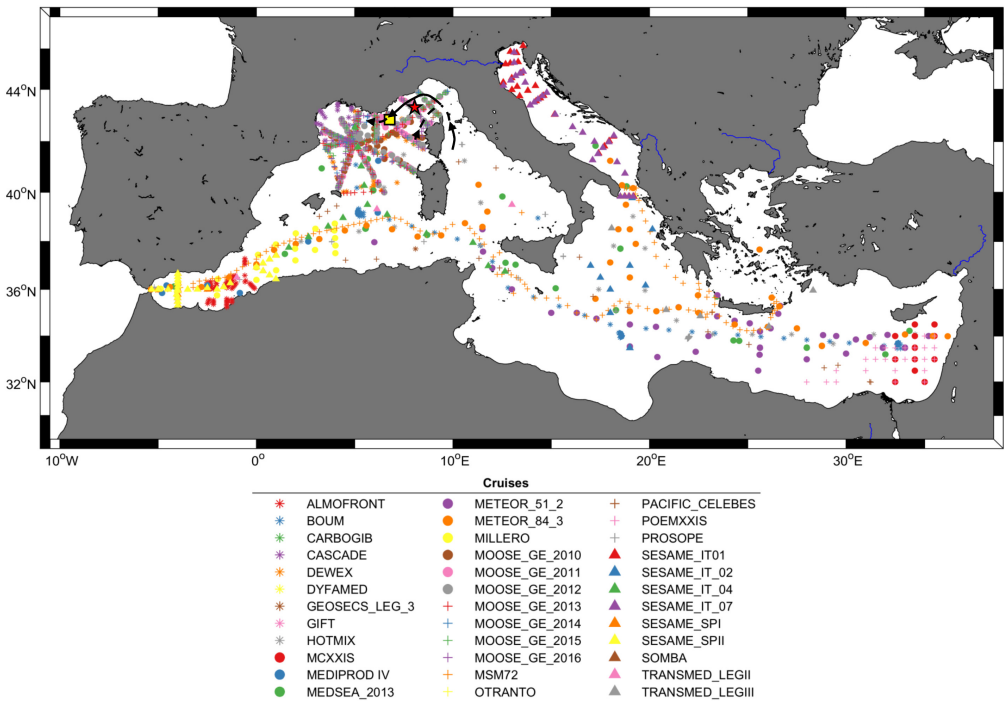

FIGURE 1 | Location of the 35 cruises used in this study, and of the DYFAMED (red star) and ANTARES (yellow square) sites in the Ligurian Sea, Northwestern Mediterranean, with a schematic representation of the North Current circulation in surface (black arrows). The DYFAMED time series and the 35 cruises constitute the training dataset whereas the ANTARES time series is used for validation.

of any continuous and derivable function (Hornik et al., 1989). A MLP is an ANN organized in several layers (i.e., input, hidden and output layers) containing neurons that are connected to each other and able to exchange information through their connections (**Figure 3**). These connections are directional, and each connection is associated with a real number, called the "weight". The information is transmitted from one neuron to another through the weights that are readjusted iteratively during the training phase to minimize the difference between MLP outputs and observations.

MLPs use an activation function between the neurons (here the sigmoid function f (**Figure 3**), with A and α equal to 4/3 and 1.7159, respectively) to ensure a quasi-linear behavior between −1 and 1 (Jamet, 2004; Sauzède et al., 2017):

$$f(x) = A * \frac{exp^{\alpha x} - 1}{exp^{\alpha x} + 1} \quad (1)$$

The backpropagation algorithm used for the MLP (Bishop, 1995) can be divided into two steps. First, the forward propagation of a stimulus (from the inputs) through the MLP generates an output. Second, the errors are propagated backward from the output through the MLP to change the weights in the opposite direction to the error gradient.

The input data were normalized to have an average of zero and a standard deviation of one using the mean and standard deviation of the training data to improve convergence (Goodfellow et al., 2016) and to prevent neural networks saturation (caused by the difference in the range of the different input variables) according to:

$$x = \frac{2}{3} * \frac{x - \bar{x}}{\sigma} \quad (2)$$

Where x, $\bar{x}$, and σ are, respectively, the input data, their mean and their standard deviation. The factor 2/3 brings at least 80% of the data in the range [−1;1] (Jamet et al., 2012).

In order to improve the generalization capabilities of the ANNs, Bayesian regularization (Bishop, 1995) was used. This method minimizes over-fitting by considering the goodness of fit as well as the network architecture. The training algorithm used was a supervised iterative training method updating weights according to Levenberg-Marquardt optimization (Linares-Rodriguez et al., 2013). This algorithm was chosen because it is better suited for function fitting and does not require

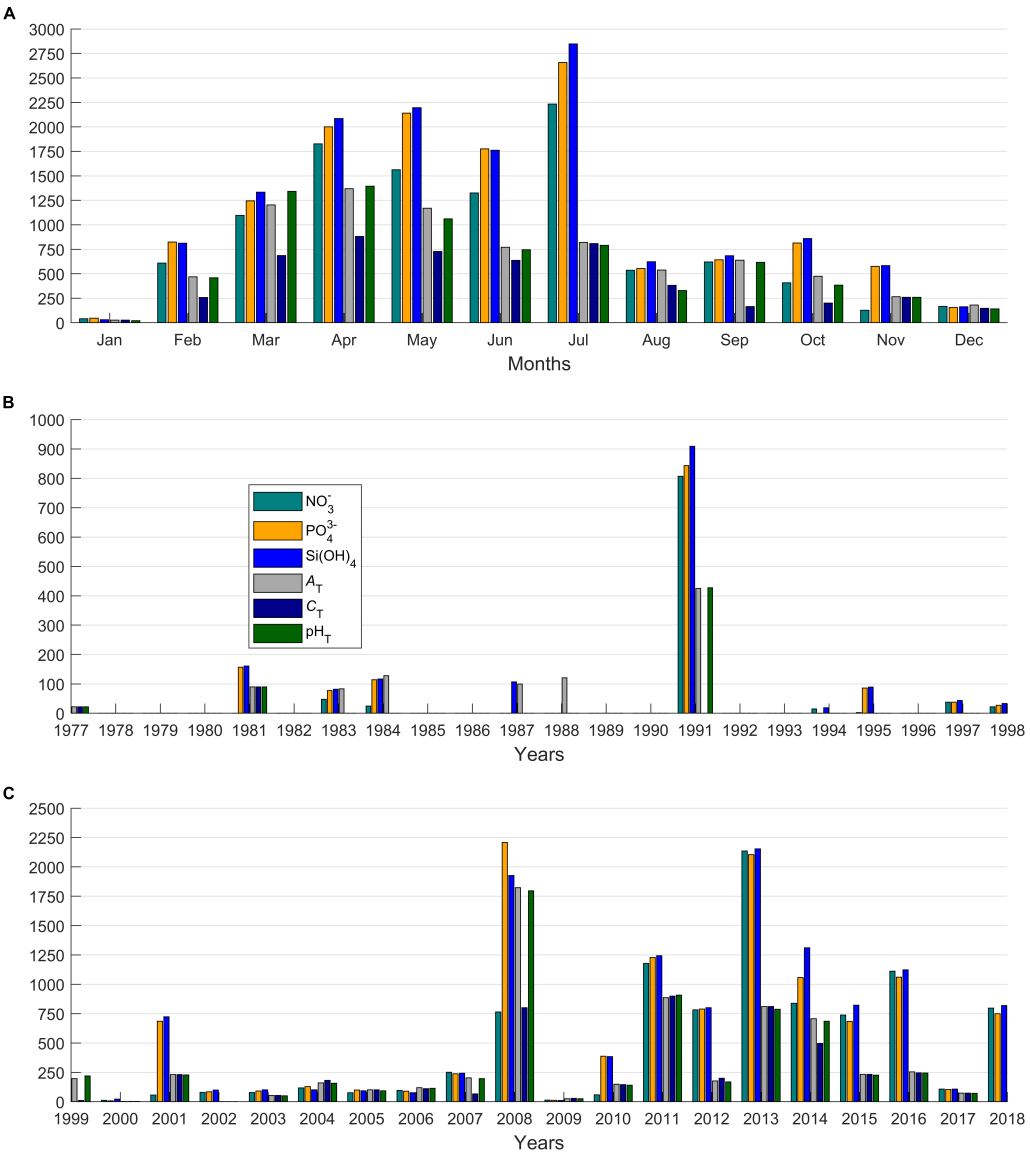

FIGURE 2 | Distribution of sample numbers **(A)** per month and **(B,C)** per year provided by the scientific cruises, after quality control. Note the difference in the y-axis for the early distributions.

excessive computing time and power, while still appropriately generalizing (Beale et al., 2018). To avoid falling to a local minimum, a linear combination of weights and quadratic errors was minimized through gradient descent, and multiple initializations with random weights were performed. Then, to determine the appropriate combination of weights and errors, Bayesian regularization was used. This allowed the generalization of the neural network through the optimization of the linear

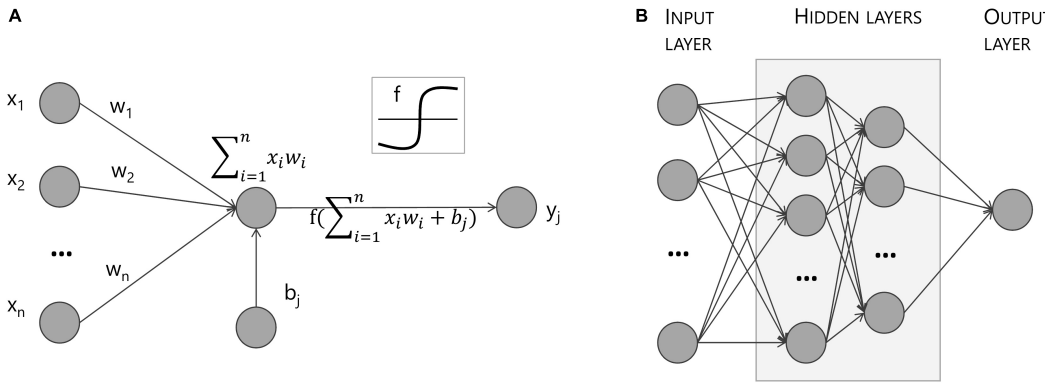

FIGURE 3 | Schematic representation of the signal-flow of a perceptron **(A)** and a Multi-Layered Perceptron **(B)**. The inputs are connected to a neuron and each connection is associated with a weight "w." The output is produced by combining the inputs and weights and adding the neuron's bias "b_j" before going through a sigmoid activation function "f." A Multi-Layered Perceptron is composed of multiple neurons in hidden layers combined in the same manner to produce a single output.

combination of weights and errors (MacKay, 1992a,b; Foresee and Hagan, 1997; Hagan et al., 2014). The Matlab Neural Network Toolbox, and more specifically the algorithm "trainbr," has been chosen for the ANN implementation. The ANN optimal architecture or topology (number of inputs, outputs, number of hidden layers and neurons in each hidden layer) hinges on the complexity of the relations between inputs and outputs. After testing several different configurations through a trial-and-error process, the topologies for neural networks producing the best results were determined with 2 hidden layers and a number varying between 15 and 50 neurons for the first layer and between 8 and 30 for the second hidden layer.

ANN Ensemble Model

The robustness and reliability of an ANN can be significantly improved by combining several ANNs into an ANN ensemble model (Sharkey, 1999; Linares-Rodriguez et al., 2013). The construction of an ANN ensemble is done in two main steps. First, the individual members of the model are created (as described above in section "Multi-Layered Perceptron"). Second, the combination of the outputs of these members is averaged to obtain the unique ensemble output. Thus, for each neural network [NO_3^-, PO_4^{3-}, $Si(OH)_4$, A_T, C_T, pH_T], the ten best topologies were chosen according to their statistics (as defined in section "Validation Statistics Metrics"). The final output of each neural network ensemble model (ANN-E) corresponds to the mean of the outputs of these ten best ANNs. Additionally, the best topology (ANN-1) among the ten best was also selected to compare between a one ANN structure and a neural network ensemble.

CANYON-MED

Based on the CANYON networks (Sauzède et al., 2017) principle, the CANYON-MED neural networks corresponding to neural-network ensemble models (ANN-E) (as described in "ANN Ensemble Model") were developed. Similarly to the work by Sauzède et al. (2017), the chosen input variables for the networks are *in situ* measurements of pressure, temperature, salinity (water mass characteristics), and oxygen together with geolocation (latitude and longitude), date of sampling (day of year or day, representing the seasonality of processes) and year of sampling (representing global trends linked to anthropogenic changes). Compared to the CANYON networks, where the year is an input only for pH_T and C_T, it has been chosen as an input for the six CANYON-MED networks [i.e., NO_3^-, PO_4^{3-}, $Si(OH)_4$, A_T, C_T, and pH_T]. This change, namely the addition of the year for each network, was based on the long-term increases in deep nutrients observed in the western basin by Béthoux et al. (1998, 2002), as well as the increases in temperature and salinity in the deep Mediterranean Sea over the past 40 years (Borghini et al., 2014) which demonstrate the need of a temporal component in CANYON-MED networks.

According to the work by Sauzède et al. (2017), the pressure input was transformed according to the combination of a linear and a logistic curve to limit the degrees of freedom of the ANN in deep waters and to account for the large range of pressure values (from the surface to 4000 m depth) and a non-homogeneous distribution of data within this range:

$$P = \frac{P}{20000dbar} + \frac{1}{\left(1 + exp\ \left(-\frac{P}{300dbar}\right)\right)^3} \quad (3)$$

Furthermore, in agreement with the CANYON networks, the day has been modified to account for the periodicity of this measurement [day 365 (end of December) of a year is similar to day 1 (beginning of January) of the next year from a

chronological perspective]. It was therefore transformed into radians according to:

$$doy_{rad} = \frac{doy * \pi}{\frac{365}{2}} \quad (4)$$

Furthermore, similarly to the aforementioned method, and due to the nature of the transfer function (a sigmoid varying in the range [−1;1]), the inputs and outputs of the neural networks have been centered and reduced to also fall into the range [−1;1] (Sauzède et al., 2016, 2017).

Moreover, also building on the CANYON networks, Bittig et al. (2018) developed CANYON-B, a Bayesian neural network improvement of CANYON. CANYON-B is constructed as a committee of neural networks and provides estimates of nutrients and carbonate system variables with a local uncertainty (whereas CANYON provides global uncertainties). Neural networks committees are composed of several neural networks and use the spread of predictions between individual members of the committee to improve the estimation of uncertainty of the committee output (Bishop, 1995). This other neural network method was also used for comparative purposes.

The Matlab and R code are available at https://github.com/MarineFou/CANYON-MED/.

Validation Statistics Metrics

Results were validated using four statistical metrics chosen to evaluate the performance of the CANYON-MED algorithms on the validation datasets: the MAE (Mean Absolute Error, Equation 5), the RMSE (Root Mean Squared Error, Equation 6), the coefficient of determination (r^2, Equation 7) as well as the slope (Equation 8) of the linear regression between the CANYON-MED-retrieved values and the corresponding *in situ* measured values. The absolute uncertainties are expressed as concentrations for NO_3^-, PO_4^{3-}, $Si(OH)_4$, A_T, and C_T (in $\mu mol.kg^{-1}$) and pH_T (pH unit) parameters.

$$MAE = \frac{1}{N} * \sum_{i=1}^{N} |X_{CANYON-MEDi} - X_{DATAi}| \quad (5)$$

$$RMSE = \sqrt{\frac{1}{N} * \sum_{i=1}^{N} (X_{CANYON-MEDi} - X_{DATAi})^2} \quad (6)$$

$$r^2 = \left(\frac{1}{N} \sum_{i=1}^{N} \frac{\left(X_{DATAi} - \overline{X_{DATAi}}\right)\left(X_{CANYON-MEDi} - \overline{X_{CANYON-MEDi}}\right)}{\sigma_{X_{DATA}} * \sigma_{X_{CANYON-MED}}} \right)^2 \quad (7)$$

$$Slope = \frac{X_{CANYON-MED} - CANYON - MED_{intercept}}{X_{DATA}} \quad (8)$$

RESULTS AND DISCUSSION

Neural Network Ensemble Improvement and Overall CANYON-MED Performance

For each studied variable [i.e., NO_3^-, PO_4^{3-}, $Si(OH)_4$, A_T, C_T, and pH_T], a CANYON-MED ensemble neural network was created as described in section "ANN Ensemble Model." Comparing the statistics for the case using a single neural network (ANN-1) and the ensemble neural network model (ANN-E, corresponding to CANYON-MED), the ANN-E model provides the most accurate nutrient and carbonate system estimates (**Table 2**). For most variables, an increase in the determination coefficient is shown (i.e., from 0.94 to 0.95, 0.90 to 0.92, 0.93 to 0.96, 0.91 to 0.94, 0.84 to 0.86 for NO_3^-, PO_4^{3-}, A_T, C_T, and pH_T, respectively) as well as a decrease in MAE and RMSE (up to 20% and 30% of the errors, respectively). The low MAE values suggest that the ANN-E model is not biased, although the slopes are slightly less than 1, resulting in an underestimation of neural network outputs.

Using the validation dataset, the performance of the CANYON-MED method was evaluated by comparing CANYON-MED's results with the corresponding *in situ* values. **Figure 4** shows these results as a function of pressure while the corresponding statistics are in **Table 2**. The accuracies obtained are very satisfactory with, for example, an accuracy of NO_{3-} extracted from the neural network method (0.73 $\mu mol.kg^{-1}$) comparable to that obtained with optical sensors such as those mounted on BGC-Argo floats (1 $\mu mol.kg^{-1}$; Johnson et al., 2017). Owing to the lower number of data presently available in our training dataset for C_T and pH_T, the ability of the corresponding neural networks to generalize correctly is lowered, explaining the less robust statistics for C_T and pH_T with slopes around 0.9, and determination coefficients of 0.91 and 0.84, respectively (**Table 2**).

In **Figure 4**, two different deep value ranges (i.e., two "patches" of dark blue points) can be distinguished for NO_{3-} and PO_4^{3-} corresponding to the deep values of the Western and Eastern Basins. The Eastern Mediterranean Sea is known to be more oligotrophic than its western counterpart (Ribera d'Alcalà et al., 2003; Pujo-Pay et al., 2011). Indeed, deep NO_3^- and PO_4^{3-} values (**Figures 4A,B**) are lower in the ultraoligotrophic eastern Mediterranean than in the oligotrophic western Mediterranean, as evidenced by the differences in concentrations of the deep values (5 and 10 $\mu mol.kg^{-1}$ for eastern and western NO_3^-, respectively and 0.2 and 0.4 $\mu mol.kg^{-1}$ for PO_4^{3-}, respectively). The deep $Si(OH)_4$ values are quite similar between the two Mediterranean basins as it is not a limiting nutrient (Krom et al., 1991). A larger dispersion is observed for low concentrations of PO_4^{3-} and NO_3^- (**Figures 4A,B**) recovered by CANYON-MED, coinciding with the low concentrations of surface nutrients in the Eastern Basin (Tanhua et al., 2013; Kress et al., 2014).

Furthermore, deep A_T ranges between 2590 and 2610 $\mu mol.kg^{-1}$ (**Figure 4D**) corresponding to the deep waters of the Western and Eastern Mediterranean Sea respectively. The difference between the two basins stems from an eastward increasing trend for A_T mirroring the increase in salinity and an eastward increase in pH_T (Hassoun et al., 2015). However,

TABLE 2 | Number of points in the training and validation datasets and statistics between *in situ* measurements from the validation database and the values predicted by CANYON-MED's "best topology" (ANN-1) and CANYON-MED (ANN-E) for NO_3^-, PO_4^{3-}, $Si(OH)_4$, A_T, C_T and pH_T.

	CANYON-MED									
	N		r^2		Slope		MAE		RMSE	
	Training	Validation	ANN-1	ANN-E	ANN-1	ANN-E	ANN-1	ANN-E	ANN-1	ANN-E
NO_3^- (μmol kg^{-1})	8439	2113	0.94	**0.95**	0.96	**0.96**	0.50	**0.47**	0.79	**0.73**
PO_4^{3-} (μmol kg^{-1})	10785	2644	0.90	**0.92**	0.95	**0.95**	0.030	**0.026**	0.050	**0.045**
$Si(OH)_4$ (μmol kg^{-1})	11071	2909	0.96	**0.96**	0.95	**0.95**	0.45	**0.40**	**0.66**	0.70
A_T (μmol kg^{-1})	6406	1516	0.93	**0.96**	0.97	**0.98**	8.0	**6.5**	12.1	**11.1**
C_T (μmol kg^{-1})	4154	1024	0.91	**0.94**	0.92	**0.92**	8.9	**7.0**	13.6	**10.0**
pH_T	6090	1447	0.84	**0.86**	0.93	**0.93**	0.011	**0.010**	0.017	**0.016**

Bold values highlight the best statistic result.

this difference is not very visible owing to the large range of A_T. For C_T, the difference between the two Mediterranean basins is lower (**Figure 4E**). C_T variability is controlled by salinity, biological processes (such as photosynthesis, oxidation of organic matter, dissolution and precipitation of $CaCO_3$), as well as air-sea CO_2 exchange (Lovato and Vichi, 2015). Additionally, pH_T (**Figure 4F**) exhibits a large range below 1500 m (7.98 to 8.1). This also stems from the difference between the two Mediterranean basins, a pattern similar to that of A_T, with higher surface and deep values in the Eastern Mediterranean Sea (Rivaro et al., 2010).

Validation on Independent Time Series: ANTARES

The ANTARES time series was chosen as an additional independent validation dataset because, among the few time series in the deep offshore Mediterranean, it is one of the few where measurements of nutrients and carbonate system variables are performed semi-regularly and over the entire water column (Lefevre, 2010). The vertical profiles of the differences between *in situ* measurements of the ANTARES dataset and the values predicted by CANYON-MED are represented (**Figure 5**) along with their mean value and associated standard deviation. In general, the accuracies (**Table 3**) of each variable are comparable, albeit slightly worse, to those determined on the CANYON-MED validation dataset (**Table 2**). These accuracies are even lower for A_T and C_T probably due to the smaller ranges covered by the ANTARES site. The errors seem quite homogeneous over the whole water column (**Figure 5**), with higher errors when lacking data at specific depths [e.g., NO_3^- and $Si(OH)_4$ at around 1250 dbar]. In addition, we can also note the clear overestimation of PO_4^{3-} at the ANTARES time series, evident from the slope of 1.06 (**Table 3**) as well as from the observation of a clear shift in **Figure 5B**.

However, it is important to note that the ANTARES dataset, although subject to quality control, still exhibits a high nutrient dispersion along the water column. This variability may result from natural phenomena or potential issues in the measurement accuracy (e.g., measurement uncertainty, sampling procedure, change of operator, evolution of techniques). In the latter case, it can explain the dispersion of errors found for nutrients in **Figure 5**.

Comparison to Other Methods Available

CANYON Methods

The performance of the CANYON, CANYON-B, and CANYON-MED methods were compared using the validation dataset (the remaining 20% of the database not used for training). The performances were computed by comparing the neural network outputs for nutrients and carbonate system parameters with the *in situ* measurements according to the metrics defined in section "Validation Statistics Metrics." Scatterplots of neural network-retrieved variables against their corresponding *in situ* measurements (**Figure 6**) reveal that the CANYON-MED method gives much better results than its global counterparts (i.e., CANYON and CANYON-B). The accuracies (RMSE) have been reduced, for each variable, by more than half between CANYON-B and CANYON-MED and by a third for nutrients and A_T between CANYON and CANYON-MED, as shown by statistics in **Table 4**. The differences are primarily due to the under-representation of Mediterranean Sea cruises in CANYON and CANYON-B's training dataset (Mediterranean data poorly represented in the GLODAPv2), as opposed to the training dataset specifically designed for the Mediterranean Sea in CANYON-MED.

Specifically, for the CANYON and CANYON-B networks, a higher scatter is observed for NO_3^- and PO_4^{3-} near-zero values (**Figures 6A,B**). CANYON-MED's MAE and RMSE are halved compared to CANYON and CANYON-B's (**Table 4**). In addition, a significant number of values are predicted to be negative (around -0.1 μmol.kg^{-1}). This feature is mainly caused by the difference in the nutrient concentrations for the oligotrophic to ultra-oligotrophic Mediterranean Sea which are close to the detection limits of the nutrients analysis method (Krom et al., 1991) compared to the higher concentrations found in the global ocean (high concentrations present in GLODAPv2, CANYON, and CANYON-B training data).

A very high scatter is also present for $Si(OH)_4$ CANYON and CANYON-B-retrieved values, especially for the lower values (i.e., <4 μmol.kg^{-1}) (**Figure 6C**). In the global ocean, $Si(OH)_4$

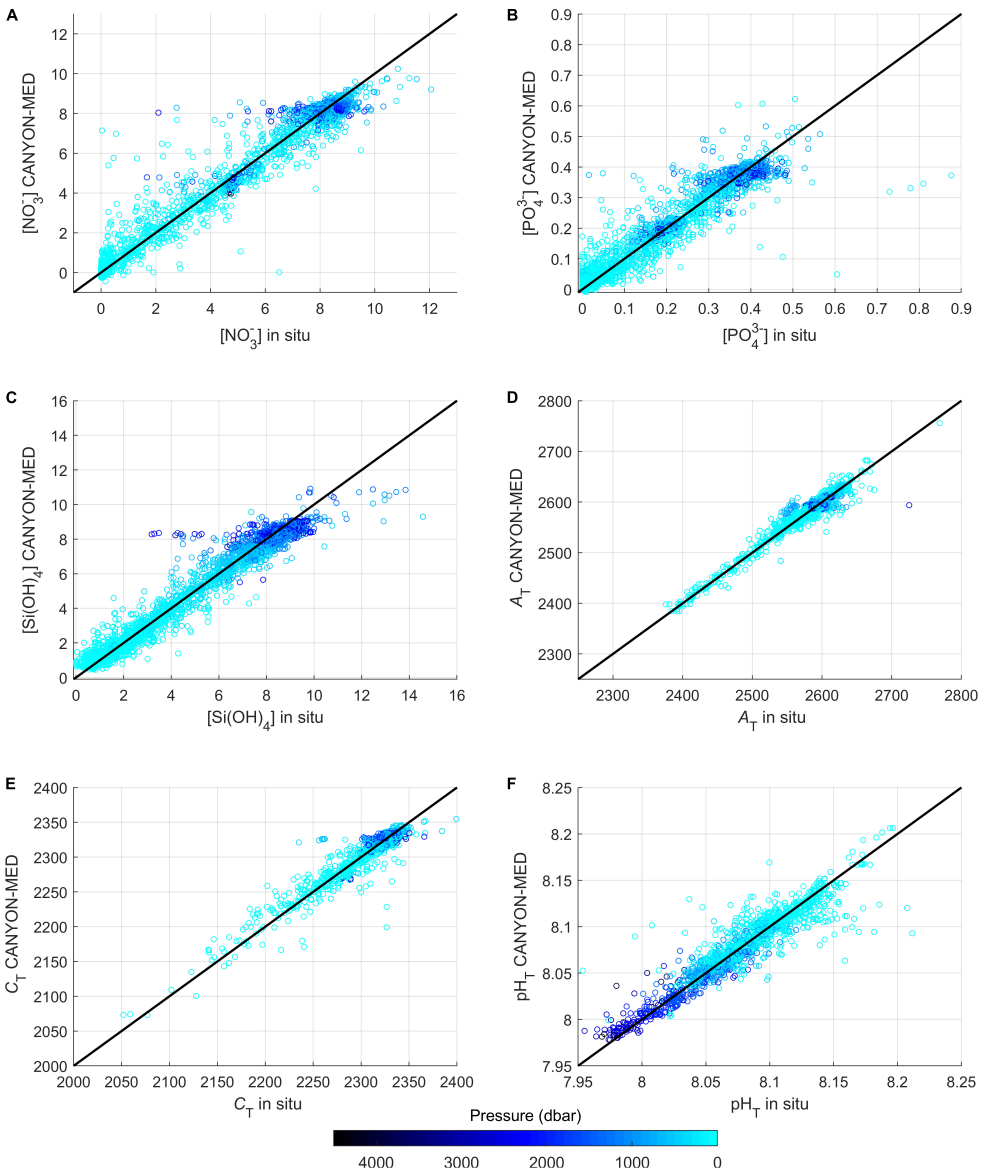

FIGURE 4 | Comparison of the CANYON-MED-retrieved values with the corresponding *in situ* measurements according to pressure for **(A)** NO_3^-, **(B)** PO_4^{3-}, **(C)** $Si(OH)_4$, **(D)** A_T, **(E)** C_T, and **(F)** pH_T. The darker blue points correspond to the deeper points whereas the lighter ones correspond to values closer to the surface. The 1:1 line is shown in black. The corresponding statistics are shown in **Table 2**.

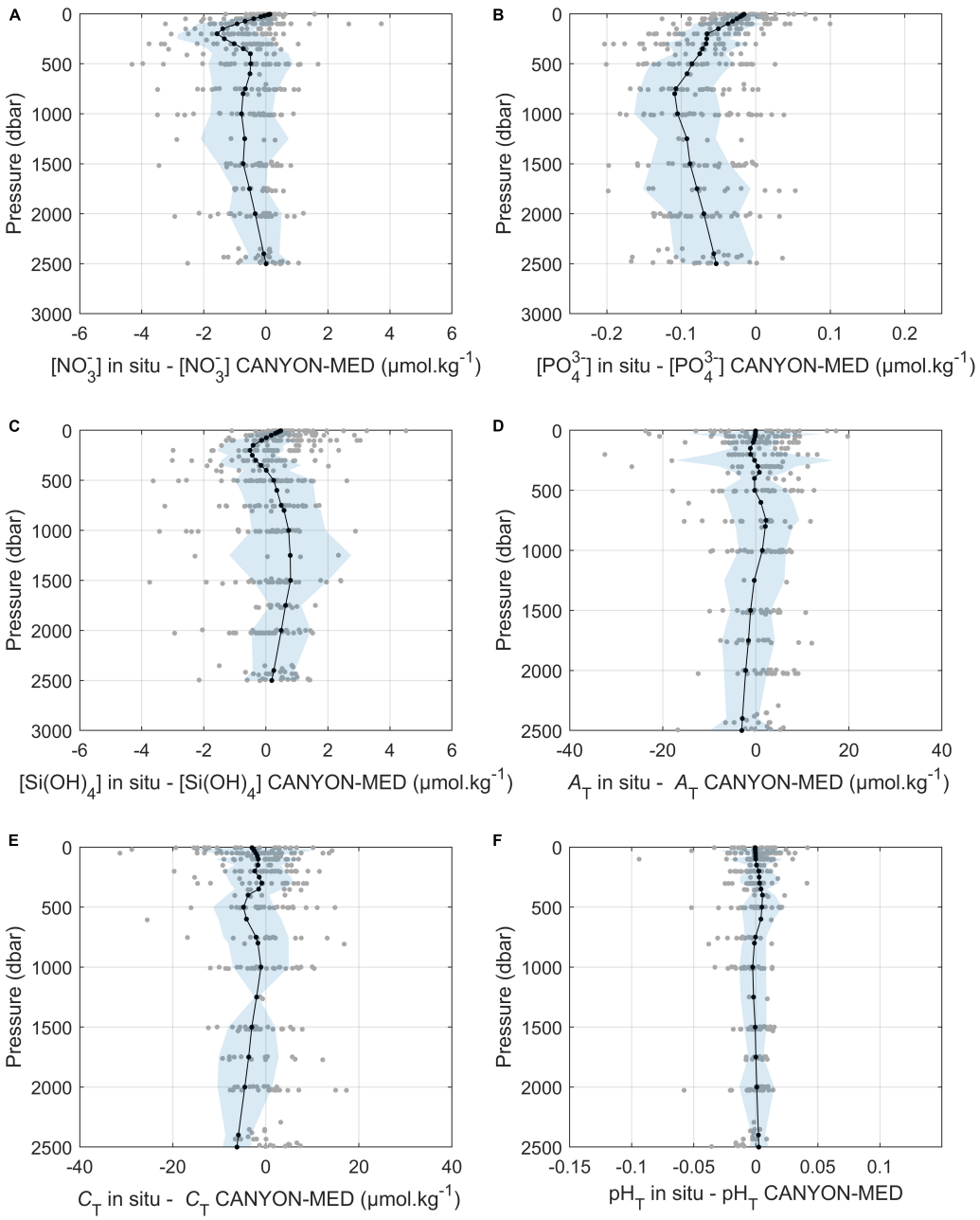

FIGURE 5 | Vertical profiles of the differences between *in situ* measurements from the ANTARES time series and the values predicted by CANYON-MED for **(A)** NO_3^-, **(B)** PO_4^{3-}, **(C)** $Si(OH)_4$, **(D)** A_T, **(E)** C_T, and **(F)** pH_T. The black line represents the mean value and the shaded area represents the standard deviation around this mean value. The statistics of the corresponding regression are presented in **Table 3**.

TABLE 3 | Statistics between *in situ* measurements from the ANTARES time series and the values predicted by CANYON-MED for NO_3^-, PO_4^{3-}, $Si(OH)_4$, A_T, C_T and pH_T.

	N	r^2	Slope	MAE	RMSE
NO_3^- (μmol kg^{-1})	411	0.89	0.97	0.70	1.09
PO_4^{3-} (μmol kg^{-1})	390	0.85	1.06	0.064	0.079
$Si(OH)_4$ (μmol kg^{-1})	410	0.86	0.95	0.8	1.1
A_T (μmol kg^{-1})	294	0.80	0.86	5.2	6.8
C_T (μmol kg^{-1})	295	0.94	0.90	5.2	7.4
pH_T	293	0.85	0.85	0.0099	0.0142

concentrations range from low concentrations (<10 μmol.kg^{-1}) similar to those found in the Mediterranean Sea to very high concentrations (up to 200 μmol.kg^{-1}) at high latitudes (Ragueneau et al., 2000; Pujo-Pay et al., 2011), thus explaining the difference in scatter between the $Si(OH)_4$ values obtained by CANYON and CANYON-MED.

A_T and C_T retrieval performance appears to be relatively similar using the three methods (**Figures 6D,E**) due to the wide range of values of these two variables, which reduces differences between approaches. However, for A_T a large spread is present in CANYON estimates. Indeed, the MAE and RMSE range to a third less than CANYON and CANYON-B (**Table 4**). Moreover, a larger dispersion remains perceptible in the values predicted by CANYON and CANYON-B with predicted values lower by up to 100 μmol.kg^{-1} than their *in situ* measurements.

Likewise, pH_T values are comparable between the three neural network-based methods (**Figure 6F**), with CANYON-MED projecting pH_T with the lowest spread. Compared to the global average surface ocean, the Mediterranean Sea will be subject to amplified acidification (Touratier and Goyet, 2009, 2011; Palmiéri et al., 2015). The Mediterranean Sea is known to absorb more anthropogenic CO_2 per unit area (Palmiéri et al., 2015). Essentially, the Mediterranean's high A_T increases its capacity to absorb anthropogenic CO_2 and the short timescales at which its deep waters are ventilated (Schneider et al., 2014) allow for deeper penetration of this CO_2, thus resulting in a lower pH_T.

Other Methods

A key advantage of CANYON-MED lies in the few inputs required to use it, but other methodologies exist to predict nutrients and carbonate system variables. CANYON-MED and the methods described in this section were applied to our validation dataset and their results evaluated by the MAE and RMSE (as defined in section "Validation Statistics Metrics") are presented in **Table 5**.

First of all, Carter et al. (2018) developed methods for locally interpolated estimations of NO_3^-, PO_4^{3-}, $Si(OH)_4$, A_T, and pH_T (LINR, LIPR, LISIR, LIARv2, and LIPHR, respectively). These methods base their computations on equations requiring salinity, Apparent Oxygen Utilization (derived from O_2), depth, temperature, as well as nutrients concentrations. For comparability to our method and its possible application on BGC-Argo floats, these regressions were applied on our validation dataset using only the equations with similar inputs as our neural networks (i.e., temperature, depth or pressure for CANYON-MED, salinity, and O_2). The computations with Locally Interpolated Regressions (LIRs) were performed using their functionality that selects, using the given inputs, the lowest-uncertainty estimate among possible estimates (Carter et al., 2018).

Furthermore, also building on the CANYON networks, and in addition to CANYON-B presented in section "CANYON-MED," Bittig et al. (2018) developed another neural network-based method: CONTENT. This method predicts carbonate system variables. In CONTENT, CANYON-B estimates of the four carbonate system variables (i.e., A_T, C_T, pH_T, pCO_2) are combined through calculations of every pair (as the four variables can be derived from any pair of them). CONTENT therefore provides better estimates through the use of all four parameters of the carbonate system, whereas CANYON-B provides a unique direct estimate. These methods have the same inputs as CANYON-MED, except for the year which is only an input for the C_T, pH_T and pCO_2 neural networks in CANYON-B.

In addition, specifically for the Mediterranean Sea, Hassoun et al. (2015) derived equations to calculate A_T and C_T from salinity hereafter referred to as A_T-S and C_T-S. Equations are available for the entire Mediterranean Sea as well as specific equations for each sub-basin and several depth layers. For our comparison, the global equations were used since some equations for specific depth layers and locations had low performance. Furthermore, it is possible to use a single equation over the whole Mediterranean Sea, to derive A_T from salinity, if marginal seas and regions of important freshwater influence are not considered (Cossarini et al., 2015), which is relevant because CANYON-MED is not suited for coastal areas.

As shown in **Table 5**, CANYON-MED has lower errors for all predicted variables than the methods presented above. CONTENT has very similar errors in the prediction of carbonate system parameters compared to CANYON-B. The equations from Hassoun et al. (2015), predict A_T and C_T with errors up to four times the errors of CANYON-MED. Moreover, the LIRs clearly stand out, with errors up to ten times higher than the other methods. However, it should be stressed that the results from the LIRs would have been more robust (errors 10% lower but still higher than the other methods, data not shown) if they had been applied using all inputs, that is including nutrients as predictors, but as mentioned before, for aims of comparability, they were not.

Generally, CANYON-MED neural networks are more accurate than other methods with the same inputs. This is not

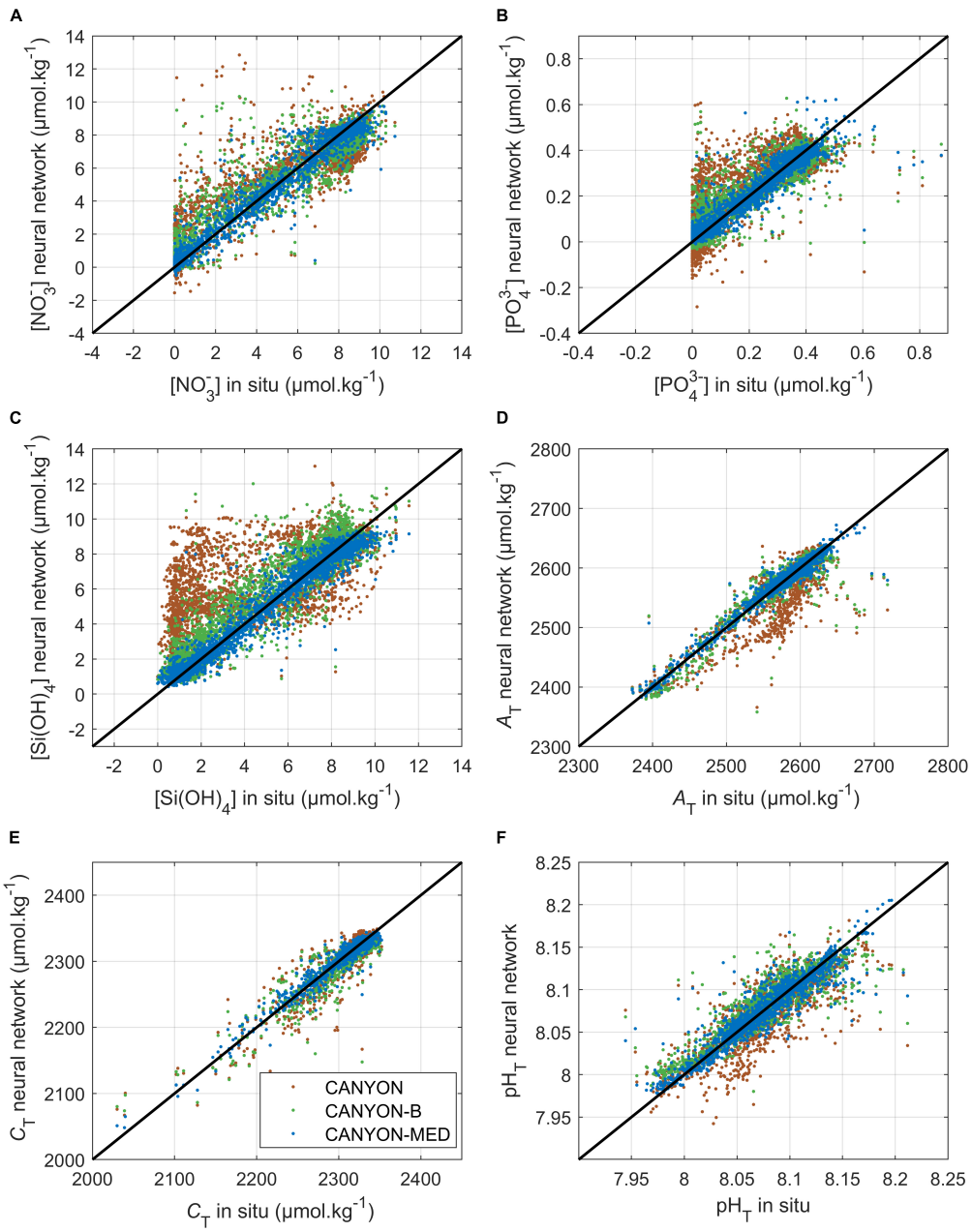

FIGURE 6 | Comparison of the CANYON (brown dots), CANYON-B (green dots) and CANYON-MED (blue dots) -retrieved values with the corresponding *in situ* measurements for **(A)** NO_3^-, **(B)** PO_4^{3-}, **(C)** $Si(OH)_4$, **(D)** A_T, **(E)** C_T, and **(F)** pH_T. The 1:1 line is shown in black.

TABLE 4 | Statistics between the CANYON, CANYON-B, and CANYON-MED -retrieved values with the corresponding *in situ* measurements applied on the entire database for NO_3^-, PO_4^{3-}, $Si(OH)_4$, A_T, C_T and pH_T.

	CANYON				CANYON-B				CANYON-MED			
	r^2	Slope	MAE	RMSE	r^2	Slope	MAE	RMSE	r^2	Slope	MAE	RMSE
NO_3^- (μmol kg^{-1})	0.71	0.69	1.37	1.81	0.84	0.82	0.95	1.34	0.95	0.96	0.47	0.73
PO_4^{3-} (μmol kg^{-1})	0.60	0.81	0.075	0.107	0.78	0.85	0.049	0.074	0.92	0.95	0.026	0.045
$Si(OH)_4$ (μmol kg^{-1})	0.38	0.46	2.28	2.98	0.86	0.92	0.97	1.30	0.96	0.95	0.40	0.70
A_T (μmol kg^{-1})	0.77	0.99	21.5	32.7	0.88	0.99	11.2	20.1	0.96	0.98	6.5	11.1
C_T (μmol kg^{-1})	0.79	0.91	13.6	19.9	0.83	0.84	12.3	17.8	0.94	0.92	7.0	10.0
pH_T	0.68	0.83	0.018	0.025	0.78	0.83	0.014	0.020	0.86	0.93	0.010	0.016

TABLE 5 | Performance indicators on the 20% validation dataset of CANYON (Sauzède et al., 2017), CANYON-B (Bittig et al., 2018), CANYON-MED (this paper), CONTENT (Bittig et al., 2018), A_T-S and C_T-S (Hassoun et al., 2015), LIARv2, LINR, and LIPHR (Carter et al., 2018) for NO_3^-, PO_4^{3-}, $Si(OH)_4$, A_T, C_T, pH_T.

	Method	MAE	RMSE
NO_3^- (μmol kg^{-1})	CANYON	1.37	1.81
	CANYON-B	0.95	1.34
	CANYON-MED	**0.47**	**0.74**
	LINR	4.14	5.90
PO_4^{3-} (μmol kg^{-1})	CANYON	0.076	0.107
	CANYON-B	0.049	0.075
	CANYON-MED	**0.026**	**0.045**
	LIPR	0.228	0.308
$Si(OH)_4$ (μmol kg^{-1})	CANYON	2.28	2.98
	CANYON-B	0.97	1.30
	CANYON-MED	**0.43**	**0.66**
	LISIR	4.32	7.93
A_T (μmol kg^{-1})	CANYON	21.53	32.74
	CANYON-B	11.18	20.07
	CANYON-MED	**6.51**	**11.09**
	CONTENT	11.52	21.24
	LIARv2	47.64	67.08
	A_T-S	15.59	30.21
C_T (μmol kg^{-1})	CANYON	13.64	19.88
	CANYON-B	12.34	17.85
	CANYON-MED	**6.98**	**10.03**
	CONTENT	12.54	17.58
	C_T-S	45.24	90.37
pH_T	CANYON	0.0181	0.0254
	CANYON-B	0.0140	0.0204
	CANYON-MED	**0.0102**	**0.0158**
	CONTENT	0.0156	0.0216
	LIPHR	0.0672	0.1173

Bold values highlight the best statitstic result.

surprising as it was built specifically for the Mediterranean Sea whereas CANYON, CANYON-B, CONTENT, and the LIRs were developed for the global ocean. However, high MAE and RMSE were obtained using A_T-S and C_T-S from Hassoun et al. (2015). This can be explained by the fact that, while having been developed specifically for the Mediterranean Sea, these equations were derived using data collected only in May whereas our validation dataset covers as much as possible the whole year. Furthermore, we only used the global equations developed for the entire Mediterranean Sea and for all depths. It is acknowledged that the equations derived for specific areas and depth layers would have produced more accurate results in targeted areas, but the aim was to compare the methods on a global basin scale. Therefore, it is suggested that, while allowing for easy computations of carbonate system variables in cases where they are lacking, the simple approximation from salinity might not always produce the best results on a varied dataset.

Overall, CANYON-MED stands out as the most robust method for the prediction of nutrients and carbonate system parameters in the Mediterranean Sea. The variables required are limited to systematically measured variables such as temperature, pressure, and salinity as well as high-quality O_2 measurements as inputs which are also widely measured (Bittig and Körtzinger, 2015). Thus, with the increased densification of high-quality O_2 measurements from BGC-Argo floats, as well as ocean gliders and moorings in the Mediterranean Sea (Testor et al., 2019; Tintoré et al., 2019; D'Ortenzio et al., 2020), CANYON-MED has a strong potential to support the development of new applications for marine biogeochemistry.

As is the case for all neural networks, the combination of the weights connecting the different hidden layers is not transparent, contrary to the weights obtained with linear regressions (Cortez and Embrechts, 2013). Nevertheless, a sensitivity analysis of the relative contribution showed no significant difference between the inputs of CANYON-MED, also indicating that no input parameter stands out over the others in an unrealistic manner. Thus, confirming the relevance of the chosen inputs and their balance as none is superfluous nor solely driving the neural network's outputs.

It should be underlined that other approaches allow for the prediction of nutrients and carbonate system variables with higher accuracies than ours. But these methods are often developed for the global ocean and might therefore not be as satisfactory in the semi-enclosed Mediterranean Sea. Furthermore, they often require a larger amount of inputs to predict a single variable. For example, Broullón et al. (2019) developed a neural network method called NNGv2 to derive A_T from geolocation, depth, temperature, salinity, and O_2 as well as nitrate, phosphate and silicate concentrations. NNGv2 predicts A_T, for the global ocean, with a RMSE of 5–6 μmol.kg^{-1}, about half the RMSE obtained when retrieving A_T using CANYON-MED. However, it is highly likely that those results would worsen in the Mediterranean Sea as NNGv2 was trained using the GLODAPv2 database (Olsen et al., 2016), similarly to CANYON,

CANYON-B, and CONTENT, in which the Mediterranean Sea is poorly described. Furthermore, NNGv2 requires more predictors than CANYON-MED. The additional variables [$Si(OH)_4$, PO_4^{3-}, NO_3^-] are not systematically measured, which hinders the use of this method, especially with the long-term objective to be applied on BGC-Argo, which are only equipped with O_2 sensors (Claustre et al., 2020 and references therein).

Example of Application: Mediterranean Deep Values

Using our 20% validation dataset, the averages of CANYON-MED outputs were calculated for each variable [i.e., NO_3^-, PO_4^{3-}, $Si(OH)_4$, A_T, C_T, and pH_T] from 1000 m depth to the bottom of the water column (4000 m) and averaged. The corresponding *in situ* measurements were averaged in the same way. The differences between *in situ* values and those predicted by CANYON-MED are presented in **Figure 7**. The choice of deep values relies on their seasonal stability.

Overall, the variables provided by CANYON-MED and the corresponding *in situ* measurements are in satisfactory agreement, i.e., the difference is close to zero. No spatial trend is observed in the differences between the *in situ* data and neural network's outputs indicating that CANYON-MED adequately predicts without bias values along the known oligotrophy and acidity gradients between the Eastern and Western basins (Krom et al., 1991; Flecha et al., 2015). However, a few outlier points stand out for each parameter. These larger differences may be due to seasonal imprints (the data presented in **Figure 7** refer to the complete validation dataset, regardless of their date and time).

In the Algero-Provencal basin, a deep A_T value stands out with a high difference (**Figure 7D**). The same occurs for a few C_T and pH_T values in the Gulf of Lion (**Figures 7E,F**). These extreme values could be explained by local phenomena also impacting temperature, salinity and/or O_2, the neural network's inputs, consequently impacting the retrieved values. Indeed, these areas are known to be dynamic with an eddy-driven mesoscale circulation, where the anomalous biogeochemical profiles could originate from (Pessini et al., 2018). We therefore hypothesize that discrete data may not sufficiently reflect the vertical distribution of these variables in a dynamic region such as the Gulf of Lion, owing to the lack of adequate observational resolution. High differences can also stem from erroneous stations not detected by the quality controls but being highlighted in CANYON-MED's outputs, causing the differences to deviate from zero values.

Additionally, some points standing out as high differences (exceptionally low values) for C_T (and A_T) in the Alboran Sea, Gulf of Lion and Algero-Provencal basin appear, after further investigation, to correspond to the first sampling campaign of the carbonate system in our database (i.e., in 1981). We, therefore, hypothesize that a difference in the quality of the measurements could explain some of the extreme deviations. Furthermore, for all variables, a larger variability can be found in the Alboran Sea than in the rest of the Mediterranean Sea. This variability can be a result of the influence of the Atlantic Ocean through the Gibraltar Strait and the strong associated mesoscale activity (Viúdez et al., 1998; Baldacci et al., 2001).

TABLE 6 | Statistics between the CANYON-MED retrieved values and the corresponding *in situ* measurements on the validation database according to Basin (West and East) for NO_3^-, PO_4^{3-}, $Si(OH)_4$, A_T, C_T, pH_T.

		CANYON-MED		
		r^2	MAE	RMSE
NO_3^- (μmol kg^{-1})	**West**	0.95	0.48	0.79
	East	0.89	0.45	0.67
PO_4^{3-} (μmol kg^{-1})	**West**	0.89	0.031	0.052
	East	0.87	0.021	0.029
$Si(OH)_4$ (μmol kg^{-1})	**West**	0.96	0.43	0.63
	East	0.96	0.43	0.70
A_T (μmol kg^{-1})	**West**	0.95	6.73	10.57
	East	0.87	7.88	11.81
C_T (μmol kg^{-1})	**West**	0.92	8.56	12.35
	East	0.73	9.19	17.60
pH_T	**West**	0.85	0.0098	0.0156
	East	0.83	0.0112	0.0165

Given the disparate spatial coverage of the training data available, we expected CANYON-MED to predict nutrients and carbonate system variables with higher errors in the Eastern Basin compared to the Western Basin. As shown by the statistics for each basin, gathered in **Table 6**, carbonate system parameters are indeed predicted with less accuracy in the Eastern Basin. As for nutrients, the difference between Eastern and Western Basin is less marked: a slightly lower MAE and RMSE for NO_3^- and PO_4^{3-} in the East are linked to a lower r^2. The difference between basins is mainly caused by the disparity in spatial and temporal coverage in our training database, stemming from a lack of cruises in the Eastern part of the Mediterranean Sea.

CANYON-MED remains unsatisfactory in areas where training data are too scarce (e.g., South Ionian Sea, off the Libyan coasts) and results accuracy might be lowered during anomalous events (extreme meteorological conditions impacting physical variables, such as deep convection). It should also be recalled that CANYON-MED is not suited for coastal areas.

CONCLUSION AND PERSPECTIVES

We have demonstrated the limited performance of the CANYON and CANYON-B methods to retrieve nutrients and carbonate system variables in the Mediterranean Sea. A new approach, CANYON-MED, was subsequently created and trained using an artificial neural network ensemble model. The approach takes advantage of the accuracy of EOVs systematically measured today (Wang et al., 2019), whether during scientific cruises or by autonomous platforms. The model was built as an ensemble of 10 optimized multi-layered perceptron feed-forward neural networks. CANYON-MED inputs were *in situ* measurements of pressure, temperature, salinity, and O_2 as well as geolocation (latitude and longitude) and sampling date (day of year and year).

The resulting ensemble model produces accurate estimates of nutrients and carbonate system variables [0.73, 0.045, and

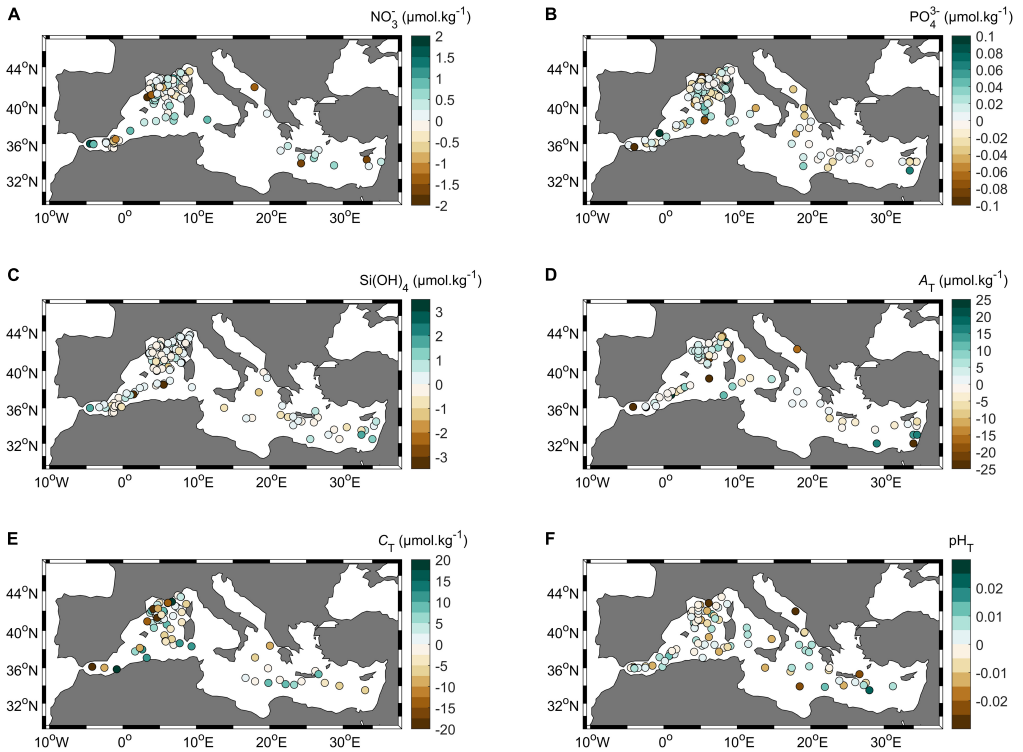

FIGURE 7 | Difference between *in situ* measurements and the corresponding values predicted by CANYON-MED averaged from 1000 m to the bottom for **(A)** NO_3^-, **(B)** PO_4^{3-}, **(C)** $Si(OH)_4$, **(D)** A_T, **(E)** C_T, and **(F)** pH_T.

0.70 µmol.kg^{-1} for NO_3^-, PO_4^{3-} and $Si(OH)_4$, respectively, and 0.016 units, 11 µmol.kg^{-1} and 10 µmol.kg^{-1} for pH_T, A_T, and C_T, respectively]. With such accuracy, CANYON-MED can produce estimates of variables that are not currently measured by autonomous platforms, as is the case for PO_4^{3-}, $Si(OH)_4$, A_T, and C_T. CANYON-MED can also help identify periods and areas in the Mediterranean Sea where the data density remains too low in space and/or time, which limits the understanding of some processes and the assessment of long-term variability. Indeed, the spatial and temporal domains where the method provides the least satisfactory results are related to weaknesses in the training database that does not sufficiently capture variability in space and time. Furthermore, more dynamic regions such as deep convection zones and mesoscale eddies may be less well reproduced by CANYON-MED.

Ship-based sampling remains imperfect either because of limited ship-time or human resources or because of weather conditions that prevent sampling in specific areas or at certain times of the year such as winter. CANYON-MED has the capability to fill gaps in observations in a cost-effective way, for example by filling the gaps in time series (subject to the absence of exceptional events). It can also be applied to a large network of BGC-Argo profiling floats and underwater gliders equipped with CTD and oxygen sensors, thus increasing the flow of biogeochemical data from systematically measured basic variables. CANYON-MED can also contribute to the quality control of NO_3^- and pH_T obtained from these autonomous platforms by providing data to correct for sensor drift during deployments and adjust deep values (e.g., Johnson et al., 2016, 2015; Sauzède et al., 2020). In line with this, multiple Eulerian moorings acquire and provide high-quality and high-frequency measurements of temperature, salinity, and O_2 over the water column at fixed locations in the Mediterranean Sea (e.g., HYDROCHANGES, EMSO, and OceanSITES networks). CANYON-MED can be applied to data collected at these sites, complementing the measured core variables, and generating high-frequency biogeochemical datasets, hence supplementing temporally limited oceanographic cruises.

Finally, since the accuracy of the virtual data obtained for NO_3^- by this approach is comparable to that obtained with autonomous platforms, their use in oceanography would be beneficial, in particular by increasing the datasets used for

the assimilation of some regional models that still lack crucial reference data (Doney et al., 2009; Cossarini et al., 2019).

DATA AVAILABILITY STATEMENT

All datasets generated for this study are included in the article/supplementary material.

AUTHOR CONTRIBUTIONS

HC, LC, FD'O, and MF initiated the study and designed the neural network configurations with the help of RS. MF collected and QCed the dataset and trained CANYON-MED. The manuscript was drafted by MF and LC. MF ran simulations and created the plots. All authors contributed to analysis and discussion of results, commented on, and contributed to the improvement of several versions of the manuscript.

ACKNOWLEDGMENTS

Thanks are due to Henry C. Bittig (IOW, Rostock) for helpful discussions on neural network development. We are extremely grateful to Marta Álvarez (IEO, La Coruña) and collaborators for making available to us the first version of the CARIMED database. We deeply acknowledge the work from analysts, investigators, and crew who collected the data at sea. We are thankful to the MOOSE program financially supported by CNRS-INSU, for providing annual cruises and fixed time series dataset for CANYON-MED training.

REFERENCES

Abram, N., Gattuso, J.-P., Prakash, A., Cheng, L., Chidichimo, M. P., Crate, S., et al. (2019). "Framing and context of the report," in *IPCC Special Report on the Ocean and Cryosphere in a Changing Climate*, ed. H.-O. Portner (Geneva: IPCC).

Álvarez, M., Sanleón-Bartolomé, H., Tanhua, T., Mintrop, L., Luchetta, A., Cantoni, C., et al. (2014). The CO_2 system in the Mediterranean Sea: a basin wide perspective. *Ocean Sci.* 10, 69–92. doi: 10.5194/os-10-69-2014

Baldacci, A., Corsini, G., Grasso, R., Manzella, G., Allen, J. T., Cipollini, P., et al. (2001). A study of the Alboran sea mesoscale system by means of empirical orthogonal function decomposition of satellite data. *J. Mar. Syst.* 29, 293–311. doi: 10.1016/S0924-7963(01)00021-25

Beale, M. H., Hagan, M. T., and Demuth, H. B. (2018). *Neural Network ToolboxTM User's Guide*. Natick, MA: The MathWorks Inc. Available online at: https://es.mathworks.com/help/pdf_doc/deeplearning/nnet_ug.pdf (accessed June 5, 2020).

Ben Mustapha, Z., Alvain, S., Jamet, C., Loisel, H., and Dessailly, D. (2014). Automatic classification of water-leaving radiance anomalies from global SeaWiFS imagery: application to the detection of phytoplankton groups in open ocean waters. *Remote Sens. Environ.* 146, 97–112. doi: 10.1016/j.rse.2013.08.046

Béthoux, J. P. (1989). Oxygen consumption, new production, vertical advection and environmental evolution in the Mediterranean Sea. *Deep Sea Res. Part A Oceanogr. Res. Pap.* 36, 769–781. doi: 10.1016/0198-0149(89)90150-90157

Béthoux, J. P., Morin, P., Chaumery, C., Connan, O., Gentili, B., and Ruiz-Pino, D. (1998). Nutrients in the Mediterranean Sea, mass balance and statistical analysis of concentrations with respect to environmental change. *Mar. Chem.* 63, 155–169. doi: 10.1016/S0304-4203(98)00059-50

Béthoux, J. P., Morin, P., Madec, C., and Gentili, B. (1992). Phosphorus and nitrogen behaviour in the Mediterranean Sea. *Deep Sea Res. Part A Oceanogr. Res. Pap.* 39, 1641–1654. doi: 10.1016/0198-0149(92)90053-V

Béthoux, J. P., Morin, P., and Ruiz-Pino, D. P. (2002). Temporal trends in nutrient ratios: chemical evidence of Mediterranean ecosystem changes driven by human activity. *Deep Sea Res. Part II Top. Stud. Oceanogr.* 49, 2007–2016. doi: 10.1016/S0967-0645(02)00024-23

Bishop, C. M. (1995). *Neural Networks for Pattern Recognition*. Oxford: Clarendon Press.

Bittig, H. C., and Körtzinger, A. (2015). Tackling oxygen optode drift: near-surface and in-air oxygen optode measurements on a float provide an accurate in situ reference. *J. Atmos. Ocean. Technol.* 32, 1536–1543. doi: 10.1175/JTECH-D-14-00162.1

Bittig, H. C., Steinhoff, T., Claustre, H., Fiedler, B., Williams, N. L., Sauzède, R., et al. (2018). An alternative to static climatologies: robust estimation of open ocean CO_2 variables and nutrient concentrations from T, S, and O2 data using bayesian neural networks. *Front. Mar. Sci.* 5:328. doi: 10.3389/fmars.2018.00328

Bittig, H. C., Maurer, T. L., Plant, J. N., Schmechtig, C., Wong, A. P. S., Claustre, H., et al. (2019). A BGC-Argo guide: planning, deployment, data handling and usage. *Front. Mar. Sci.* 6:502. doi: 10.3389/fmars.2019.00502

Borghini, M., Bryden, H., Schroeder, K., Sparnocchia, S., and Vetrano, A. (2014). The Mediterranean is becoming saltier. *Ocean Sci.* 10, 693–700. doi: 10.5194/os-10-693-2014

Broullón, D., Pérez, F. F., Velo, A., Hoppema, M., Olsen, A., Takahashi, T., et al. (2019). A global monthly climatology of total alkalinity: a neural network approach. *Earth Syst. Sci. Data* 11, 1109–1127. doi: 10.5194/essd-11-1109-2019

Carter, B. R., Feely, R. A., Williams, N. L., Dickson, A. G., Fong, M. B., and Takeshita, Y. (2018). Updated methods for global locally interpolated estimation of alkalinity, pH, and nitrate. *Limnol. Oceanogr. Methods* 16, 119–131. doi: 10.1002/lom3.10232

Chai, F., Johnson, K. S., Claustre, H., Xing, X., Wang, Y., Boss, E., et al. (2020). Monitoring ocean biogeochemistry with autonomous platforms. *Nat. Rev. Earth Environ.* 1, 315–326. doi: 10.1038/s43017-020-0053-y

Claustre, H., Johnson, K. S., and Takeshita, Y. (2020). Observing the global ocean with biogeochemical-argo. *Annu. Rev. Mar. Sci.* 12, 23–48. doi: 10.1146/annurev-marine-010419-010956

Conan, P. (2013). *DEWEX-MERMEX 2013 LEG2 Cruise, Le Suroît R/V*. doi: 10.17600/13020030

Copin-Montégut, C., and Bégovic, M. (2002). Distributions of carbonate properties and oxygen along the water column (0-2000m) in the central part of the NW Mediterranean Sea (Dyfamed site): influence of winter vertical mixing on air-sea CO_2 and O2 exchanges. *Deep Sea Res. Part II* 49, 2049–2066. doi: 10.1016/S0967-0645(02)00027-29

Coppola, L., Diamond Riquier, E., and Carval, T. (2019a). *Dyfamed Observatory Data*. London: SEANOE.

Coppola, L., Raimbault, P., Mortier, L., and Testor, P. (2019b). Monitoring the environment in the northwestern Mediterranean Sea. *EOS* 100:951. doi: 10.1029/2019EO125951

Coppola, L., Legendre, L., Lefevre, D., Prieur, L., Taillandier, V., and Diamond Riquier, E. (2018). Seasonal and inter-annual variations of dissolved oxygen in the northwestern Mediterranean Sea (DYFAMED site). *Prog. Oceanogr.* 162, 187–201. doi: 10.1016/j.pocean.2018.03.001

Claustre, H. (1999). *PROSOPE Cruise, Thalassa R/V*. Available online at: https://campagnes.flotteoceanographique.fr/campagnes/99040060/

Coppola, L. (2016). *MOOSE-GE 2016 Cruise, L'Atalante R/V*. Available online at: https://campagnes.flotteoceanographique.fr/campagnes/16000700/

Cortez, P., and Embrechts, M. J. (2013). Using sensitivity analysis and visualization techniques to open black box data mining models. *Inform. Sci.* 225, 1–17. doi: 10.1016/j.ins.2012.10.039

Cossarini, G., Lazzari, P., and Solidoro, C. (2015). Spatiotemporal variability of alkalinity in the Mediterranean Sea. *Biogeosciences* 12, 1647–1658. doi: 10.5194/bg-12-1647-2015

Cossarini, G., Mariotti, L., Feudale, L., Mignot, A., Salon, S., Taillandier, V., et al. (2019). Towards operational 3D-Var assimilation of chlorophyll

biogeochemical-argo float data into a biogeochemical model of the mediterranean Sea. *Ocean Model.* 133, 112–128. doi: 10.1016/j.ocemod.2018.11.005

Crispi, G., Mosetti, R., Solidoro, C., and Crise, A. (2001). Nutrients cycling in Mediterranean basins: the role of the biological pump in the trophic regime. *Ecol. Model.* 138, 101–114. doi: 10.1016/S0304-3800(00)00396-393

Dickson, A. G. (1990). Standard potential of the reaction: AgCl(s) + $^1/_2$H2(g) = Ag(s) + HCl(aq), and the standard acidity constant of the ion HSO4- in synthetic sea water from 273.15 to 318.15 K. *J. Chem. Thermodyn.* 22, 113–127. doi: 10.1016/0021-9614(90)90074-z

Dickson, A. G., and Millero, F. J. (1987). A comparison of the equilibrium constants for the dissociation of carbonic acid in seawater media. *Deep Sea Res.* 34, 1733–1743. doi: 10.1016/0198-0149(87)90021-5

Diffenbaugh, N. S., Pal, J. S., Giorgi, F., and Gao, X. (2007). Heat stress intensification in the Mediterranean climate change hotspot. *Geophys. Res. Lett.* 34:GL030000. doi: 10.1029/2007GL030000

Doney, S. C., Fabry, V. J., Feely, R. A., and Kleypas, J. A. (2009). Ocean acidification: the other CO_2 problem. *Annu. Rev. Mar. Sci.* 1, 169–192. doi: 10.1146/annurev.marine.010908.163834

D'Ortenzio, F., Taillandier, V., Claustre, H., Prieur, L. M., Leymarie, E., Mignot, A., et al. (2020). Biogeochemical Argo: the test case of the NAOS Mediterranean array. *Front. Mar. Sci.* 7:120. doi: 10.3389/fmars.2020.00120

Durrieu De MadronXavier (2011). *CASCADE Cruise, L'Atalante R/V*. Available online at: https://campagnes.flotteoceanographique.fr/campagnes/11010020/

Environmental Sciences Division, O. R. N. L. (1988). *GEOSECS Atlantic, Pacific, Indian, and Mediterranean Radiocarbon Data*. doi: 10.3334/CDIAC/OTG.NDP027

Flecha, S., Pérez, F. F., García-Lafuente, J., Sammartino, S., Ríos, A. F., and Huertas, I. E. (2015). Trends of pH decrease in the Mediterranean Sea through high frequency observational data: indication of ocean acidification in the basin. *Sci. Rep.* 5:16770. doi: 10.1038/srep16770

Foresee, F. D., and Hagan, M. T. (1997). "Gauss-newton approximation to bayesian learning," in *Proceedings of International Conference on Neural Networks (ICNN'97)*, Piscataway, NJ.

Fourrier, M. (2020). Dataset used for CANYON-MED training and validation. *figshare*. doi: 10.6084/m9.figshare.12452795.v1

Gattuso, J.-P., and Hansson, L. (2011). *Ocean Acidification*. Oxford: Oxford University Press.

Giorgi, F. (2006). Climate change hot-spots. *Geophys. Rese. Lett.* 33:734. doi: 10.1029/2006GL025734

Goodfellow, I., Bengio, Y., and Courville, A. (2016). *Deep Learning*. Cambridge, MA: MIT Press.

GOOS (2018). Available online at: https://www.goosocean.org/index.php?option=com_content &view=article&id=14&Itemid=114 (accessed October 31, 2019).

Goyet, C., Hassoun, A. E. R., and Gemayel, E. (2015). *Carbonate System During the May 2013 MedSeA Cruise*. London: PANGAEA. doi: 10.1594/PANGAEA.841933

Gregor, L., Lebehot, A. D., Kok, S., and Scheel Monteiro, P. M. (2019). A comparative assessment of the uncertainties of global surface ocean CO_2 estimates using a machine-learning ensemble (CSIR-ML6 version 2019a) - have we hit the wall? *Geosci. Model. Dev.* 12, 5113–5136. doi: 10.5194/gmd-12-5113-2019

Hagan, M. T., Demuth, H. B., Beale, M. H., and De Jesus, O. (2014). *Neural Network Design*, 2nd Edn. Wrocław: Martin T. Hagan.

Hassoun, A. E. R., Gemayel, E., Krasakopoulou, E., Goyet, C., Saab, M. A. A., and Ziveri, P. (2015). Modeling of the total alkalinity and the total inorganic carbon in the mediterranean Sea. *J. Water Resour. and Ocean Sci.* 4:24. doi: 10.11648/j.wros.20150401.14

Hornik, K., Stinchcombe, M., and White, H. (1989). Multilayer feedforward networks are universal approximators. *Neural Netw.* 2, 359–366. doi: 10.1016/0893-6080(89)90020-90028

Huertas, I. E. (2007a). *Hydrochemistry Measured on Water Bottle Samples During Al Amir Moulay Abdallah Cruise CARBOGIB-2*. London: PANGAEA. doi: 10.1594/PANGAEA.618899

Huertas, I. E. (2007b). *Hydrochemistry Measured on Water Bottle Samples During Al Amir Moulay Abdallah Cruise CARBOGIB-3*. London: PANGAEA. doi: 10.1594/PANGAEA.618898

Huertas, I. E. (2007c). *Hydrochemistry Measured on Water Bottle Samples During Al Amir Moulay Abdallah Cruise CARBOGIB-4*. London: PANGAEA. doi: 10.1594/PANGAEA.618897

Huertas, I. E. (2007d). *Hydrochemistry Measured on Water Bottle Samples During Al Amir Moulay Abdallah Cruise CARBOGIB-5*. London: PANGAEA. doi: 10.1594/PANGAEA.618896

Huertas, I. E. (2007e). *Hydrochemistry Measured on Water Bottle Samples During Al Amir Moulay Abdallah Cruise CARBOGIB-6*. London: PANGAEA. doi: 10.1594/PANGAEA.618895

Huertas, I. E. (2007f). *Hydrochemistry Measured on Water Bottle Samples During Garcia del Cid Cruise GIFT-1*. London: PANGAEA. doi: 10.1594/PANGAEA.618916

Huertas, I. E. (2007g). *Hydrochemistry Measured on Water Bottle Samples During Garcia del Cid Cruise GIFT-2*. London: PANGAEA. doi: 10.1594/PANGAEA.618915

Hydes, D., Jiang, Z.-P., Hartman, M. C., Campbell, J., Hartman, S. E., Pagnani, M., et al. (2011). *Dissolved Inorganic Carbon, Alkalinity, Temperature, Salinity and DISSOLVED OXYGEN Collected From Profile and Discrete Sample Observations Using Alkalinity titrator, CTD and Other Instruments From the Pacific Celebes in the Alboran Sea, Arabian Sea and Others From 2007-06-11 to 2012-03-18 (NCEI Accession 0081040)*. Silver Spring, MD: NOAA. doi: 10.3334/CDIAC/OTG.VOS_PC_2007-2012

Jamet, C. (2004). *Inversion Neuro-Variationnelle Des Images De La Couleur De L'océan - Restitution des Propriétés Optiques Des Aérosols Et De La Concentration En Chlorophylle-A Pour Les Eaux Du cas I*. Available online at: https://tel.archives-ouvertes.fr/tel-00007377/document (accessed February 8, 2018).

Jamet, C., Loisel, H., and Dessailly, D. (2012). Retrieval of the spectral diffuse attenuation coefficient Kd in open and coastal ocean waters using a neural network inversion. *J. Geophys. Res. Oceans* 117:C10023. doi: 10.1029/2012JC008076

Johnson, K. S., and Claustre, H. (2016). Bringing biogeochemistry into the Argo age. *EOS* 97:427. doi: 10.1029/2016EO062427

Johnson, K. S., Jannasch, H. W., Coletti, L. J., Elrod, V. A., Martz, T. R., Takeshita, Y., et al. (2016). Deep-Sea DuraFET: a pressure tolerant pH sensor designed for global sensor networks. *Analyt. Chem.* 88, 3249–3256. doi: 10.1021/acs.analchem.5b04653

Johnson, K. S., Plant, J. N., Coletti, L. J., Jannasch, H. W., Sakamoto, C. M., Riser, S. C., et al. (2017). Biogeochemical sensor performance in the SOCCOM profiling float array. *J. Geophys. Res. Oceans* 122, 6416–6436. doi: 10.1002/2017JC012838

Johnson, K. S., Plant, J. N., Riser, S. C., and Gilbert, D. (2015). Air oxygen calibration of oxygen optodes on a profiling float array. *J. Atmos. Ocean. Technol.* 32, 2160–2172. doi: 10.1175/JTECH-D-15-0101.1

Krasakopoulou, E., and Souvermezoglou, E. (2013). *Discrete measurements of carbon dioxide and other parameters in the Aegean Sea during the HCMR OTRANTO-5 cruise from February 9 to February 10, 1995 (NCEI Accession 0084544)*. Silver Spring, MD: NOAA. doi: 10.3334/CDIAC/OTG.HCMR_OTR5_1995

Kress, N., Gertman, I., and Herut, B. (2014). Temporal evolution of physical and chemical characteristics of the water column in the Easternmost Levantine basin (Eastern Mediterranean Sea) from 2002 to 2010. *J. Mar. System* 135, 6–13. doi: 10.1016/j.jmarsys.2013.11.016

Körtzinger, A., Schimanski, J., Send, U., and Wallace, D. (2004). The ocean takes a deep breath. *Science* 306, 1337–1337. doi: 10.1126/science.1102557

Krom, M. D., Kress, N., Brenner, S., and Gordon, L. I. (1991). Phosphorus limitation of primary productivity in the eastern Mediterranean Sea. *Limnol. Oceanogr.* 36, 424–432. doi: 10.4319/lo.1991.36.3.0424

Krom, M. D., Woodward, E. M. S., Herut, B., Kress, N., Carbo, P., Mantoura, R. F. C., et al. (2005). Nutrient cycling in the south east Levantine basin of the eastern Mediterranean: results from a phosphorus starved system. *Deep Sea Res. Part II Top. Stud. Oceanogr.* 52, 2879–2896. doi: 10.1016/j.dsr2.2005.08.009

Landschützer, P., Gruber, N., Bakker, D. C. E., and Schuster, U. (2014). Recent variability of the global ocean carbon sink. *Glob. Biogeochem. Cycles* 28, 927–949. doi: 10.1002/2014GB004853

Le Quéré, C., Andrew, R. M., Friedlingstein, P., Sitch, S., Pongratz, J., Manning, A. C., et al. (2018). Global carbon budget 2017. *Earth Syst. Sci. Data* 10, 405–448. doi: 10.5194/essd-10-405-2018

Lee, K., Sabine, C. L., Tanhua, T., Kim, T.-W., Feely, R. A., and Kim, H.-C. (2011). Roles of marginal seas in absorbing and storing fossil fuel CO_2. *Energy Environ. Sci.* 4, 1133–1146. doi: 10.1039/C0EE00663G

Lefevre, D. (2010). *MOOSE (ANTARES)*. doi: 10.18142/233

Lefevre, N., Watson, A. J., and Watson, A. R. (2005). A comparison of multiple regression and neural network techniques for mapping in situ pCO_2 data. *Tellus B* 57, 375–384. doi: 10.1111/j.1600-0889.2005.00164.x

Lewis, E., Wallace, D., and Allison, L. J. (1998). *Program Developed for CO_2 System Calculations. Environmental Sciences Division Publication No. 4735*. Oak Ridge, TN: Carbon Dioxide Information Analysis Center.

Linares-Rodriguez, A., Ruiz-Arias, J. A., Pozo-Vazquez, D., and Tovar-Pescador, J. (2013). An artificial neural network ensemble model for estimating global solar radiation from Meteosat satellite images. *Energy* 61, 636–645. doi: 10.1016/j.energy.2013.09.008

Lindstrom, E., Gunn, J., Fischer, A., McCurdy, A., Glover, L. K., and Members, T. T. (2012). *A Framework For Ocean Observing*. Paris: UNESCO.

Lovato, T., and Vichi, M. (2015). An objective reconstruction of the Mediterranean Sea carbonate system. *Deep Sea Res. Part I Oceanogr. Res. Pap.* 98, 21–30. doi: 10.1016/j.dsr.2014.11.018

MacKay, D. J. C. (1992a). A practical bayesian framework for backpropagation networks. *Neural Comput.* 4, 448–472. doi: 10.1162/neco.1992.4.3.448

MacKay, D. J. C. (1992b). Bayesian interpolation. *Neural Comput.* 4, 415–447. doi: 10.1162/neco.1992.4.3.415

Marty, J.-C., Chiavérini, J., Pizay, M.-D., and Avril, B. (2002). Seasonal and interannual dynamics of nutrients and phytoplankton pigments in the western Mediterranean Sea at the DYFAMED time-series station (1991-1999). *Deep Sea Res. Part II Top. Stud. Oceanogr.* 49, 1965–1985. doi: 10.1016/S0967-0645(02)00022-X

Marzban, C. (2009). "Basic statistics and basic AI: neural networks," in *Artificial Intelligence Methods in the Environmental Sciences*, eds S. E. Haupt, A. Pasini, and C. Marzban (Dordrecht: Springer), 15–47. doi: 10.1007/978-1-4020-9119-3_2

McGill, D. A. (1966). *The Relative Supplies Of Phosphate, Nitrate And Silicate In The Mediterranean Sea*. Madrid: CIESM.

Mehrbach, C., Culberson, C. H., Hawley, J. E., and Pytkowicx, R. M. (1973). Measurement of the apparent dissociation constants of carbonic acid in seawater at atmospheric pressure. *Limnol. Oceanogr.* 18, 897–907. doi: 10.4319/lo.1973.18.6.0897

Millot, C. (1999). Circulation in the western Mediterranean Sea. *J. Mar. Syst.* 20, 423–442. doi: 10.1016/S0924-7963(98)00078-75

Millot, C., and Taupier-Letage, I. (2005). "Circulation in the mediterranean Sea," in *The Mediterranean Sea*, ed. A. Saliot (Berlin: Springer), 29–66. doi: 10.1007/b107143

Minas, H. J. (1981). *MEDIPROD IV Cruise, Jean Charcot R/V*. doi: 10.17600/81006511

Mortier, L., Ait Ameur, N., and Taillandier, V. (2014). *SOMBA-GE-2014 Cruise, Téthys II R/V*. doi: 10.17600/14007500

Moutin, T. (2008). *BOUM Cruise, L'Atalante R/V*. doi: 10.17600/8010090

Niewiadomska, K., Claustre, H., Prieur, L., and d'Ortenzio, F. (2008). Submesoscale physical-biogeochemical coupling across the Ligurian current (northwestern Mediterranean) using a bio-optical glider. *Limnol. Oceanogr.* 53, 2210–2225. doi: 10.4319/lo.2008.53.5_part_2.2210

Olsen, A., Key, R. M., van Heuven, S., Lauvset, S. K., Velo, A., Lin, X., et al. (2016). The Global Ocean Data analysis project version 2 (GLODAPv2) - an internally consistent data product for the world ocean. *Earth Syst. Sci. Data* 8, 297–323. doi: 10.5194/essd-8-297-2016

Palmiéri, J., Orr, J. C., Dutay, J.-C., Béranger, K., Schneider, A., Beuvier, J., et al. (2015). Simulated anthropogenic CO_2 storage and acidification of the Mediterranean Sea. *Biogeosciences* 12, 781–802. doi: 10.5194/bg-12-781-2015

Pasqueron de Fommervault, O., Migon, C., D×Ortenzio, F., Ribera d'Alcalà, M., and Coppola, L. (2015). Temporal variability of nutrient concentrations in the northwestern Mediterranean Sea (DYFAMED time-series station). *Deep Sea Res. Part I Oceanogr. Res. Pap.* 100, 1–12. doi: 10.1016/j.dsr.2015.02.006

Pessini, F., Olita, A., Cotroneo, Y., and Perilli, A. (2018). Mesoscale eddies in the Algerian Basin: do they differ as a function of their formation site? *Ocean Sci.* 14, 669–688. doi: 10.5194/os-14-669-2018

Piron, A., Thierry, V., Mercier, H., and Caniaux, G. (2016). Argo float observations of basin-scale deep convection in the Irminger sea during winter 2011-2012. *Deep Sea Res. Part I Oceanogr. Res. Pap.* 109, 76–90. doi: 10.1016/j.dsr.2015.12.012

Piron, A., Thierry, V., Mercier, H., and Caniaux, G. (2017). Gyre-scale deep convection in the subpolar North Atlantic Ocean during winter 2014-2015. *Geophys. Res. Lett.* 44, 1439–1447. doi: 10.1002/2016GL071895

Prieur, L. (1991). *ALMOFRONT*. doi: 10.18142/30

Pujo-Pay, M., Conan, P., Oriol, L., Cornet-Barthaux, V., Falco, C., Ghiglione, J.-F., et al. (2011). Integrated survey of elemental stoichiometry (C, N, P) from the western to eastern Mediterranean Sea. *Biogeosciences* 8, 883–899. doi: 10.5194/bg-8-883-2011

Ragueneau, O., Tréguer, P., Leynaert, A., Anderson, R. F., Brzezinski, M. A., DeMaster, D. J., et al. (2000). A review of the Si cycle in the modern ocean: recent progress and missing gaps in the application of biogenic opal as a paleoproductivity proxy. *Glob. Planet. Chang.* 26, 317–365. doi: 10.1016/S0921-8181(00)00052-57

Redfield, A. C. (1934). "On the proportions of organic derivatives in sea water and their relation to the composition of plankton," in *James Johnstone Memorial Volume*, ed. R. Daniel (Liverpool: University Press of Liverpool), 176–192.

Ribera d'Alcalà, M., Civitarese, G., Conversano, F., and Lavezza, R. (2003). Nutrient ratios and fluxes hint at overlooked processes in the Mediterranean Sea. *J. Geophys. Res. Oceans* 108, C001650. doi: 10.1029/2002JC001650

Riser, S. C., Freeland, H. J., Roemmich, D., Wijffels, S., Troisi, A., Belbéoch, M., et al. (2016). Fifteen years of ocean observations with the global argo array. *Nat. Clim. Chang.* 6, 145–153. doi: 10.1038/nclimate2872

Rivaro, P., Messa, R., Massolo, S., and Frache, R. (2010). Distributions of carbonate properties along the water column in the Mediterranean Sea: spatial and temporal variations. *Mar. Chem.* 121, 236–245. doi: 10.1016/j.marchem.2010.05.003

Robinson, C. (2019). Microbial respiration, the engine of ocean deoxygenation. *Front. Mar. Sci.* 5:533. doi: 10.3389/fmars.2018.00533

Roemmich, D., Alford, M. H., Claustre, H., Johnson, K., King, B., Moum, J., et al. (2019). On the future of argo: a global, full-depth, multi-disciplinary array. *Front. Mar. Sci.* 6:439. doi: 10.3389/fmars.2019.00439

Rumelhart, D. E., Hintont, G. E., and Williams, R. J. (1986). Learning representations by back-propagating errors. *Nature* 523, 533–536. doi: 10.1038/323533a0

Sanleón-Bartolomé, H., Alvarez, M., Velo, A., Tanhua, T., and Fajar, N. M. (2017). *The CARIMED (CARbon In the MEDiterranean Sea) Data Synthesis Initiative: Overview And Quality Control Procedures*. Available online at: http://www.repositorio.ieo.es/e-ieo/handle/10508/11313 (accessed October 31, 2019).

Sauzède, R., Bittig, H. C., Claustre, H., Pasqueron de Fommervault, O., Gattuso, J.-P., Legendre, L., et al. (2017). Estimates of water-column nutrient concentrations and carbonate system parameters in the global ocean: a novel approach based on neural networks. *Front. Mar. Sci.* 4:128. doi: 10.3389/fmars.2017.00128

Sauzède, R., Claustre, H., Uitz, J., Jamet, C., Dall'Olmo, G., D'Ortenzio, F., et al. (2016). A neural network-based method for merging ocean color and Argo data to extend surface bio-optical properties to depth: retrieval of the particulate backscattering coefficient: bbp vertical profile from satellite data. *J. Geophys. Res. Oceans* 121, 2552–2571. doi: 10.1002/2015JC011408

Sauzède, R., Martinez, E., Maes, C., Pasqueron de Fommervault, O., Poteau, A., Mignot, A., et al. (2020). Enhancement of phytoplankton biomass leeward of Tahiti as observed by Biogeochemical-Argo floats. *J. Mar. Syst.* 204:103284. doi: 10.1016/j.jmarsys.2019.103284

Schneider, A., Tanhua, T., Körtzinger, A., and Wallace, D. W. R. (2010). High anthropogenic carbon content in the eastern Mediterranean. *J. Geophys. Res.* 115:C006171. doi: 10.1029/2010JC006171

Schneider, B., Roether, W., and University Of Bremen (2013). *Dissolved Inorganic Carbon, Alkalinity, Temperature, Salinity and Other Variables Collected From Discrete Sample and Profile Observations Using CTD, Bottle and Other Instruments From METEOR in the Aegean Sea, Mediterranean Sea and Others From 2001-10-18 to 2001-11-11 (NCEI Accession 0084620)*. Silver Spring, MD: NODC. doi: 10.3334/CDIAC/OTG.CARINA_06MT20011018

Schneider, A., Tanhua, T., Roether, W., and Steinfeldt, R. (2014). Changes in ventilation of the Mediterranean Sea during the past 25 year. *Ocean Sci.* 10, 1–16. doi: 10.5194/os-10-1-2014

Sharkey, A. J. C. (ed.) (1999). *Combining Artificial Neural Nets: Ensemble and Modular Multi-Net Systems*. Berlin: Springer.

Tanhua, T., Hainbucher, D., Schroeder, K., Cardin, V., Álvarez, M., and Civitarese, G. (2013). The Mediterranean Sea system: a review and an introduction to the special issue. *Ocean Sci.* 9, 789–803. doi: 10.5194/os-9-789-2013

Tanhua, T., McCurdy, A., Fischer, A., Appeltans, W., Bax, N., Currie, K., et al. (2019). What we have learned from the framework for ocean observing: evolution of the global ocean observing system. *Front. Mar. Sci.* 6:471. doi: 10.3389/fmars.2019.00471

Testor, P. (2013). *DEWEX-MERMEX 2013 LEG1 Cruise, Le Suroît R/V*. doi: 10.17600/13020010

Testor, P., Coppola, L., and Mortier, L. (2010). *MOOSE-GE 2010 Cruise, Téthys II R/V*. Washington, DC: AGU. doi: 10.17600/10450080

Testor, P., Coppola, L., and Mortier, L. (2011). *MOOSE-GE 2011 Cruise, Téthys II R/V*. Washington, DC: AGU. doi: 10.17600/11450160

Testor, P., Coppola, L., and Mortier, L. (2012). *MOOSE-GE 2012 Cruise, Le Suroît R/V*. Washington, DC: AGU. doi: 10.17600/12020030

Testor, P., Coppola, L., and Mortier, L. (2013). *MOOSE-GE 2013 Cruise, Téthys II R/V*. Washington, DC: AGU. doi: 10.17600/13450110

Testor, P., Coppola, L., and Mortier, L. (2014). *MOOSE-GE 2014 Cruise, Le Suroît R/V*. Washington, DC: AGU. doi: 10.17600/14002300

Testor, P., Coppola, L., and Mortier, L. (2015). *MOOSE-GE 2015 Cruise, Le Suroît R/V*. Washington, DC: AGU. doi: 10.17600/15002500

Testor, P., de Young, B., Rudnick, D. L., Glenn, S., Hayes, D., Lee, C. M., et al. (2019). OceanGliders: a component of the Integrated GOOS. *Front. Mar. Sci.* 6:422. doi: 10.3389/fmars.2019.00422

Tintoré, J., Pinardi, N., Álvarez-Fanjul, E., Aguiar, E., Álvarez-Berastegui, D., Bajo, M., et al. (2019). Challenges for sustained observing and forecasting systems in the mediterranean Sea. *Front. Mar. Sci.* 6:568. doi: 10.3389/fmars.2019.00568

Touratier, F., and Goyet, C. (2009). Decadal evolution of anthropogenic CO_2 in the northwestern Mediterranean Sea from the mid-1990s to the mid-2000s. *Deep Sea Res. Part I Oceanogr. Res. Pap.* 56, 1708–1716. doi: 10.1016/j.dsr.2009.05.015

Touratier, F., and Goyet, C. (2011). Impact of the eastern mediterranean transient on the distribution of anthropogenic CO_2 and first estimate of acidification for the mediterranean Sea. *Deep Sea Res. Part I Oceanogr. Res. Pap.* 58, 1–15. doi: 10.1016/j.dsr.2010.10.002

Uppström, L. R. (1974). The boron/chlorinity ratio of deep-sea water from the Pacific Ocean. *Deep Sea Res.* 21, 161–162. doi: 10.1016/0011-7471(74)90074-6

van Heuven, S., Pierrot, D., Rae, J., Lewis, E., and Wallace, D. W. R. (2011). *CO_2SYS v 1.1, MATLAB Program Developed for CO_2 System Calculations. ORNL/CDIAC-105b*. Oak Ridge, TN: Oak Ridge National Laboratory.

Velo, A., Pérez, F. F., Tanhua, T., Gilcoto, M., Ríos, A. F., and Key, R. M. (2013). Total alkalinity estimation using MLR and neural network techniques. *J. Mar. Syst.* 111–112, 11–18. doi: 10.1016/j.jmarsys.2012.09.002

Viúdez, A., Pinot, J.-M., and Haney, R. L. (1998). On the upper layer circulation in the Alboran Sea. *J. Geophys. Res. Oceans* 103, 21653–21666. doi: 10.1029/98JC01082

Wang, Z. A., Moustahfid, H., Mueller, A. V., Michel, A. P. M., Mowlem, M., Glazer, B. T., et al. (2019). Advancing observation of ocean biogeochemistry, biology, and ecosystems with cost-effective *in situ* sensing technologies. *Front. Mar. Sci.* 6:519. doi: 10.3389/fmars.2019.00519

Weller, R. A., Baker, D. J., Glackin, M. M., Roberts, S. J., Schmitt, R. W., Twigg, E. S., et al. (2019). The challenge of sustaining ocean observations. *Front. Mar. Sci.* 6:105. doi: 10.3389/fmars.2019.00105

Ziveri, P., and Grelaud, M. (2015). *Physical Oceanography Measured on Water Bottle Samples During ÁngelesAlvario Cruise MedSeA2013*. London: PANGAEA. doi: 10.1594/PANGAEA.846051

Conflict of Interest: The authors declare that the research was conducted in the absence of any commercial or financial relationships that could be construed as a potential conflict of interest.

4.4 Corrigendum publié dans *Frontiers in Marine Science*

frontiers in Marine Science

CORRECTION
published: 25 January 2021
doi: 10.3389/fmars.2021.650509

Corrigendum: A Regional Neural Network Approach to Estimate Water-Column Nutrient Concentrations and Carbonate System Variables in the Mediterranean Sea: CANYON-MED

Marine Fourrier[1]*, *Laurent Coppola*[1,2], *Hervé Claustre*[1], *Fabrizio D'Ortenzio*[1], *Raphaëlle Sauzède*[2] *and Jean-Pierre Gattuso*[1,3]

[1] Sorbonne Université, CNRS, Laboratoire d'Océanographie de Villefranche, Villefranche-sur-Mer, France, [2] Sorbonne Université, CNRS, Institut de la Mer de Villefranche, Villefranche-sur-Mer, France, [3] Institute for Sustainable Development and International Relations, Sciences Po, Paris, France

Keywords: nutrients, carbonate system, Mediterranean Sea, neural network, CANYON

OPEN ACCESS

Edited and reviewed by:
Ananda Pascual, Mediterranean Institute for Advanced Studies (IMEDEA), Spain

***Correspondence:**
Marine Fourrier
marine.fourrier@obs-vlfr.fr

Specialty section:
This article was submitted to Ocean Observation, a section of the journal Frontiers in Marine Science

Received: *07 January 2021*
Accepted: *14 January 2021*
Published: *25 January 2021*

Citation:
Fourrier M, Coppola L, Claustre H, D'Ortenzio F, Sauzède R and Gattuso J-P (2021) Corrigendum: A Regional Neural Network Approach to Estimate Water-Column Nutrient Concentrations and Carbonate System Variables in the Mediterranean Sea: CANYON-MED. Front. Mar. Sci. 8:650509. doi: 10.3389/fmars.2021.650509

A Corrigendum on

A Regional Neural Network Approach to Estimate Water-Column Nutrient Concentrations and Carbonate System Variables in the Mediterranean Sea: CANYON-MED
by Fourrier, M., Coppola, L., Claustre, H., D'Ortenzio, F., Sauzède, R., and Gattuso, J.-P. (2020). Front. Mar. Sci. 7:620. doi: 10.3389/fmars.2020.00620

In the original article, there was an error. The published version of the neural network created a fake seasonality in the output parameters at depth. This has been corrected and a second version of the CANYON-MED neural networks was created.

A correction has been made to the ***Abstract***:

A regional neural network-based method, "CANYON-MED" is developed to estimate nutrients and carbonate system variables specifically in the Mediterranean Sea over the water column from pressure, temperature, salinity, and oxygen together with geolocation and date of sampling. Six neural network ensembles were developed, one for each variable (i.e., three macronutrients: nitrates (NO_3^-), phosphates (PO_4^{3-}) and silicates ($Si(OH)_4$), and three carbonate system variables: pH on the total scale (pH_T), total alkalinity (A_T), and dissolved inorganic carbon or total carbon (C_T), trained using a specific quality-controlled dataset of reference "bottle" data in the Mediterranean Sea. This dataset is representative of the peculiar conditions of this semi-enclosed sea, as opposed to the global ocean. For each variable, the neural networks were trained on 80% of the data chosen randomly and validated using the remaining 20%. CANYON-MED retrieved the variables with good accuracies (Root Mean Squared Error): 0.78 $\mu mol.kg^{-1}$ for NO_3^-, 0.043 $\mu mol.kg^{-1}$ for PO_4^{3-} and 0.71 $\mu mol.kg^{-1}$ for $Si(OH)_4$, 0.014 units for pH_T, 13 $\mu mol.kg^{-1}$ for A_T and 12 $\mu mol.kg^{-1}$ for C_T. A second validation on the ANTARES independent time series confirmed the method's applicability in the Mediterranean Sea. After comparison to other existing methods to estimate nutrients and carbonate system variables, CANYON-MED stood out as the most robust, using the aforementioned inputs. The application of CANYON-MED on the Mediterranean Sea data from autonomous observing systems (integrated network of Biogeochemical-Argo floats, Eulerian moorings and ocean gliders measuring hydrological properties together with oxygen

concentration) could have a wide range of applications. These include data quality control or filling gaps in time series, as well as biogeochemical data assimilation and/or the initialization and validation of regional biogeochemical models still lacking crucial reference data. Matlab and R code are available at https://github.com/MarineFou/CANYON-MED/v2/.

A correction has been made to ***Material and methods, ANN ensemble model*, *Paragraph 1***:

The robustness and reliability of an ANN can be significantly improved by combining several ANNs into an ANN ensemble model (Sharkey, 1999; Linares-Rodriguez et al., 2013). The construction of an ANN ensemble is done in two main steps. First, the individual members of the model are created (as described above in section "Multi-Layered Perceptron"). Second, the combination of the outputs of these members is averaged to obtain the unique ensemble output. Thus, for each neural network [NO_3^-, PO_4^{3-}, $Si(OH)_4$, A_T, C_T, pH_T], the ten best topologies were chosen according to their statistics (as defined in section "Validation Statistics Metrics"). The final output of each neural network ensemble model (ANN-E) corresponds to the mean of the outputs of these ten best ANNs (if falling less than a standard deviation from the mean). Additionally, the best topology (ANN-1) among the ten best was also selected to compare between a one ANN structure and a neural network ensemble.

A correction has been made to ***Material and methods, CANYON-MED, Paragraph 1***:

Based on the CANYON networks (Sauzède et al., 2017) principle, the CANYON-MED neural networks corresponding to neural-network ensemble models (ANN-E) (as described in "ANN Ensemble Model") were developed. Similarly to the work by Sauzède et al. (2017), the chosen input variables for the networks are *in situ* measurements of pressure, temperature, salinity (water mass characteristics), and oxygen together with geolocation (latitude and longitude) and date of sampling. Compared to the CANYON networks, where the year is an input only for pH_T and C_T, the decimal year has been chosen as an input for the six CANYON-MED networks [i.e., NO_3^-, PO_4^{3-}, $Si(OH)_4$, A_T, C_T and pH_T]. This change, namely the transformation from day of year and year to decimal year for each network, was based on the long-term increases in deep nutrients observed in the western basin by Béthoux et al. (1998, 2002), as well as the increases in temperature and salinity in the deep Mediterranean Sea over the past 40 years (Borghini et al., 2014) which demonstrate the need of a temporal component in CANYON-MED networks.

A correction has been made to ***Material and methods, CANYON-MED*, *Paragraph 3***: the following text has been removed.

"Furthermore, in agreement with the CANYON networks, the doy has been modified to account for the periodicity of this measurement [doy 365 (end of December) of a year is similar to doy 1 (beginning of January) of the next year from a chronological perspective]. It was therefore transformed into radians according to:

$$doy_{rad} = \frac{doy^{*}\pi''}{\frac{365}{2}}$$

The authors apologize for this error and state that this does not change the scientific conclusions of the article in any way. The original article has been updated.

REFERENCES

Béthoux, J. P., Morin, P., Chaumery, C., Connan, O., Gentili, B., and Ruiz-Pino, D. (1998). Nutrients in the Mediterranean Sea, mass balance and statistical analysis of concentrations with respect to environmental change. Mar. Chem. 63, 155–169. doi: 10.1016/S0304-4203(98)00059-50

Béthoux, J. P., Morin, P., and Ruiz-Pino, D. P. (2002). Temporal trends in nutrient ratios: chemical evidence of Mediterranean ecosystem changes driven by human activity. Deep Sea Res. Part II Top. Stud. Oceanogr. 49, 2007–2016. doi: 10.1016/S0967-0645(02)00024-23

Borghini, M., Bryden, H., Schroeder, K., Sparnocchia, S., and Vetrano, A. (2014). The Mediterranean is becoming saltier. Ocean Sci. 10, 693–700. doi: 10.5194/os-10-693-2014

Linares-Rodriguez, A., Ruiz-Arias, J. A., Pozo-Vazquez, D., and Tovar-Pescador, J. (2013). An artificial neural network ensemble model for estimating global solar radiation from Meteosat satellite images. Energy 61, 636–645. doi: 10.1016/j.energy.2013.09.008

Sauzède, R., Bittig, H. C., Claustre, H., Pasqueron de Fommervault, O., Gattuso, J.-P., Legendre, L., et al. (2017). Estimates of water-column nutrient concentrations and carbonate system parameters in the global ocean: a novel approach based on neural networks. Front. Mar. Sci. 4:128. doi: 10.3389/fmars.2017.00128

Sharkey, A. J. C. (ed.) (1999). Combining Artificial Neural Nets: Ensemble and Modular Multi-Net Systems. Berlin: Springer.

4.5 Conclusions et perspectives de l'étude

En mer Méditerranée, les méthodes neuronales CANYON et dérivées produisent des estimations peu satisfaisantes des nutriments et des variables du système des carbonates. Une nouvelle approche, CANYON-MED, a ainsi été créée et entraînée comme un ensemble de réseaux de neurones. Cette approche tire profit de la précision élevée avec laquelle les EOVs sont mesurées systématiquement de nos jours (Wang et al. 2019) lors de campagnes en mer ou sur des plateformes autonomes. La méthode est constituée d'un ensemble de 10 perceptrons multi-couches, un type de réseau de neurones. Les paramètres d'entrée de CANYON-MED sont des mesures *in situ* de pression, température, salinité et O_2 ainsi que la position dans l'espace (latitude et longitude) et dans le temps (année décimale). La méthode prédit les nutriments et les variables du système des carbonates avec une précision élevée (0.73, 0.045, et 0.70 μmol kg^{-1} pour NO_3^-, PO_4^{3-} et $Si(OH)_4$ respectivement, et 0.016 unités, 11 μmol kg^{-1} et 10 μmol kg^{-1} pour pH_T, A_T et C_T respectivement). Avec de telles précisions, CANYON-MED peut estimer des variables qui ne sont pas actuellement mesurées par les plateformes autonomes telles que PO_4^{3-}, $Si(OH)_4$, A_T et C_T. CANYON-MED peut également aider à identifier les périodes et les zones de la mer Méditerranée où la densité de données reste trop faible dans l'espace et/ou le temps, ce qui limite la compréhension de certains processus et l'évaluation de la variabilité à long terme. En effet, les domaines spatiaux et temporels où la méthode fournit les résultats les moins satisfaisants sont liés aux faiblesses de la base de données d'entraînement qui ne capture pas suffisamment la variabilité spatio-temporelle. De plus, des régions plus dynamiques telles que les tourbillons de mésoéchelle ou les zones de formation d'eau dense pourraient être moins bien reproduites par CANYON-MED. L'échantillonnage par campagne en mer demeure imparfait de part des limitations de temps bateau, de ressources humaines ou financières ou encore de par les conditions météorologiques qui limitent l'échantillonnage de certaines zones ou à certaines périodes de l'année telles que l'hiver. CANYON-MED a la capacité de « combler les trous » dans les systèmes d'observations de façon rentable, par exemple en complétant les trous dans les séries temporelles (sous réserve de l'absence d'évènements exceptionnels). La méthode peut également être appliquée au large réseau de flotteurs-profileurs BGC-Argo et de planeurs sous-marins équipés de CTD et de capteurs d'O_2, augmentant ainsi le flux de données biogéochimiques à partir de variables de base systématiquement mesurées. CANYON-MED peut également contribuer au contrôle qualité des NO_3^- et du pH_T obtenus à partir de ces plateformes autonomes en fournissant des données pour corriger la dérive des capteurs pendant les déploiements et ajuster les valeurs profondes (e.g. Johnson et al. 2015 ; Johnson et Claustre 2016 ; Sauzède et al. 2020. Dans cette optique, de multiples mouillages eulériens acquièrent et fournissent des mesures de haute qualité et de haute fréquence de la température, de la salinité et de l'O_2 dans la colonne d'eau à des observatoires fixes de la mer Méditerranée (par exemple, les réseaux HYDROCHANGES, EMSO et OceanSITES Schroeder et al. 2013 ;

Dañobeitia et al. 2020). Enfin, puisque la précision des données virtuelles obtenues pour le NO_3^- par cette approche est comparable à celle obtenue avec des plateformes autonomes, son utilisation en océanographie serait bénéfique, notamment pour augmenter les jeux de données utilisés pour l'assimilation de certains modèles régionaux qui manquent encore cruellement de données de référence (Doney et al. 2009 ; Cossarini et al. 2019).

Chapitre 5

Impact de la convection intermittente en Méditerranée nord-occidentale sur le contenu en oxygène, nutriments et carbonates

Sommaire du présent chapitre

5.1 Contexte

Ces dernières décennies, plusieurs modifications rapides ont été observées au niveau des processus physiques et biogéochimiques (Tanhua et al. 2013 ; Malanotte-Rizzoli et al. 2014 ; Schroeder et al. 2016), bien que partiellement masquées par des évènements épisodiques et une forte variabilité régionale. Par exemple, la température et la salinité des eaux profondes ont augmenté depuis 40 ans (respectivement 0,04°C et 0,015, Borghini et al. 2014), phénomène accentué par l'augmentation de température et de salinité dans les eaux intermédiaires qui s'est ensuite propagée dans les eaux profondes par les événements récents de formation intense d'eau dense dans le bassin occidental (Schroeder et al. 2008b). La LIW caractérisée par un minimum d'O_2 dans toute la Méditerranée, est sensible à une diminution globale de l'O_2 prédit par les modèles climatiques et biogéochimiques dans un contexte de dérèglement climatique et notamment face à une augmentation de la stratification de la colonne d'eau qui limite les

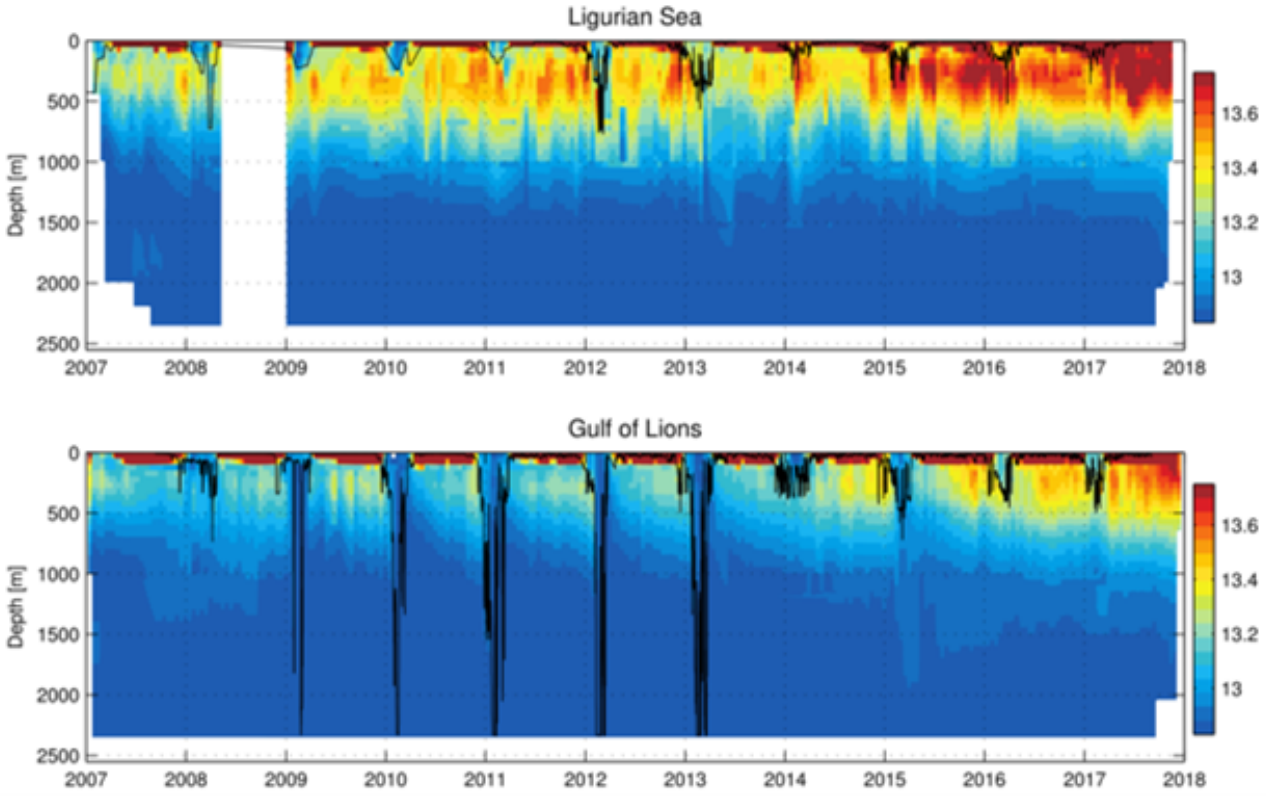

FIGURE 5.1 – Évolution de la température à (haut) DYFAMED (43.41°N 7.89°E) et (bas) LION (42.04°N 4.68°E) en mer Ligure et dans le golfe du Lion respectivement. Les profils dans un rayon de 15 km du mouillage ont été utilisés et « mergés » avec les mesures des mouillages. La ligne noire représente la MLD, calculée selon HOUPERT et al. (2016). Tiré de MARGIRIER et al. 2020.

apports d'O_2 depuis la surface (OSCHLIES 2021 ; SOMOT et al. 2018), et ainsi la ventilation des eaux intermédiaires et profondes. Le manque d'observations sur la variabilité du contenu en O_2 en Méditerranée limite la compréhension de l'impact de la désoxygénation sur le cycle du carbone et les écosystèmes marins. En Méditerranée nord-occidentale a lieu le phénomène de formation d'eaux dense (DWF) principalement dans le Golfe du Lion (HERRMANN et al. 2010 ; SOMOT et al. 2018 ; COPPOLA et al. 2017), où les mélanges hivernaux de LIW avec les eaux de surface produisent les WMDW. En mer Ligure, des phénomènes moins intenses de DWF ont lieu de manière épisodique (SPARNOCCHIA et al. 1994 ; SOMOT et al. 2018). La convection verticale hivernale renouvelle les nutriments dans les couches de surface, et l'efficacité de la convection détermine la disponibilité en nutriments dans la couche euphotique (MAYOT et al. 2017) qui influence alors directement la production primaire. L'impact des évènements de DWF sur les variables physiques dans le bassin nord-occidental a été largement étudié (TESTOR et al. 2018 ; DURRIEU DE MADRON et al. 2017 ; MARGIRIER 2018), figure 5.1).

Les conséquences sur l'O_2 et les variables biogéochimiques ont été étudiées lors d'un effort intense d'observation lors de l'hiver 2012-2013. Ainsi COPPOLA et al. (2017) ont étudié la

ventilation des couches profondes et Kessouri et al. (2017) ont analysé l'effet de la DWF sur les budgets biogéochimiques et la production primaire. En mer Ligure, une étude par Coppola et al. (2018) a analysé l'évolution des caractéristiques des masses d'eau et de la dynamique de l'O_2 au niveau de la série temporelle DYFAMED. Les changements dans les propriétés des eaux profondes du bassin occidental sont principalement le résultat des propriétés des eaux de surface et intermédiaires modifiées par les changements liés au climat qui se propagent en profondeur par l'intermédiaire de la convection profonde (Touratier et Goyet 2011). Il est prévu que l'intensité de la convection profonde diminue en mer Méditerranée (Somot et al. 2006 ; Soto-Navarro et al. 2020), ce qui pourrait entraîner une hypoxie dans les couches intermédiaires et profondes, ayant ainsi des répercussions importantes sur le biotope marin. Pourtant, aucune étude n'a caractérisé les changements temporels de l'O_2 dans les deux zones de la Méditerranée nord-occidentale soumises à la DWF avec des résolutions spatiales et temporelles permettant d'évaluer la réponse de l'O_2 aux événements de mélange hivernal. Ceci est d'autant plus important que les études de modélisation prévoient une évolution vers une stratification accrue et une profondeur de couche de mélange (MLD) plus faible dans le nord-ouest de la mer Méditerranée (Somot et al. 2006 ; Pagès et al. 2020 ; Soto-Navarro et al. 2020), réduisant ainsi les apports de nutriments issus de la convection vers les eaux de surface appauvries en nutriments et impactant directement la reminéralisation de la matière organique et l'export de carbone par une séquestration réduite lors des événements de DWF (Kessouri et al. 2018). Des tendances d'évolution des nutriments ont été déduites d'études réalisées à partir de campagnes en mer mais celles-ci restent limitées dans l'espace, à des stations fixes comme DYFAMED (O. Pasqueron de Fommervault et al. 2015b) ou dans le temps, lors de campagnes en mer annuelles (Kessouri et al. 2018). Quant à l'évolution du système des carbonates en Méditerranée nord-occidentale, la majorité des études se sont concentrées sur la couche de surface et ont soit été restreintes dans l'espace (DYFAMED, Merlivat et al. 2018 ; Coppola et al. 2020a), soit ont estimé des changements par rapport à l'ère préindustrielle (Touratier et al. 2016 ; El Rahman Hassoun 2015).

Au cours de la dernière décennie, un grand nombre de flotteurs Argo équipés de capteurs d'O_2 ont été déployés en mer Méditerranée dans le cadre de multiples programmes tels que l'initiative nationale française « Novel Argo ocean Observing System » (NAOS), un projet visant à promouvoir, consolider et développer le réseau Argo (ex, D'Ortenzio et al. 2020 ; Le Traon et al. 2020) ou MOOXY (projet GMMC 2014-2019, CNRS) complétant ainsi les systèmes d'observation traditionnels (mouillages, campagnes mensuelles et annuelles) et permettant un meilleur suivi de la dynamique de l'O_2 dans la zone. De plus, une méthode basée sur des réseaux de neurones, CANYON-MED (Fourrier et al. 2020) a été développée pour la mer Méditerranée permettant d'estimer NO_3^-, PO_4^{3-}, $Si(OH)_4$, et les variables du système des carbonates : A_T, C_T et pH sur l'échelle totale (pH_T) à partir de la température, de la salinité,

de l'O_2, de la position dans le temps et l'espace. Ainsi, en appliquant CANYON-MED sur le large réseau de flotteurs Argo mesurant l'O_2 et les mouillages fixes dans le bassin nord-occidental, il est possible de dériver ces variables biogéochimiques et d'étudier leurs variations temporelles, par exemple en réponse à la convection dans un contexte de réduction des événements de DWF (Somot et al. 2006 ; Pagès et al. 2020 ; Soto-Navarro et al. 2020).

5.2 Résumé de l'étude

La présente étude analyse les séries temporelles d'O_2 reconstituées à partir de campagnes, de mouillages et de flotteurs Argo dans le golfe du Lion et la mer Ligure, en mettant l'accent sur les eaux intermédiaires appauvries en oxygène (LIW). Les nutriments et les variables du système des carbonates sont décrits et leurs réponses aux évènements de DWF ainsi que leurs tendances en surface, dans les eaux intermédiaires et en profondeur sont discutées. Dans les eaux intermédiaires, le minimum d'O_2 est fortement affecté par le processus de convection intermittent, et les deux zones présentent des réponses différentes aux événements convectifs. Dans les deux zones, au cours de la période 2012-2020, on observe une augmentation globale des nutriments dans les couches intermédiaires et profondes, avec un impact concomitant sur les rapports stoechiométriques augmentant la limitation en phosphore. Les estimations d'acidification dérivées dans différentes couches de la colonne d'eau montrent une augmentation globale de l'A_T et du C_T et une diminution concomitante du pH. Ces tendances ont été fortement affectées par les événements de convection.

5.3 Papier en révision dans *Journal of Geophysical Research : Oceans*

Impact of intermittent Convection in the northwestern Mediterranean Sea on Oxygen content, Nutrients and the Carbonate system

Marine Fourrier [1], Laurent Coppola[1,2], Fabrizio D'Ortenzio[1], Christophe Migon[1], Jean-Pierre Gattuso[1,3]

[1] Sorbonne Université, CNRS, Laboratoire d'Océanographie de Villefranche, F-06230 Villefranche-sur-Mer, France

[2] Sorbonne Université, CNRS, Institut de la Mer de Villefranche, F-06230 Villefranche-sur-Mer, France

[3] Institute for Sustainable Development and International Relations, Sciences Po, Paris, France

Corresponding author : Marine Fourrier (marine.fourrier@imev-mer.fr)

Key Points :

— The strong effect of winter convection on the O_2 minimum in the Mediterranean Sea is investigated through multiple observation platforms
— We provide estimates of nitrate, phosphate and silicate trends.
— Dissolved inorganic carbon increases in intermediate and deep waters with a concurrent pH decrease.

Abstract Using Argo profiling floats, cruises and mooring data, we reconstructed the dissolved oxygen (O_2) dynamics in the Gulf of Lion and in the Ligurian Sea, with a focus on the intermediate waters. By applying the CANYON-MED neural network-based method on the large network of O_2-equipped Argo floats we derived nutrients and carbonate system variables in the Gulf of Lion and the Ligurian Sea at different depths in the water column and derived trends over the 2012-2020 period. In these waters, the O_2 minimum is strongly affected by the intermittent convection process, and the two areas show dissimilar responses to the mixing events. In both areas, over the 2012-2020 period, nutrients increase overall in deep layers, with a concomitant impact on nutrient molar ratios tending towards an increase in P-limitation. Acidification estimates derived in different layers of the water column show an overall increase in dissolved inorganic carbon and a concurrent pH decrease. These trends were strongly affected by convection events.

Plain Language Summary Using multiple observation platforms such as Argo profiling floats (autonomous, free-floating instruments equipped with sensors and profiling regularly in the first 2000 m of the water column), at sea cruises on oceanographic vessels, and moorings (fixed position stations), we reconstructed the dissolved oxygen (O_2) dynamics in the northwestern Mediterranean Sea. The intermediate waters are characterized by an O_2 minimum strongly affected by the intermittent convection process (due to winter forcings and density changes, mixing of water masses occurs over the water column). We also derived nutrients and carbonate system variables (related to acidification) from a neural network methodology developed for the Mediterranean Sea, CANYON-MED, applied on Argo floats equipped with O_2 sensors in different layers of the water column. Over the 2012-2020 period, the derived trends show an overall increase of nutrients in deep layers, with an impact on nutrient limitations. Acidification estimates show an overall acidification. These trends were strongly affected by convection events.

1. Introduction

The Mediterranean Sea is a semi-enclosed marginal sea characterized by a rapid overturning circulation (Millot et Taupier-Letage 2005) where deep-water formation processes happen in both the Western and Eastern basins (Schroeder et al. 2012 and references therein, Pinardi et al. 2019). In the northwestern Mediterranean Sea, the intermediate water masses are characterized by a temperature and salinity maximum in subsurface corresponding to the Levantine Intermediate Waters (LIW) formed in the Eastern basin in late February/early March (Lascaratos et al. 1993). This saline and relatively warm water mass spreads at intermediate

depths (between 200 and 600 m) over the Mediterranean in a westward pathway, entering the Ligurian Sea and flowing within the Northern Current along the southern French coasts on its way to the Strait of Gibraltar. During its transit from the eastern basin, the consumption of organic matter sinking from the surface decreases the O_2 content in this water mass creating an O_2 minimum in the water column (160-170 μmol kg^{-1}, Coppola et al. 2018) and lowering pH_T and increasing dissolved inorganic carbon (C_T ; Álvarez et al. 2014). In the northwestern Mediterranean Sea, which is well ventilated compared to the global ocean (Schneider et al. 2014), Dense Water Formation (DWF) mainly occurs in the Gulf of Lion (Herrmann et al. 2010 ; Somot et al. 2018), where winter mixing of LIW with surface waters produces Western Mediterranean Deep Water (WMDW). In the Ligurian Sea, less intense DWF also occurs episodically (Sparnocchia et al. 1994 ; Somot et al. 2018). The Mediterranean Sea is considered an oligotrophic basin with low annual primary production (Sournia 1973 ; Moutin et Raimbault 2002 ; Reale et al. 2020) and an eastward increasing gradient of oligotrophy (Pujo-Pay et al. 2011). Winter vertical convection replenishes nutrients in the surface layers, and the efficiency of convection determines the availability of nutrients in photic waters (Mayot et al. 2017). The impact of these DWF events on physical variables has been thoroughly documented (Testor et al. 2018 ; Durrieu De Madron et al. 2017 ; Margirier 2018). The consequences on O_2 and biogeochemistry were investigated during an intense observing effort in 2012-2013. Coppola et al. (2017) studied the ventilation of the deeper layers and Kessouri et al. (2017) analyzed the effect of DWF on biogeochemical budgets and primary production. In the Ligurian Sea, a study by Coppola et al. (2018) analyzed the evolution of water mass characteristics and O_2 dynamics at the DYFAMED time-series station.

Changes in the deep-water properties of the western basin are primarily the result of surface properties modified by climate-related changes taking place at the air-sea interfaces which are propagated downwards through deep formation (Touratier et Goyet 2011). It is predicted that the intensity of deep convection will lessen in the Mediterranean Sea (Somot et al. 2006 ; Soto-Navarro et al. 2020) which could lead to hypoxia in intermediate and deep layers, thus having significant impacts on marine biota. Yet, no study has characterized the temporal changes of O_2 in the two areas of the northwestern Mediterranean Sea subjected to DWF with spatial and temporal resolutions enabling to assess the O_2 response to winter mixing events. This is especially important as modeling studies predict an evolution towards enhanced stratification and shallower Mixed Layer Depth (MLD, in meters) in the northwestern Mediterranean Sea (Somot et al. 2006 ; Pagès et al. 2020 ; Soto-Navarro et al. 2020), therefore reducing nutrient inputs from convection to the nutrient-depleted surface waters and directly impacting remineralization of organic matter and carbon export through reduced sequestration during DWF events (Kessouri et al. 2018). Trends in the evolution of nutrients have been derived from ship-based studies but these remain limited in space through fixed stations such as DYFAMED

(O. Pasqueron de Fommervault et al. 2015b) or limited in time through yearly cruises (Kessouri et al. 2018). As for the evolution of the carbonate system in the northwestern Mediterranean Sea, most studies have focused on the surface layer and were either restrained spatially (DYFAMED, Coppola et al. 2020a) or estimated changes relative to the preindustrial era (Touratier et al. 2016 ; El Rahman Hassoun 2015).

In the past decade, a large number of Argo floats equipped with O_2 sensors have been deployed in the Mediterranean Sea through multiple programs such as the French national initiative "Novel Argo ocean Observing System" (NAOS), a project to promote, consolidate, and develop the Argo network (e.g., D'Ortenzio et al. 2020 ; Le Traon et al. 2020) or MOOXY (2014-2019 GMMC project, CNRS) complementing the traditional observing systems (moorings, monthly and yearly cruises) and allowing better monitoring of O_2 dynamics in the area. Moreover, a neural network-based method CANYON-MED (Fourrier et al. 2020) has been developed for the Mediterranean Sea allowing to estimate nitrate (NO_3^-), phosphate (PO_4^{3-}), silicate ($Si(OH)_4$), and carbonate system variables total alkalinity (A_T), total inorganic carbon (C_T), and pH on the total scale (pH_T) from temperature, salinity, O_2, geolocation and date of sampling. Therefore, by applying CANYON-MED on the large network of O_2-equipped Argo floats, biogeochemical variables can be derived and their temporal variations investigated, for example in response to convection in a context of reduction of DWF events (Somot et al. 2006 ; Pagès et al. 2020 ; Soto-Navarro et al. 2020). In the present study, the O_2 time series reconstructed from Argo floats, moorings, and cruises in the Gulf of Lion and the Ligurian Sea, with a focus on the oxygen-depleted intermediate layer (LIW), are analyzed. Nutrients and carbonate system variables derived from Argo float data are described and the responses to DWF and trends at the surface, in intermediate waters, and at depth are discussed.

2. Materials and Methods

2.1. Study area and observational data

2.1.1. DYFAMED and LION sites

The DYFAMED site (Coppola et al. 2020b) is located in the Ligurian Sea (43.41°N, 7.89°E, water depth of 2350 m ; purple star in the blue box figure 5.2). It is surrounded by the permanent geostrophic Ligurian frontal jet flow caused by the Northern Current's cyclonic circulation, separating the sampling area from coastal inputs by a density gradient (Millot 1999 ; Niewiadomska et al. 2008). Monthly cruises with full water column profiles have been performed at the DYFAMED site since 1991 and are included in the MOOSE network since 2010 (J.-C. Marty et al. 2002 ; Coppola et al. 2019). This is the longest open-sea time series in the Mediterranean Sea in terms of O_2, nutrients, and carbonate system measurements. The LION site (Testor et al. 2020) is located in the Gulf of Lion (42.04°N, 4.68°E, water depth of 2400 m, red triangle in the orange box in figure 5.2) in the vicinity of the center of the DWF. At the two sites, moorings are equipped with CTD and oxygen sensors at intermediate depth (around

350 m) and 2000 m. The oxygen data were corrected by applying a slope-offset correction to the Winkler reference data on samples collected monthly and yearly at DYFAMED and yearly at LION (Coppola et al. 2019).

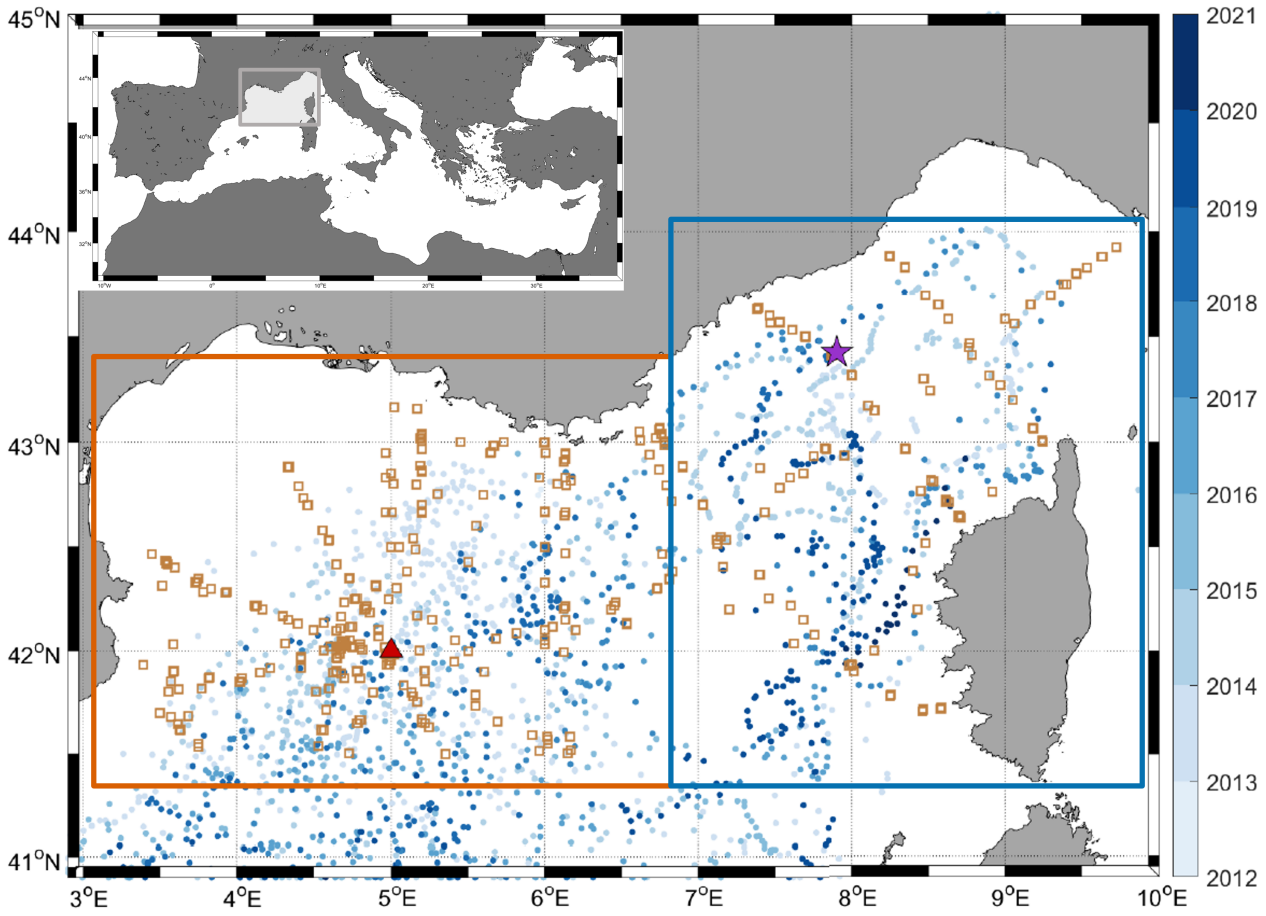

Figure 5.2 – Position of Argo profiling floats profiles equipped with O_2 sensors according to the time of the profile (blue circles), stations from cruises (brown squares), and of the LION (red triangle) and DYFAMED (purple star) mooring sites in the Gulf of Lion (orange box) and Ligurian Sea (blue box) respectively.

Two regions are distinguished : the Gulf of Lion and the Ligurian Sea (figure 5.2, orange and blue box respectively), with a limit chosen at 6.9°E taking into account regional dynamics and ensuring sufficient data in each area.

2.1.2. Argo floats

Data from 18 Argo (Argo 2020) profiling floats deployed in the Mediterranean Sea were used. They were equipped with O_2 sensors (optode Aanderaa) from October 2012 (first deployments of Argo-O_2 floats in the area) to July 2020 (see Supplementary Table 1 and figure 5.2). To ensure data consistency, only the O_2 adjusted in "Delayed Mode" was used. This signifies that the O_2 was checked by the Principal Investigator responsible for the float after adjustment (Bittig et al., 2019). Most of the floats were calibrated during "Delayed Mode" to a reference CTD cast or

climatological value. Only the more recent floats were able to do in air measurements which they were corrected with, enabling a higher quality correction. Of the 18 floats in this study, 4 were corrected for drift during the "Delayed Mode" procedures. Argo floats have been set up to profile every 1 to 5 days to catch the O_2 variability at a 1000 m parking depth. Some floats profiled upwards from 2000 m to the surface while others profiled from 1000 m to the surface.

2.1.3. MOOSE-GE yearly basin-scale cruises

Observations from the yearly MOOSE-GE cruises (Coppola et Diamond Riquier 2008) have also been used. The O_2 measurements were performed using a Seabird SBE43 sensor calibrated with Winkler measurements performed on board. Water samples were collected from CTD-rosette casts equipped with Niskin bottles. Seawater was sampled at different depths from the surface to just above the seafloor once per day. The calibration coefficients of the SBE43 sensor were adjusted for the whole cruise using the least-squares method as described by Coppola et al. (2018). Samples for dissolved inorganic nutrients were collected from Niskin bottles in 20 mL polyethylene bottles. They were analyzed by a standard colorimetric method on a segmented flow analyzer (Autoanalyser II Seal Bran & Luebbe) following Aminot et Kérouel (2007). Samples for C_T and A_T were collected into acid-washed 500 cm^3 borosilicate glass bottles and poisoned with 100 mm^3 of $HgCl_2$, following the recommendation of Dickson et al. (2007). Samples were stored in the dark at 4°C pending analysis. Measurements of C_T and A_T were performed simultaneously by potentiometric acid titration using a closed cell following the methods described by Edmond (1970) and (Dickson et Goyet 1994). Analyses were performed at the National facility for the analysis of carbonate system parameters (SNAPO-CO_2, LOCEAN, Sorbonne Université – CNRS, France).

2.2. Derived variables

Seawater pH on the total scale at in situ pressure and temperature was derived from A_T and C_T data for the MOOSE-GE cruises. Calculations were performed using CO_2SYS-MATLAB (Lewis et Wallace 1998 ; Heuven et al. 2011) using the carbonic acid dissociation constants of Mehrbach et al. (1973) as refit by Dickson et Millero (1987), the dissociation constant for bisulfate of Dickson (1990) and Uppström (1974) for the ratio of total boron to salinity. The MLD was estimated for each float profile based on potential density profiles calculated from pressure, temperature, and salinity data. The MLD was derived using a 0.03 $kg.m^{-3}$ threshold density criterion with a reference depth of 10 meters (D'Ortenzio et al. 2005). The maximum Argo-derived MLD is restricted to 2000 m, i.e. the maximum depth reached by the Argo floats. In the Ligurian Sea over the period of study, few Argo floats were located close to the DYFAMED mooring. As the position of these Argo floats did not allow us to resolve the temporal variation of MLD at the position of the fixed time series, the MLDs calculated from a 3D numerical simulation were used. These estimates were obtained from a simulation of the Mediterranean basin using the SYMPHONIE model (Marsaleix et al. 2008). This model has

already been used to simulate convection in the northwestern Mediterranean (Estournel et al. 2016 ; Herrmann et al. 2008) and its impact on biogeochemistry (Kessouri et al. 2018) and oxygen budget (Ulses et al. 2021) for which the MLD is a key parameter. Furthermore, the MLD calculated by this model at DYFAMED was also used by Heimbürger et al. (2013) and O. Pasqueron de Fommervault et al. (2015c). The numerical domain of the model has a mesh size ranging from 0.8 km in the north to 1.4 km in the south of the Mediterranean Sea (Ulses et al. 2021). In the present study, the daily median MLD using the 0.03 $kg.m^{-3}$ criterion over a 20 km area around the DYFAMED location was extracted from the simulation (supplementary data) and is used in figures 5.3, 5.4 and Supplementary figure 1.

In the western Mediterranean Sea, the O_2 Minimum Layer (OML) often coincides with the mean LIW depth (300-450 m ; Tanhua et al. 2013). In this layer, O_2 consumption is higher than O_2 replenishment through diffusive and advective processes (Packard et al. 1988 ; Tanhua et al. 2013 ; Coppola et al. 2018). In this study, the depth of the LIW was determined as either the salinity or temperature maxima deeper than the 29 kg m^{-3} isopycnal. Margirier et al. (2020) proposed this method as a way to better track the LIW in T/S space rather than restricting it to a fixed depth. In some cases for winter profiles, the water column is completely homogenized because of mixing, therefore the depth of the LIW was determined in this homogeneous layer. To study the impact of winter convection events on intermediate layers, Argo float data are compared with mooring data (DYFAMED for the Ligurian Sea profiles, and LION for the Gulf of Lion profiles) at the corresponding depth, and with bottle data less than 15 days apart and less than 20 km apart. By applying the CANYON-MED neural networks (Fourrier et al. 2020), NO_3^-, PO_4^{3-}, $Si(OH)_4$, A_T, C_T, and pH_T were derived from float data.

2.3. Statistical analyses

Temporal trends over the period 2013-2020 were computed at different depths for the biogeochemical variables of interest. After removing the seasonal component through a yearly moving average, we used a Student test to detect trend significance (p-value < 0.01).

3. Results

3.1. Variability of the O_2 concentrations in the northwestern basin

figure 5.3 shows the time series of O_2 in the Gulf of Lion (figure 5.3a) and Ligurian Sea (figure 5.3b) as reconstructed from Argo floats, mooring data, and monthly and yearly cruises. For each area, O_2 data was interpolated over a grid with a 5-day step and with an adapted vertical resolution (metric over the first 10 m, with a 10 m-step until 200 m, and a 25 m-step until the bottom). Mooring data, monthly and yearly cruises were filtered down to a five-day sampling frequency and gridded on the same grid as the Argo data. The coupling of these high-frequency measuring platforms allows for a reconstruction of O_2 dynamics in the two areas. In the Gulf of Lion, MLD increases to around 2000 m in the winter 2012-2013 and to 1900 m at the beginning

of 2018. In the Ligurian Sea, monthly cruises allow for a reconstruction of the O_2 time series with fewer gaps than for the Gulf of Lion (figure 5.3b). However, fewer Argo floats are located in the area, and float-derived MLD data is sparse. Therefore, specifically for the Ligurian Sea, a modeled MLD (median of 20 km around DYFAMED) is also used to complement the incomplete Argo-derived MLD. O_2 follows the classical vertical distribution with higher O_2 in surface waters in contact with the atmosphere (> 225 μmol kg^{-1}), a minimum in intermediate layers (LIW), and a subsequent increase with depth. The O_2 minimum spreads in the Gulf of Lion between 300 and 600 m with concentrations lower than 170 μmol kg^{-1}. In the Ligurian Sea, the O_2 minimum in intermediate waters spans from 250 to more than 600 m with a mean concentration of around 165 μmol kg^{-1}. In both areas, the O_2 minimum is periodically interrupted in winter.

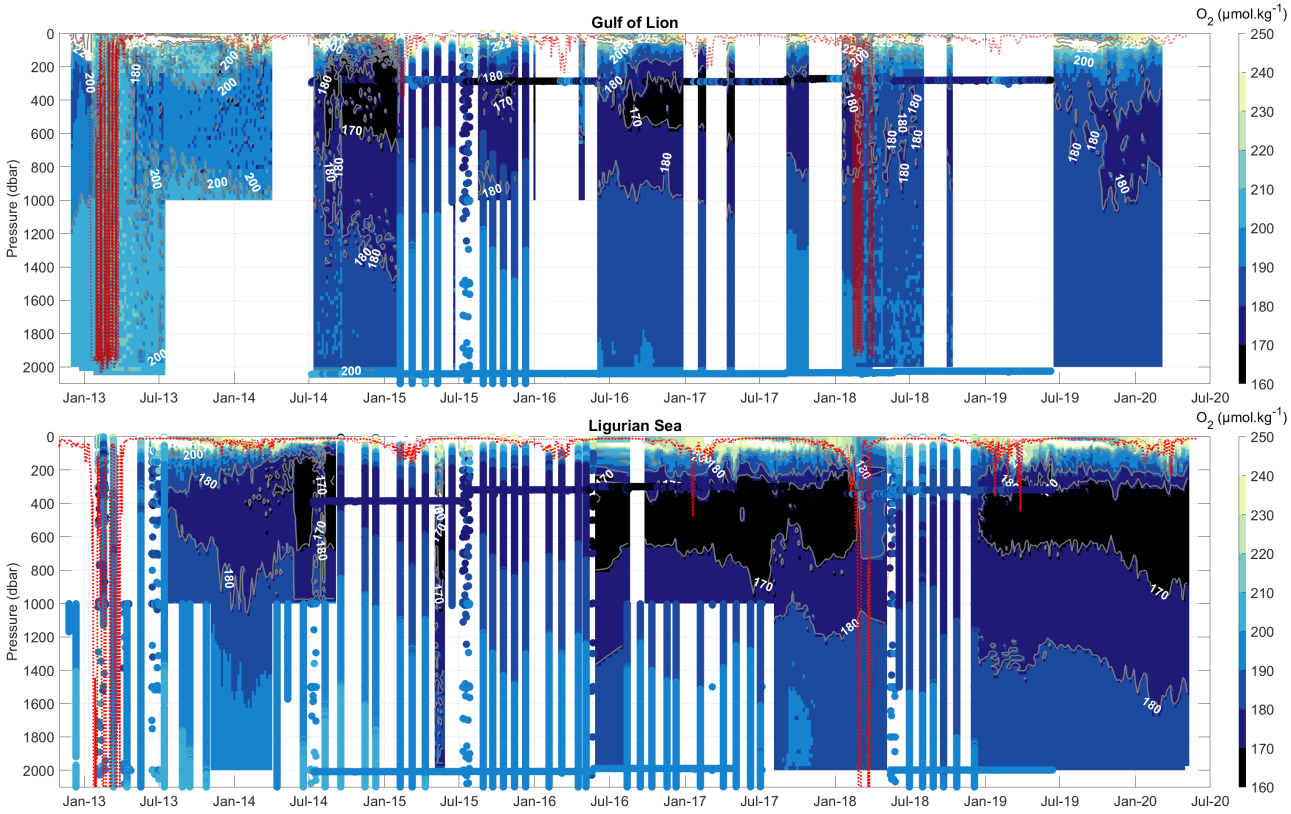

FIGURE 5.3 – Time series of O_2 from profiling floats, moorings and cruises in the Gulf of Lion (a) and Ligurian Sea (b), and Mixed Layer Depth (MLD ; dark red line). For the Ligurian Sea, the median modelled MLD (bright red line) completes the MLD derived from Argo floats.

To better study the effect of deep-water formation on the O_2 minimum in the intermediate layers of the northwestern Mediterranean Sea, Argo, mooring, and cruise data were extracted at the depth of the mooring (around 350 m), for the Gulf of Lion (figure 5.4a) and the Ligurian Sea (figure 5.4b). In the Gulf of Lion at the depth of the mooring, O_2 ranges from 160 to 210 μmol kg^{-1}. All instrumental platforms show periodic increases of O_2 followed by subsequent decreases over time. There is a strong covariance of O_2 from Argo, mooring, and cruise data

at the mooring depths (supplementary figure 1). These platforms used together allow a better reconstruction of the O_2 dynamics. In the Ligurian Sea, Argo floats data is scarce. O_2 also ranges from 160 to 210 μmol kg^{-1} in this area. All platforms capture a strong O_2 increase in winter 2013 (around 30 μmol kg^{-1}) and at the beginning of 2018 (up to 40 μmol kg^{-1}).

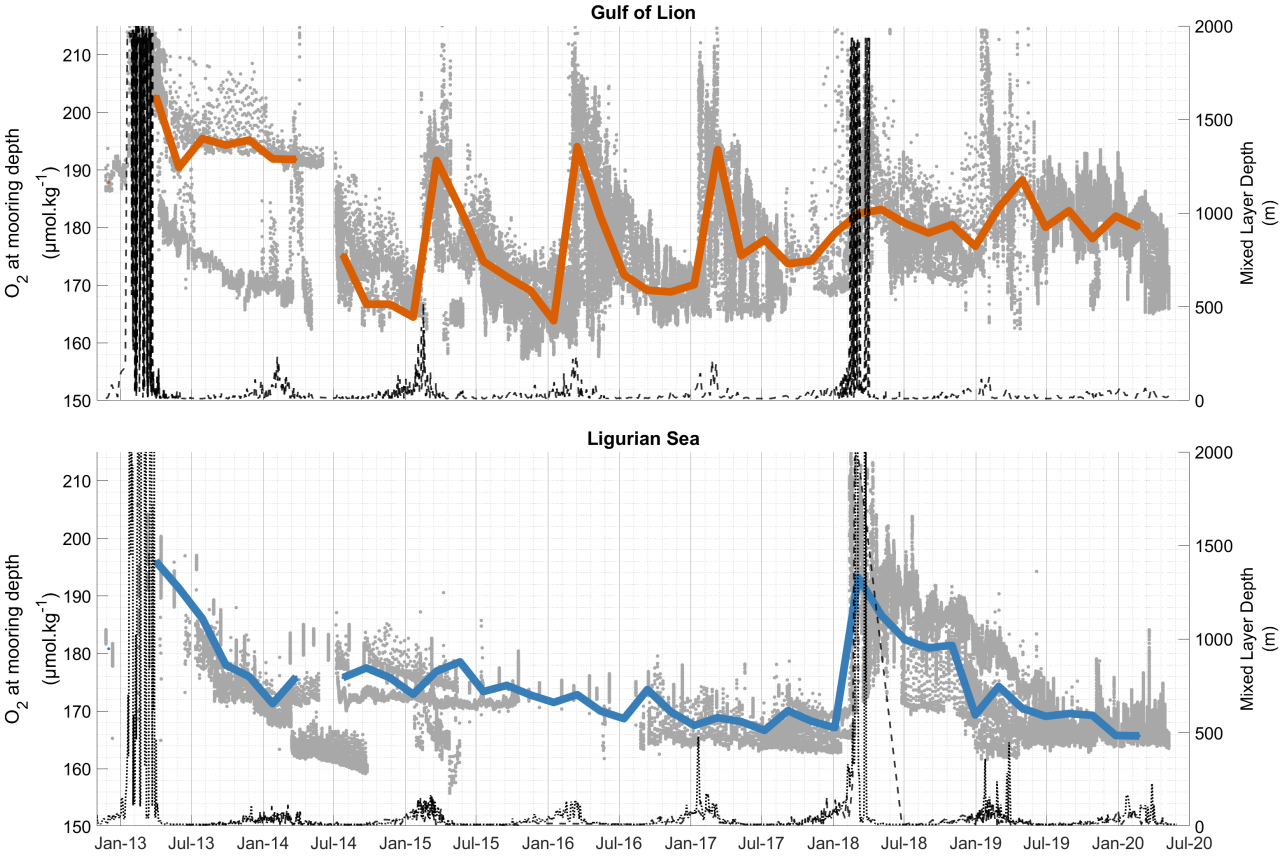

FIGURE 5.4 – Time series of median O_2 at the depth of the mooring in the Gulf of Lion (a, orange) and the Ligurian Sea (b, blue) from all platforms. The colored line represents the median signal. The Mixed Layer Depth (MLD in meters, black line) was computed with a 0.03 density threshold (D'ORTENZIO et al. 2005). For the Ligurian Sea, the median modelled MLD completes the MLD derived from Argo floats.

Based on the consistency of the different platforms used in this study at the depth of the mooring (detailed in figure S2), a median O_2 signal using all available data was derived in both areas of study at the mooring depth and is presented in figure 5.4, together with the MLD from Argo floats and modeled MLD for the Ligurian Sea (same as in figure 5.3) in both areas. In the Gulf of Lion (figure 5.4a), there is a yearly seasonal cycle with increases in winter of about 30 μmol kg^{-1} (highest values around February) and decreases from April onwards until the following winter. In winter 2012-2013, O_2 increased in the intermediate layers up to 210 μmol kg^{-1}. The spatial variability remained high in summer 2013 as demonstrated by the spread around the median value (about 20 μmol kg^{-1} of difference). From January 2013 to January

2014, an Argo float left the mixed area explaining the decreasing signal from 190 to 170 μmol kg^{-1} by January 2014. Variations occur in the yearly seasonal cycle with an increase in the minimum values of around 10 μmol kg^{-1} between the end of 2014 and the end of 2019. In the Ligurian Sea (figure 5.4b), O_2 in the intermediate waters does not exhibit the same yearly seasonal cycle as the Gulf of Lion. In winter 2013, O_2 increased from 170 μmol kg^{-1} at the end of 2012 to a higher amount (higher than 200 μmol kg^{-1}) and returned to 170 μmol kg^{-1} almost a year later. Afterwards, O_2 steadily decreased between January 2014 and January 2018 by 0.75 μmol kg^{-1} year-1 in that area. At the beginning of 2018 O_2 increased up to 210 μmol kg^{-1} in the intermediate waters with a slow decrease afterward. A year later, in June 2019, O_2 remained higher than the year before leveling with values around 170 μmol kg^{-1}. From October 2019 onwards, O_2 remained stable.

3.2. Carbonate and nutrient variability

CANYON-MED-derived nutrients and carbonate system variables at the surface, in intermediate layers (in the LIW), and at depth (around 2000 m) in the Gulf of Lion and the Ligurian Sea are in agreement with the data collected during the monthly and yearly cruises (figure 5.5 ; Supplementary figure 2).

At the surface, all variables display clear seasonal cycles with large amplitudes, also present in the bottle reference data (squares on figure 5.5) and no clear trend emerges at that depth. Nutrients exhibit a maximum at the end of winter and a minimum in summer, with a seasonal range twice larger in the Gulf of Lion than in the Ligurian Sea. A_T, C_T, and pH_T also vary seasonally with maxima in winter and minimal values in summer. There is no clear difference between the two areas in terms of seasonal range. In both areas, lacking data in specific seasons or years hinders the analysis of the seasonal cycles. In the LIW and at depth, nutrients, C_T increased throughout the 2013-2020 period as pH_T decreased (figure 5.5, table 5.1). However, the rate of change differs between regions (Gulf of Lion vs Ligurian Sea) and depths (LIW vs 2000 m). In the Gulf of Lion in the LIW, only NO_3^- exhibit an increase over the 2013-2020 period. During the winters 2012-2013 and 2017-2018, nutrients present a large range (up to 2 μmol kg^{-1} for NO_3^-). In the Ligurian Sea, no trend is significant in the LIW. At about 2000 m, the three macronutrients increase over the study period, and the impact of the 2012-2013 winter event and, to a lesser extent, the 2017-2018 winter event, are visible. While NO_3^- and $Si(OH)_4$ have similar rates of increase between the two study areas, at depth, PO_4^{3-} increases twice faster in the Ligurian Sea than in the Gulf of Lion (0.0034 and 0.0016 μmol kg^{-1} year^{-1} respectively). In the LIW, C_T increases in both areas with a concomitant pH_T decrease. In intermediate layers, lower A_T, C_T, and higher pH_T are observed in winter than in other seasons. The periodic increase in pH_T is large enough to affect the slope of decrease, but with pH_T reaching similar values by the end of 2020 in both areas. At depth, C_T increases at a similar rate in both areas, while for pH_T the trend is only significant in the Gulf of Lion.

TABLEAU 5.1 – Estimates of nutrients and carbonate variable changes in the northwestern Mediterranean Sea. For the area, GOL corresponds to the Gulf of Lion and LIG to the Ligurian Sea. If not specified, pH is on the total scale, (S) refers to pH on the seawater scale, and the asterisk to deltas over the period. Only significant trends are reported in the table.

Variable	Area	Data type	Period	Surface trend	LIW trend	Deep trend	Reference
NO_3^- (μmol kg^{-1})	GOL	CANYON-MED	2013-2020		0.158±0.03	0.135±0.05	this study
	LIG	CANYON-MED	2013-2020			0.129±0.08	this study
	LIG	Shipborne	1991-2011			0.23%	O. PASQUERON DE FOMMERVAULT et al. (2015a)
PO_4^{3-} (μmol kg^{-1})	GOL	CANYON-MED	2013-2020			0.0016±0.0016	this study
	LIG	CANYON-MED	2013-2020			0.0034±0.002	this study
	LIG	Shipborne	1991-2011			-0.62 %	O. PASQUERON DE FOMMERVAULT et al. (2015a)
$Si(OH)_4$ (μmol kg^{-1})	GOL	CANYON-MED	2013-2020			0.175±0.078	this study
	LIG	CANYON-MED	2013-2020			0.187±0.111	this study
	LIG	Shipborne	1991-2011			0.60%	O. PASQUERON DE FOMMERVAULT et al. (2015a)
A_T (μmol kg^{-1})	GOL	CANYON-MED	2013-2020				this study
	LIG	CANYON-MED	2013-2020				this study
	LIG	Shipborne	1998-2016	0.5±0.21	0.80±0.08	0.84±0.132	COPPOLA et al. (2020a)
C_T (μmol kg^{-1})	GOL	CANYON-MED	2013-2020		2.743±0.60	1.20±0.39	this study
	LIG	CANYON-MED	2013-2020		2.56±1.31	1.60±1.13	this study
	LIG	Shipborne	1998-2016	0.59±0.34	1.18±0.09	1.36±0.161	COPPOLA et al. (2020a)
	LIG	Mooring	1995-1997, 2013-2015	1.40±0.15			MERLIVAT et al. (2018)
pH_T	GOL	CANYON-MED	2013-2020		-0.0022±0.016	-0.0016±0.0005	this study
	GOL	TrOCA method	Preindustrial-2011	-0.15 to -0.11	-0.15 to -0.11	-0.12 to -0.11	TOURATIER et al. (2016)
	GOL	Modelling	Preindustrial-2001	-0.084±0.001		-0.006 to -0.005	PALMIÉRI et al. (2015)
	GOL	Shipborne	Preindustrial-2013		-0.075 (S)*	-0.12 (S)*	EL RAHMAN HASSOUN (2015)
	LIG	CANYON-MED	2013-2020		-0.0016±0.016		this study
	LIG	Shipborne	1998-2016	-0.003±0.001	-0.001±0	-0.002±0	COPPOLA et al. (2020a)
	LIG	Mooring	1995-1997, 2013-2015	-0.0022±0.0002 (S)			MERLIVAT et al. (2018)
	LIG	Shipborne	1995-2011	-0.003±0.001 (S)			MARCELLIN YAO et al. (2016)

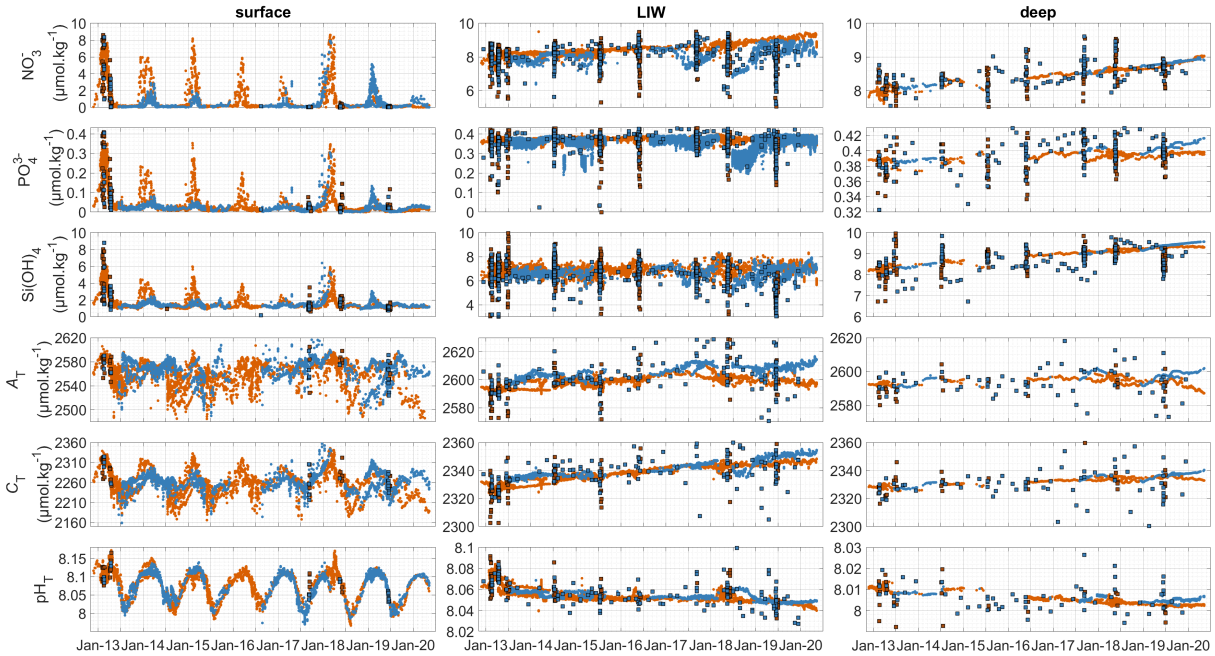

FIGURE 5.5 – Biogeochemical evolution of the northwestern Mediterranean Sea. Panels a-f shows the evolution in the surface waters (with high seasonal variability), panels g-l at the intermediate waters (at the depth of the LIW), and panels m-r at 2000 m, for nitrates (a, g, m), phosphates (b, h, n), silicates (c, i, o), total alkalinity (d, j, p), total carbon (e, k, q) and pH_T (f, l, r). The range changes between panels to better represent the values in the corresponding layer. CANYON-MED derived values from Argo float data are represented as dots (orange for the Gulf of Lion and blue for the Ligurian Sea). Bottle measurements are superimposed as colored squares according to their area. The bottle data come from a 15 day- 25 km- matchup with the CANYON-MED derived values from Argo floats.

4. Discussion

4.1. O_2 evolution with DWF events

The episodic ventilation of the intermediate and deeper layers by deep convection is a major source of O_2 for these water masses that are propagated in the western Mediterranean Sea through circulation. TAMBURINI et al. (2013) have shown that the spreading of dense waters from the Gulf of Lion ventilates deep layers, moving south and east, thus affecting areas such as the Ligurian Sea. ULSES et al. (2021) have also demonstrated that the newly formed deep waters flow south and west, which might be the case for highly convective events such as winter 2012-2013. In the Gulf of Lion, convection is especially intense due to the strong wind forcings preconditioning the area combined with the cyclonic circulation (TESTOR et al. 2018). In the Gulf of Lion, annual bottom-reaching convection occurred in winter from 2009 to 2013 (MARGIRIER et al. 2020), ventilating the intermediate waters where the OML is present. In winter 2012-2013, mixing reached more than 2000 m (figure 5.3a, 5.4a) and homogenized the whole water column.

The O_2 minimum disappeared and O_2 increased to more than 200 μmol kg^{-1} in intermediate waters. After restratification, the O_2 minimum reformed with a thickness ranging from 200 to 550 m, and values down to less than 170 μmol kg^{-1}. From 2014 to 2017, the winter convection remained limited to 500 m (Margirier et al. 2020), leading to an increase in temperature and salinity in the intermediate layers. In 2018, intense deep convection occurred reaching at least 1900 m (as captured by the Argo floats), weakening the O_2 minimum (figure 5.3a, 5.4a). Consequently, O_2 remained at relatively high values in the intermediate layer (around 175 μmol kg^{-1}) from March 2018 to January 2019 without an O_2 minimum until the last mixing event in winter 2018-2019 as captured by the fixed mooring data (LION and DYFAMED). By the end of 2019, the O_2 minimum had reformed with values around 170 μmol kg^{-1} but deeper (400 m to 750 m). In the deep layers, the lack of data prevents getting a clear picture of the effects of the deepening of the mixed layer depth on O_2, with the exception of the winter of 2012-2013 when a deepening to more than 2000 m was captured by Argo floats and increased the O_2 concentration at depth to about 205 μmol kg^{-1} (figure 5.3a). O_2 slowly decreased from 203 μmol kg^{-1} to 193 μmol kg^{-1} in this layer between summer 2014 to summer 2019. In contrast to the 2012-2013 winter mixing, the event of winter 2018-2019 did not affect much the O_2 concentration trend at the depth of the mooring. Furthermore, the 2013 convective event in the Gulf of Lion may have induced increases in O_2 at depth in the Ligurian Sea through dense water spreading (Coppola et al. 2017), and the 2018 increase in O_2 at depth may result from a combination of the Ligurian Sea deep convection and the spreading of water masses from the Gulf of Lion deep convection. However, the OML is ventilated through local convective events. The detection of the convective events with Argo floats is consistent with previous studies, although Margirier et al. (2020), using the MLD criterion of Houpert et al. (2016), reported a maximum depth of convection of 2330 m in 2013, which cannot be captured by Argo floats that profile down to 2000 m. Between 2014 and 2017, Margirier et al. (2020) detected maximum depths reached by winter convection ranging between 420 m and 710 m while the Argo floats detected shallower deepenings (500 m at most). This difference is due to the irregularity of the Argo data and the location of the floats relative to the convective area (figure 5.2). The 2018 convective event in the Gulf of Lion is a result of multiple ML deepenings (with a cold winter period in 2018-2019) and its effect on the O_2 distribution over the water column appears limited with no ventilation of deep waters as compared to the 2013 DWF event, during which the volume of deep water formed ranged from 1.5x10^{13} m^3 (Coppola et al. 2017) to 5 to 7x10^{13} m^3 (Testor et al. 2018). The difference between the 2012-2013 and 2017-2018 events can be attributed to several factors : (1) the convective surface area estimated by Margirier et al. (2020) is half the surface reported by Houpert et al. (2016) or Testor et al. (2018) for intensive convective years, (2) large-scale to submesoscale structures mixing waters varied between the two events (eddies, SCVs ; Bosse et al. 2015 ; Bosse et al. 2017 ; Testor et al. 2018, and (3) preconditioned

states differed. Indeed, from 2009 to 2013, all winter convections reached the bottom, while between 2014 and 2018, in the absence of convection, the intermediate layers rapidly evolved to a warmer and saltier state. This led to a thickening of the LIW and thus to a considerable input of salt into the intermediate layers. This amount of salt in the intermediate layers is a good indication of the future convective state for the following winter (Testor et al. 2018; Margirier et al. 2020). In the Ligurian Sea, weaker atmospheric forcings than in the Gulf of Lion lead to episodically occurring convection events (Estournel et al. 2016). In the Ligurian Sea, lacking MLD data due to the limited number of Argo floats in the area was compensated using modeled MLD data around the DYFAMED mooring (figure 5.3b, 5.4b). At the beginning of 2013, glider transects from Nice to Calvi captured a strong mixing event with a deepening of the mixed layer to at least 800 m (gliders in their study being limited to 1000 m) (Bosse et al. 2017) and modeled MLDs increased to more than 2000 m (whereas no Argo float were present in the area hindering the retrieval of Argo-derived MLDs). In the following summer, shipborne observations revealed an O_2-enriched (around 195 μmol kg^{-1}) layer between 300 and 1200 m (Bosse et al. 2017). The O_2 minimum was reformed more than a year later by summer 2014 and its O_2 content decreased from January 2014 by 1 μmol kg^{-1} per year until the convection event of 2018 (figure 5.4b). This slow decrease differs from the one reported at the DYFAMED site by Coppola et al. (2018) who reported a decrease of 5 μmol kg^{-1} per year on average over the 1994-2005 period. However, in the period 2007-2014, their results showed a stable concentration of around 180 μmol kg^{-1}. In winter 2018, modeled MLD data reveal a mixing event up to 2000 m with an increase in O_2 up to more than 210 μmol kg^{-1}. This episodic mixing event may also have slowed the decreasing trend in O_2 in the OML as the 2006 intense mixing in the Gulf of Lion (Coppola et al. 2018) is considered to have happened before. With no apparent mixing until the end of our time series, the O_2 minimum remained stable (168 μmol kg^{-1}) and spread from 350 m to more than 800 m by July 2020. In the Ligurian Sea, the high variability in O_2 along the time series (figures 5.4b and 5.5b, Supplementary figure 1) stems from the different locations of the mooring and Argo data. The Argo profiles were mainly located West of Corsica, where a vein of LIW is strongly located with lower O_2 concentrations. In the Ligurian Sea, the 2018 winter was the last cold winter with important heat loss at the beginning of March, inducing mixing up to 1000 m caught by the DYFAMED mooring or up to 2000 m as modeled. The ventilation of the OML is especially important as the Mediterranean circulation influences the Atlantic Ocean through the intermediate and deep waters flowing through Gibraltar where changes in temperature, salinity, and O_2 in the outflowing waters could affect the North Atlantic (Schroeder et al. 2016).

4.2. Nutrient dynamics

In the oligotrophic northwestern Mediterranean Sea, one of the only regions where a yearly phytoplankton bloom occurs (Lavigne et al. 2013), winter mixing of the water column induces

the upwelling of bioavailable nutrients from deep water masses to the surface (J. C. Marty et Chiavérini 2010 ; Estrada et al. 2014 ; Severin et al. 2014 ; Ulses et al. 2016) and the refueling of the photic layer influencing the intensity of the spring phytoplankton blooms (Lévy et al. 1999 ; Migon et al. 2002 ; Ulses et al. 2016). The efficiency of winter vertical convection is a main determinant of the availability of nutrients in surface waters and of phytoplanktonic blooms during the subsequent late spring (Lavigne et al. 2013) and the consecutive export of particulate organic carbon (POC) at depth. However, Macias et al. (2018) projected that, by the year 2030, the main control of primary production in the northwestern Mediterranean Sea may likely change from deep winter convection to a condition where mesoscale activity will have a predominant role for nutrient delivery into the euphotic layer, which could in return cause a phenological change of plankton seasonality.

At the surface (figure 5.5a-c, Table 5.1, Supplementary figure 2), no trends were significant. During our study period (2013-2020), nitrate concentrations increased in the LIW (figure 5.5g) and nutrients increased at depth (figure 5.5m-o) in the Gulf of Lion and at depth in the Ligurian Sea for nitrates and siliactes (Table 5.1). Specifically NO_3^-, and $Si(OH)_4$ increased at depth with no significant difference between the two areas (figure 5.5m,o table 5.1). In the Ligurian Sea, at the DYFAMED site, O. Pasqueron de Fommervault et al. (2015b) found a significant increase in NO_3^- of 0.23% per year, while $Si(OH)_4$ had no significant trend (Table 5.1). They also detected an abrupt change in 2005-2006 for NO_3^-, PO_4^{3-}, $Si(OH)_4$, characterized by a slight but statistically significant increase in nutrient concentration linked to the intense winter convection observed in 2005 and in 2006 that led to the formation of new warmer and saltier Western Mediterranean Deep Water (WMDW ; Smith et al. 2008 ; López-Jurado et al. 2005 ; Font et al. 2007 ; Schröder et al. 2006 ; Schroeder et al. 2010). This can be compared to the impact the 2012-2013 DWF event had on nutrients at depth with a high dispersion of NO_3^- and $Si(OH)_4$ in the Gulf of Lion and, to a lesser extent, on PO_4^{3-} (figure 5.5 g-i, m-o), the mixing of enriched deep waters with depleted surface waters causing a large dispersion in nutrients (up to 2, 0.1 and 3 μmol kg^{-1} respectively for NO_3^-, PO_4^{3-} and $Si(OH)_4$) in intermediate and deep waters.

The response of nutrients to ML dynamics remains nuanced : to a certain extent, deeper MLDs lead to more efficient refueling of nutrients in surface waters. However, Heimbürger et al. (2013) suggested that a succession of ML deepenings, even though of lesser magnitude, can be more efficient than a single one. While our data show increasing trends in both areas with an increase three times larger in the Ligurian Sea than in the Gulf of Lion, O. Pasqueron de Fommervault et al. (2015b) found a decrease in PO_4^{3-} at depth of -0.62%/year over the period 1991-2011. However, their study considered the layer from 800 m to the bottom whereas the focus of the present paper is on the layer around 2000 m. Furthermore, O. Pasqueron de Fommervault et al. (2015b) hypothesized that the formation of new warmer and saltier

WMDW in 2006 led to the uplift of the old WMDW by several hundreds of meters (Schroeder et al. 2008b ; Schroeder et al. 2013), increasing nutrient concentrations over the 800 to 2000 m depth range. In the intermediate layer, the increase of nutrients is linked to remineralization along the LIW's path (Schroeder et al. 2020) and the periodic inputs through convective winter events. Moreover, high productivity in the upper layers caused more intense remineralization in the intermediate layers. At the annual scale for 2013, Kessouri et al. (2017), estimated that the DWF area was a sink of NO_3^- and PO_4^{3-} in intermediate layers and a source of organic nitrogen and phosphorus throughout the water column for the surrounding regions through circulation. Below 200 m depth, O. Pasqueron de Fommervault et al. (2015b) found no clear seasonal variability in nutrients. In our data, the large scatter of nutrient concentration in the intermediate layer is linked to the spatial distribution of the float profiles (figure 5.2) and to the consequences of the mixing events. The nutrient increases in intermediate waters are close to the Redfield's model (C :N :Si :P :-O_2 = 106 :16 :15 :1 :-172 ; Pujo-Pay et al. 2011), indicating faster remineralization of NO_3^- than of $Si(OH)_4$ and PO_4^{3-} (Schroeder et al. 2020). Higher N :P ratios in intermediate waters could be a signature of the original eastern Mediterranean waters contributing to its formation (Krom et al. 2005) or of the activity of heterotrophic communities in the Mediterranean mesopelagic layer (Rahav et al. 2019).

The concurrent increase of some nutrients in both the LIW and at 2000 m can be the result of many interplaying factors. First, the different evolutions between nutrients led to a significant increase in the N :P ratio at all depths (data not shown), yielding an increasing P-limitation relative to Redfield's model, consistent with the findings of O. Pasqueron de Fommervault et al. (2015b) at DYFAMED. Indeed, the N :P ratio is always high in the atmospheric material (Bartoli et al. 2005 ; Krishnamurthy et al. 2010 ; O. Pasqueron de Fommervault et al. 2015c), and the impact of atmospheric deposition is particularly important in the whole Mediterranean Sea (Christodoulaki et al. 2013 ; O. Pasqueron de Fommervault et al. 2015c). This P-limitation increased faster in the Gulf of Lion than in the Ligurian Sea through a decoupling between NO_3^- and PO_4^{3-} trends (nitrates increased while phosphates did not significantly evolve). Second, physical circulation of the water masses in this area may have brought nutrient inputs from the southeast through advection and isopycnal diffusion from the West Corsica current. Third, due to the marked decrease in convection and mixing, water masses might have evolved from a structure with multiple water masses overlapping at the bottom to a more homogeneous monolayer situation. This enables a better detection of nutrient increases in the deep water masses through remineralization processes. O_2 decreased at depth in both the Gulf of Lion and Ligurian Sea, which is consistent with the signature of remineralization caused by higher microbial activity. Fourth, the decrease of local convective events would likely result in weaker replenishment in surface and accumulation of nutrients at depth. In the North Atlantic, Williams et Follows (2003) have shown the accumulation of nitrates at the bottom

in the absence of advection. Similarly, in the absence of convection these nutrients are no longer upwelled to the surface and/or diffused through advection.

4.3. Carbonate system variability

The characteristics of acidification of the Mediterranean Sea are linked to its biogeochemical characteristics and circulation features (Álvarez et al. 2014 ; Hainbucher et al. 2014). Specifically, it is known to absorb more anthropogenic CO_2 per unit area (Palmiéri et al. 2015) due to the high A_T values (linked to the high salinities of the Mediterranean Sea caused by evaporation). This increases its capacity to absorb but also buffer anthropogenic CO_2. The short timescale at which the deep waters are ventilated (Schneider et al. 2014) allows for deeper penetration of CO_2, therefore lowering pH_T. Specifically, carbon sequestration stems from two main causes, the physical and biological pumps, both intricately linked to the intermediate waters (Schroeder et al. 2020). First, the cooling of surface waters increases CO_2 absorption, and during DWF events CO_2-enriched water masses deepen and consequently sequester CO_2 through the physical pump (Touratier et al. 2016 ; Cantoni et al. 2016). Second, through the biological pump, the uptake of CO_2 during photosynthesis is followed by its release at depth when the sinking organic matter is remineralized, mainly occurring in the intermediate layers (Bethoux et al. 2005). The distribution of pH is a result of the equilibrium between ocean mixing, biological production and remineralization, precipitation and dissolution of calcium carbonate, and temperature and pressure changes across the water column (Lauvset et al. 2020). In the global ocean, the most important natural process controlling pH in the ocean interior is organic matter remineralization (Lauvset et al. 2020). In the Mediterranean Sea, high rates of organic matter remineralization are observed in intermediate and deep waters related to the downward export of dissolved organic carbon (Lefévre et al. 1996), especially during winter DWF events (Copin-Montégut et Avril 1993), thus having a large influence on pH. In the intermediate layers, increased respiration and organic matter remineralization also lower pH_T and increase C_T, decreasing the buffering capacity (Urbini et al. 2020 ; Álvarez et al. 2014). At the surface, no trend is significant. In intermediate waters, our results for C_T and pH_T are similar to estimates by previous studies. However, at depth, the rate of decrease is two to four times lower than previously described. This difference may be explained by the peculiar location of Argo floats, west of Corsica, for most of our Ligurian Sea profiles. C_T increased twice faster in intermediate waters than previously estimated (Coppola et al. 2020a ; Table 5.1) while at depth the results were much more similar. It should be noted that the trends at intermediate depths described by Coppola et al. (2020a) spanned over the 300-800 m layer whereas ours focused on the area around the O_2 minimum, therefore covering a smaller vertical portion. Furthermore, the periods studied while having an overlap are different (1998-2016 for Coppola et al. (2020a) versus 2013-2020 for the present study) and were subjected to different winter mixing events (both in terms of frequency and intensity) between both periods. The

distribution of C_T in the water column is driven by an equilibrium between the biological pump, which lowers C_T at the surface and increases it at intermediate depths, and the physical pump which exchanges CO_2 at the air-sea interface. Strong mixing events episodically bring together intermediate waters with cold surface waters poorer in A_T and C_T, with a higher pH_T and depending on convection strength C_T-enriched deep waters with a lower pH_T as compared to the intermediate waters. The effect is particularly strong on pH_T changing the slope of decrease, but with pH_T reaching similar values by the end of 2020 in both areas. The large impact of winter mixing on the C_T and pH signal is crucial as it drives the acidification signal : pH trends between both areas would be similar were it not for convective events that increase pH in intermediate layers and strong events (such as in 2013 and 2018) that increase pH in the deep layers. Furthermore, Touratier et Goyet (2011) have shown that the deep convection and cascading in the Gulf of Lion could explain the relatively high rate of acidification estimated in the deep layers of the western Mediterranean Sea. Therefore, these convection events seem to induce a slowing down of the acidification process in intermediate waters, essential in weakening the acidification process already reported in the Mediterranean Sea (Hassoun et al. 2015 ; Palmiéri et al. 2015 ; Touratier et Goyet 2011). It has also been shown that the CO_2 chemistry is less sensitive to temperature in the Mediterranean Sea than in the Atlantic because of the low C_T/A_T ratio and high buffer factors (Álvarez et al. 2014). Moreover, the increase in atmospheric CO_2 increases C_T and has little effect on A_T which is consistent with our results with an increase in C_T with no significant change in A_T (figure 5.5).

5. Conclusion

The consequences of climate change on the physical properties of water masses are well established, with warming and salinification of the Levantine Intermediate Water in the northwestern Mediterranean Sea (Margirier et al. 2020) and in the deep waters of the western Mediterranean Sea (Borghini et al. 2014). These changes lead to an increase in stratification and a decrease in the intensity and frequency of dense water formation events (Macias et al. 2018 ; Soto-Navarro et al. 2020 ; Somot et al. 2006). The intensity of winter mixing is likely to reduce the ventilation of the water column and specifically of the O_2-depleted Levantine Intermediate Layer and to decrease the supply of nutrients required for phytoplankton growth in the upper layers (Severin et al. 2017). An intensification of the O_2 minimum in the intermediate layers is already visible in the Ligurian Sea (Coppola et al. 2018) and the combination of mooring, Argo, and ship-based observations show that the O_2 minimum is very strongly affected by the intermittent convection process. In the absence of deep convection events, the O_2-depleted layer spreads vertically and intensifies even more so in the Ligurian Sea, where the mixing events are less regular and intense than in the Gulf of Lion. When these events occur, the O_2 minimum is affected with an increase of O_2 in intermediate layers depending on the intensity of the winter convection, accompanied by a decrease afterward. Our results also show a difference

in ventilation of the deeper layers between the Gulf of Lion and the Ligurian Sea, with the latter seemingly more easily ventilated by deep convection events, maybe through recirculation between the two areas. Integrated observing networks and multi-platforms approaches are fundamental in studying dense water formation events (Tintoré et al. 2019) and their impacts on biogeochemistry (monthly and yearly cruises, moorings, Argo floats, ...). The application of the CANYON-MED neural networks (Fourrier et al. 2020 ; Fourrier et al. 2021) on the large network of O_2-equipped Argo floats in the northwestern Mediterranean Sea allowed the study of reconstructed time series of nutrients and carbonate system variables with large spatial and temporal coverage. Nevertheless, they are limited by their technical capacities to a profiling depth of 2000 m and as drifting platforms, sometimes offer biased representations of the studied areas (e.g. the accumulation of floats west of Corsica in the Ligurian Sea area). However, we were able to describe how convective events impact nutrients and carbonate system variables changing their overall evolutions over time and at different depths. In the Gulf of Lion, nitrates increase in intermediate layers and all nutrients increase at depth, whereas in the Ligurian Sea only nitrates and silicates at depth increase over the period of study. However, the decoupling between nitrates and phosphates might lead to an evolution in the nutrient molar ratios as compared to Redfield's model. Complementary studies are required to further investigate the exact cause of the nutrient increases between the atmospheric, physical and biological factors interconnected. Ocean acidification time series of consistent sampling over many years are still lacking for the Mediterranean Sea (Durrieu de Madron et al. 2011). Our approach using neural-network derived pH_T allowed for acidification estimates in different layers of the water column. Overall, C_T increased with a concurrent pH_T decrease and were strongly affected by mixing events.

Acknowledgments

We thank Claude Estournel for the simulation performed using the HPC CALMIP platform under grant P09115. The SYMPHONIE model is distributed by the SIROCCO group (https ://sirocco.obs-mip.fr). We also thank Louis Legendre (LOV, SU), Louis Prieur (LOV, SU) and Dominique Lefevre (MIO) for fruitful discussions about the results and the exploration of hypotheses in our study. We acknowledge the MOOSE program (Mediterranean Ocean Observing System for the Environment) coordinated by CNRS-INSU and the Research Infrastructure ILICO (CNRS-IFREMER). For seawater sample analyses, we also thank the SNAPO-CO_2 at LOCEAN, Sorbonne Université – CNRS, France). Argo data are available at https://doi.org/10.17882/42182#78698 or at ftp://ftp.ifremer.fr/ifremer/argo/dac/coriolis. These data were collected and made freely available by the International Argo Program and the national programs that contribute to it (https://argo.ucsd.edu, https://www.ocean-ops.org). The Argo Program is part of the Global Ocean Observing System. This study represents a contribution to the NAOS project (funded by the Agence Nationale de la Recherche in the

framework of the French “Equipement d’avenir” program grant ANR J11R107-F).

5.4 Conclusions et perspectives de l'étude

Les conséquences du changement climatique sur les propriétés physiques des masses d'eau sont connues, avec un réchauffement et une salinisation de la LIW dans le nord-ouest de la mer Méditerranée (Margirier et al. 2020) et dans les eaux profondes de la mer Méditerranée occidentale (Borghini et al. 2014). Ces changements entraînent une augmentation de la stratification et une diminution de l'intensité et de la fréquence des événements de DWF (Macias et al. 2018 ; Soto-Navarro et al. 2020 ; Somot et al. 2006). L'intensité du mélange hivernal est susceptible de réduire la ventilation de la colonne d'eau, spécifiquement des eaux intermédiaires appauvries en O_2, et de diminuer l'apport de nutriments nécessaires à la croissance du phytoplancton dans les couches de surface (Severin et al. 2017). Une intensification du minimum d'O_2 dans les couches intermédiaires est déjà visible en mer Ligure (Coppola et al. 2018) et la combinaison d'observations issues de mouillages, de flotteurs Argo et de campagnes en mer montre que le minimum d'O_2 est très fortement affecté par le processus de convection intermittente. En l'absence d'événements de convection profonde, la couche appauvrie en O_2 s'étend verticalement et s'intensifie encore plus en mer Ligure, où les événements de mélange sont moins réguliers et moins intenses que dans le Golfe du Lion. Lorsque ces événements se produisent, le minimum d'O_2 est affecté avec une augmentation de l'O_2 dans les couches intermédiaires relative à l'intensité de la convection hivernale, accompagnée d'une diminution par la suite. Nos résultats montrent également une différence dans la ventilation des couches profondes entre le Golfe du Lion et la mer Ligure . Dans cette dernière, les eaux intermédiaires sont plus facilement ventilées lors des évènements de mélange. De plus, on retrouve en mer Ligure la dispersion des eaux profondes formées dans le Golfe du Lion qui pourraient impacter l'O_2 dans les eaux profondes de la mer Ligure . Les réseaux d'observation intégrés et les approches multi-plateformes sont fondamentaux pour étudier les événements de DWF (Tintoré et al. 2019) et leurs impacts sur la biogéochimie (campagnes mensuelles et annuelles, mouillages, flotteurs profileurs Argo, ...).

L'application des réseaux de neurones CANYON-MED (Fourrier et al. 2020) au vaste réseau de flotteurs Argo mesurant l'O_2 dans le nord-ouest de la Méditerranée a permis l'étude de séries temporelles reconstituées de nutriments et de variables du système des carbonates avec une large couverture spatio-temporelle. Néanmoins, ils sont limités techniquement à une profondeur maximale de 2000 m et en tant que plateformes dérivantes, offrent parfois des représentations biaisées des zones étudiées (par exemple l'accumulation de flotteurs à l'ouest de la Corse dans la zone de la mer Ligure). Cependant, nous avons pu décrire comment les événements convectifs impactent les nutriments et les variables du système des carbonates en modifiant leurs évolutions globales dans le temps et à différentes profondeurs. Le Golfe du Lion et la mer Ligure montrent des réponses similaires aux événements de mélange avec une augmentation globale des nutriments dans les couches intermédiaires et profondes et un

impact limité de la convection sur les tendances à long terme. Les évènements de mélange ont cependant un impact sur les rapports stoechiométriques des nutriments, augmentant la limitation en phosphore. Des études complémentaires seraient nécessaires pour approfondir la cause exacte de l'augmentation des nutriments entre les facteurs atmosphériques, physiques et biologiques fortement liés. En Méditerranée nord-occidentale, une acidification des eaux de surface a été mise en évidence (Kapsenberg et al. 2017 ; Merlivat et al. 2018) ainsi qu'une acidification des couches intermédiaires et profondes (Coppola et al. 2020a). Ces tendances ne permettent pas de refléter les variabilités saisonnières et interannuelles affectant cette acidification. Ainsi, une approche par des plateformes autonome mesurant le pH ou en couplant des plateformes autonomes équipées de capteurs d'O_2 avec des méthodes de réseau de neurones comme CANYON-MED sont nécessaires pour mieux prédire ces tendances. Dans cette étude, la seconde approche a permis d'estimer des tendances de diminution du pH à différentes profondeurs ainsi que l'augmentation concomitante de C_T, tous les deux fortement affectés par les événements de mélange.

Chapitre 6

Ventilation dans le bassin Levantin

Sommaire du présent chapitre

6.1 Contexte

La LIW, masse d'eau clé pour la circulation générale de la mer Méditerranée (Robinson et al. 2010), se forme dans le bassin Levantin en mer Méditerranée orientale (détails en partie 1.3.3 Formation d'eau dense en mer Méditerranée Orientale). Les masses d'eau de la Méditerranée orientale sont plus chaudes, avec une salinité et une teneur en oxygène plus élevées que celles de la Méditerranée occidentale (Álvarez et al. 2014). Le long de son parcours vers le bassin occidental et vers Gibraltar, les caractéristiques de la LIW évoluent. Elle maintient une température et une salinité élevées, influençant ainsi la circulation et la formation d'eau dense le long de son parcours, mais sa teneur en oxygène évolue avec une diminution d'O_2 associée à une reminéralisation accrue (Tanhua et al. 2013). Dans le bassin oriental, la couche de minimum d'oxygène est fortement étendue sur la verticale avec un coeur autour de 500-700 m (Tanhua et al. 2013). Les eaux de cette zone sont fortement stratifiées, ce qui limite le mélange diffusif sur la verticale.

Cependant, les processus biogéochimiques qui se produisent pendant le mélange dans cette zone restent mal compris en raison de la faible couverture de données (principalement des croisières historiques) due entre autres au contexte géopolitique difficile. Il a été démontré que le gyre de Rhodes, dans le nord-ouest du bassin Levantin, est un des lieux de formation de la LIW sous les vents du nord froids et secs provenant des continents (The LIWEX Group 2003).

Cette étude préliminaire vise en s'appuyant sur des flotteurs BGC-Argo équipés de capteurs d'O_2 déployés dans la zone d'étude à caractériser la ventilation dans le patch sur la période

automne 2018 - été 2019.

6.2 Étude préliminaire

1. Introduction

The LIW, a key water mass for the general circulation of the Mediterranean Sea (Robinson et al, 2001), is mainly formed in the Rhodes Gyre in the eastern Mediterranean Sea. The Levantine basin is considered one of the most oligotrophic regions in the world (Azam et al. 1983). The water masses of the Eastern Mediterranean Sea are warmer, with higher salinity and oxygen content than those in the Western Mediterranean Sea (Álvarez et al. 2014) and the LIW is no exception. Along its path to the western basin and to Gibraltar, the characteristics of the LIW evolve. It maintains a high temperature and high salinity, therefore influencing circulation and dense water formation along its path but its oxygen content evolves with an O_2 decrease associated with increased remineralisation. In the eastern basin, the oxygen minimum layer is spread vertically with its core around 500-700 m (Tanhua et al. 2013). The waters in this area are highly stratified restricting diffusive mixing on the vertical.

However, the biogeochemical processes occurring during the mixing in this area remain poorly understood because of the low data coverage (mostly historical cruises) amongst others due to the difficult geopolitical context. Mixing events associated to LIW formation can inject nutrients in the surface layer therefore triggering phytoplankton growth (D'Ortenzio et al. 2021) (Sur et al. 1993). The Rhodes Gyre in the northwestern Levantine has been shown to be the main location of the formation of the LIW under the cold and dry north winds from the continents (The LIWEX Group 2003).

We hypothesize that the main ventilation of the LIW occurs in the area where the MLD is the deepest, thus allowing O_2 injection in the water column.

In the framework of the PERLE (Pelagic Ecosystem Response to deep water formation in the Levant Experiment) project, cruises took place in the Levantine basin during the 2018-2019 period (D'Ortenzio et al. 2021). During those cruises, BGC-Argo floats equipped with O_2 sensors were also deployed to acquire data in between cruises and increase our monitoring of this area. Wimart-Rousseau et al. (2021) have described the inorganic carbon in the area thanks to the data from the PERLE cruises and D'Ortenzio et al. (2021) have reported on nitrate and phytoplancton dynamics in the area combining BGC-Argo, satellite and cruise data. Our study is based on O_2 from BGC-Argo data and we hypothesize that the main ventilation of the LIW occurs in the area where the MLD is the deepest. We also hypothesize that the MLD maximum patch could be identified by region of annual minimum SST as in D'Ortenzio et al. (2021).

2. Material and methods

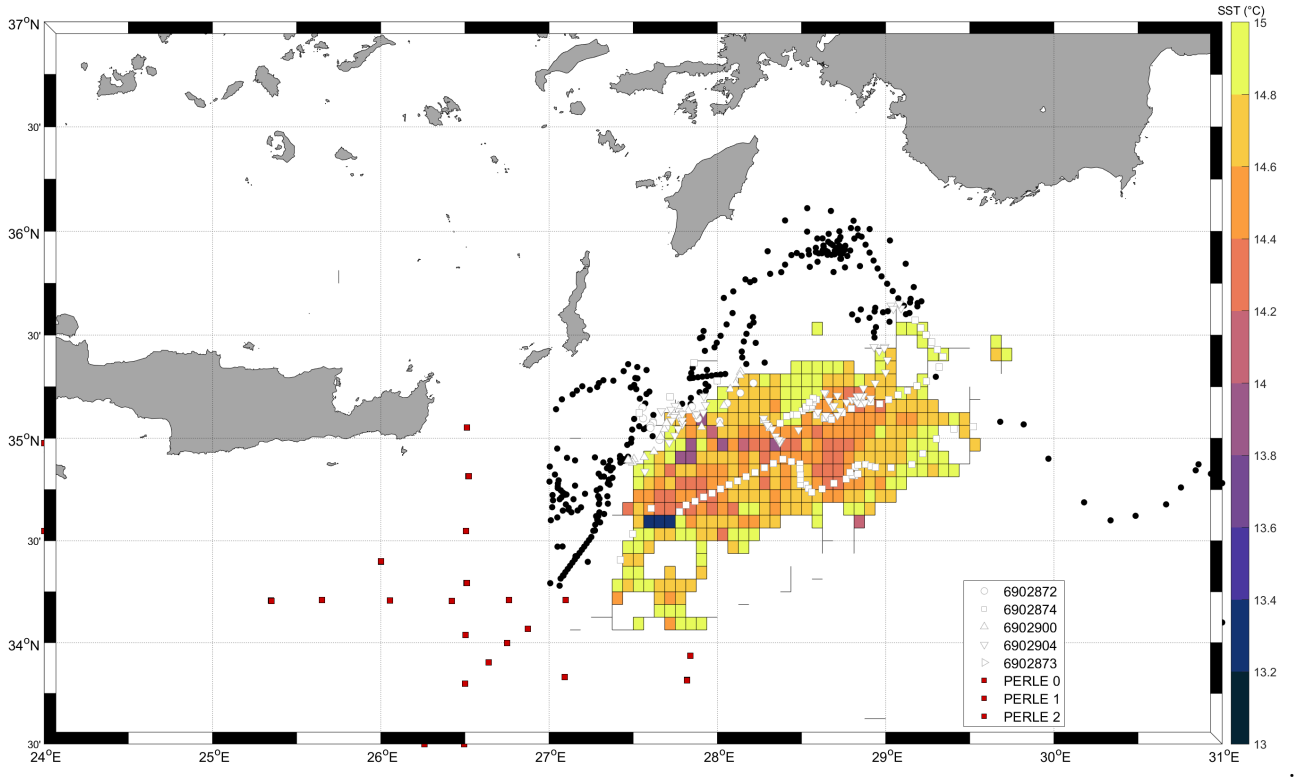

FIGURE 6.1 – Argo float locations in the Levantine basin. The coloured Sea Surface Temperature (SST) patch depicts the waters < 15°C as in D'ORTENZIO et al. (2021). The Argo float profiles are colored according to their location inside (white circles) or outside (black circles) the patch. Red squares show the location of the PERLE cruise stations. Argo locations have been filtered keeping only locations above 27°E, *i.e.* closer to the SST patch.

Sea surface temperature data

Sea Surface Temperature (SST) observations form the Copernicus Marine Service were extracted as in D'ORTENZIO et al. (2021) for the fall 2018 to summer 2019 period and the annual absolute minimum value per pixel was identified. The resulting SST "patch" is shown in figure 6.1.

BGC-Argo data

Five BGC-Argo floats were deployed in the Levantine basin equipped with O_2 sensors over the 2018-2019 period (figure 6.1). The floats O_2 measurements were corrected by the Coriolis Data Assembly Center either using in air measurements compared to NCEP climatology data (for floats 6902872, 690873, 6902874, and 6902900) or with subsurface measurements compared to climatology data (float 690904) (THIERRY et al. 2021). For each profile, a distinction was made between the floats inside or outside the patch.

Derived variables

The Mixed Layer Depth (MLD) was estimated for each float profile based on potential density

profiles calculated from pressure, temperature, and salinity data. The MLD was derived using a 0.03 kg.m^{-3} threshold density criterion with a reference depth of 10 meters (D'Ortenzio et al. 2005). The maximum Argo-derived MLD is restricted to 2000 m, i.e. the maximum depth reached by the Argo floats.

For each Argo profile the oxygen content over the water column was calculated by integrating the oxygen content from the surface to the maximum depth reached by the Argo float. The mean O_2 value in the 300-600 meters layer was also extracted.

3. Results and discussion

Argo float profiles located inside the mixed patch show higher MLDs, up to 1100 m (figure 6.2), whereas MLDs outside the patch only reach 300 meters, confirming that the mixing occurs mainly inside the SST patch as defined in D'Ortenzio et al. (2021). The O_2 integrated content increases from around 180 μmol kg^{-1} between November 2018 and mid-January 2019 to 185 μmol kg^{-1} by March 2019. The O_2 in the 300-600 m displays similar dynamics with a stable value around 172 μmol kg^{-1} up to mid-January 2019 followed by an increase to 189 μmol kg^{-1} by March 2019. Afterwards, both the integrated content and the O_2 in intermediate layers decrease slowly to revert back to their original value at the beginning of the period. The O_2 increase starts around the 20th of January when the MLD deepens and reaches around 1000 m. The integrated content inside and outside the patch shows similar values. Profiles were extracted at six dates and for similar oxygen contents to allow for a comparison between the O_2 inside and outside the patch on the vertical (figure 6.2 d-i). The O_2 profiles from October and December show similar distributions between the profiles inside and outside the patch. In January, the overall O_2 is similar with a small difference at the surface with the profile inside the patch 10 μmol kg^{-1} lower than the one outside in the first 100 meters. In February 2019, after the ML deepenings, the profiles inside and outside the patch show a different vertical structure with O_2 variations in the upper 300 m probably associated to vertical mixing and oxygenation of the upper part of the water column. In April 2019, outside the patch the float shows a different dynamic with an intrusion of a different water mass between 100 and 300m, whereas the float inside the patch has homogeneous O_2 in the upper 200 meters and decreases with depth. In June 2019, there is a subsurface maximum of O_2 in the first 100 meters that doesn't seem to be associated with biological activity. The O_2 increase and homogenization are similar between the Argo profiles inside and outside the patch leading to believe that the main ventilation isn't restricted to the patch and is quickly advected to the sides.

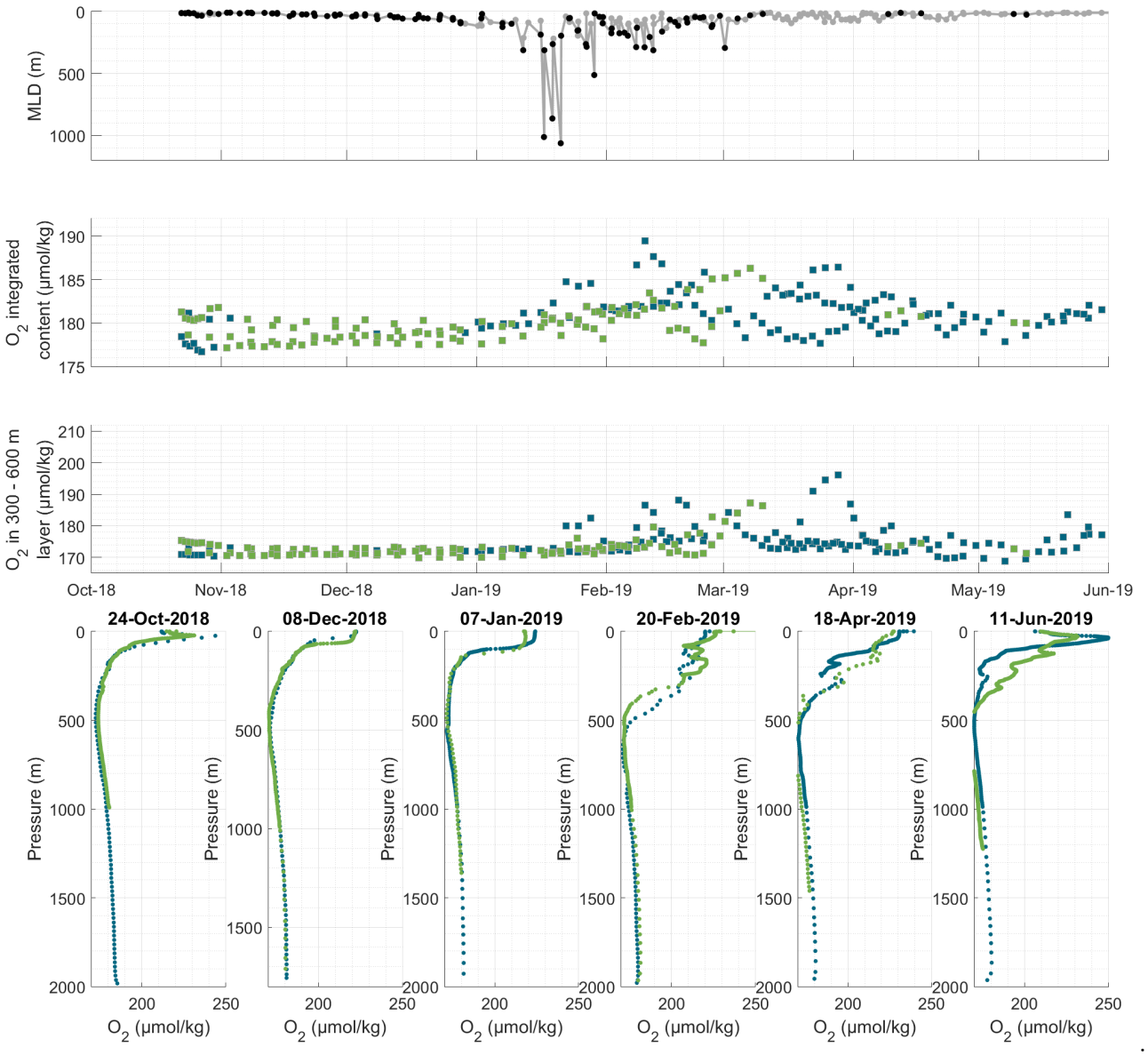

FIGURE 6.2 – Time series of a. MLD, b. O_2 content over the water column, c. O_2 in the 300-600 m layer, d-i. O_2 profiles at selected dates. Black and green markers correspond to Argo profiles inside the patch whereas gray and blue markers correspond to profiles outside the patch.

Chapitre 7

Conclusions et perspectives

Sommaire du présent chapitre

7.1 Conclusions

Ces travaux de thèse sont à l'origine d'une méthode neuronale adaptée à la Méditerranée pour estimer les nutriments et les variables du système des carbonates à partir de variables systématiquement mesurées. Cette méthode a ensuite été appliquée en Méditerranée nord-occidentale pour mieux comprendre la dynamique de variables biogéochimiques (O_2, nutriments et variables du système des carbonates) en réponse aux évènements de mélange intense. Enfin, la ventilation de la LIW au niveau de sa zone de formation a été estimée.

Les principales questions scientifiques présentées dans la partie 1.6 Objectifs de la thèse et traitées au cours de cette thèse ainsi que les résultats majeurs sont décrits ci-après.

Quel est l'impact de la formation d'eau dense, en Méditerranée nord-occidentale, sur l'O_2, sur les nutriments et sur les variables du système des carbonates ?
Dans le Golfe du Lion et en mer Ligure, des évènements de mélange hivernal et de formation d'eau dense ont lieu de manière alternée selon les années avec une forte variabilité saisonnière ventilant les couches intermédiaires et profondes, et permettant la remontée de nutriments vers la surface. Le jeu de données utilisées est limité dans le temps, et pour estimer l'impact du changement climatique un jeu de données plus long serait nécessaire (30 ans). Néanmoins, dans un contexte d'augmentation de la stratification et de réduction de ces évènements de mélange (Somot et al. 2006 ; Soto-Navarro et al. 2020), l'analyse des séries temporelles 2012-2020

d'O_2 reconstituées à partir de campagnes, mouillages et flotteurs Argo dans le Golfe du Lion et la mer Ligure ont permis de montrer que le minimum d'O_2 dans la LIW est fortement affecté par le processus de convection intermittent qui ventile les couches intermédiaires. Une différence de réponse entre la mer Ligure et le Golfe du Lion a également pu être mise en évidence. Les tendances sur la période 2012-2020 ont été calculées pour les nutriments et les variables du système des carbonates en surface, dans la LIW et en profondeur. Dans les deux zones, au cours de la période 2012-2020, on observe une augmentation globale des nutriments dans les couches intermédiaires et profondes, avec un impact sur les rapports stoechiométriques augmentant la limitation en phosphore. Les estimations d'acidification dérivées dans différentes couches de la colonne d'eau montrent une augmentation globale de l'A_T et du C_T et une diminution concomitante du pH. Ces tendances ont été fortement affectées par les événements de convection et semblent avoir des conséquences sur l'ensemble de la colonne d'eau.

Peut-on améliorer notre caractérisation de la distribution spatio-temporelle des concentrations en nutriments, O_2 et carbonates en combinant les observations *in situ* et de nouvelles méthodes de machine learning ?
Les mesures de nutriments et de variables du système des carbonates en Méditerranée sont nombreuses mais certaines régions et périodes temporelles restent sous-échantillonnées. Les mesures d'O_2 sont devenues de plus en plus fréquentes et de bonnes qualités qu'elles proviennent de mouillages, de flotteur Argo ou de planeurs. La méthode CANYON-MED constituée d'un ensemble de réseaux de neurones et développée au cours de cette thèse s'appuie sur la méthode CANYON créée pour l'océan global. Cette méthode permet d'estimer nutriments (nitrates, phosphates, silicates) et variables du système des carbonates (A_T, C_T et pH_T) avec des précisions connues à l'aide de mesures de température, salinité, pression et O_2 ainsi que la position dans le temps et dans l'espace. De plus, les variables prédites ont des précisions équivalentes aux précisions des capteur existants ce qui permettrait d'appliquer les méthodes CANYON-MED pour résoudre des verrous scientifiques. Par exemple, de nombreuses applications voient le jour en s'appuyant sur le large réseau de flotteurs-profileurs ainsi que sur les planeurs et mouillages présents en mer Méditerranée.

7.2 Perspectives

Les travaux présentés au cours de cette thèse on été concentrés sur la partie hauturière de la mer Méditerranée. Cependant, des études préliminaires ont pu montrer des perspectives d'application de la méthode CANYON-MED en milieu côtier. Le milieu côtier est une zone complexe où se mêlent de nombreux processus physiques et biogéochimiques ayant des échelles de temps et d'espace très variables (variabilités diurnes, de marées, saisonnières, interannuelles, etc.). La zone côtière est en général plus sensible aux pressions que le large. Les impacts

sociétaux et économiques face au réchauffement et à l'occurrence des évènements extrêmes ont des répercussions considérables. Ces changements sont même souvent irréversibles. Dans ce contexte, les séries temporelles côtières sont sujettes aux facteurs environnementaux et des trous apparaissent dans ces séries limitant la compréhension des processus côtiers. Par ailleurs, des mesures *in situ* côtières sont effectuées régulièrement et permettent le contrôle qualité des capteurs installés en milieu côtier au delà de leur exploitation scientifique, mais ces mesures restent basse fréquence. Afin d'obtenir une meilleure compréhension de l'évolution des nutriments (notamment face aux apports variables) et des variables du système des carbonates (Kapsenberg et al. 2017) ainsi que pour mieux appréhender la réponse du plancton à leurs variations dans le milieu côtier, il est nécessaire de densifier les données existantes. Ainsi, les méthodes neuronales comme CANYON-MED peuvent permettre de compléter les trous dans les séries temporelles (figure 7.1).

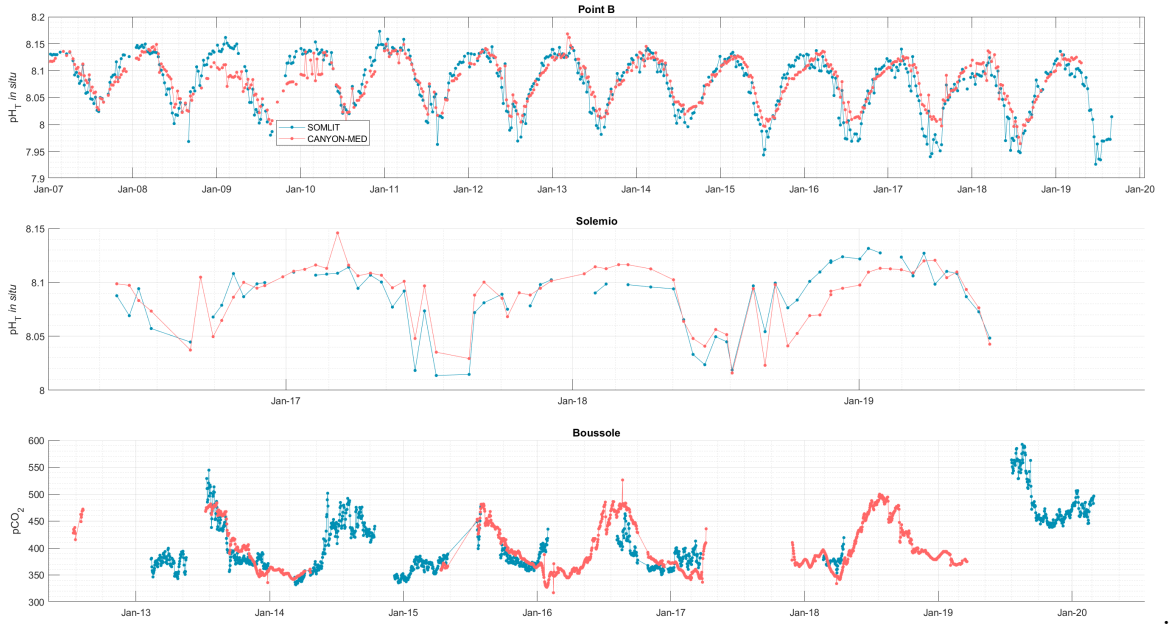

Figure 7.1 – Comparaisons entre les données *in situ* (en bleu) et les sorties de CANYON-MED (en orange) à la position correspondante pour a. le pH_T au point B, b. le pH_T à Solemio, c. la pCO_2 à Boussole.

De plus, appliquées au données de planeurs sous-marin, elles permettent d'explorer le continuum côte-large (figure 7.2).

Ces résultats restent préliminaires mais indiquent la possibilité de développer des méthodes similaires à CANYON-MED spécifiques pour le milieu côtier.

Par ailleurs, comme mentionné dans la partie 2.2.5 Sorties de modèles, la méthode CANYON-MED est un atout pour améliorer les simulations issues de modèle, que ce soit pour l'assimilation de ces données prédites ou pour comparer les sorties de modèles qui manquent encore cruellement de données de référence (Doney et al. 2009 ; Cossarini et al. 2019).

De par leurs capacités à générer des données « virtuelles », les méthodes neuronales peuvent être utilisées pour la génération d'indicateurs climatiques. En particulier, leur utilisation peut permettre l'estimation de tendances dans différentes sous-régions de la mer Méditerranée, à différentes profondeurs caractéristiques correspondant à des masses d'eau d'intérêt dans un contexte de changement climatique. En particulier, un produit de nutriments (Produit : MULTIOBS_GLO_BIO_NUTRIENTS_PROFILES_REP_015_009) à l'échelle globale, dérivé de données de flotteurs Argo à l'aide de méthodes neuronales, est distribué par CMEMS (Copernicus Marine Environment Monitoring Service). La partie Méditerranée de ce produit est issue d'estimations par la méthode CANYON-MED, en complément des méthodes CANYON pour l'océan global. Ce produit peut être utilisé par la communauté de modélisateurs pour l'assimilation de données.

Enfin, CANYON-MED peut servir pour des utilisations plus dérivées telles que le calcul de la Production Communautaire Nette (Net Community Production, NCP). En effet Possenti et al. (2021) ont dérivé la NCP via l'O_2 mesuré sur les planeurs sous-marins, mais aussi via le C_T dérivé de la CO_2 mesurée par le planeur. En s'appuyant uniquement sur l'O_2 mesuré par planeur, CANYON-MED permettrait de faire une estimation robuste de C_T et donc de retrouver la NCP selon la méthode de Possenti et al. (2021). Les précisions du C_T estimé par CANYON-MED et du C_T recalculé à partir du CO_2 sont similaires. Cette méthode permettrait ainsi de tirer profit des mesures gliders équipés de capteur d'O_2 mais encore peu équipés de capteurs de CO_2.

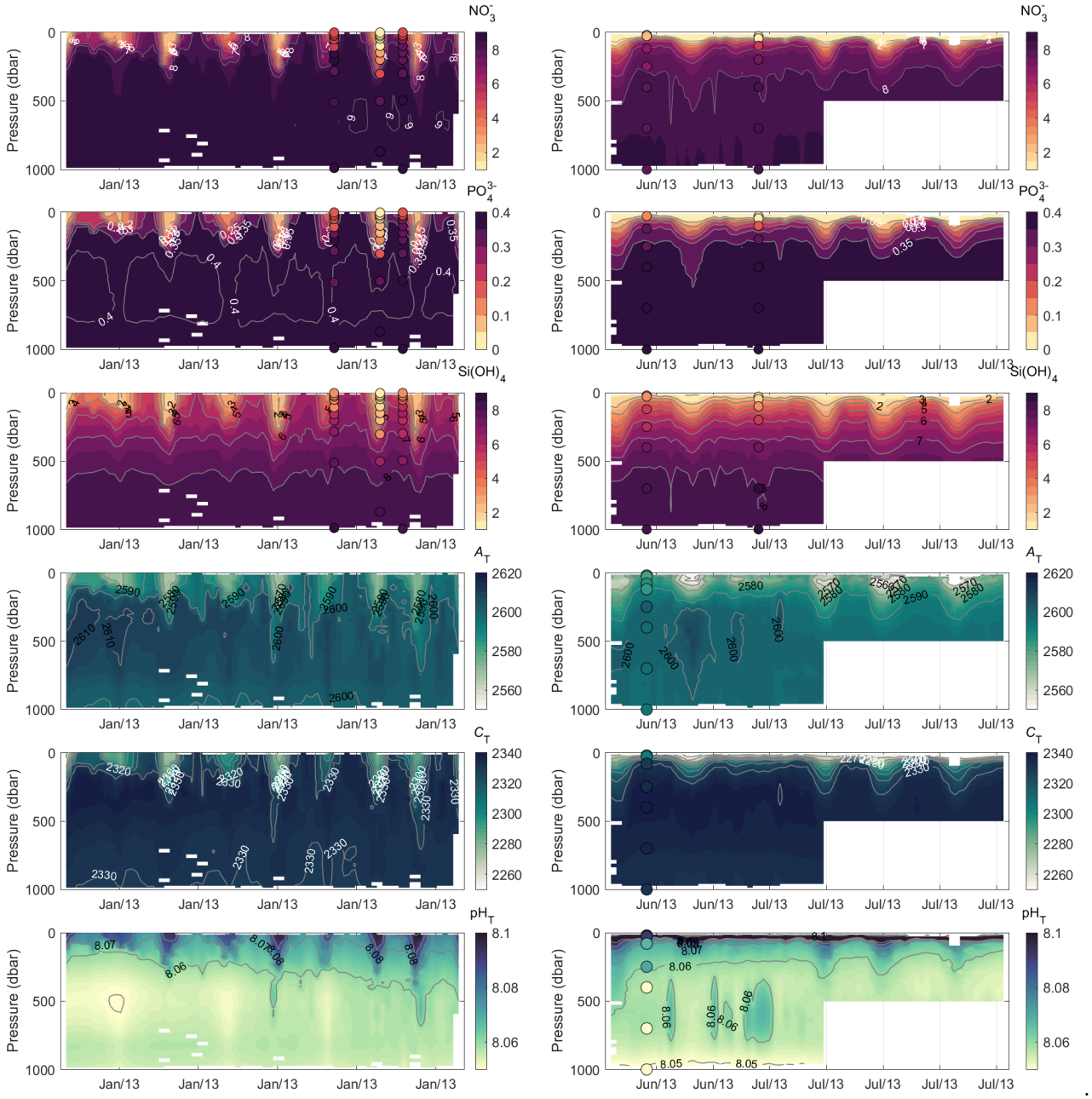

FIGURE 7.2 – Séries temporelles de nitrates, phosphates, silicates, A_T, C_T et pH_T dérivées de CANYON-MED pour les données gliders de la section T00 23 (panneau gauche) et T00 26 (panneau droit). Les données bouteilles suffisamment proches dans le temps et l'espace ont été représentées sous forme de cercles pour comparaison avec les données virtuelles générées par CANYON-MED.

Bibliographie

[1] M. Álvarez, H. Sanleón-Bartolomé, T. Tanhua, L. Mintrop, A. Luchetta, C. Cantoni, K. Schroeder et G. Civitarese. « The CO2 system in the Mediterranean Sea : a basin wide perspective ». In : *Ocean Science* 10.1 (14 fév. 2014), p. 69-92. doi : 10.5194/os-10-69-2014.

[2] A. Aminot et R. Kérouel. *Dosage automatique des nutriments dans les eaux marines : méthodes en flux continu*. Google-Books-ID : WJa03AhDIGoC. Editions Quae, 2007. 191 p.

[3] Argo. « Argo float data and metadata from Global Data Assembly Centre (Argo GDAC) ». In : (2020). type : dataset. doi : 10.17882/42182.

[4] S. B. Argo. *SAGE_O2*. original-date : 2018-04-17T20 :03 :07Z. 24 juin 2021.

[5] F. Azam, T. Fenchel, J. G. Field, J. S. Gray, L. A. Meyer-Reil et F. Thingstad. « The Ecological Role of Water-Column Microbes in the Sea ». In : *Marine Ecology Progress Series* 10.3 (1983). Publisher : Inter-Research Science Center, p. 257-263.

[6] G. Bartoli, C. Migon et R. Losno. « Atmospheric input of dissolved inorganic phosphorus and silicon to the coastal northwestern Mediterranean Sea : Fluxes, variability and possible impact on phytoplankton dynamics ». In : *Deep Sea Research Part I : Oceanographic Research Papers* 52.11 (1er nov. 2005), p. 2005-2016. doi : 10.1016/j.dsr.2005.06.006.

[7] M. H. Beale, M. T. Hagan et H. B. Demuth. *Neural Network Toolbox™ User's Guide*. Beale, M. H., Hagan, T. M., and Demuth, H. B. : Deep Learning Toolbox ™ , User's Guide, Release 2018a, The MathWorks, Inc., Natick, Massachusetts, United States, available at : https ://es. mathworks.com/help/pdf_doc/deeplearning/nnet_ug.pdf, last ac- cess : 20 August 2018. Natick, Massachusetts, United States : The MathWorks, Inc.

[8] M. Bégovic. « Contribution à l'étude du système des carbonates en Méditerranée-Distribution et variation spatio-temporelle de la pression partielle de CO2 dans les eaux superficielles du bassin Liguro-Provençal ». Thèse de doct. Université Pierre et Marie Curie - Paris VI, 20 sept. 2001.

[9] A. Bergamasco et P. Malanotte-Rizzoli. « The circulation of the Mediterranean Sea : a historical review of experimental investigations ». In : *Advances in Oceanography and Limnology* 1.1 (1er juin 2010). Publisher : Taylor & Francis _eprint : https ://-doi.org/10.1080/19475721.2010.491656, p. 11-28. doi : 10.1080/19475721.2010.491656.

[10] J. P. Bethoux, B. Gentili, P. Morin, E. Nicolas, C. Pierre et D. Ruiz-Pino. « The Mediterranean Sea : a miniature ocean for climatic and environmental studies and a key for the climatic functioning of the North Atlantic ». In : *Progress in Oceanography* 44.1 (1er août 1999), p. 131-146. doi : 10.1016/S0079-6611(99)00023-3.

[11] J. P. Bethoux, M. S. El Boukhary, D. Ruiz-Pino, P. Morin et C. Copin-Montégut. « Nutrient, Oxygen and Carbon Ratios, CO2 Sequestrationand Anthropogenic Forcing in the Mediterranean Sea ». In : *The Mediterranean Sea*. Sous la dir. d'A. Saliot. T. 5K. Berlin, Heidelberg : Springer Berlin Heidelberg, 2005, p. 67-86. doi : 10.1007/b107144.

[12] J. Béthoux, P. Morin, C. Chaumery, O. Connan, B. Gentili et D. Ruiz-Pino. « Nutrients in the Mediterranean Sea, mass balance and statistical analysis of concentrations with respect to environmental change ». In : *Marine Chemistry* 63.1 (déc. 1998), p. 155-169. doi : 10.1016/S0304-4203(98)00059-0.

[13] J. P. Béthoux, P. Morin et D. P. Ruiz-Pino. « Temporal trends in nutrient ratios : chemical evidence of Mediterranean ecosystem changes driven by human activity ». In : *Deep Sea Research Part II : Topical Studies in Oceanography* 49.11 (jan. 2002), p. 2007-2016. doi : 10.1016/S0967-0645(02)00024-3.

[14] N. Bindoff, W. W. L. Cheung, J. Kairo, J. Arístegui, V. Guinder, R. Hallberg, N. Hilmi, N. Jiao, M. Karim, L. Levin, S. O'Donoghue, S. Purca Cuicapusa, B. Rinkevich, T. Suga, A. Tagliabue et P. Williamson. « Chapter 5 : Changing Ocean, Marine Ecosystems, and Dependent Communities ». In : *IPCC Special Report on the Ocean and Cryosphere in a Changing Climate*. H.-O. Pörtner, D.C. Roberts, V. Masson-Delmotte, P. Zhai, M. Tignor, E. Poloczanska, K. Mintenbeck, A. Alegría, M. Nicolai, A. Okem, J. Petzold, B. Rama, N.M. Weyer (eds.) In press., 2019.

[15] C. M. Bishop. *Neural Networks for Pattern Recognition*. Google-Books-ID : T0S0BgAAQBAJ. Clarendon Press, 23 nov. 1995. 501 p.

[16] H. C. Bittig et A. Körtzinger. « Tackling Oxygen Optode Drift : Near-Surface and In-Air Oxygen Optode Measurements on a Float Provide an Accurate in Situ Reference ». In : *Journal of Atmospheric and Oceanic Technology* 32.8 (août 2015), p. 1536-1543. doi : 10.1175/JTECH-D-14-00162.1.

[17] H. C. Bittig, A. Körtzinger, C. Neill, E. van Ooijen, J. N. Plant, J. Hahn, K. S. Johnson, B. Yang et S. R. Emerson. « Oxygen Optode Sensors : Principle, Characterization, Calibration, and Application in the Ocean, suppl. material ». In : *Frontiers in Marine Science* 4 (24 jan. 2018). doi : 10.3389/fmars.2017.00429.

[18] H. C. Bittig, T. L. Maurer, J. N. Plant, C. Schmechtig, A. P. S. Wong, H. Claustre, T. W. Trull, T. V. S. Udaya Bhaskar, E. Boss, G. Dall'Olmo, E. Organelli, A. Poteau, K. S. Johnson, C. Hanstein, E. Leymarie, S. Le Reste, S. C. Riser, A. R. Rupan, V. Taillandier, V. Thierry et X. Xing. « A BGC-Argo Guide : Planning, Deployment, Data Handling and Usage ». In : *Frontiers in Marine Science* 6 (22 août 2019), p. 502. doi : 10.3389/fmars.2019.00502.

[19] M. Borghini, H. Bryden, K. Schroeder, S. Sparnocchia et A. Vetrano. « The Mediterranean is becoming saltier ». In : *Ocean Science* 10 (7 août 2014). Avec la coll. de M. Borghini, H. Bryden, K. Schroeder, S. Sparnocchia et A. Vetrano, p. 693-700. doi : 10.5194/os-10-693-2014.

[20] G. L. E. Borzelli, M. Gačić, V. Cardin et G. Civitarese. « Eastern Mediterranean Transient and reversal of the Ionian Sea circulation ». In : *Geophysical Research Letters* 36.15 (2009). _eprint : https ://agupubs.onlinelibrary.wiley.com/doi/pdf/10.1029/2009GL039261. doi : 10.1029/2009GL039261.

[21] R. Boscolo et H. Bryden. « Causes of long-term changes in Aegean sea deep water ». In : *Oceanologica Acta* 24.6 (1er nov. 2001), p. 519-527. doi : 10.1016/S0399-1784(01)01172-0.

[22] A. Bosse. « Circulation générale et couplage physique-biogéochimie à (sous-)mésoéchelle en Méditerranée Nord-occidentale à partir de données in situ ». Thèse de doct. 2016.

[23] A. Bosse, P. Testor, N. Mayot, L. Prieur, F. D'Ortenzio, L. Mortier, H. Le Goff, C. Gourcuff, L. Coppola, H. Lavigne et P. Raimbault. « A submesoscale coherent vortex in the Ligurian Sea : From dynamical barriers to biological implications ». In : *Journal of Geophysical Research : Oceans* 122.8 (août 2017), p. 6196-6217. doi : 10.1002/2016JC012634.

[24] A. Bosse, P. Testor, L. Mortier, L. Prieur, V. Taillandier, F. d'Ortenzio et L. Coppola. « Spreading of Levantine Intermediate Waters by submesoscale coherent vortices in the northwestern Mediterranean Sea as observed with gliders ». In : *Journal of Geophysical Research : Oceans* 120.3 (2015), p. 1599-1622. doi : 10.1002/2014JC010263.

[25] T. Boyer, H. E. Garcia, R. A. Locarnini, M. M. Zweng, A. V. Mishonov, J. R. Reagan, K. A. Weathers, O. K. Baranova, D. Seidov et I. V. Smolyar. *World Ocean Atlas 2018. NOAA National Centers for Environmental Information. Dataset.* 2018.

[26] C. de Boyer Montégut. « Mixed layer depth over the global ocean : An examination of profile data and a profile-based climatology ». In : *Journal of Geophysical Research* 109 (C12 2004). doi : 10.1029/2004JC002378.

[27] W. S. Broecker et T.-H. Peng. *Tracers in the sea.* New-York : Eldigio Press, 1982.

[28] D. Broullón, F. F. Pérez, A. Velo, M. Hoppema, A. Olsen, T. Takahashi, M. Key, M. González-Dávila, T. Tanhua, E. Jeansson, A. Kozyr et van Heuven. « A global monthly climatology of total alkalinity : a neural network approach ». In : *Earth System Science Data* 11.3 (31 juil. 2019), p. 1109-1127. doi : 10.5194/essd-11-1109-2019.

[29] D. Broullón, F. F. Pérez, A. Velo Lanchas, M. Hoppema, A. Olsen, T. Takahashi, R. M. Key, T. Tanhua, J. M. Santana-Casiano et A. Kozyr. « A global monthly climatology of oceanic total dissolved inorganic carbon : a neural network approach ». In : *Earth System Science Data* (2020). doi : 10.5194/essd-2020-37.

[30] H. L. Bryden, J. Candela et T. H. Kinder. « Exchange through the Strait of Gibraltar ». In : *Progress in Oceanography* 33.3 (1er jan. 1994), p. 201-248. doi : 10.1016/0079-6611(94)90028-0.

[31] M. Canals, P. Puig, X. D. de Madron, S. Heussner, A. Palanques et J. Fabres. « Flushing submarine canyons ». In : *Nature* 444.7117 (nov. 2006). Bandiera_abtest : a Cg_type : Nature Research Journals Number : 7117 Primary_atype : Research Publisher : Nature Publishing Group, p. 354-357. doi : 10.1038/nature05271.

[32] C. Cantoni, A. Luchetta, J. Chiggiato, S. Cozzi, K. Schroeder et L. Langone. « Dense water flow and carbonate system in the southern Adriatic : A focus on the 2012 event ». In : *Marine Geology*. Cascading Dense water Flow and its Impact on the Sea Floor in the Adriatic and Aegean Sea, Eastern Mediterranean 375 (1er mai 2016), p. 15-27. doi : 10.1016/j.margeo.2015.08.013.

[33] S. Cherif, E. Doblas-Miranda, P. Lionello, C. Borrego, F. Giorgi, A. Iglesias, S. Jebari, M. Moriondo, O. Pringault, G. Rilov, S. Somot, A. Tsikliras, M. Vilà et G. Zittis. « Chapter 2 Drivers of Change ». In : *Climate and Environmental Change in the Mediterranean Basin - Current situation and Risks for the Future. first Mediterranean Assessment Report*. Cramer W, Guiot J, Marini K (eds.) This chapter should be cited as : Cherif S, Doblas-Miranda E, Lionello P, Borrego C, Giorgi F, Iglesias A, Jebari S, Mahmoudi E, Moriondo M, Pringault O, Rilov G, Somot S, Tsikliras A, Vila M, Zittis G 2020 Drivers of change. In : Climate and Environmental Change in the Mediterranean Basin – Current Situation and Risks for the Future. First Mediterranean Assessment Report [Cramer W, Guiot J, Marini K (eds.)] Union for the Mediterranean, Plan Bleu, UNEP/MAP, Marseille, France, 128pp, in press. Marseille, France : Union for the Mediterranean, Plan Bleu, UNEP/MAP, p. 128.

[34] S. Christodoulaki, G. Petihakis, M. Kanakidou, N. Mihalopoulos, K. Tsiaras et G. Triantafyllou. « Atmospheric deposition in the Eastern Mediterranean. A driving force for ecosystem dynamics ». In : *Journal of Marine Systems*. Large-scale regional comparisons of marine biogeochemistry and ecosystem processes - research approaches and results 109-110 (1er jan. 2013), p. 78-93. doi : 10.1016/j.jmarsys.2012.07.007.

[35] G. Civitarese, M. Gačić, M. Lipizer et G. L. Eusebi Borzelli. « On the impact of the Bimodal Oscillating System (BiOS) on the biogeochemistry and biology of the Adriatic and Ionian Seas (Eastern Mediterranean) ». In : *Biogeosciences* 7.12 (15 déc. 2010), p. 3987-3997. doi : 10.5194/bg-7-3987-2010.

[36] H. Claustre, J. Bishop, E. Boss, S. Bernard, J.-F. Berthon, C. Coatanoan, K. Johnson, A. Lotiker, O. Ulloa, M. J. Perry, F. D'Ortenzio, O. Fanton D'andon et J. Uitz. « Bio-optical profiling floats as new observational tools for biogeochemical and ecosystem studies : potential synergies with ocean color remote sensing ». In : *Proceedings of OceanObs*. OceanObs. 2009.

[37] H. Claustre, K. S. Johnson et Y. Takeshita. « Observing the Global Ocean with Biogeochemical-Argo ». In : *Annual Review of Marine Science* 12.1 (3 jan. 2020), p. 23-48. doi : 10.1146/annurev-marine-010419-010956.

[38] G. Copin-Montégut et B. Avril. « Vertical distribution and temporal variation of dissolved organic carbon in the North-Western Mediterranean Sea ». In : *Deep Sea Research Part I : Oceanographic Research Papers* 40.10 (1er oct. 1993), p. 1963-1972. doi : 10.1016/0967-0637(93)90041-Z.

[39] L. Coppola, L. Prieur, I. Taupier-Letage, C. Estournel, P. Testor, D. Lefevre, S. Belamari, S. LeReste et V. Taillandier. « Observation of oxygen ventilation into deep waters through targeted deployment of multiple Argo-O2 floats in the north-western Mediterranean Sea in 2013 ». In : *Journal of Geophysical Research : Oceans* 122.8 (août 2017), p. 6325-6341. doi : 10.1002/2016JC012594.

[40] L. Coppola, J. Boutin, J.-P. Gattuso, D. Lefevre et N. Metzl. « The Carbonate System in the Ligurian Sea ». In : *The Mediterranean Sea in the Era of Global Change 1*. Section : 4 _eprint : https ://onlinelibrary.wiley.com/doi/pdf/10.1002/9781119706960.ch4. John Wiley & Sons, Ltd, 2020, p. 79-103. doi : 10.1002/9781119706960.ch4.

[41] L. Coppola et E. Diamond Riquier. « MOOSE (DYFAMED) ». In : (2008). Publisher : Sismer. doi : 10.18142/131.

[42] L. Coppola, E. Diamond Riquier et T. Carval. *Dyfamed observatory data*. type : dataset. 2020. doi : 10.17882/43749.

[43] L. Coppola, L. Legendre, D. Lefevre, L. Prieur, V. Taillandier et E. Diamond Riquier. « Seasonal and inter-annual variations of dissolved oxygen in the northwestern Mediterranean Sea (DYFAMED site) ». In : *Progress in Oceanography* 162 (mar. 2018), p. 187-201. doi : 10.1016/j.pocean.2018.03.001.

[44] L. Coppola, P. Raimbault, L. Mortier et P. Testor. « Monitoring the Environment in the Northwestern Mediterranean Sea ». In : *Eos* 100 (25 juil. 2019). doi : 10.1029/2019EO125951.

[45] G. Cossarini, L. Mariotti, L. Feudale, A. Mignot, S. Salon, V. Taillandier, A. Teruzzi et F. D'Ortenzio. « Towards operational 3D-Var assimilation of chlorophyll Biogeochemical-Argo float data into a biogeochemical model of the Mediterranean Sea ». In : *Ocean Modelling* 133 (jan. 2019), p. 112-128. doi : 10.1016/j.ocemod.2018.11.005.

[46] W. Cramer, J. Guiot, K. Marini, B. Azzopardi, M. V. Balzan, S. Cherif, E. Doblas-Miranda et P. Drobinski. « MedECC 2020 Résumé à l'intention des décideurs ». In : *Changement climatique et environnemental dans le bassin méditerranéen – Situation actuelle et risques pour le futur. Premier rapport d'évaluation sur la Méditerranée*. Cramer W, Guiot J, Marini K (eds.) MedECC 2020 Résumé à l'intention des décideurs. Dans Changement climatique et environnemental dans le bassin méditerranéen – Situation actuelle et risques pour le futur. Premier rapport d'évaluation sur la Méditerranée [Cramer W, Guiot J, Marini K (eds.)] Union pour la Mediterranée, Plan Bleu, UNEP/MAP, Marseille, France, 36pp, sous presse. Marseille, France : Plan Bleu, UNEP/MAP, p. 36.

[47] F. D'Ortenzio, V. Taillandier, H. Claustre, L. Coppola, P. Conan, F. Dumas, X. Durrieu du Madron, M. Fourrier, A. Gogou, A. Karageorgis, D. Lefevre, E. Leymarie, A. Oviedo, A. Pavlidou, A. Poteau, P. M. Poulain, L. Prieur, S. Psarra, M. Puyo-Pay, M. Ribera d'Alcalà, C. Schmechtig, L. Terrats, D. Velaoras, T. Wagener et C. Wimart-Rousseau. « BGC-Argo Floats Observe Nitrate Injection and Spring Phytoplankton Increase in the Surface Layer of Levantine Sea (Eastern Mediterranean) ». In : *Geophysical Research Letters* 48.8 (28 avr. 2021). doi : 10.1029/2020GL091649.

[48] F. D'Ortenzio, D. Antoine et S. Marullo. « Satellite-driven modeling of the upper ocean mixed layer and air–sea CO2 flux in the Mediterranean Sea ». In : *Deep Sea Research Part I : Oceanographic Research Papers* 55.4 (avr. 2008), p. 405-434. doi : 10.1016/j.dsr.2007.12.008.

[49] F. D'Ortenzio, D. Iudicone, C. de Boyer Montegut, P. Testor, D. Antoine, S. Marullo, R. Santoleri et G. Madec. « Seasonal variability of the mixed layer depth in the Mediterranean Sea as derived from in situ profiles ». In : *Geophysical Research Letters* 32.12 (juin 2005), n/a-n/a. doi : 10.1029/2005GL022463.

[50] F. D'Ortenzio et L. M. Prieur. « The upper mixed layer ». In : *Life in the Mediterranean Sea : a look at habitat changes*. Sous la dir. de N. Stambler. Hauppauge, N.Y : Nova Science, 2012.

[51] F. D'Ortenzio, V. Taillandier, H. Claustre, L. M. Prieur, E. Leymarie, A. Mignot, A. Poteau, C. Penkerc'h et C. M. Schmechtig. « Biogeochemical Argo : The Test Case of the NAOS Mediterranean Array ». In : *Frontiers in Marine Science* 7 (24 mar. 2020), p. 120. doi : 10.3389/fmars.2020.00120.

[52] J. J. Dañobeitia, S. Pouliquen, T. Johannessen, A. Basset, M. Cannat, B. G. Pfeil, M. I. Fredella, P. Materia, C. Gourcuff, G. Magnifico, E. Delory, J. del Rio Fernandez, I. Rodero, L. Beranzoli, I. Nardello, D. Iudicone, T. Carval, J. M. Gonzalez Aranda, G. Petihakis, J. Blandin, W. L. Kutsch, J.-M. Rintala, A. R. Gates et P. Favali. « Toward a Comprehensive and Integrated Strategy of the European Marine Research Infrastructures for Ocean Observations ». In : *Frontiers in Marine Science* 7 (2020), p. 180. doi : 10.3389/fmars.2020.00180.

[53] A. G. Dickson et C. Goyet. *Handbook of methods for the analysis of the various parameters of the carbon dioxide system in sea water. Version 2*. ORNL/CDIAC-74. Oak Ridge National Lab., TN (United States), 1er sept. 1994. doi : https://doi.org/10.2172/10107773.

[54] A. G. Dickson et F. J. Millero. « A comparison of the equilibrium constants for the dissociation of carbonic acid in seawater media ». In : *Deep Sea Research* 34.10 (1987), p. 1733-1743.

[55] A. G. Dickson, C. L. Sabine et J. R. Christian. *Guide to Best Practices for Ocean CO2 Measurements*. Report. Accepted : 2015-01-05T00 :12 :27Z ISBN : 9781897176078 Journal Abbreviation : Dickson Bible. North Pacific Marine Science Organization, 2007.

[56] A. G. Dickson. « Standard potential of the reaction : AgCl(s) +iH,(g) = Ag(s) + HCl(aq), and and the standard acidity constant of the ion HSO4- in synthetic sea water from 273.15 to 318.15 K ». In : *Journal of Chemical Thermodynamics* 22 (1990), p. 113-127.

[57] A. G. Dickson. « pH buffers for sea water media based on the total hydrogen ion concentration scale ». In : *Deep Sea Research Part I : Oceanographic Research Papers* 40.1 (1er jan. 1993), p. 107-118. doi : 10.1016/0967-0637(93)90055-8.

[58] N. S. Diffenbaugh, J. S. Pal, F. Giorgi et X. Gao. « Heat stress intensification in the Mediterranean climate change hotspot ». In : *Geophysical Research Letters* 34.11 (2007). doi : 10.1029/2007GL030000.

[59] S. C. Doney, V. J. Fabry, R. A. Feely et J. A. Kleypas. « Ocean Acidification : The Other CO2 Problem ». In : *Annual Review of Marine Science* 1.1 (jan. 2009), p. 169-192. doi : 10.1146/annurev.marine.010908.163834.

[60] X. Durrieu De Madron, S. Ramondenc, L. Berline, L. Houpert, A. Bosse, S. Martini, L. Guidi, P. Conan, C. Curtil, N. Delsaut, S. Kunesch, J. F. Ghiglione, P. Marsaleix, M. Pujo-Pay, T. Séverin, P. Testor et C. Tamburini. « Deep sediment resuspension and thick nepheloid layer generation by open-ocean convection ». In : *Journal of Geophysical Research : Oceans* 122.3 (2017). _eprint : https ://agupubs.onlinelibrary.wiley.com/doi/pdf/10.1002/2016JC012062, p. 2291-2318. DOI : https://doi.org/10.1002/2016JC012062.

[61] X. Durrieu de Madron, V. Zervakis, A. Theocharis et D. Georgopoulos. « Comments on "Cascades of dense water around the world ocean" ». In : *Progress in Oceanography* 64.1 (1er jan. 2005), p. 83-90. DOI : 10.1016/j.pocean.2004.08.004.

[62] X. Durrieu de Madron et al. « Marine ecosystems' responses to climatic and anthropogenic forcings in the Mediterranean ». In : *Progress in Oceanography* 91.2 (1er oct. 2011), p. 97-166. DOI : 10.1016/j.pocean.2011.02.003.

[63] J. M. Edmond. « High precision determination of titration alkalinity and total carbon dioxide content of sea water by potentiometric titration ». In : *Deep Sea Research and Oceanographic Abstracts* 17.4 (1er août 1970), p. 737-750. DOI : 10.1016/0011-7471(70)90038-0.

[64] A. El Rahman Hassoun. « Modeling of the Total Alkalinity and the Total Inorganic Carbon in the Mediterranean Sea ». In : *Journal of Water Resources and Ocean Science* 4.1 (2015), p. 24. DOI : 10.11648/j.wros.20150401.14.

[65] C. Estournel, P. Marsaleix et C. Ulses. « A new assessment of the circulation of Atlantic and Intermediate Waters in the Eastern Mediterranean ». In : *Progress in Oceanography* 198 (1er nov. 2021), p. 102673. DOI : 10.1016/j.pocean.2021.102673.

[66] C. Estournel, P. Testor, P. Damien, F. D'Ortenzio, P. Marsaleix, P. Conan, F. Kessouri, X. Durrieu de Madron, L. Coppola, J.-M. Lellouche, S. Belamari, L. Mortier, C. Ulses, M.-N. Bouin et L. Prieur. « High resolution modeling of dense water formation in the north-western Mediterranean during winter 2012-2013 ». In : *Journal of Geophysical Research : Oceans* 121.7 (juil. 2016), p. 5367-5392. DOI : 10.1002/2016JC011935.

[67] M. Estrada, M. Latasa, M. Emelianov, A. Gutiérrez-Rodríguez, B. Fernández-Castro, J. Isern-Fontanet, B. Mouriño-Carballido, J. Salat et M. Vidal. « Seasonal and mesoscale variability of primary production in the deep winter-mixing region of the NW Mediterranean ». In : *Deep Sea Research Part I : Oceanographic Research Papers* 94 (déc. 2014), p. 45-61. DOI : 10.1016/j.dsr.2014.08.003.

[68] J. Font, P. Puig, J. Salat, A. Palanques et M. Emelianov. « Sequence of hydrographic changes in NW Mediterranean deep water due to the exceptional winter of 2005 ». In : *Scientia Marina* 71.2 (30 juin 2007). Number : 2, p. 339-346. DOI : 10.3989/scimar.2007.71n2339.

[69] F. D. Foresee et M. T. Hagan. « Gauss-Newton approximation to Bayesian learning ». In : *Proceedings of International Conference on Neural Networks (ICNN'97)*. T. 3. FORESEE, F. Dan et HAGAN, Martin T. Gauss-Newton approximation to Bayesian learning. In : Proceedings of International Conference on Neural Networks (ICNN'97). IEEE, 1997. p. 1930-1935. IEEE, juin 1997, p. 1930-1935.

[70] M. Fourrier, L. Coppola, H. Claustre, F. D'Ortenzio, R. Sauzède et J.-P. Gattuso. « A Regional Neural Network Approach to Estimate Water-Column Nutrient Concentrations and Carbonate System Variables in the Mediterranean Sea : CANYON-MED ». In : *Frontiers in Marine Science* 7 (2020). Publisher : Frontiers. doi : 10.3389/fmars.2020.00620.

[71] M. Fourrier, L. Coppola, H. Claustre, F. D'Ortenzio, R. Sauzède et J.-P. Gattuso. « Corrigendum : A Regional Neural Network Approach to Estimate Water-Column Nutrient Concentrations and Carbonate System Variables in the Mediterranean Sea : CANYON-MED ». In : *Frontiers in Marine Science* 8 (25 jan. 2021), p. 650509. doi : 10.3389/fmars.2021.650509.

[72] E. Frajka-Williams, P. B. Rhines et C. C. Eriksen. « Horizontal Stratification during Deep Convection in the Labrador Sea ». In : *Journal of Physical Oceanography* 44.1 (1er jan. 2014). Publisher : American Meteorological Society Section : Journal of Physical Oceanography, p. 220-228. doi : 10.1175/JPO-D-13-069.1.

[73] M. Gačić, G. L. E. Borzelli, G. Civitarese, V. Cardin et S. Yari. « Can internal processes sustain reversals of the ocean upper circulation ? The Ionian Sea example ». In : *Geophysical Research Letters* 37.9 (2010). _eprint : https ://agupubs.onlinelibrary.wiley.com/doi/pdf/10.1029/2010GL043216. doi : 10.1029/2010GL043216.

[74] J. C. Gascard et C. Richez. « Water masses and circulation in the Western Alboran sea and in the Straits of Gibraltar ». In : *Progress in Oceanography* 15.3 (1er jan. 1985), p. 157-216. doi : 10.1016/0079-6611(85)90031-X.

[75] T. D. Gedeon, P. M. Wong et D. Harris. *Balancing bias and variance : Network topology and pattern set reduction techniques*. Lecture Notes in Computer Science. Springer, Berlin, Heidelberg, 7 juin 1995.

[76] F. Giorgi. « Climate change hot-spots ». In : *Geophysical Research Letters* 33.8 (2006). doi : 10.1029/2006GL025734.

[77] L. Grignon, D. A. Smeed, H. L. Bryden et K. Schroeder. « Importance of the variability of hydrographic preconditioning for deep convection in the Gulf of Lion, NW Mediterranean ». In : *Ocean Science* 6.2 (14 juin 2010), p. 573-586. doi : 10.5194/os-6-573-2010.

[78] N. Gruber, S. C. Doney, S. R. Emerson, D. Gilbert, T. Kobayashi, A. Körtzinger, G. C. Johnson, K. S. Johnson, S. C. Riser et O. Ulloa. *The ARGO-Oxygen Program : A white paper to promote the addition of oxygen sensors to the international Argo float program*. Working Paper. Accepted : 2017-06-08T17 :52 :48Z. Prepared for distribution to the Argo Steering Committee, 14 fév. 2007.

[79] M. T. Hagan, H. B. Demuth, M. H. Beale et O. De Jesus. *Neural network design*. 2nd edition. Wrocław, 2014. 800 p.

[80] D. Hainbucher, A. Rubino, V. Cardin, T. Tanhua, K. Schroeder et M. Bensi. « Hydrographic situation during cruise M84/3 and P414 (spring 2011) in the Mediterranean Sea ». In : *Ocean Science* 10.4 (29 juil. 2014). Publisher : Copernicus GmbH, p. 669-682. doi : https://doi.org/10.5194/os-10-669-2014.

[81] N. Hamad, C. Millot et I. Taupier-Letage. « A new hypothesis about the surface circulation in the eastern basin of the mediterranean sea ». In : *Progress in Oceanography*. Mediterranean physical oceanography and biogeochemical cycles : Mediterranean general circulation and climate variability 66.2 (1er août 2005), p. 287-298. doi : 10.1016/j.pocean.2005.04.002.

[82] A. E. R. Hassoun, E. Gemayel, E. Krasakopoulou, C. Goyet, M. Abboud-Abi Saab, V. Guglielmi, F. Touratier et C. Falco. « Acidification of the Mediterranean Sea from anthropogenic carbon penetration ». In : *Deep Sea Research Part I : Oceanographic Research Papers* 102 (août 2015), p. 1-15. doi : 10.1016/j.dsr.2015.04.005.

[83] L.-E. Heimbürger, H. Lavigne, C. Migon, F. D'Ortenzio, C. Estournel, L. Coppola et J.-C. Miquel. « Temporal variability of vertical export flux at the DYFAMED time-series station (Northwestern Mediterranean Sea) ». In : *Progress in Oceanography* 119 (déc. 2013), p. 59-67. doi : 10.1016/j.pocean.2013.08.005.

[84] M. Herrmann, F. Sevault, J. Beuvier et S. Somot. « What induced the exceptional 2005 convection event in the northwestern Mediterranean basin ? Answers from a modeling study ». In : *Journal of Geophysical Research : Oceans* 115 (C12 2010). _eprint : https ://agupubs.onlinelibrary.wiley.com/doi/pdf/10.1029/2010JC006162. doi : https://doi.org/10.1029/2010JC006162.

[85] M. Herrmann, S. Somot, F. Sevault, C. Estournel et M. Déqué. « Modeling the deep convection in the northwestern Mediterranean Sea using an eddy-permitting and an eddy-resolving model : Case study of winter 1986–1987 ». In : *Journal of Geophysical Research : Oceans* 113 (C4 2008). _eprint : https ://agupubs.onlinelibrary.wiley.com/doi/pdf/10.1029/20
doi : https://doi.org/10.1029/2006JC003991.

[86] S. van Heuven, D. Pierrot, J. Rae, E. Lewis et D. Wallace. « CO2SYS v 1.1, MATLAB program developed for CO2 system calculations ». In : *ORNL/CDIAC-105b. Carbon Dioxide Information Analysis Center, Oak Ridge National Laboratory, U.S. DoE, Oak Ridge, TN.* (1er jan. 2011).

[87] K. Hornik, M. Stinchcombe et H. White. « Multilayer feedforward networks are universal approximators ». In : *Neural Networks* 2.5 (jan. 1989), p. 359-366. doi : 10.1016/0893-6080(89)90020-8.

[88] L. Houpert, X. Durrieu de Madron, P. Testor, A. Bosse, F. D'Ortenzio, M. N. Bouin, D. Dausse, H. Le Goff, S. Kunesch, M. Labaste, L. Coppola, L. Mortier et P. Raimbault. « Observations of open-ocean deep convection in the northwestern Mediterranean Sea : Seasonal and interannual variability of mixing and deep water masses for the 2007-2013 Period : DEEP CONVECTION OBS. NWMED 2007-2013 ». In : *Journal of Geophysical Research : Oceans* 121.11 (nov. 2016), p. 8139-8171. doi : 10.1002/2016JC011857.

[89] L. Houpert, P. Testor, X. Durrieu de Madron, S. Somot, F. D'Ortenzio, C. Estournel et H. Lavigne. « Seasonal cycle of the mixed layer, the seasonal thermocline and the upper-ocean heat storage rate in the Mediterranean Sea derived from observations ». In : *Progress in Oceanography*. Oceanography of the Arctic and North Atlantic Basins 132 (1er mar. 2015), p. 333-352. doi : 10.1016/j.pocean.2014.11.004.

[90] L. Houpert. « Contribution to the Study of Transfer Processes from the Surface to the Deep Ocean in the Mediterranean Sea using in situ Measurements ». Thèse de doct. Université de Perpignan via Domitia, 2013.

[91] V. V. Ivanov, G. I. Shapiro, J. M. Huthnance, D. L. Aleynik et P. N. Golovin. « Cascades of dense water around the world ocean ». In : *Progress in Oceanography* 60.1 (1er jan. 2004), p. 47-98. doi : 10.1016/j.pocean.2003.12.002.

[92] C. Jamet, H. Loisel et D. Dessailly. « Retrieval of the spectral diffuse attenuation coefficient Kd in open and coastal ocean waters using a neural network inversion ». In : *Journal of Geophysical Research : Oceans* 117 (C10023 oct. 2012). doi : 10.1029/2012JC008076.

[93] C. Jamet. « Inversion neuro-variationnelle des images de la couleur de l'ocean - Restitution des proprietes optiques des aerosols et de la concentration en chlorophylle-a pour les eaux du cas I ». Thèse de doct. Université Pierre et Marie Curie - Paris VI, 10 jan. 2004.

[94] K. S. Johnson et H. Claustre. « Bringing Biogeochemistry into the Argo Age ». In : *Eos* 97 (2016). doi : 10.1029/2016EO062427.

[95] K. S. Johnson, H. W. Jannasch, L. J. Coletti, V. A. Elrod, T. R. Martz, Y. Takeshita, R. J. Carlson et J. G. Connery. « Deep-Sea DuraFET : A Pressure Tolerant pH Sensor Designed for Global Sensor Networks ». In : *Analytical Chemistry* 88.6 (15 mar. 2016), p. 3249-3256. doi : 10.1021/acs.analchem.5b04653.

[96] K. S. Johnson, J. N. Plant, S. C. Riser et D. Gilbert. « Air Oxygen Calibration of Oxygen Optodes on a Profiling Float Array ». In : *Journal of Atmospheric and Oceanic Technology* 32.11 (30 sept. 2015), p. 2160-2172. doi : 10.1175/JTECH-D-15-0101.1.

[97] L. Kapsenberg, S. Alliouane, F. Gazeau, L. Mousseau et J.-P. Gattuso. « Coastal ocean acidification and increasing total alkalinity in the northwestern Mediterranean Sea ». In : *Ocean Science* 13.3 (15 mai 2017), p. 411-426. doi : 10.5194/os-13-411-2017.

[98] F. Kessouri. « Biogeochemical cycles of the Mediterranean sea ». Thèse de doct. Université Paul Sabatier - Toulouse III, 21 déc. 2015.

[99] F. Kessouri, C. Ulses, C. Estournel, P. Marsaleix, F. D'Ortenzio, T. Severin, V. Taillandier et P. Conan. « Vertical Mixing Effects on Phytoplankton Dynamics and Organic Carbon Export in the Western Mediterranean Sea ». In : *Journal of Geophysical Research : Oceans* 123.3 (mar. 2018), p. 1647-1669. doi : 10.1002/2016JC012669.

[100] F. Kessouri, C. Ulses, C. Estournel, P. Marsaleix, T. Severin, M. Pujo-Pay, J. Caparros, P. Raimbault, O. Pasqueron de Fommervault, F. D'Ortenzio, V. Taillandier, P. Testor et P. Conan. « Nitrogen and Phosphorus Budgets in the Northwestern Mediterranean Deep Convection Region ». In : *Journal of Geophysical Research : Oceans* 122.12 (déc. 2017), p. 9429-9454. doi : 10.1002/2016JC012665.

[101] B. Klein, W. Roether, B. B. Manca, D. Bregant, V. Beitzel, V. Kovacevic et A. Luchetta. « The large deep water transient in the Eastern Mediterranean ». In : *Deep Sea Research Part I : Oceanographic Research Papers* 46.3 (mar. 1999), p. 371-414. doi : 10.1016/S0967-0637(98)00075-2.

[102] A. Körtzinger, J. Schimanski, U. Send et D. Wallace. « The Ocean Takes a Deep Breath ». In : *Science* 306.5700 (19 nov. 2004). Publisher : American Association for the Advancement of Science Section : Brevia, p. 1337-1337. doi : 10.1126/science.1102557.

[103] A. Krishnamurthy, J. K. Moore, N. Mahowald, C. Luo et C. S. Zender. « Impacts of atmospheric nutrient inputs on marine biogeochemistry ». In : *Journal of Geophysical Research : Biogeosciences* 115 (G1 2010). _eprint : https ://agupubs.onlinelibrary.wiley.com/doi/pdf/10.1029/2009JG001115. doi : https://doi.org/10.1029/2009JG001115.

[104] M. Krom, E. Woodward, B. Herut, N. Kress, P. Carbo, R. Mantoura, G. Spyres, T. Thingstad, P. Wassmann, C. Wexels-Riser, V. Kitidis, C. Law et G. Zodiatis. « Nutrient cycling in the south east Levantine basin of the eastern Mediterranean : Results from a phosphorus starved system ». In : *Deep Sea Research Part II : Topical Studies in Oceanography* 52.22 (nov. 2005), p. 2879-2896. doi : 10.1016/j.dsr2.2005.08.009.

[105] H. Lacombe, P. Tchernia et L. Gamberoni. « Variable bottom water in the Western Mediterranean basin ». In : *Progress in Oceanography* 14 (1er jan. 1985), p. 319-338. doi : 10.1016/0079-6611(85)90015-1.

[106] P. Landschützer, N. Gruber et D. C. E. Bakker. « Decadal variations and trends of the global ocean carbon sink ». In : *Global Biogeochemical Cycles* 30.10 (oct. 2016), p. 1396-1417. doi : 10.1002/2015GB005359.

[107] P. Landschützer, G. G. Laruelle, A. Roobaert et P. Regnier. « A uniform pCO2 climatology combining open and coastal oceans ». In : *Earth System Science Data Discussions* (6 mai 2020). doi : 10.5194/essd-2020-90.

[108] A. Lascaratos et K. Nittis. « A high-resolution three-dimensional numerical study of intermediate water formation in the Levantine Sea ». In : *Journal of Geophysical Research : Oceans* 103 (C9 1998). _eprint : https ://agupubs.onlinelibrary.wiley.com/doi/pdf/10.1029/98JC01196 p. 18497-18511. doi : 10.1029/98JC01196.

[109] A. Lascaratos, W. Roether, K. Nittis et B. Klein. « Recent changes in deep water formation and spreading in the eastern Mediterranean Sea : a review ». In : *Progress in Oceanography* 44.1 (août 1999), p. 5-36. doi : 10.1016/S0079-6611(99)00019-1.

[110] A. Lascaratos, R. G. Williams et E. Tragou. « A mixed-layer study of the formation of Levantine intermediate water ». In : *Journal of Geophysical Research : Oceans* 98 (C8 1993). _eprint : https ://agupubs.onlinelibrary.wiley.com/doi/pdf/10.1029/93JC00912, p. 14739-14749. doi : https://doi.org/10.1029/93JC00912.

[111] S. K. Lauvset, B. R. Carter, F. F. Pèrez, L.-Q. Jiang, R. A. Feely, A. Velo et A. Olsen. « Processes Driving Global Interior Ocean pH Distribution ». In : *Global Biogeochemical Cycles* 34.1 (jan. 2020). doi : 10.1029/2019GB006229.

[112] H. Lavigne. « Impact of mixed layer depth seasonal variations on the phytoplankton phenology in the Mediterranean Sea ». Thèse de doct. Université Pierre et Marie Curie, 2013.

[113] H. Lavigne, F. D'Ortenzio, C. Migon, H. Claustre, P. Testor, M. R. d'Alcalà, R. Lavezza, L. Houpert et L. Prieur. « Enhancing the comprehension of mixed layer depth control on the Mediterranean phytoplankton phenology : Mediterranean Phytoplankton Phenology ». In : *Journal of Geophysical Research : Oceans* 118.7 (juil. 2013), p. 3416-3430. doi : 10.1002/jgrc.20251.

[114] P.-Y. Le Traon, F. D'Ortenzio, M. Babin, E. Leymarie, C. Marec, S. Pouliquen, V. Thierry, C. Cabanes, H. Claustre, D. Desbruyères, L. Lacour, J.-L. Lagunas, G. Maze, H. Mercier, C. Penkerc'h, N. Poffa, A. Poteau, L. Prieur, V. Racapé, A. Randelhoff, E. Rehm, C. M. Schmechtig, V. Taillandier, T. Wagener et X. Xing. « Preparing the New Phase of Argo : Scientific Achievements of the NAOS Project ». In : *Frontiers in Marine Science* 7 (14 oct. 2020), p. 577408. doi : 10.3389/fmars.2020.577408.

[115] N. Lefevre, A. J. Watson et A. R. Watson. « A comparison of multiple regression and neural network techniques for mapping in situ pCO2 data ». In : *Tellus B* 57.5 (nov. 2005), p. 375-384. doi : 10.1111/j.1600-0889.2005.00164.x.

[116] D. Lefévre, M. Denis, C. E. Lambert et J. .-C. Miquel. « Is DOC the main source of organic matter remineralization in the ocean water column ? » In : *Journal of Marine Systems*. The Coastal Ocean in a Global Change Perspective 7.2 (1er fév. 1996), p. 281-291. doi : 10.1016/0924-7963(95)00003-8.

[117] S. Lek et J. Guégan. « Artificial neural networks as a tool in ecological modelling, an introduction ». In : *Ecological Modelling* 120.2 (août 1999), p. 65-73. doi : 10.1016/S0304-3800(99)00092-7.

[118] M. Lévy, M. Visbeck et N. Naik. « Sensitivity of primary production to different eddy parameterizations : A case study of the spring bloom development in the northwestern Mediterranean Sea ». In : *Journal of Marine Research* 57.3 (1er mai 1999), p. 427-448. doi : 10.1357/002224099764805147.

[119] E. Lewis et D. W. R. Wallace. *Program developed for CO2 system calculations*. 1998.

[120] T. Liblik, J. Karstensen, P. Testor, P. Alenius, D. Hayes, S. Ruiz, K. Heywood, S. Pouliquen, L. Mortier et E. Mauri. « Potential for an underwater glider component as part of the Global Ocean Observing System ». In : *Methods in Oceanography* 17 (déc. 2016), p. 50-82. doi : 10.1016/j.mio.2016.05.001.

[121] A. Linares-Rodriguez, J. A. Ruiz-Arias, D. Pozo-Vazquez et J. Tovar-Pescador. « An artificial neural network ensemble model for estimating global solar radiation from Meteosat satellite images ». In : *Energy* 61 (nov. 2013), p. 636-645. doi : 10.1016/j.energy.2013.09.008.

[122] *LOCODOX*. original-date : 2020-05-19T12 :13 :53Z. 9 nov. 2020.

[123] J.-L. López-Jurado, C. González-Pola et P. Vélez-Belchí. « Observation of an abrupt disruption of the long-term warming trend at the Balearic Sea, western Mediterranean Sea, in summer 2005 ». In : *Geophysical Research Letters* 32.24 (2005). _eprint : https ://agupubs.onlinelibrary.wiley.com/doi/pdf/10.1029/2005GL024430. doi : https://doi.org/10.1029/2005GL024430.

[124] W. Ludwig, E. Dumont, M. Meybeck et S. Heussner. « River discharges of water and nutrients to the Mediterranean and Black Sea : Major drivers for ecosystem changes during past and future decades ? » In : *Progress in Oceanography* 80.3 (1er mar. 2009), p. 199-217. doi : 10.1016/j.pocean.2009.02.001.

[125] D. Macias, E. Garcia-Gorriz et A. Stips. « Deep winter convection and phytoplankton dynamics in the NW Mediterranean Sea under present climate and future (horizon 2030) scenarios ». In : *Scientific Reports* 8.1 (déc. 2018). doi : 10.1038/s41598-018-24965-0.

[126] D. J. C. MacKay. « A Practical Bayesian Framework for Backpropagation Networks ». In : *Neural Computation* 4.3 (mai 1992), p. 448-472. doi : 10.1162/neco.1992.4.3.448.

[127] D. J. C. MacKay. « Bayesian Interpolation ». In : *Neural Computation* 4.3 (1er mai 1992), p. 415-447. doi : 10.1162/neco.1992.4.3.415.

[128] P. Malanotte-Rizzoli, V. Artale, G. L. Borzelli-Eusebi, S. Brenner, A. Crise, M. Gacic, N. Kress, S. Marullo, M. Ribera d\&amp ;apos ;Alcalà, S. Sofianos, T. Tanhua, A. Theocharis, M. Alvarez, Y. Ashkenazy, A. Bergamasco, V. Cardin, S. Carniel, G. Civitarese, F. D\&amp ;apos ;Ortenzio, J. Font, E. Garcia-Ladona, J. M. Garcia-Lafuente, A. Gogou, M. Gregoire, D. Hainbucher, H. Kontoyannis, V. Kovacevic, E. Kraskapoulou, G. Kroskos, A. Incarbona, M. G. Mazzocchi, M. Orlic, E. Ozsoy, A. Pascual, P.-M. Poulain, W. Roether, A. Rubino, K. Schroeder, J. Siokou-Frangou, E. Souvermezoglou, M. Sprovieri, J. Tintoré et G. Triantafyllou. « Physical forcing and physical/biochemical variability of the Mediterranean Sea : a review of unresolved issues and directions for future research ». In : *Ocean Science* 10.3 (6 mai 2014), p. 281-322. doi : 10.5194/os-10-281-2014.

[129] B. B. Manca, L. Ursella et P. Scarazzato. « New Development of Eastern Mediterranean Circulation based on Hydrological Observations and Current Measurements ». In : *Marine Ecology* 23 (s1 2002). _eprint : https ://onlinelibrary.wiley.com/doi/pdf/10.1111/j.1439-0485.2002.tb00023.x, p. 237-257. doi : 10.1111/j.1439-0485.2002.tb00023.x.

[130] K. Marcellin Yao, O. Marcou, C. Goyet, V. Guglielmi, F. Touratier et J.-P. Savy. « Time variability of the north-western Mediterranean Sea pH over 1995–2011 ». In : *Marine Environmental Research* 116 (mai 2016), p. 51-60. doi : 10.1016/j.marenvres.2016.02.016.

[131] F. Margirier. « Etude de la variabilité physique et biogéochimique des masses d'eaux en Mer Méditerranée ». Thèse de doct. Paris : Sorbonne Université, 29 nov. 2018.

[132] F. Margirier, P. Testor, E. Heslop, K. Mallil, A. Bosse, L. Houpert, L. Mortier, M.-N. Bouin, L. Coppola, F. D'Ortenzio, X. Durrieu de Madron, B. Mourre, L. Prieur, P. Raimbault et V. Taillandier. « Abrupt warming and salinification of intermediate waters interplays with decline of deep convection in the Northwestern Mediterranean Sea ». In : *Scientific Reports* 10.1 (déc. 2020), p. 20923. doi : 10.1038/s41598-020-77859-5.

[133] P. Marsaleix, F. Auclair, J. W. Floor, M. J. Herrmann, C. Estournel, I. Pairaud et C. Ulses. « Energy conservation issues in sigma-coordinate free-surface ocean models ». In : *Ocean Modelling* 20.1 (jan. 2008), p. 61-89. doi : 10.1016/j.ocemod.2007.07.005.

[134] J. Marshall et F. Schott. « Open-ocean convection : Observations, theory, and models ». In : *Reviews of Geophysics* 37.1 (fév. 1999), p. 1-64. doi : 10.1029/98RG02739.

[135] J. C. Marty et J. Chiavérini. « Hydrological changes in the Ligurian Sea (NW Mediterranean, DYFAMED site) during 1995–2007 and biogeochemical consequences ». In : *Biogeosciences* 7.7 (7 juil. 2010), p. 2117-2128. doi : 10.5194/bg-7-2117-2010.

[136] J.-C. Marty, J. Chiavérini, M.-D. Pizay et B. Avril. « Seasonal and interannual dynamics of nutrients and phytoplankton pigments in the western Mediterranean Sea at the DYFAMED time-series station (1991–1999) ». In : *Deep Sea Research Part II : Topical Studies in Oceanography* 49.11 (jan. 2002), p. 1965-1985. doi : 10.1016/S0967-0645(02)00022-X.

[137] C. Marzban. « Basic Statistics and Basic AI : Neural Networks ». In : *Artificial Intelligence Methods in the Environmental Sciences*. Springer, Dordrecht, 2009, p. 15-47. doi : 10.1007/978-1-4020-9119-3_2.

[138] N. Mayot, F. D'Ortenzio, V. Taillandier, L. Prieur, O. P. de Fommervault, H. Claustre, A. Bosse, P. Testor et P. Conan. « Physical and Biogeochemical Controls of the Phytoplankton Blooms in North Western Mediterranean Sea : A Multiplatform Approach Over a Complete Annual Cycle (2012-2013 DEWEX Experiment) ». In : *Journal of Geophysical Research : Oceans* 122.12 (déc. 2017), p. 9999-10019. doi : 10.1002/2016JC012052.

[139] MEDOC GROUP. « Observation of Formation of Deep Water in the Mediterranean Sea, 1969 ». In : *Nature* 227.5262 (sept. 1970). Bandiera_abtest : a Cg_type : Nature Research Journals Number : 5262 Primary_atype : Research Publisher : Nature Publishing Group, p. 1037-1040. doi : 10.1038/2271037a0.

[140] C. Mehrbach, C. H. Culberson, J. E. Hawley et R. M. Pytkowicx. « Measurement of the apparent dissociation constants of carbonic acid in seawater at atmospheric pressure ». In : *Limnology and Oceanography* 18.6 (nov. 1973), p. 897-907. doi : 10.4319/lo.1973.18.6.0897.

[141] L. Merlivat, J. Boutin, D. Antoine, L. Beaumont, M. Golbol, V. Vellucci, S. Université-CNRS-IRD-MNHN et S. Université-CNRS. « Increase of dissolved inorganic carbon and decrease in pH in near-surface waters in the Mediterranean Sea during the past two decades ». In : *Biogeosciences* 15 (2018), p. 5653-5662.

[142] C. Migon, V. Sandroni, J.-C. Marty, B. Gasser et J.-C. Miquel. « Transfer of atmospheric matter through the euphotic layer in the northwestern Mediterranean : seasonal pattern and driving forces ». In : *Deep Sea Research Part II : Topical Studies in Oceanography*. Studies at the DYFAMED (France JGOFS) Time-Series Station, N.W. M editerranean Sea 49.11 (1er jan. 2002), p. 2125-2141. doi : 10.1016/S0967-0645(02)00031-0.

[143] C. Millot. « Circulation in the Western Mediterranean Sea ». In : *Journal of Marine Systems* 20.1 (1er avr. 1999), p. 423-442. doi : 10.1016/S0924-7963(98)00078-5.

[144] C. Millot et I. Taupier-Letage. « Circulation in the Mediterranean Sea ». In : *The Mediterranean Sea*. Sous la dir. d'A. Saliot. T. 5K. Berlin, Heidelberg : Springer Berlin Heidelberg, 2005, p. 29-66. doi : 10.1007/b107143.

[145] T. Moltmann, J. Turton, H.-M. Zhang, G. Nolan, C. Gouldman, L. Griesbauer, Z. Willis, Á. M. Piniella, S. Barrell, E. Andersson, C. Gallage, E. Charpentier, M. Belbeoch, P. Poli, A. Rea, E. F. Burger, D. M. Legler, R. Lumpkin, C. Meinig, K. O'Brien, K. Saha, A. Sutton, D. Zhang et Y. Zhang. « A Global Ocean Observing System (GOOS), Delivered Through Enhanced Collaboration Across Regions, Communities, and New Technologies ». In : *Frontiers in Marine Science* 6 (28 juin 2019), p. 291. doi : 10.3389/fmars.2019.00291.

[146] T. Moutin et P. Raimbault. « Primary production, carbon export and nutrients availability in western and eastern Mediterranean Sea in early summer 1996 (MINOS cruise) ». In : *Journal of Marine Systems*. MATER : MAss Transfer and Ecosystem Response 33-34 (1er juin 2002), p. 273-288. doi : 10.1016/S0924-7963(02)00062-3.

[147] K. Niewiadomska, H. Claustre, L. Prieur et F. d'Ortenzio. « Submesoscale physical-biogeochemical coupling across the Ligurian current (northwestern Mediterranean) using a bio-optical glider ». In : *Limnology and Oceanography* 53.5 (sept. 2008), p. 2210-2225. doi : 10.4319/lo.2008.53.5_part_2.2210.

[148] A. Olsen, R. M. Key, S. van Heuven, S. K. Lauvset, A. Velo, X. Lin, C. Schirnick, A. Kozyr, T. Tanhua, M. Hoppema, S. Jutterström, R. Steinfeldt, E. Jeansson, M. Ishii, F. F. Pérez et T. Suzuki. « The Global Ocean Data Analysis Project version 2 (GLODAPv2) – an internally consistent data product for the world ocean ». In : *Earth System Science Data* 8.2 (15 août 2016), p. 297-323. doi : 10.5194/essd-8-297-2016.

[149] J. de Oña et C. Garrido. « Extracting the contribution of independent variables in neural network models : a new approach to handle instability ». In : *Neural Computing and Applications* 25.3 (sept. 2014), p. 859-869. doi : 10.1007/s00521-014-1573-5.

[150] A. Oschlies. « A committed fourfold increase in ocean oxygen loss ». In : *Nature Communications* 12.1 (déc. 2021), p. 2307. doi : 10.1038/s41467-021-22584-4.

[151] A. Oschlies, K. G. Schulz, U. Riebesell et A. Schmittner. « Simulated 21st century's increase in oceanic suboxia by CO2-enhanced biotic carbon export ». In : *Global Biogeochemical Cycles* 22.4 (2008). _eprint : https ://agupubs.onlinelibrary.wiley.com/doi/pdf/10.1029/2
doi : 10.1029/2007GB003147.

[152] T. Packard, H. Minas, B. Coste, R. Martinez, M. Bonin, J. Gostan, P. Garfield, J. Christensen, Q. Dortch, M. Minas, G. Copin-Montegut et C. Copin-Montegut. « Formation of the Alboran oxygen minimum zone ». In : *Deep Sea Research Part A. Oceanographic Research Papers* 35.7 (juil. 1988), p. 1111-1118. doi : 10.1016/0198-0149(88)90003-9.

[153] R. Pagès, M. Baklouti, N. Barrier, M. Ayache, F. Sevault, S. Somot et T. Moutin. « Projected Effects of Climate-Induced Changes in Hydrodynamics on the Biogeochemistry of the Mediterranean Sea Under the RCP 8.5 Regional Climate Scenario ». In : *Frontiers in Marine Science* 7 (19 nov. 2020), p. 563615. doi : 10.3389/fmars.2020.563615.

[154] J. Palmiéri, J. C. Orr, J.-C. Dutay, K. Béranger, A. Schneider, J. Beuvier et S. Somot. « Simulated anthropogenic CO2 storage and acidification of the Mediterranean Sea ». In : *Biogeosciences* 12.3 (10 fév. 2015), p. 781-802. doi : 10.5194/bg-12-781-2015.

[155] O. Pasqueron de Fommervault, F. D'Ortenzio, A. Mangin, R. Serra, C. Migon, H. Claustre, H. Lavigne, M. Ribera d'Alcalà, L. Prieur, V. Taillandier, C. Schmechtig, A. Poteau, E. Leymarie, A. Dufour, F. Besson et G. Obolensky. « Seasonal variability of nutrient concentrations in the Mediterranean Sea : Contribution of Bio-Argo floats ». In : *Journal of Geophysical Research : Oceans* 120.12 (déc. 2015), p. 8528-8550. doi : 10.1002/2015JC011103.

[156] O. Pasqueron de Fommervault, C. Migon, F. D'Ortenzio, M. Ribera d'Alcalà et L. Coppola. « Temporal variability of nutrient concentrations in the northwestern Mediterranean sea (DYFAMED time-series station) ». In : *Deep Sea Research Part I : Oceanographic Research Papers* 100 (juin 2015), p. 1-12. doi : 10.1016/j.dsr.2015.02.006.

[157] O. Pasqueron de Fommervault, C. Migon, A. Dufour, F. D'Ortenzio, F. Kessouri, P. Raimbault, N. Garcia et V. Lagadec. « Atmospheric input of inorganic nitrogen and phosphorus to the Ligurian Sea : Data from the Cap Ferrat coastal time-series station ». In : *Deep Sea Research Part I : Oceanographic Research Papers* 106 (1er déc. 2015), p. 116-125. doi : 10.1016/j.dsr.2015.08.010.

[158] O. P. Pasqueron de Fommervault. « Dynamique des nutriments en Méditerranée : des campagnes océanographiques aux flotteurs Bio-Argo ». Thèse de doct. Université Pierre et Marie Curie, 2015.

[159] N. Pinardi, P. Cessi, F. Borile et C. L. P. Wolfe. « The Mediterranean Sea Overturning Circulation ». In : *Journal of Physical Oceanography* 49.7 (1er juil. 2019). Publisher : American Meteorological Society Section : Journal of Physical Oceanography, p. 1699-1721. doi : 10.1175/JPO-D-18-0254.1.

[160] N. Pinardi et A. Navarra. « Baroclinic wind adjustment processes in the Mediterranean Sea ». In : *Deep Sea Research Part II : Topical Studies in Oceanography* 40.6 (1er jan. 1993), p. 1299-1326. doi : 10.1016/0967-0645(93)90071-T.

[161] L. Possenti, I. Skjelvan, D. Atamanchuk, A. Tengberg, M. P. Humphreys, S. Loucaides, L. Fernand et J. Kaiser. « Norwegian Sea net community production estimated from O2 and prototype CO2 optode measurements on a Seaglider ». In : *Ocean Science* 17.2 (30 avr. 2021), p. 593-614. doi : 10.5194/os-17-593-2021.

[162] P.-M. Poulain, M. Menna et E. Mauri. « Surface Geostrophic Circulation of the Mediterranean Sea Derived from Drifter and Satellite Altimeter Data ». In : *Journal of Physical Oceanography* 42.6 (1er juin 2012). Publisher : American Meteorological Society Section : Journal of Physical Oceanography, p. 973-990. doi : 10.1175/JPO-D-11-0159.1.

[163] I. Puillat, I. Taupier-Letage et C. Millot. « Algerian Eddies lifetime can near 3 years ». In : *Journal of Marine Systems* 31.4 (1er jan. 2002), p. 245-259. doi : 10.1016/S0924-7963(01)00056-2.

[164] M. Pujo-Pay, P. Conan, L. Oriol, V. Cornet-Barthaux, C. Falco, J.-F. Ghiglione, C. Goyet, T. Moutin et L. Prieur. « Integrated survey of elemental stoichiometry (C, N, P) from the western to eastern Mediterranean Sea ». In : *Biogeosciences* 8.4 (8 avr. 2011), p. 883-899. doi : 10.5194/bg-8-883-2011.

[165] E. Rahav, J. Silverman, O. Raveh, O. Hazan, M. Rubin-Blum, C. Zeri, A. Gogou, M. Kralj, A. Pavlidou et N. Kress. « The deep water of Eastern Mediterranean Sea is a hotspot for bacterial activity ». In : *Deep Sea Research Part II : Topical Studies in Oceanography* (mar. 2019). doi : 10.1016/j.dsr2.2019.03.004.

[166] M. Reale, F. Giorgi, C. Solidoro, V. Di Biagio, F. Di Sante, L. Mariotti, R. Farneti et G. Sannino. « The Regional Earth System Model RegCM-ES : Evaluation of the Mediterranean Climate and Marine Biogeochemistry ». In : *Journal of Advances in Modeling Earth Systems* 12.9 (sept. 2020). doi : 10.1029/2019MS001812.

[167] A. Redfield. « On the Proportions of Organic Derivatives in Seawater and their Relation to the Composition of Plankton ». In : Liverpool University Press. T. James Johnstone Memorial Volume. Chapitre 5. Liverpool, UK : R.J. Danial, 1934, p. 176-192.

[168] M. Ribera d'Alcalà, G. Civitarese, F. Conversano et R. Lavezza. « Nutrient ratios and fluxes hint at overlooked processes in the Mediterranean Sea ». In : *Journal of Geophysical Research : Oceans* 108 (C9 2003). doi : 10.1029/2002JC001650.

[169] M. .-H. Rio, P. .-M. Poulain, A. Pascual, E. Mauri, G. Larnicol et R. Santoleri. « A Mean Dynamic Topography of the Mediterranean Sea computed from altimetric data, in-situ measurements and a general circulation model ». In : *Journal of Marine Systems*. Marine Environmental Monitoring and Prediction 65.1 (1er mar. 2007), p. 484-508. doi : 10.1016/j.jmarsys.2005.02.006.

[170] S. C. Riser et K. S. Johnson. « Net production of oxygen in the subtropical ocean ». In : *Nature* 451.7176 (jan. 2008), p. 323-325. doi : 10.1038/nature06441.

[171] R. A. Robinson, W. G. Leslie, A. Theocharis et A. Lascaratos. « Mediterranean Sea circulation ». In : *Ocean Currents*. Google-Books-ID : FYSCUH235E8C. Academic Press, 2010, p. 283-306.

[172] D. Roemmich et al. « On the Future of Argo : A Global, Full-Depth, Multi-Disciplinary Array ». In : *Frontiers in Marine Science* 6 (2 août 2019), p. 439. doi : 10.3389/fmars.2019.00439.

[173] W. Roether, B. Klein, B. B. Manca, A. Theocharis et S. Kioroglou. « Transient Eastern Mediterranean deep waters in response to the massive dense-water output of the Aegean Sea in the 1990s ». In : *Progress in Oceanography* 74.4 (1er sept. 2007), p. 540-571. doi : 10.1016/j.pocean.2007.03.001.

[174] F. Rosenblatt. « The perceptron : A probabilistic model for information storage and organization in the brain ». In : *Psychological Review* 65.6 (1958). Place : US Publisher : American Psychological Association, p. 386-408. doi : 10.1037/h0042519.

[175] F. Rosenblatt. « Perceptron Simulation Experiments ». In : *Proceedings of the IRE* 48.3 (mar. 1960). Conference Name : Proceedings of the IRE, p. 301-309. doi : 10.1109/JRPROC.1960.287598.

[176] S. Samuel, K. Haines, S. Josey et P. G. Myers. « Response of the Mediterranean Sea thermohaline circulation to observed changes in the winter wind stress field in the period 1980–1993 ». In : *Journal of Geophysical Research : Oceans* 104 (C4 1999). _eprint : https ://agupubs.onlinelibrary.wiley.com/doi/pdf/10.1029/1998JC900130, p. 7771-7784. doi : 10.1029/1998JC900130.

[177] R. Sauzède, H. C. Bittig, H. Claustre, O. Pasqueron de Fommervault, J.-P. Gattuso, L. Legendre et K. S. Johnson. « Estimates of water-column nutrient concentrations and carbonate system parameters in the global ocean : a novel approach based on neural networks ». In : *Frontiers in Marine Science* 4 (22 mai 2017). doi : 10.3389/fmars.2017.00128.

[178] R. Sauzède, E. Martinez, C. Maes, O. Pasqueron de Fommervault, A. Poteau, A. Mignot, H. Claustre, J. Uitz, L. Oziel, K. Maamaatuaiahutapu, M. Rodier, C. Schmechtig et V. Laurent. « Enhancement of phytoplankton biomass leeward of Tahiti as observed by Biogeochemical-Argo floats ». In : *Journal of Marine Systems* 204 (avr. 2020), p. 103284. doi : 10.1016/j.jmarsys.2019.103284.

[179] M. Scardi. « Artificial neural networks as empirical models for estimating phytoplankton production ». In : (), p. 11.

[180] A. Schneider, T. Tanhua, A. Körtzinger et D. W. R. Wallace. « High anthropogenic carbon content in the eastern Mediterranean ». In : *Journal of Geophysical Research* 115 (C12 21 déc. 2010). doi : 10.1029/2010JC006171.

[181] A. Schneider, T. Tanhua, W. Roether et R. Steinfeldt. « Changes in ventilation of the Mediterranean Sea during the past 25 year ». In : *Ocean Science* 10.1 (27 jan. 2014), p. 1-16. doi : 10.5194/os-10-1-2014.

[182] K. Schröder, G. P. Gasparini, M. Tangherlini et M. Astraldi. « Deep and intermediate water in the western Mediterranean under the influence of the Eastern Mediterranean Transient ». In : *Geophysical Research Letters* 33.21 (2006). _eprint : https ://agupubs.onlinelibrary.wiley.com/doi/pdf/10.1029/2006GL027121. doi : https://doi.org/10.1029/2006GL027121.

[183] K. Schroeder, J. Chiggiato, H. L. Bryden, M. Borghini et S. Ben Ismail. « Abrupt climate shift in the Western Mediterranean Sea ». In : *Scientific Reports* 6.1 (11 mar. 2016). Number : 1 Publisher : Nature Publishing Group, p. 23009. doi : 10.1038/srep23009.

[184] K. Schroeder, S. A. Josey, M. Herrmann, L. Grignon, G. P. Gasparini et H. L. Bryden. « Abrupt warming and salting of the Western Mediterranean Deep Water after 2005 : Atmospheric forcings and lateral advection ». In : *Journal of Geophysical Research* 115 (C8 27 août 2010), p. C08029. doi : 10.1029/2009JC005749.

[185] K. Schroeder, C. Millot, L. Bengara, S. Ben Ismail, M. Bensi, M. Borghini, G. Budillon, V. Cardin, L. Coppola, C. Curtil, A. Drago, B. El Moumni, J. Font, J. L. Fuda, J. García-Lafuente, G. P. Gasparini, H. Kontoyiannis, D. Lefevre, P. Puig, P. Raimbault, G. Rougier, J. Salat, C. Sammari, J. C. Sánchez Garrido, A. Sanchez-Roman, S. Sparnocchia, C. Tamburini, I. Taupier-Letage, A. Theocharis, M. Vargas-Yáñez et A. Vetrano. « Long-term monitoring programme of the hydrological variability in the Mediterranean Sea : a first overview of the HYDROCHANGES network ». In : *Ocean Science* 9.2 (19 mar. 2013), p. 301-324. doi : 10.5194/os-9-301-2013.

[186] K. Schroeder, A. Ribotti, M. Borghini, R. Sorgente, A. Perilli et G. P. Gasparini. « An extensive western Mediterranean deep water renewal between 2004 and 2006 ». In : *Geophysical Research Letters* 35.18 (2008). _eprint : https ://agupubs.onlinelibrary.wiley.com/doi/pdf/10.1029/2008GL035146. doi : 10.1029/2008GL035146.

[187] K. Schroeder, V. Taillandier, A. Vetrano et G. P. Gasparini. « The circulation of the western Mediterranean Sea in spring 2005 as inferred from observations and from model outputs ». In : *Deep Sea Research Part I : Oceanographic Research Papers* 55.8 (1er août 2008), p. 947-965. doi : 10.1016/j.dsr.2008.04.003.

[188] K. Schroeder, S. Cozzi, M. Belgacem, M. Borghini, C. Cantoni, S. Durante, A. Petrizzo, A. Poiana et J. Chiggiato. « Along-Path Evolution of Biogeochemical and Carbonate System Properties in the Intermediate Water of the Western Mediterranean ». In : *Frontiers in Marine Science* 7 (29 mai 2020), p. 375. doi : 10.3389/fmars.2020.00375.

[189] K. Schroeder, J. Lafuente, S. Josey, V. Artale, B. Buongiorno Nardelli, M. Gacic, G. Gasparini, M. Herrmann, P. Lionello, W. Ludwig, C. Millot, E. Özsoy, G. Pisacane, J. Sánchez-Garrido, G. Sannino, R. Santoleri, S. Somot, M. Struglia, E. Stanev et G. Zodiatis. « Circulation of the Mediterranean Sea and its variability ». In : *The mediterranean climate : from past to future*. 1er jan. 2012.

[190] K. Schroeder, T. Tanhua, H. Bryden, M. Alvarez, J. Chiggiato et S. Aracri. « Mediterranean Sea Ship-based Hydrographic Investigations Program (Med-SHIP) ». In : *Oceanography* 28.3 (1er sept. 2015), p. 12-15. doi : 10.5670/oceanog.2015.71.

[191] T. Severin, P. Conan, X. Durrieu de Madron, L. Houpert, M. J. Oliver, L. Oriol, J. Caparros, J. F. Ghiglione et M. Pujo-Pay. « Impact of open-ocean convection on nutrients, phytoplankton biomass and activity ». In : *Deep Sea Research Part I : Oceanographic Research Papers* 94 (1er déc. 2014), p. 62-71. doi : 10.1016/j.dsr.2014.07.015.

[192] T. Severin, F. Kessouri, M. Rembauville, E. D. Sánchez-Pérez, L. Oriol, J. Caparros, M. Pujo-Pay, J.-F. Ghiglione, F. D'Ortenzio, V. Taillandier, N. Mayot, X. Durrieu De Madron, C. Ulses, C. Estournel et P. Conan. « Open-ocean convection process : A driver of the winter nutrient supply and the spring phytoplankton distribution in the Northwestern Mediterranean Sea ». In : *Journal of Geophysical Research : Oceans* 122.6 (juin 2017), p. 4587-4601. doi : 10.1002/2016JC012664.

[193] G. I. Shapiro, J. M. Huthnance et V. V. Ivanov. « Dense water cascading off the continental shelf ». In : *Journal of Geophysical Research : Oceans* 108 (C12 2003). _eprint : https ://agupubs.onlinelibrary.wiley.com/doi/pdf/10.1029/2002JC001610. doi : 10.1029/2002JC001610.

[194] A. J. C. Sharkey, éd. *Combining Artificial Neural Nets : Ensemble and Modular Multi-Net Systems*. Perspectives in Neural Computing. London : Springer-Verlag, 1999.

[195] R. O. Smith, H. L. Bryden et K. Stansfield. « Observations of new western Mediterranean deep water formation using Argo floats 2004-2006 ». In : *Ocean Science* 4.2 (14 mai 2008). Publisher : Copernicus GmbH, p. 133-149. doi : https://doi.org/10.5194/os-4-133-2008.

[196] S. Somot, F. Sevault et M. Déqué. « Transient climate change scenario simulation of the Mediterranean Sea for the twenty-first century using a high-resolution ocean circulation model ». In : *Climate Dynamics* 27.7 (12 oct. 2006), p. 851-879. doi : 10.1007/s00382-006-0167-z.

[197] S. Somot, L. Houpert, F. Sevault, P. Testor, A. Bosse, I. Taupier-Letage, M.-N. Bouin, R. Waldman, C. Cassou, E. Sanchez-Gomez, X. Durrieu de Madron, F. Adloff, P. Nabat et M. Herrmann. « Characterizing, modelling and understanding the climate variability of the deep water formation in the North-Western Mediterranean Sea ». In : *Climate Dynamics* 51.3 (août 2018), p. 1179-1210. doi : 10.1007/s00382-016-3295-0.

[198] J. Soto-Navarro, G. Jordá, A. Amores, W. Cabos, S. Somot, F. Sevault, D. Macías, V. Djurdjevic, G. Sannino, L. Li et D. Sein. « Evolution of Mediterranean Sea water properties under climate change scenarios in the Med-CORDEX ensemble ». In : *Climate Dynamics* 54.3 (fév. 2020), p. 2135-2165. doi : 10.1007/s00382-019-05105-4.

[199] A. Sournia. « La production primaire planctonique en Méditerranée. Essai de mise à jour ». In : *LA PRODUCTION PRIMAIRE PLANCTONIQUE EN MEDITERRANEE. ESSAI DE MISE A JOUR*. Bull. Etud. Commun. Medit. Monaco, 1973, p. 1-128.

[200] S. Sparnocchia, G. M. R. Manzella et P. E. L. Violette. « The Interannual and Seasonal Variability of the MAW and LIW Core Properties in the Western Mediterranean Sea ». In : *Seasonal and Interannual Variability of the Western Mediterranean Sea*. Section : 10 _eprint : https ://agupubs.onlinelibrary.wiley.com/doi/pdf/10.1029/CE046p0117. American Geophysical Union (AGU), 1994, p. 177-194. doi : 10.1029/CE046p0117.

[201] H. Sur, E. Ozsoy et U. Unluata. « Simultaneous deep and intermediate depth convection in the northern levantine sea, winter 1992 ». In : *Oceanologica Acta* 16.1 (1er jan. 1993). Publisher : Gauthier-Villars, p. 33-43.

[202] Y. Takeshita, T. R. Martz, K. S. Johnson, J. N. Plant, D. Gilbert, S. C. Riser, C. Neill et B. Tilbrook. « A climatology-based quality control procedure for profiling float oxygen data : Qc Procedure for Profiling Float Oxygen ». In : *Journal of Geophysical Research : Oceans* 118.10 (oct. 2013), p. 5640-5650. doi : 10.1002/jgrc.20399.

[203] C. Tamburini et al. « Deep-Sea Bioluminescence Blooms after Dense Water Formation at the Ocean Surface ». In : *PLoS ONE* 8.7 (10 juil. 2013). Sous la dir. de J. M. Roberts, e67523. doi : 10.1371/journal.pone.0067523.

[204] T. Tanhua, D. Hainbucher, K. Schroeder, V. Cardin, M. Álvarez et G. Civitarese. « The Mediterranean Sea system : a review and an introduction to the special issue ». In : *Ocean Science* 9.5 (6 sept. 2013), p. 789-803. doi : 10.5194/os-9-789-2013.

[205] M. Telszewski, A. Chazottes, U. Schuster, A. J. Watson, C. Moulin, D. C. E. Bakker, M. González-Dávila, T. Johannessen, A. Körtzinger, H. Lüger, A. Olsen, A. Omar, X. A. Padin, A. F. Ríos, T. Steinhoff, M. Santana-Casiano, D. W. R. Wallace et R. Wanninkhof. « Estimating the monthly pCO2 distribution in the North Atlantic using a self-organizing neural network ». In : *Biogeosciences* 6.8 (5 août 2009), p. 1405-1421. doi : 10.5194/bg-6-1405-2009.

[206] P. Testor, X. Durrieu De Madron, L. Mortier, F. D'ortenzio, H. Legoff, D. Dausse, M. Labaste et L. Houpert. *LION observatory data*. type : dataset. 2020. doi : 10.17882/44411.

[207] P. Testor, U. Send, J.-C. Gascard, C. Millot, I. Taupier-Letage et K. Béranger. « The mean circulation of the southwestern Mediterranean Sea : Algerian Gyres ». In : *Journal of Geophysical Research : Oceans* 110 (C11 2005). _eprint : https ://agupubs.onlinelibrary.wiley.com/doi/pdf/10.1029/2004JC002861. doi : 10.1029/2004JC002861.

[208] P. Testor, A. Bosse, L. Houpert, F. Margirier, L. Mortier, H. Legoff, D. Dausse, M. Labaste, J. Karstensen, D. Hayes, A. Olita, A. Ribotti, K. Schroeder, J. Chiggiato, R. Onken, E. Heslop, B. Mourre, F. D'ortenzio, N. Mayot, H. Lavigne, O. d. Fommervault, L. Coppola, L. Prieur, V. Taillandier, X. D. d. Madron, F. Bourrin, G. Many, P. Damien, C. Estournel, P. Marsaleix, I. Taupier-Letage, P. Raimbault, R. Waldman, M.-N. Bouin, H. Giordani, G. Caniaux, S. Somot, V. Ducrocq et P. Conan. « Multiscale Observations of Deep Convection in the Northwestern Mediterranean Sea During Winter 2012–2013 Using Multiple Platforms ». In : *Journal of Geophysical Research : Oceans* 123.3 (2018), p. 1745-1776. doi : 10.1002/2016JC012671.

[209] P. Testor, G. Meyers, C. Pattiaratchi, R. Bachmayer, D. Hayes, S. Pouliquen, L. Petit de la Villeon, T. Carval, A. Ganachaud, L. Gourdeau, L. Mortier, H. Claustre, V. Taillandier, P. Lherminier, T. Terre, M. Visbeck, J. Karstensen, G. Krahmann, A. Alvarez, M. Rixen, P.-M. Poulain, S. Osterhus, J. Tintore, S. Ruiz, B. Garau, D. Smeed, G. Griffiths, L. Merckelbach, T. Sherwin, C. Schmid, J. A. Barth, O. Schofield, S. Glenn, J. Kohut, M. J. Perry, C. Eriksen, U. Send, R. David, D. Rudnick, J. Sherman, C. Jones, D. Webb, V. Lee et B. Owens. « Gliders as a Component of Future Observing Systems ». In : *Proceedings of OceanObs'09 : Sustained Ocean Observations and Information for Society*. OceanObs'09 : Sustained Ocean Observations and Information for Society. European Space Agency, 31 déc. 2010, p. 961-978. doi : 10.5270/OceanObs09.cwp.89.

[210] P. Testor et al. « OceanGliders : A Component of the Integrated GOOS ». In : *Frontiers in Marine Science* 6 (2 oct. 2019), p. 422. doi : 10.3389/fmars.2019.00422.

[211] The LIWEX Group. « The Levantine Intermediate Water Experiment (LIWEX) Group : Levantine basin—A laboratory for multiple water mass formation processes ». In : *Journal of Geophysical Research* 108 (C9 2003), p. 8101. doi : 10.1029/2002JC001643.

[212] A. Theocharis, D. Georgopoulos, A. Lascaratos et K. Nittis. « Water masses and circulation in the central region of the Eastern Mediterranean : Eastern Ionian, South Aegean and Northwest Levantine, 1986–1987 ». In : *Deep Sea Research Part II : Topical Studies in Oceanography* 40.6 (1er jan. 1993), p. 1121-1142. doi : 10.1016/0967-0645(93)90064-T.

[213] A. Theocharis, E. Balopoulos, S. Kioroglou, H. Kontoyiannis et A. Iona. « A synthesis of the circulation and hydrography of the South Aegean Sea and the Straits of the Cretan Arc (March 1994–January 1995) ». In : *Progress in Oceanography* 44.4 (1er déc. 1999), p. 469-509. doi : 10.1016/S0079-6611(99)00041-5.

[214] A. Theocharis, K. Nittis, H. Kontoyiannis, E. Papageorgiou et E. Balopoulos. « Climatic changes in the Aegean Sea influence the eastern Mediterranean thermohaline circulation (1986–1997) ». In : *Geophysical Research Letters* 26.11 (1999). _eprint : https ://agupubs.onlinelibrary.wiley.com/doi/pdf/10.1029/1999GL900320, p. 1617-1620. doi : 10.1029/1999GL900320.

[215] V. Thierry, H. Bittig, D. Gilbert, T. Kobayashi, S. Kanako et C. Schmid. *Processing Argo oxygen data at the DAC level*. Medium : pdf Version Number : 2.3.1. Ifremer, 2018. doi : 10.13155/39795.

[216] V. Thierry, H. Bittig et T. A.-B. Team. « Argo quality control manual for dissolved oxygen concentration ». In : (24 fév. 2021).

[217] J. Tintoré et al. « Challenges for Sustained Observing and Forecasting Systems in the Mediterranean Sea ». In : *Frontiers in Marine Science* 6 (13 sept. 2019), p. 568. doi : 10.3389/fmars.2019.00568.

[218] F. Touratier, C. Goyet, L. Houpert, X. D. de Madron, D. Lefèvre, M. Stabholz et V. Guglielmi. « Role of deep convection on anthropogenic CO2 sequestration in the Gulf of Lions (northwestern Mediterranean Sea) ». In : *Deep Sea Research Part I : Oceanographic Research Papers* 113 (juil. 2016), p. 33-48. doi : 10.1016/j.dsr.2016.04.003.

[219] F. Touratier et C. Goyet. « Decadal evolution of anthropogenic CO2 in the northwestern Mediterranean Sea from the mid-1990s to the mid-2000s ». In : *Deep Sea Research Part I : Oceanographic Research Papers* 56.10 (oct. 2009), p. 1708-1716. doi : 10.1016/j.dsr.2009.05.015.

[220] F. Touratier et C. Goyet. « Impact of the Eastern Mediterranean Transient on the distribution of anthropogenic CO2 and first estimate of acidification for the Mediterranean Sea ». In : *Deep Sea Research Part I : Oceanographic Research Papers* 58.1 (jan. 2011), p. 1-15. doi : 10.1016/j.dsr.2010.10.002.

[221] M. N. Tsimplis, V. Zervakis, S. A. Josey, E. L. Peneva, M. V. Struglia, E. V. Stanev, A. Theocharis, P. Lionello, P. Malanotte-Rizzoli, V. Artale, E. Tragou et T. Oguz. « Chapter 4 Changes in the oceanography of the Mediterranean Sea and their link to climate variability ». In : *Developments in Earth and Environmental Sciences*. T. 4. Elsevier, 2006, p. 227-282. doi : 10.1016/S1571-9197(06)80007-8.

[222] C. Ulses, P.-A. Auger, K. Soetaert, P. Marsaleix, F. Diaz, L. Coppola, M. Herrmann, F. Kessouri et C. Estournel. « Budget of organic carbon in the North-Western Mediterranean open sea over the period 2004-2008 using 3-D coupled physical-biogeochemical modeling ». In : *Journal of Geophysical Research : Oceans* 121.9 (sept. 2016), p. 7026-7055. doi : 10.1002/2016JC011818.

[223] C. Ulses, C. Estournel, M. Fourrier, L. Coppola, F. Kessouri, D. Lefèvre et P. Marsaleix. « Oxygen budget of the north-western Mediterranean deep-convection region ». In : *Biogeosciences* 18.3 (10 fév. 2021), p. 937-960. doi : 10.5194/bg-18-937-2021.

[224] L. R. Uppström. « The boron/chlorinity ratio of deep-sea water from the Pacific Ocean ». In : *Deep Sea Research* 21 (1974), p. 161-162.

[225] L. Urbini, G. Ingrosso, T. Djakovac, S. Piacentino et M. Giani. « Temporal and Spatial Variability of the CO2 System in a Riverine Influenced Area of the Mediterranean Sea, the Northern Adriatic ». In : *Frontiers in Marine Science* 7 (2020). Publisher : Frontiers. doi : 10.3389/fmars.2020.00679.

[226] J. J. Vega, R. Reynoso et H. C. Calvet. « Effect of signal noise on the learning capability of an artificial neural network ». In : *Nuclear Instruments and Methods in Physics Research Section A : Accelerators, Spectrometers, Detectors and Associated Equipment* 606.3 (21 juil. 2009), p. 693-699. doi : 10.1016/j.nima.2009.04.021.

[227] D. Velaoras, D. Kassis, L. Perivoliotis, P. Pagonis, A. Hondronasios et K. Nittis. « Temperature and salinity variability in the Greek Seas based on POSEIDON stations time series : preliminary results ». In : *Mediterranean Marine Science* 14.3 (21 juin 2013). Number : 3, p. 5-18. doi : 10.12681/mms.446.

[228] D. Velaoras, V. P. Papadopoulos, H. Kontoyiannis, V. Cardin et G. Civitarese. « Water masses and hydrography during April and June 2016 in the Cretan Sea and Cretan Passage (Eastern Mediterranean Sea) ». In : *Deep Sea Research Part II : Topical Studies in Oceanography* (sept. 2018), S0967064518300857. doi : 10.1016/j.dsr2.2018.09.005.

[229] Z. A. Wang, H. Moustahfid, A. V. Mueller, A. P. M. Michel, M. Mowlem, B. T. Glazer, T. A. Mooney, W. Michaels, J. S. McQuillan, J. C. Robidart, J. Churchill, M. Sourisseau, A. Daniel, A. Schaap, S. Monk, K. Friedman et P. Brehmer. « Advancing Observation of Ocean Biogeochemistry, Biology, and Ecosystems With Cost-Effective in situ Sensing Technologies ». In : *Frontiers in Marine Science* 6 (6 sept. 2019), p. 519. doi : 10.3389/fmars.2019.00519.

[230] R. G. Williams et M. J. Follows. « Physical Transport of Nutrients and the Maintenance of Biological Production ». In : *Ocean Biogeochemistry : The Role of the Ocean Carbon Cycle in Global Change*. Sous la dir. de M. J. R. Fasham. Global Change — The IGBP Series (closed). Berlin, Heidelberg : Springer, 2003, p. 19-51. doi : 10.1007/978-3-642-55844-3_3.

[231] C. Wimart-Rousseau, T. Wagener, M. Álvarez, T. Moutin, M. Fourrier, L. Coppola, L. Niclas-Chirurgien, P. Raimbault, F. D'Ortenzio, X. Durrieu de Madron, V. Taillandier, F. Dumas, P. Conan, M. Pujo-Pay et D. Lefèvre. « Seasonal and Interannual Variability of the CO2 System in the Eastern Mediterranean Sea : A Case Study in the North Western Levantine Basin ». In : *Frontiers in Marine Science* 8 (17 mai 2021), p. 649246. doi : 10.3389/fmars.2021.649246.

[232] X. Xing, H. Claustre, J. Uitz, A. Mignot, A. Poteau et H. Wang. « Seasonal variations of bio-optical properties and their interrelationships observed by Bio-Argo floats in the subpolar North Atlantic ». In : *Journal of Geophysical Research : Oceans* 119.10 (2014). _eprint : https ://agupubs.onlinelibrary.wiley.com/doi/pdf/10.1002/2014JC010189, p. 7372-7388. doi : 10.1002/2014JC010189.

[233] M. Zavatarielli et G. L. Mellor. « A Numerical Study of the Mediterranean Sea Circulation ». In : *Journal of Physical Oceanography* 25.6 (1er juin 1995). Publisher : American Meteorological Society Section : Journal of Physical Oceanography, p. 1384-1414. doi : 10.1175/1520-0485(1995)025<1384:ANSOTM>2.0.CO;2.

[234] R. E. Zeebe et D. Wolf-Gladrow. *CO2 in Seawater : Equilibrium, Kinetics, Isotopes*. Google-Books-ID : g3j3Zn4kEscC. Gulf Professional Publishing, 29 oct. 2001. 382 p.

[235] V. Zervakis, D. Georgopoulos et P. G. Drakopoulos. « The role of the North Aegean in triggering the recent Eastern Mediterranean climatic changes ». In : *Journal of Geophysical Research : Oceans* 105 (C11 2000). _eprint : https ://agupubs.onlinelibrary.wiley.com/doi/ p. 26103-26116. doi : 10.1029/2000JC900131.

Liste des publications

Sommaire du présent chapitre

Publications dans des revues à comités de lecture

1. Wimart-Rousseau, C., Wagener, T., Álvarez, M., Moutin, T., Fourrier, M., Coppola, L., Niclas-Chirurgien, L., Raimbault, P., D'Ortenzio, F., Durrieu de Madron, X., Taillandier, V., Dumas, F., Conan, P., Pujo-Pay, M., and Lefèvre, D. (2021). ***Seasonal and Interannual Variability of the CO_2 System in the Eastern Mediterranean Sea : A Case Study in the North Western Levantine Basin***. Frontiers in Marine Science, 8, 649246. DOI : 10.3389/fmars.2021.649246
2. D'Ortenzio, F., Taillandier, V., Claustre, H., Coppola, L., Conan, P., Dumas, F., Durrieu de Madron X., Fourrier, M., Gogou A., Karageorgis, A., Lefevre, D., Lymarie, E., Oviedo, A., Pavlidou, A., Poteau, A., Poulain, P. M., Prieur, L., Psarra, S, Pujo-Pay, M., Ribera d'Alcalà, M., Schmechtig, C., Terrats, L., Velaoras, D., Wagener, T., and Wimart-Rousseau, C. (2021). ***BGC-Argo Floats Observe Nitrate Injection and Spring Phytoplankton Increase in the Surface Layer of Levantine Sea (Eastern Mediterranean)***. Geophysical Research Letters, 48(8). DOI : 10.1029/2020GL091649
3. Ulses, C., Estournel, C., Fourrier, M., Coppola, L., Kessouri, F., Lefèvre, D., Marsaleix, P. (2021). ***Oxygen budget of the north-western Mediterranean deep-convection region***. Biogeosciences, 18(3), 937–960. DOI : 10.5194/bg-18-937-2021
4. Fourrier, M., Coppola, L., Claustre, H., D'Ortenzio, F., Sauzède, R., Gattuso, J.-P. (2020). ***A Regional Neural Network Approach to Estimate Water-Column Nutrient Concentrations and Carbonate System Variables in the Mediterranean Sea : CANYON-MED***. Frontiers in Marine Science, 7. DOI : 10.3389/fmars.2020.00620

Présentations et posters

1. Fourrier, M., Coppola, L., D'Ortenzio, F. (2-5 Novembre 2021). ***Apport des méthodes neuronales pour le suivi des paramètres biogéochimiques, perspectives d'application au domaine côtier***. Colloque ILICO-EVOLECO, La Rochelle, France. Présentation Orale. *Prix du meilleur oral doctorant.*

2. Fourrier, M., Coppola, L., D'Ortenzio, F., Gattuso, J.-P. (Online, 22-27 June 2021). ***Changes in the carbonate system evolution of the northwestern Mediterranean Sea using a neural network based method and potential applications to the coastal environment***. ASLO 2021 Aquatic Sciences Meeting. Présentation orale.
3. Fourrier, M., Coppola, L., D'Ortenzio, F. (Online, 24-25 November 2020). ***Evolution of dissolved O_2, nutrients and carbonate system variables in the northwestern Mediterranean Sea using a machine learning method***. 9th MONGOOS Workshop. Présentation orale.
4. Fourrier, M., Coppola, L., D'Ortenzio, F. (Online, 16-18 November 2020). ***Evolution de l'O_2, des nutriments et des carbonates en Méditerranée Nord-Occidentale par une méthode de machine learning***. Med2020. Poster.
5. Fourrier, M., Coppola, L., D'Ortenzio, F. (Online, 4-8 May 2020). ***New insights into nutrients dynamics and the carbonate system using a neural network approach in the Mediterranean Sea***. European Geosciences Union General Assembly 2020. EGU2020-9520. Poster. DOI : 10.5194/egusphere-egu2020-9520.
6. Fourrier, M., Coppola, L., D'Ortenzio, F., Claustre, H. (22-23 October 2019). ***A neural network approach to estimate water-column nutrient concentrations and carbonate system parameters in the Mediterranean Sea : CANYON-MED***. 7th Euro Argo Science Meeting, Athens, Greece. Poster.
7. Fourrier, M., Coppola, L., D'Ortenzio, F., Claustre, H., Sauzède, R., Bittig, H. C., Àlvarez, M. (7-12 April 2019). ***A neural network approach to estimate water-column nutrient concentrations and carbonate system parameters in the Mediterranean Sea : CANYON-MED***. European Geosciences Union General Assembly 2019, Vienna, Austria. Poster.

Annexes

Sommaire du présent chapitre

Annexe 1 : Matériel auxiliaire de l'article - Chapitre 5
Convection et biogéochimie en Méditerranée nord-occidentale

Journal of Geophysical Research : Oceans

Supporting Information for

Impact of intermittent Convection in the northwestern Mediterranean Sea on Oxygen content, Nutrients and the Carbonate system

Marine Fourrier[1], Laurent Coppola[1,2], Fabrizio D'Ortenzio[1], Christophe Migon[1], Jean-Pierre Gattuso[1,3]

[1]Sorbonne Université, CNRS, Laboratoire d'Océanographie de Villefranche, F-06230 Villefranche-sur-Mer, France
[2]Sorbonne Université, CNRS, Institut de la Mer de Villefranche, F-06230 Villefranche-sur-Mer, France
[3]Institute for Sustainable Development and International Relations, Sciences Po, Paris, France

Contents of this file

Figures S1 to S3

Introduction

Supporting information consists of three supporting figures, one supplementary dataset and one supporting table. The first supporting figures provides an intercomparison between the different data platforms used to study O_2 dynamics in figure 3 of the manuscript. The second supporting figure details the regressions between *in situ* data and the CANYON-MED derived data used in this study according to matchup distance to verify the accuracy of the method and its use for the study. The third supporting figure details the variations in terms of biogeochemistry at different depths of the water column with data for the two areas (Ligurian Sea and Gulf of Lion) pooled by year. This figure uses the same data as Figure 4 of the manuscript but allows for a different and complementary description of the data.

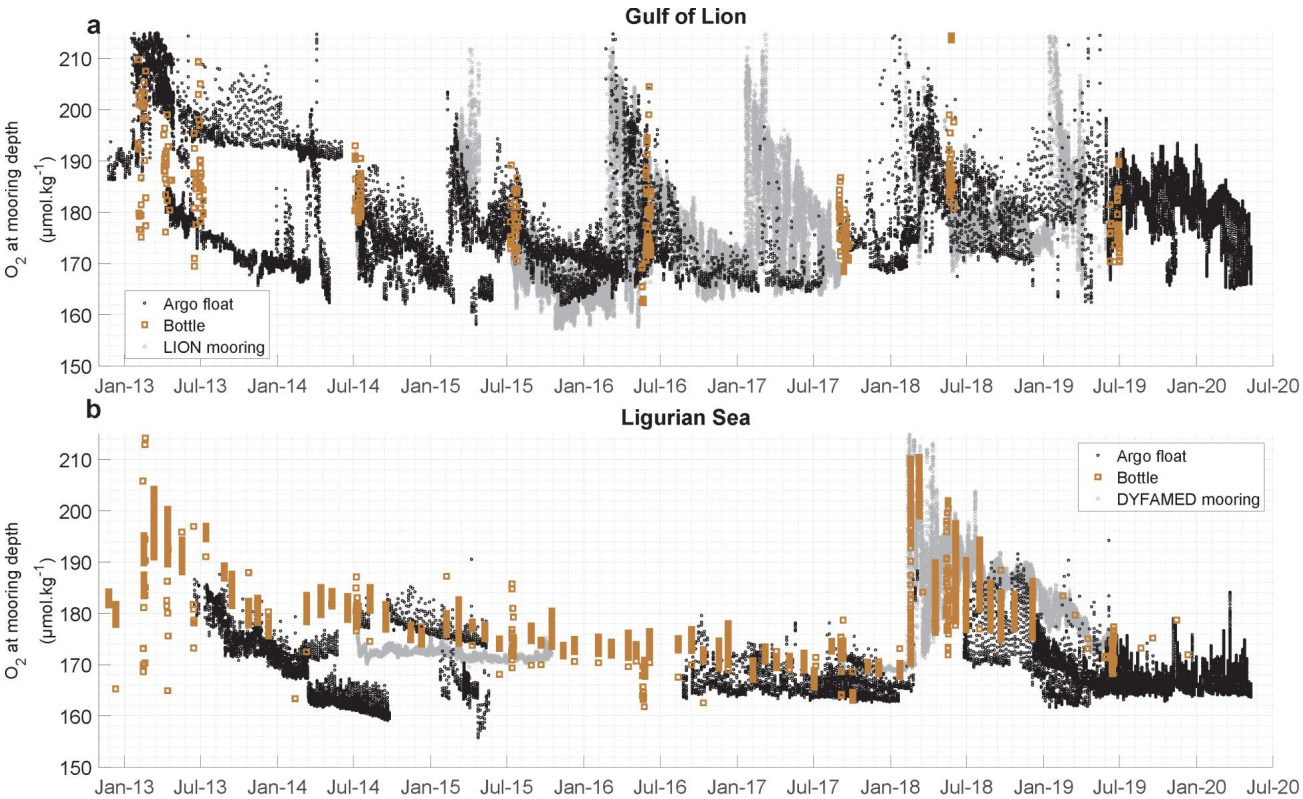

Figure S1. Time series of O_2 at the moorings depth in the Gulf of Lion (a) and the Ligurian Sea (b) from Argo data (black dots), mooring data (grey stars), and cruise data (brown squares). In the Gulf of Lion, low Argo O_2 values between January 2013 and 2014 correspond to a float that left the mixed patch.

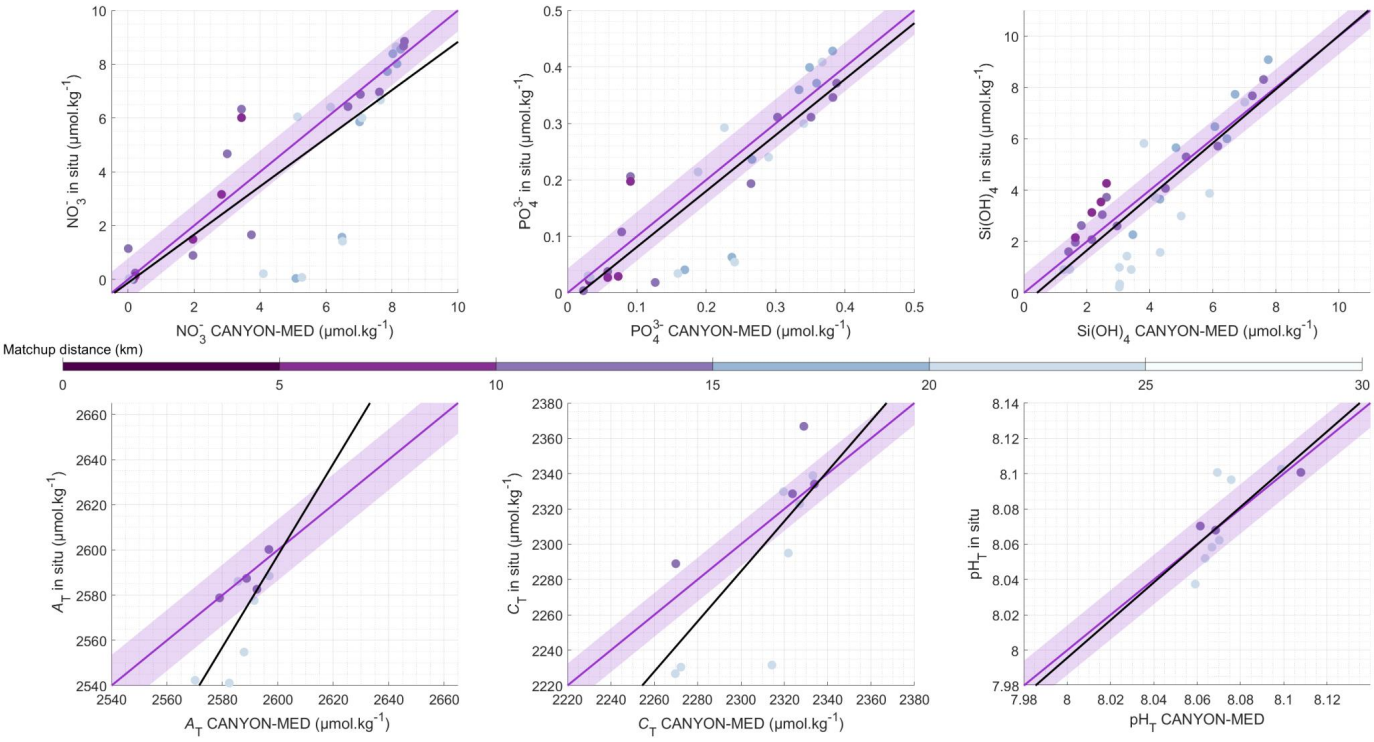

Figure S2. Model II linear regressions between the *in situ* and CANYON-MED derived biogeochemical variables according to matchup distance (light blue points are further away). The purple line corresponds to the 1:1 line and the purple shaded area corresponds to the CANYON-MED error (*Fourrier et al., 2021*). The black line corresponds to the actual regression line between the *in situ* values and CANYON-MED outputs. The matchup is for data less than 15 days and less than 5 dbar apart.

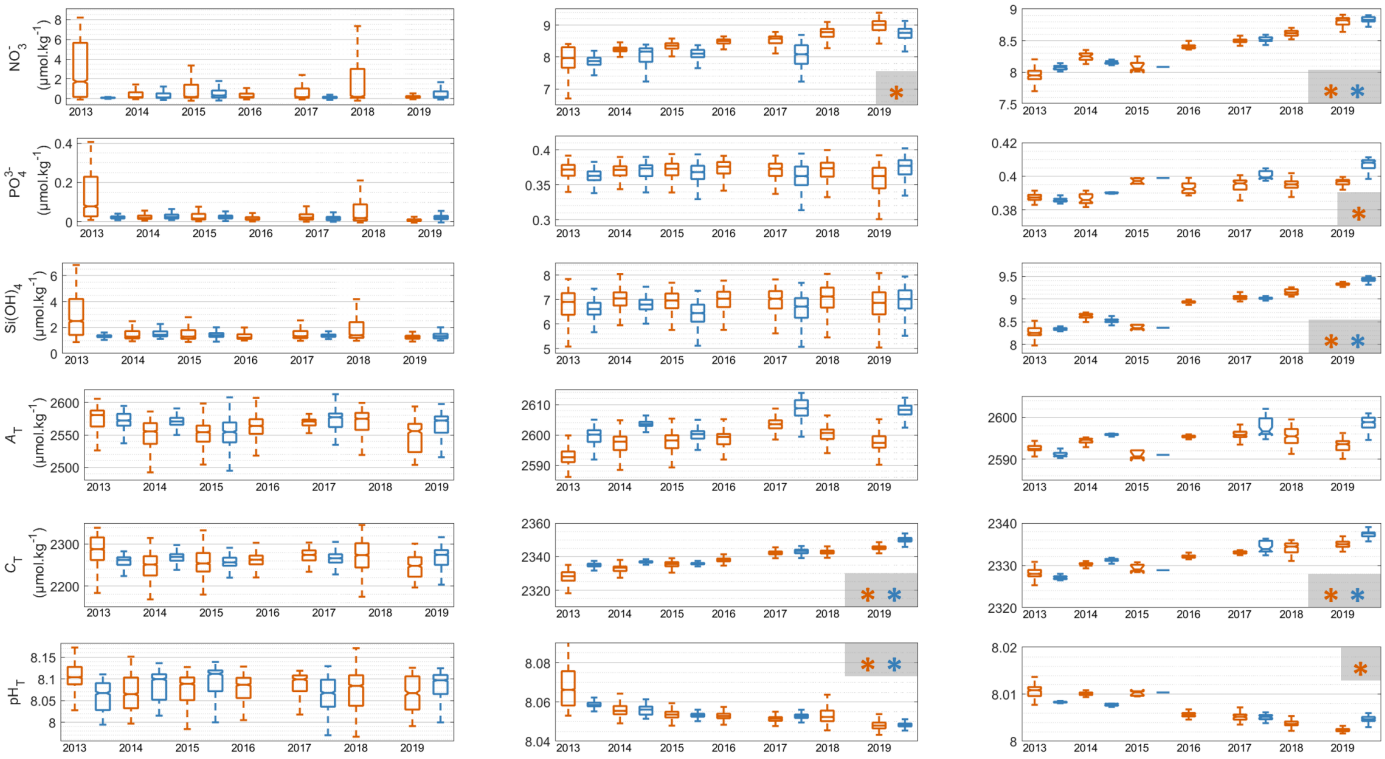

Figure S3. Changes in key biogeochemical evolution in the northwestern Mediterranean Sea. Panels a-f shows the evolution in the surface waters (with high seasonal variability), panels g-l in the LIW, and panels m-r at 2000 m, for nitrates (a, g, m), phosphates (b, h, n), silicates (c, i, o), total alkalinity (d, j, p), total carbon (e, k, q) and pH_T (f, l, r). Boxplots for each year are constructed from CANYON-MED derived values from Argo float data (orange for the Gulf of Lion and green for the Ligurian Sea), only for years when every season is represented. For the sake of readability, the time axis is discontinuous and the boxplots for each region do not overlap. The trends

Journal of Geophysical Research : Oceans

Supporting Information for

Impact of intermittent Convection in the northwestern Mediterranean Sea on Oxygen content, Nutrients and the Carbonate system

Marine Fourrier[1], Laurent Coppola[1,2], Fabrizio D'Ortenzio[1], Christophe Migon[1], Jean-Pierre Gattuso[1,3]

[1]Sorbonne Université, CNRS, Laboratoire d'Océanographie de Villefranche, F-06230 Villefranche-sur-Mer, France
[2]Sorbonne Université, CNRS, Institut de la Mer de Villefranche, F-06230 Villefranche-sur-Mer, France
[3]Institute for Sustainable Development and International Relations, Sciences Po, Paris, France

Contents of this file

Introduction

Supporting information consists of three supporting figures, one supplementary dataset and one supporting table. The supporting table is a list of the Argo floats used for this study together with their location and deployment time for each area (Gulf of Lion and Ligurian Sea).

WMO	*Gulf of Lion*			*Ligurian Sea*		
	First profile	*Last profile*	*Number of profiles*	*Firstt profile*	*Last profile*	*Number of profiles*
6901460	11/08/2014	17/06/2015	15	12/07/2014	13/05/2015	54
6901463	23/07/2014	19/04/2015	40	24/01/2015	19/05/2015	21
6901464	11/08/2014	02/07/2015	61	12/07/2014	04/12/2015	42
6901465	09/07/2014	24/02/2015	47	-	-	0
6901467	24/11/2012	02/06/2014	205	-	-	0
6901470	31/01/2013	07/07/2013	98	17/06/2013	23/05/2014	67
6901471	29/01/2013	21/08/2013	112	-	-	0
6901496	04/03/2014	04/03/2014	1	16/07/2013	13/03/2014	178
6901512	10/04/2013	04/05/2014	143	-	-	0
6901648	07/07/2014	26/05/2016	186	-	-	0
6901649	16/07/2014	06/06/2016	155	23/09/2014	22/04/2015	31
6901776	-	-	0	15/03/2014	24/09/2014	140
6902687	30/05/2016	17/10/2018	128	06/12/2016	06/03/2018	46
6902733	28/05/2016	18/08/2016	19	25/08/2016	19/01/2018	74
6902803	14/11/2017	09/05/2020	213	10/09/2017	09/11/2017	13
6902804	03/09/2017	04/02/2019	125	11/12/2018	09/05/2020	103
6902901	-	-	0	07/12/2018	12/06/2019	68

Table S1. Characteristics of the floats used in this study. WMO: World Meteorological Organization float number. For each area, the dates of the first and last profiles are given together with the corresponding number of profiles in the area.

Annexe 2 : Article : Oxygen budget of the north-western Mediterranean deep-convection region

Ulses, C., Estournel, C., **Fourrier, M.**, Coppola, L., Kessouri, F., Lefèvre, D., and Marsaleix, P.
Biogeosciences (2021)

Biogeosciences, 18, 937–960, 2021
https://doi.org/10.5194/bg-18-937-2021

Biogeosciences Open Access EGU

Oxygen budget of the north-western Mediterranean deep-convection region

Caroline Ulses[1,2], Claude Estournel[1], Marine Fourrier[3], Laurent Coppola[3], Fayçal Kessouri[2,4], Dominique Lefèvre[5], and Patrick Marsaleix[1]

[1]Laboratoire d'Etudes en Géophysique et Océanographie Spatiales (LEGOS), Université de Toulouse, CNES, CNRS, IRD, UPS, Toulouse, France
[2]Laboratoire d'Aérologie (LA), Université de Toulouse, CNRS, UPS, Toulouse, France
[3]Sorbonne Université, CNRS, Laboratoire d'Océanographie de Villefranche (LOV), 06230 Villefranche-sur-Mer, France
[4]Southern California Coastal Water Research Project, Costa Mesa, CA, USA
[5]Aix-Marseille Université, Mediterranean Institute of Oceanography (MIO), 13288 Marseille CEDEX 9, France

Correspondence: Caroline Ulses (caroline.ulses@legos.obs-mip.fr)

Received: 17 July 2020 – Discussion started: 12 August 2020
Revised: 13 November 2020 – Accepted: 26 November 2020 – Published: 10 February 2021

Abstract. The north-western Mediterranean deep convection plays a crucial role in the general circulation and biogeochemical cycles of the Mediterranean Sea. The DEWEX (DEnse Water EXperiment) project aimed to better understand this role through an intensive observation platform combined with a modelling framework. We developed a three-dimensional coupled physical and biogeochemical model to estimate the cycling and budget of dissolved oxygen in the entire north-western Mediterranean deep-convection area over the period September 2012 to September 2013. After showing that the simulated dissolved oxygen concentrations are in a good agreement with the in situ data collected from research cruises and Argo floats, we analyse the seasonal cycle of the air–sea oxygen exchanges, as well as physical and biogeochemical oxygen fluxes, and we estimate an annual oxygen budget. Our study indicates that the annual air-to-sea fluxes in the deep-convection area amounted to $20\,\mathrm{mol\,m^{-2}\,yr^{-1}}$. A total of 88 % of the annual uptake of atmospheric oxygen, i.e. $18\,\mathrm{mol\,m^{-2}}$, occurred during the intense vertical mixing period. The model shows that an amount of $27\,\mathrm{mol\,m^{-2}}$ of oxygen, injected at the sea surface and produced through photosynthesis, was transferred under the euphotic layer, mainly during deep convection. An amount of $20\,\mathrm{mol\,m^{-2}}$ of oxygen was then gradually exported in the aphotic layers to the south and west of the western basin, notably, through the spreading of dense waters recently formed. The decline in the deep-convection intensity in this region predicted by the end of the century in recent projections may have important consequences on the overall uptake of atmospheric oxygen in the Mediterranean Sea and on the oxygen exchanges with the Atlantic Ocean, which appear necessary to better quantify in the context of the expansion of low-oxygen zones.

1 Introduction

Deep convection is a key process leading to a massive transfer of oxygen from the atmosphere to the ocean interior (Körtzinger et al., 2004, 2008b; Fröb et al., 2016; Wolf et al., 2018). Its weakening in some regions (de Lavergne et al., 2014; Brodeau and Koenigk, 2016), induced by enhanced stratification, is one of the primary factors, along with changing ventilation at intermediate depths, slowdown of the overturning circulation, warming-induced decrease in solubility modulated by salinity changes and changes in C : N utilisation ratios, that may explain the ongoing decline in the open-ocean oxygen inventory, or deoxygenation, observed and modelled since the middle of the 20th century (Bopp et al., 2002; Keeling and Garcia, 2002; Plattner et al., 2002; Joos et al., 2003; Keeling et al., 2010; Helm et al., 2011; Andrews et al., 2017; Ito et al., 2017; Schmidtko et al., 2017; Breitburg et al., 2018). The oxygen decline leads to an increase in the volume of hypoxic or even anoxic waters and

to the expansion of oxygen minimum zones (OMZs), which substantially affect life and habitats of marine ecosystems and have implications for biogeochemical cycles (Ingall et al., 1994; Levin, 2003; Diaz and Rosenberg, 2008; Breitburg et al., 2009; Naqvi et al., 2010; Stramma et al., 2010; Scholz et al., 2014; Bristow et al., 2017). It is crucial to gain understanding of the actual ventilation occurring in deep-convection areas and to continue developing models to predict its future evolution under climate change.

The north-western (NW) Mediterranean Sea (Fig. 1a and b) is one of the few regions of the world where deep convection takes place (Schott et al., 1996). In autumn, during the preconditioning phase, a cyclonic gyre formed by the Northern Current and the Balearic front leads to the doming of the isopycnals and the rising of high-salinity intermediate waters, the Levantine Intermediate Waters (LIW), close to the surface. In winter, cold and dry northerly winds (Mistral, Tramontane) produce the cooling, evaporation and subsequent density increase in surface waters. The instability of the water column induces convective mixing of surface waters with deeper waters, and, when the process is intense, in the formation of new deep waters that spread into the western Mediterranean Sea, such as observed in 2004–2006 (Schroeder et al., 2008a). The depth and horizontal extension of convection in the NW region show strong interannual variability, driven by both the variability of the winter buoyancy loss and the stratification magnitude prior to the convection period (Mertens and Schott, 1998; Béthoux et al., 2002; Houpert et al., 2016; Somot et al., 2016). The deepest convection takes place in the centre of the Gulf of Lion where the yearly maximum of the mixed-layer depth varies from a few hundred metres to 2500 m when the bottom is reached (MEDOC Group, 1970).

At the Mediterranean basin scale, the deep convection occurring in the north-western region is one of the major processes responsible for an enrichment of the euphotic layer with nutrients, compared to Atlantic influx as well as terrestrial and atmospheric inputs (Severin et al., 2014; Ulses et al., 2016; Kessouri et al., 2017). The replenishment of the surface layer with nutrients during deep convection is followed by an intense bloom in spring when vertical mixing weakens (Bernadello et al., 2012; Lavigne et al., 2013; Auger et al., 2014; Ulses et al., 2016; Kessouri et al., 2018). The formation of deep waters is also at the origin of a huge ventilation of the western Mediterranean Sea (Minas and Bonin, 1988; Copin-Montégut and Bégovic, 2002; Schroeder et al., 2008a; Schneider et al., 2014; Stöven and Tanhua, 2015; Touratier et al., 2016; Coppola et al., 2017; 2018; Li and Tanhua, 2020). The study of Mavropoulou et al. (2020), based on in situ observations over the period 1960–2011, indicated that its variability is one of the main drivers of the interannual variability of the dissolved oxygen (O_2) concentration in the deep waters of the western Mediterranean Sea. The oxygenation induced by recurrent intermediate and deep convection together with a relatively low primary production make the Mediterranean Sea a well-oxygenated basin (Tanhua et al., 2013). In the western Mediterranean open sea, the oxygen minimum layer (OML) is located in the LIW and shows a minimum oxygen concentration of 170–185 $\mu mol\,kg^{-1}$, above $\approx 70\,\%$ of the saturation levels (Tanhua et al., 2013; Coppola et al., 2018). Thus the OML in this region is clearly less pronounced than the OMZs in the open oceans or deep basins of other seas, such as the adjacent Black Sea, where hypoxic conditions (oxygen concentration $< 2\,mL\,O_2\,L^{-1}$ or $< 61\,\mu mol\,O_2\,kg^{-1}$; Diaz and Rosenberg, 2008; Breitburg et al., 2018) are encountered. However the semi-enclosed Mediterranean Sea with a fast warming was identified as one of the most vulnerable marine regions to climate change (Giorgi, 2006). Recently, regional ocean models of the Mediterranean Sea converged to predict a weakening of NW deep-convection intensity under climate change scenarios by the end of the 21st century (Soto-Navarro et al., 2020). Yet, Coppola et al. (2018), by analysing the evolution of observed oxygen profiles in the Ligurian Sea over a 20 year period, suggested that hypoxic conditions may be reached in water masses at intermediate depths after a period of 25 years without deep-convection events (presuming bacterial respiration remains the same).

One of the objectives of the DEWEX (DEnse Water EXperiment) project carried out in 2012/13 was to investigate the deep-convection process, the formation of north-western Mediterranean Deep Waters and the impact of deep convection on biogeochemical fluxes (Conan et al., 2018). Three cruises and the deployment of autonomous platforms (glider, Argo floats) provided an unprecedented intensive observation of this region before, during and after a deep-convection event and completed the observation effort during the stratified period operated since 2010 in the framework of the MOOSE-GE (Mediterranean Ocean Observing System for the Environment-Grande Échelle) programme (Estournel et al., 2016b). The 2012/13 event was identified by observational and modelling studies as one of the five most intense deep-convection events over the period 1980–2013 (Somot et al., 2016; Herrmann et al., 2017; Coppola et al., 2018) due to extremely strong buoyancy loss (Somot et al., 2016). Regarding the oxygen dynamics, DEWEX winter observations showed a strong increase in the O_2 inventory of the entire water column, which was concomitant to the deepening of the mixed layer and was attributed to a rapid intake of atmospheric dissolved oxygen (Coppola et al., 2017). However, these observations remain limited in time and space. Up to date, no high-resolution modelling of the oxygen dynamics in the NW deep-convection region that could complete the monitoring effort and provide quantification for the whole area has yet been proposed.

In this study, we take advantage of the DEWEX project to implement and constrain with in situ observations a 3D coupled physical–biogeochemical model representing the dynamics of dissolved oxygen and to gain understanding in the variability of the oxygen inventory in the whole NW Mediterranean deep-convection area, for the period between Septem-

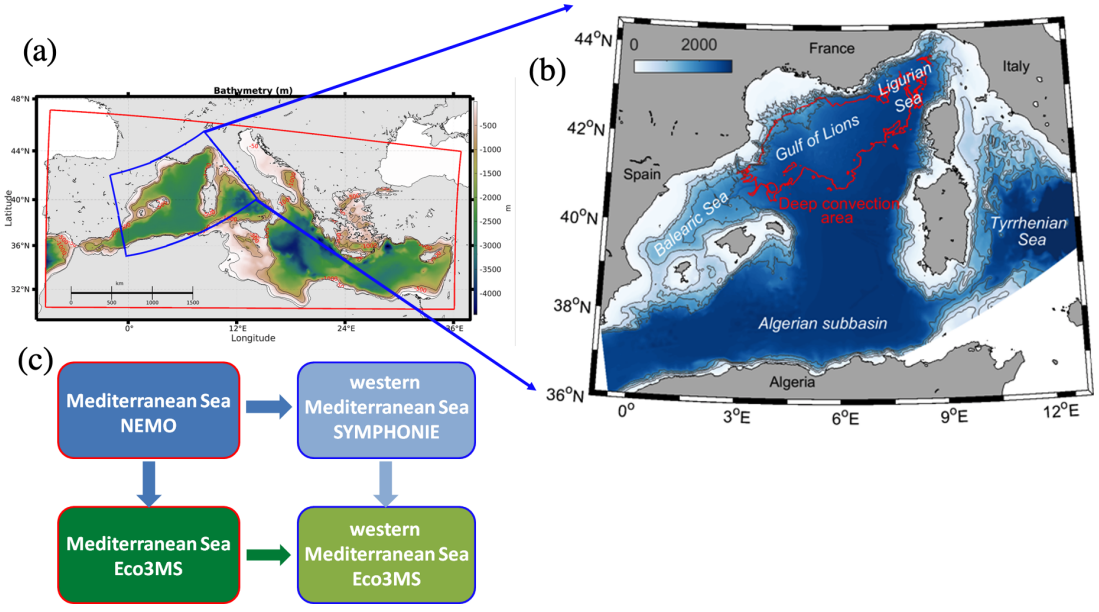

Figure 1. Domain and bathymetry (m) of **(a)** the forcing coupled NEMO-Eco3MS Mediterranean model (red contour) and of **(b)** the coupled SYMPHONIE-Eco3MS western sub-basin model. The blue contour in **(a)** indicates the limits of the western sub-basin model. The red contoured area in **(b)** corresponds to the deep-convection area. **(c)** Scheme of the downscaling strategy from the Mediterranean Sea to the western sub-basin.

ber 2012 and September 2013. In this framework, we investigate the seasonal cycle of the oxygen inventory and estimate its annual budget, and we analyse and quantify the relative contribution of air–sea exchanges, as well as of physical and biogeochemical processes in the budget. The following document is organised as follows: in Sect. 2, we describe the numerical model, its implementation and the observations used for its assessment. In Sect. 3, we compare our model results with in situ observations. In Sect. 4, we describe the seasonal cycle of atmospheric and physical conditions. In Sect. 5, we examine the seasonal cycle of oxygen inventory and fluxes, as well as the annual oxygen budget. We discuss our results in Sect. 6 and conclude in Sect. 7.

2 Material and methods

2.1 The numerical model

2.1.1 The hydrodynamic model

The SYMPHONIE model used in this study is a 3D primitive equation model, with a free surface and generalised sigma vertical coordinate, as described in Marsaleix et al. (2008). The vertical diffusion is parameterised with a prognostic equation for the turbulent kinetic energy and a diagnostic equation for the mixing and dissipation lengths, following Gaspar et al. (1990). Atmospheric forcing (turbulent fluxes) is calculated using the bulk formulae described by Large and Yeager (2004). This model was previously used in the Mediterranean Sea to simulate open-sea convection (Herrmann et al., 2008; Estournel et al., 2016a; Ulses et al., 2016), shelf dense-water cascading (Estournel et al., 2005; Ulses et al., 2008b) and continental shelf circulation on the Gulf of Lion shelf (Estournel et al., 2001; 2003; Ulses et al., 2008a).

2.1.2 The biogeochemical model

The biogeochemical model Eco3M-S is a multi-nutrient and multi-plankton functional type model that simulates the dynamics of the biogeochemical decoupled cycles of several biogenic elements (carbon, nitrogen, phosphorus, silicon) and of non-Redfieldian plankton groups (Ulses et al., 2016). The model was previously used to study the biogeochemical processes on the Gulf of Lion shelf (Auger et al., 2011) and in the NW Mediterranean deep-convection area (Herrmann et al., 2013, 2017; Auger et al., 2014; Ulses et al., 2016; Kessouri et al., 2017, 2018). In this study, the model was extended to describe the dynamics of dissolved oxygen in the ocean interior and the air–sea exchanges of oxygen. Here we only describe the rate of change of the new state variable, the dissolved oxygen concentration and the parameterisation of the air–sea flux of oxygen, which were included in the model version described in detail by Auger et al. (2011). The rate of change of dissolved oxygen concentration due to biogeochemistry in the water column is governed by the following

equation:

$$\frac{\mathrm{dDO}_x}{\mathrm{d}t} = \sum_{i=1}^{3} \left(\mathrm{GPP}_i - \mathrm{RespPhy}_i\right) \gamma_{\mathrm{C/DO}_x} - \sum_{i=1}^{3} \left(\mathrm{RespZoo}_i + \mathrm{RespZoo}_i^{\mathrm{add}}\right) \gamma_{\mathrm{C/DO}_x} - \mathrm{RespBac}\, \gamma_{\mathrm{C/DO}_x} - \mathrm{Nitrif}\, \gamma_{\mathrm{NH_4/DO}_x}, \quad (1)$$

where DO_x is the dissolved oxygen concentration; GPP_i and $\mathrm{RespPhy}_i$ are gross primary production and respiration, respectively, for phytoplankton group i; $\mathrm{RespZoo}_i$ and $\mathrm{RespZoo}_i^{\mathrm{add}}$ are basal respiration and additional respiration fluxes to maintain constant N : C and P : C internal ratios, respectively, for zooplankton group i; RespBac is bacterial respiration; and Nitrif is nitrification. $\gamma_{\mathrm{C/DO}_x}$ and $\gamma_{\mathrm{NH_4/DO}_x}$, equal to 1 and 2, respectively, are the mole of DO_x, used per mole of C in respiration and needed to oxidise 1 mol of ammonium in nitrification as described in Grégoire et al. (2008).

The flux of dissolved oxygen at the air–sea interface, $\mathrm{DO}_x\mathrm{Flux}$, is computed from

$$\mathrm{DO}_x\mathrm{Flux} = K_w \left(\mathrm{DO}_{x\,\mathrm{sat}} - \mathrm{DO}_{x\,\mathrm{surf}}\right), \quad (2)$$

where $\mathrm{DO}_{x\,\mathrm{sat}}$ and $\mathrm{DO}_{x\,\mathrm{surf}}$ ($\mathrm{mmol\,m^{-3}}$) are the concentration of dissolved oxygen at saturation level and at the surface of the ocean, respectively, and $K_w(\mathrm{m\,s^{-1}})$ is the gas transfer velocity. The oxygen solubility (or dissolved oxygen at saturation level) is determined using the equation of Garcia and Gordon (1992). The oxygen saturation anomaly (noted $\Delta\mathrm{O}_2$) is defined as $\Delta\mathrm{O}_2 = (\mathrm{DO}_x - \mathrm{DO}_{x\,\mathrm{sat}})/\mathrm{DO}_{x\,\mathrm{sat}} \times 100\,\%$. We computed here the gas transfer velocity using the parameterisation of Wanninkhof and McGillis (1999) with a cubic dependency to the wind speed, following the study in the convective Labrador Sea by Körtzinger et al. (2008b), who found that this parameterisation was one of those that gave the best results and recommended a stronger-than-quadratic wind speed dependency for the high wind speed range. In addition, sensitivity analyses using eight various parameterisations of the gas transfer velocity were performed to estimate uncertainties of air–sea exchanges and are discussed in Sect. 6.1. For these sensitivity tests, we used quadratic (Wanninkhof, 1992, 2014) and hybrid (Nightingale et al., 2000; Wanninkhof et al., 2009) wind speed dependency parameterisations, as well as parameterisations including air–sea fluxes due to bubble formation (Woolf, 1997; Stanley et al., 2009; Liang et al., 2013; Bushinsky and Emerson, 2018).

2.1.3 Implementation

The implementation of the hydrodynamic and biogeochemical simulations used in this study was described by Estournel et al. (2016a) and Kessouri et al. (2017; 2018). The numerical domain (Fig. 1a, b) covers most of the western Mediterranean basin, using a curvilinear grid with variable horizontal resolution (Bentsen et al., 1999). The mesh size ranges from 0.8 km in the north to 1.4 km in the south. The grid has 40 vertical levels with closer spacing near the surface (15 levels in the first 100 m in the centre of the convection area characterised by depths of $\approx$ 2500 m). As explained in Estournel et al. (2016a), the size of the grid is not small enough to explicitly represent convective plumes, which thus need to be parameterised. In our case, to prevent the development of static instabilities at the surface resulting in noise at the scale of the mesh, the heat and water fluxes are distributed over the whole mixed layer whose thickness is given by the depth at which the vertical density gradient becomes negative.

The biogeochemical model is forced offline by daily outputs of the hydrodynamic model. The advection and diffusion of the biogeochemical variables were calculated using the QUICKEST (QUICK with Estimated Streaming Terms) scheme (Leonard, 1979) on the horizontal and with a centred scheme on the vertical.

A strategy of downscaling from the Mediterranean basin to the western sub-basin scale was implemented in three stages (Fig. 1a and c) as described by Kessouri et al (2017). In a first step, the SYMPHONIE hydrodynamic model was initialised and forced at its lateral boundaries with daily analyses of the configuration PSY2V4R4, based on the NEMO ocean model at a resolution of 1/12° over the Atlantic and the Mediterranean Sea by the Mercator Ocean International operational system (Lellouche et al., 2013). Second, the biogeochemical model was forced at the Mediterranean basin scale by the outputs of the same NEMO simulation. In a third step, the daily outputs of the two previous simulations were used to initialise and force the Eco3M-S biogeochemical model over the western Mediterranean Sea. This nesting protocol ensures the coherence of the physical and biogeochemical fields at the open boundaries. The basin configuration of the biogeochemical model was initialised in summer 2011, with climatological fields of in situ nutrient concentrations from the oligotrophic period in the MEDAR/MEDATLAS database (Manca et al., 2004) and according to oxygen observations from the *Meteor* M84/3 cruise carried out in April 2011 (Tanhua et al., 2013) and DYFAMED station observations in August 2011 (Coppola et al., 2018). The regional biogeochemical simulation started in August 2012. Due to strong vertical diffusivities in the basin-scale model, we corrected the initial oxygen concentration for the north-western region using DYFAMED observations carried out in the summer of 2012 (Coppola et al., 2018) and for the south-western region according to *Meteor* M84/3 observations.

Meteorological parameters including downward radiative fluxes were taken from the ECMWF (European Centre for Medium-Range Weather Forecasts) operational forecasts at 1/8° horizontal resolution and 3 h temporal resolution based on daily analyses. River runoffs were considered based on realistic daily values for French rivers (data provided by Banque Hydro, http://www.hydro.eaufrance.fr/) and Ebro (data provided by SAIH Ebro, http://www.saihebro.com),

and mean annual values for the other rivers. At the Rhône River mouth, nitrate, ammonium, phosphate, silicate and dissolved organic carbon concentrations were prescribed using in situ daily data (P. Raimbault, MISTRALS database). These data, combined with those of Moutin et al. (1998) and Sempéré et al. (2000), were used to estimate dissolved organic phosphorus and nitrogen and particulate organic matter concentrations as described in Auger et al. (2011). At the other river mouths, climatological values were prescribed according to Ludwig et al. (2010). Dissolved oxygen concentration at the river mouths was set to values at saturation. The deposition of organic and inorganic matter from the atmosphere was neglected in this study. Fluxes of inorganic nutrients and oxygen at the sediment–sea interface were considered by coupling the pelagic model with a simplified version of the meta-model described by Soetaert et al. (2001). The parameters of the latter model were set following the modelling study performed by Pastor et al. (2011) for the Gulf of Lion shelf.

2.1.4 Study area

For analyses and budget purposes, we defined the deep-convection area as the area where the daily averaged mixed-layer depth exceeded 1000 m at least once during wintertime (red contoured area in Fig. 1b), according to Kessouri et al. (2017, 2018). It covered an area of 61 720 km^2 in 2013. The mixed-layer depth is defined as the depth where the potential density exceeds its value at 10 m depth by 0.01 $kg\,m^{-3}$ (Coppola et al., 2017). Heat fluxes and physical and biogeochemical parameters and fluxes presented in the following sections correspond to values averaged over all model grid points included in this area. The budget of oxygen inventory was computed in two layers based on biogeochemistry processes: in the upper layer (from the surface to 150 m) including the euphotic layer where photosynthesis influences the dynamics of oxygen and in the underlying aphotic layer (from 150 m to the bottom) where only respiration and nitrification processes are taken into account in the model. The maximum depth of the base of the euphotic layer was defined at 150 m, based on the regional minimum value of diffuse attenuation coefficient of light at 490 nm derived from satellite observations (http://marine.copernicus.eu/, products: OCEANCOLOUR_MED_OPTICS_L3_REP_-OBSERVATIONS_009_095), and following the studies by Lazzari et al. (2012) and Kessouri et al. (2018).

2.2 Observations used for the model assessment

2.2.1 Cruise observations

To assess the horizontal and vertical distribution of the simulated dissolved oxygen concentration, we use in situ observations collected during two cruises carried out in the framework of the DEWEX project on board the RV *Le Suroît*: the first one, DEWEX Leg1, was carried out during the active phase of deep convection, in February 2013 (Testor, 2013), and the second one, DEWEX Leg2, was carried out during the following spring bloom, in April 2013 (Conan, 2013). In addition, we use observations from the 2013 MOOSE-GE cruise, conducted during the stratified, oligotrophic season, in June–July 2013 on board RV *Tethys II* (Testor et al., 2013). The dissolved oxygen measurements were performed during the DEWEX (Leg1: 74 stations, Leg2: 99 stations) and MOOSE-GE (74 stations) cruises, using a Sea-Bird SBE43 sensor. The calibration and quality control of the measurements were described by Coppola et al. (2017). The accuracy of the measurements was estimated at 2 % of oxygen saturation, i.e. 4 $\mu mol\,kg^{-1}$. A Winkler analysis performed on board was used to adjust the SBE43 raw data, as specified by the GO-SHIP programme (http://www.go-ship.org/).

We also compare our model results with high-frequency measurements of wind at 10 m and of ocean surface temperature, salinity (thermosalinograph and conductivity–temperature–depth (CTD)) and dissolved oxygen concentration (optode) at 3 m depth using the sea surface water continuous acquisition system (SACES) (Dugenne, 2017) during the two DEWEX cruises.

2.2.2 Argo floats

To evaluate the temporal evolution of the modelled oxygen inventory, we use data of three Argo-O_2 floats (floats 6901467, 6901470, 6901487) deployed in the NW Mediterranean Sea during the preconditioning phase (late November 2012) and the active phase (late January 2013) of dense water formation and operational until the end of the study period (Coppola et al., 2017; Argo, 2020). Dissolved oxygen measurements were made with a standard CTD sensor, equipped with an oxygen optode with fast time response (Aanderaa 4330). Calibrations of optodes were performed before the float deployment and also during the deployment using CTD profiles and seawater samples (Niskin bottles). Details on float deployment strategy and calibration are given by Coppola et al. (2017). We calculated the oxygen inventory from 1800 m to the surface for floats 6901467 and 6901470 and only from 1000 m to the surface for float 6901487 due to poor quality salinity data below this depth.

2.3 Statistical analysis

In order to quantify the performance of the model in its ability to represent the dynamics of dissolved oxygen for the study period, we computed four complementary metrics following the recommendations of Allen et al. (2007): (1) the SD ratio ($r_\sigma = \frac{\sigma_o}{\sigma_m}$ where σ_m and σ_o are the SD of model outputs and observations, respectively); (2) the Pearson cor-

relation coefficient,

$$R = \frac{\frac{1}{K}\sum_{k=1}^{K}\left(y_k^m - \overline{y^m}\right)\left(y_k^o - \overline{y^o}\right)}{\sigma_m \sigma_o},$$

where K is the number of observations, y_k^o is the observation k, y_k^m is the corresponding model output k, and $\overline{y^o}$ and $\overline{y^m}$ are the mean of observations and model outputs, respectively; (3) the normalised root-mean-square error,

$$\mathrm{NRMSE} = \frac{\sqrt{\frac{1}{K}\sum_{k=1}^{K}\left(y_k^o - y_k^m\right)^2}}{\overline{y^o}} \times 100\,\%;$$

and (4) the percentage bias ($\mathrm{PB} = \frac{\overline{y^m} - \overline{y^o}}{\overline{y^o}} \times 100\,\%$). The model results are compared with the observations at the same dates and positions.

3 Evaluation of the model

The accurate representation of the winter mixing of water masses is an essential point for the simulation of the dissolved oxygen dynamics in this region, marked by a strong ventilation of the deep waters that plays a crucial role in its seasonal cycle (Copin-Montégut et al., 2002; Touratier et al., 2016; Coppola et al., 2017; 2018). A validation of the hydrodynamic part of the simulation is described by Estournel et al. (2016a), who showed similar spatial distribution of the modelled water column stratification in the entire deep-convection area, as well as modelled time evolution of the temperature profile in the centre of the Gulf of Lion open sea during the winter that is close to the observations.

Furthermore, an assessment of the biogeochemical part of the coupled model is presented in Kessouri et al. (2017; 2018). These studies showed that the model is able to accurately reproduce the timing and magnitude of the surface chlorophyll increase during the spring and autumnal blooms, as well as the concentrations of nutrients and depths of nutriclines and the dynamics and depth of the deep chlorophyll maximum during the stratified, oligotrophic period.

In this study, we focus the evaluation of the coupled model on its ability to realistically represent the dynamics of dissolved oxygen in the deep regions of the NW Mediterranean Sea. For this purpose, we first compare the model results to in situ observations from DEWEX and MOOSE-GE cruises conducted at three key periods: the winter mixing period, the phytoplankton bloom period and the stratified summer period. We then compare the model outputs to Argo data deployed in the area in terms of time evolution of oxygen inventory.

3.1 Comparisons to cruise observations

The comparisons of modelled wind velocity and ocean model outputs with in situ observations from the high-frequency SACES are shown in Fig. 2. Modelled wind provided by ECMWF and used to force the hydrodynamic model and to calculate the air–sea oxygen flux is highly correlated with the observations ($R = 0.96$, p value < 0.01). The low values of NRMSE (13.9 %) and percentage bias (−0.5 %) show the accuracy of this variable, found for all ranges of value. Regarding the surface ocean variables, we obtain statistically significant correlations equal to 0.64, 0.83 and 0.83 (p value < 0.01), between observed and modelled values of, respectively, surface temperature, salinity and dissolved oxygen concentration. The NRMSEs are equal to 2.0 %, 0.3 % and 5.2 %, respectively. The percentage biases remain negligible for temperature (−0.7 %), salinity (0.002 %) and dissolved oxygen concentration (−1.2 %).

Figures 3 and 4 compare the observed and modelled dissolved oxygen concentration for the stations sampled during the DEWEX and MOOSE-GE cruises, respectively, at the surface (between 5 and 10 m) and along the south–north transect passing across the convection area (stations encircled in black in Fig. 3). Overall, the simulation correctly reproduces the spatial and temporal variability of the oxygen concentration observed at the surface and in the water column during and between the three cruises. During wintertime, the model simulates low surface oxygen concentrations ($< 220\,\mu\mathrm{mol\,kg^{-1}}$) in the open sea of the Gulf of Lion and the Ligurian Sea, areas that coincide with the deep vertical mixing regions (Estournel et al., 2016a; Kessouri et al., 2017) (Fig. 3a and b). Figure 4a shows the oxygen homogenisation of the whole water column between 41.5 and 42.3° N, the core of the deep-convection area. Concentrations above $240\,\mu\mathrm{mol\,kg^{-1}}$ are modelled in the surface layer on the shelf and in the south at the Balearic front, in accordance with the observations (Figs. 3a, b and 4a). The model also agrees with observations showing a layer of low oxygen concentration (minimum concentration $< 185\,\mu\mathrm{mol\,kg^{-1}}$ at depths around 500 m) located between 150 and 1500 m, mainly in the LIW (300–800 m), outside the deep-convection area (Fig. 4a). The metrics confirm the good agreement between model outputs and observations with a significant spatial correlation of 0.81 and 0.61 (p value < 0.01), an NRMSE of 5.3 % and 15.7 %, and a negligible percentage bias of −1.1 % and 0.01 %, respectively, at the surface and along the south–north transect.

During the spring cruise period, the model represents high dissolved oxygen values ($> 240\,\mu\mathrm{mol\,kg^{-1}}$) at the surface throughout the region, as observed (Fig. 3c and d). The increase in modelled oxygen concentration in the surface layer between both campaigns is in agreement with observations (Figs. 3a–d and 4a, b). A zone of low oxygen concentration in the intermediate waters is present in the convection area in both datasets (Fig. 4b). However, it is worth noting that this zone of low oxygen concentration is heterogeneous

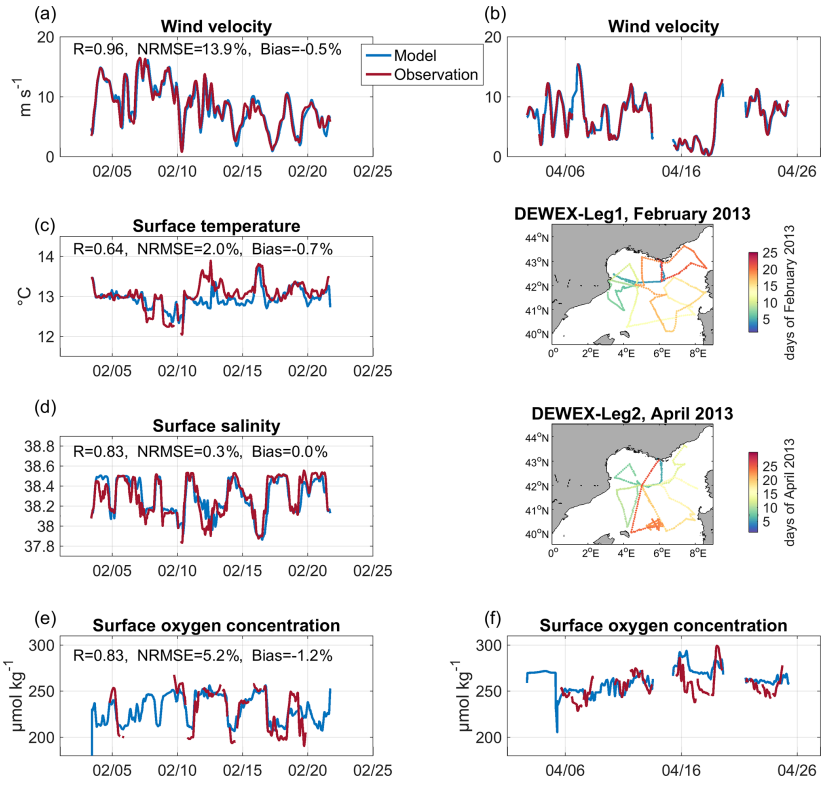

Figure 2. Time evolution during DEWEX Leg1 (in February 2013, **a**, **c**, **d** and **e**) and Leg2 (in April 2013, **b, f**) cruises of observed (red) and modelled (blue) (**a** and **b**) wind velocity ($m\,s^{-1}$), **(c)** surface temperature (°C), **(d)** surface salinity, and **(e, f)** surface dissolved oxygen concentration ($\mu mol\,kg^{-1}$). Trajectories of the measurements during DEWEX Leg1 and Leg2 cruises are indicated on inserted maps. Modelled wind velocity was provided by ECMWF. No surface temperature and salinity data are available over the period of DEWEX Leg2. The metrics indicated for the modelled wind velocity and surface oxygen concentration were calculated for both DEWEX Leg1 and Leg2 periods.

in its magnitude and thickness both in model outputs and in observations, and it is not similarly distributed in space in the model compared to the measurements. At the surface and along the transect, the spatial correlation coefficients between modelled and observed dissolved oxygen are equal to 0.59 and 0.30 (p value < 0.01), respectively, the NRMSE to 4.6 % and 19.3 %, respectively, and the percentage biases to -1.2 % and -4.4 %, respectively.

The north–south gradient, with lower surface concentrations in the south of the deep-convection area, observed during the stratified period (i.e. MOOSE-GE cruise period in June–July), is then well reproduced by the model (Fig. 3e and f). The minimum zone is more established than in spring in both in situ data and model results (Fig. 4c). Both sets of data represent a maximum in the subsurface at depths around 50 m, close to the deep chlorophyll maximum (shown in Fig. 5 in Kessouri et al., 2018), although an underestimation of its magnitude is visible between 41.5 and 42° N in the model (Fig. 4c). We find a spatial correlation coefficient of 0.64 and 0.96 (p value < 0.01), an NRMSE of 3.2 % and 3.5 %, and a negligible percentage bias (absolute values ≤ 0.4 %) between model outputs and observations at the surface and along the north–south transect, respectively.

The metrics computed using all station data from the three cruises are given in Table 1. The modelled dissolved oxygen concentration is significantly correlated with the observed concentration ($R \geq 0.81$, $p < 0.01$), in particular for the winter period when the pattern of the oxygen distribution appears to be primarily shaped by deep-convection processes, shown to be accurately represented by Estournel et al. (2016a). The model results show low percentage biases (PB < 1 %), low NRMSE (< 8 %), and SD ratios ranging between 1.13 and 1.35, which indicate a larger variability in the observations than in the model outputs.

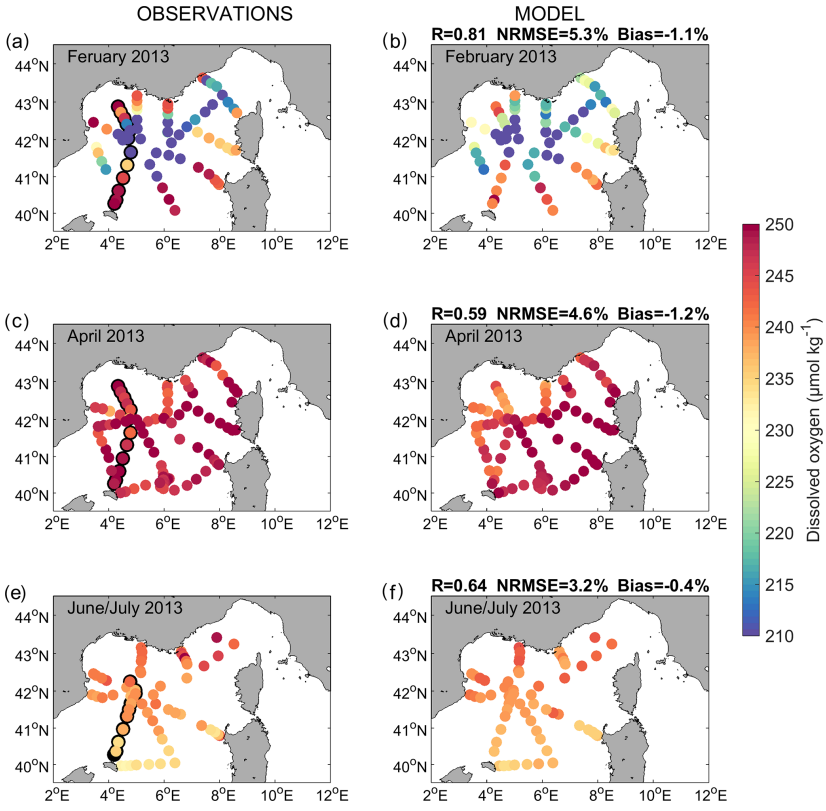

Figure 3. Surface dissolved oxygen concentration ($\mu mol\,kg^{-1}$) observed (**a**, **c** and **e**) and modelled (**b**, **d** and **f**) over the (**a** and **b**) DEWEX Leg1 (1–21 February 2013), (**c** and **d**) DEWEX Leg2 (5–24 April 2013) and (**e** and **f**) MOOSE-GE (11 June–9 July 2013) cruise periods. The black-outlined dots correspond to the measurement stations shown in Fig. 4.

Table 1. Statistical analysis of model results: Pearson correlation coefficient (R), normalised root-mean-square error (NRMSE), percentage bias (PB) and SD ratio, calculated between modelled dissolved oxygen concentrations and observations from DEWEX winter and spring cruises and the MOOSE-GE summer cruise and from Argo-O_2 platforms.

	R	NRMSE, %	PB, %	SD ratio
DEWEX Leg1	0.86 ($p < 0.01$, $n = 2960$)	5.6	−0.59	1.34
DEWEX Leg2	0.93 ($p < 0.01$, $n = 3960$)	4.9	0.55	1.13
MOOSE 2013	0.81 ($p < 0.01$, $n = 2960$)	7.6	0.51	1.35
Float 6901467	0.56 ($p < 0.01$, $n = 5120$)	10.3	−0.12	1.37
Float 6901470	0.93 ($p < 0.01$, $n = 4480$)	3.0	−0.19	0.99
Float 6901487	0.88 ($p < 0.01$, $n = 4720$)	4.1	−0.11	1.01

3.2 Comparison to Argo float data

The model accurately reproduces the magnitude of oxygen inventory in the water column and its time evolution observed using Argo floats during the study period (Fig. 5). The model simulates the increase observed between early December and late February. This increase is estimated at $\approx 20\,mol\,m^{-2}$ over a layer from the surface to 1800 m, along the trajectory of the float 6901467 (Fig. 5a), and at $\approx 10\,mol\,m^{-2}$ over a layer from the surface to 1000 m, along the trajectory of the float 6901487 (Fig. 5c), both floats being located in the Gulf of Lion at that period. The oxygen inventory remains high during the month of March and then decreases significantly from early April to early June, in model outputs and Argo observations. In both datasets, the decrease reaches up to $20\,mol\,m^{-2}$ over 1800 m along the path of the Argo float 6901470 in the Gulf of Lion (Fig. 5b) and is less pronounced ($\approx 10\,mol\,m^{-2}$) along the trajectory of the

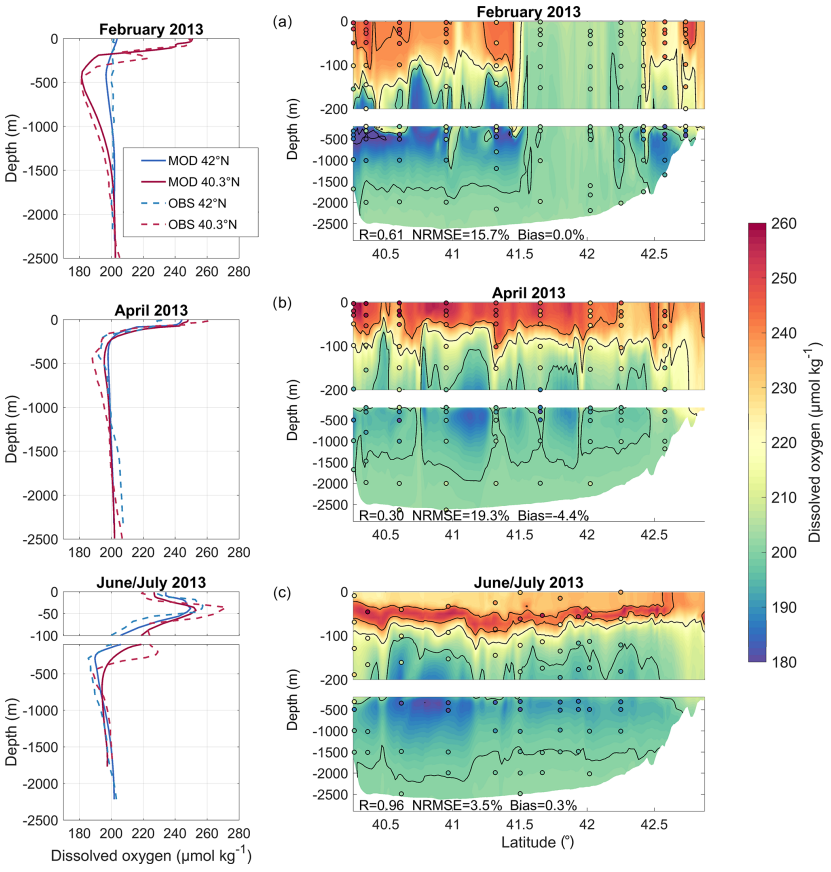

Figure 4. Comparison between model outputs and observations on a transect crossing the deep-convection area (stations are circled in black in Fig. 3a, c and e) over the (**a** and **b**) DEWEX (Leg1: 10–12 February 2013, Leg2: 8–10 April) and **(c)** MOOSE-GE (27 June–5 July 2013) cruise periods. The left column shows observed and modelled profiles at 42 and 40.3° N. The right column shows vertical section of dissolved oxygen concentration (µmol kg^{-1}) along the transect; the model is represented by background colours and observations are indicated in coloured circles.

float 6901467 in the Balearic Sea (Fig. 5a). More moderate decreases are then simulated and observed until September along all float trajectories. The statistical analysis shows that, in terms of oxygen inventory, significant correlation coefficients are obtained between the model outputs and the three float observations ($0.64 < R < 0.83$, p value < 0.01), NRMSEs are smaller than or equal to 2.4 %, and the absolute values of percentage bias are smaller than or equal to 2 % (Fig. 5). In terms of dissolved oxygen concentration in the water column, we obtain significant correlation coefficients ($0.56 < R < 0.93$, p value < 0.01), NRMSEs smaller than 10.5 %, percentage biases smaller than 1 %, and SD ratios close to 1 for floats 6901470 and 6901487 and of 1.37 for float 6901467 (Table 1).

4 Atmospheric and hydrodynamic conditions

In the NW Mediterranean Sea, deep convection takes place every winter but shows strong interannual variability in its magnitude and spatial extent. This interannual variability is partly related to the variability of heat fluxes (Somot et al., 2016). Over the study period, the convection area was marked by severe heat loss episodes from late October 2012 to mid-March 2013 (Fig. 6a). In particular, there was a first short but intense heat loss event (mean heat flux $< -1000\,\mathrm{W\,m^{-2}}$) at the end of October, followed by several long northerly wind episodes when heat loss peaks reached $500\,\mathrm{W\,m^{-2}}$, during the months of December to February (late November to mid-December, mid-January, early February and late February). Finally, a last strong heat loss episode occurred in mid-March after a period of positive heat flux. The wind velocity averaged over the convection period (15

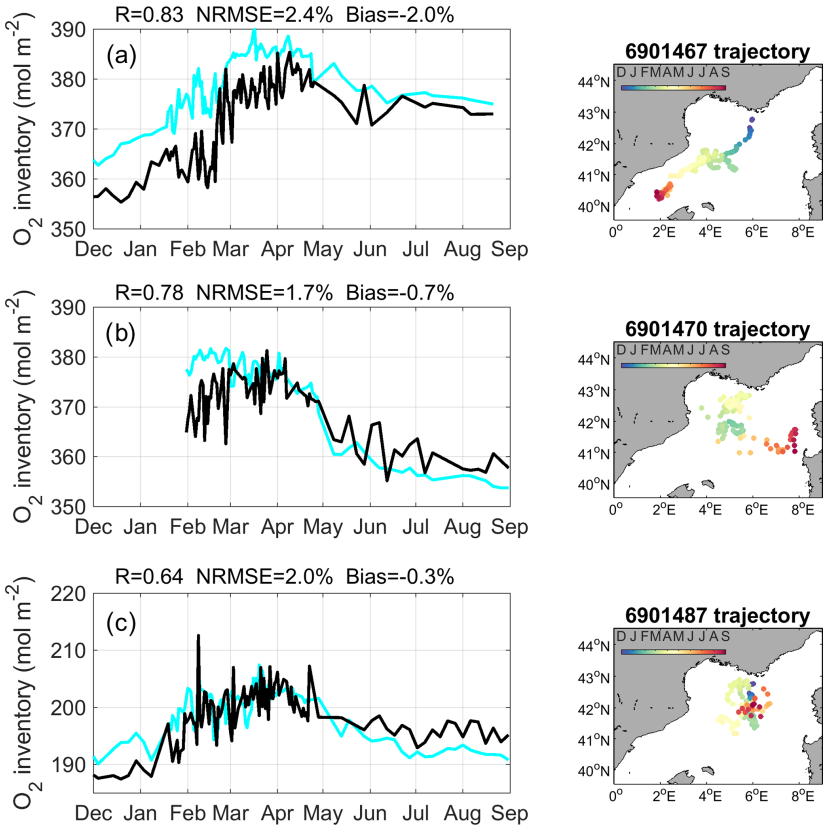

Figure 5. The left column shows oxygen inventory integrated from the surface to 1800 m depth (**a** and **b**) or 1000 m **(c)** (mol m^{-2}) in Argo float measurements (cyan) and model outputs (black) along Argo **(a)** 6901467, **(b)** 6901470 and **(c)** 6901487 float trajectories. The right column shows trajectories of corresponding Argo float.

January–8 March, 15–24 March) was maximum in the centre of the Gulf of Lion, where it reached 10 m s^{-1} (Fig. 7a). From April onwards, the convection region was mainly characterised by heat gains.

In response to the autumnal heat loss events, the mixed layer (ML) began to deepen below 50 m at the end of November (Fig. 6b). Its deepening was strongly enhanced in winter over four periods that coincided with the four episodes of intense northerly wind associated with heat loss mentioned above (Fig. 6a and b). Deep convection reached the bottom layer ($\approx$ 2000 m) in the core of the convection zone (latitude $\approx$ 42° N, 4° E < longitude < 5° E) in early February, and the spatially averaged mixed layer reached a maximum depth of about 1500 m at the end of February (Fig. 6b). At the end of the main convection event, end of February–early March, the spatially averaged mixed layer abruptly decreased to less than 100 m (Fig. 6b). Finally, during the secondary convection event from 15 to 24 March, it reached almost 800 m. Figure 7b shows the modelled mixed-layer depth (MLD) averaged over the convection periods. It exceeded 1000 m in a central area of the Gulf of Lion, between 41.5 and 42.5° N and 3.5 and 7° E and was smaller than 500 m in the Ligurian Sea. From mid-April to the end of the period, the mixed layer was shallow (depth < 50 m) and its depth remained above the nutriclines (Kessouri et al., 2017) and the deep chlorophyll maximum (Kessouri et al., 2018).

5 Results

5.1 Seasonal cycle of dissolved oxygen

The good agreement found between model results and in situ measurements (Sect. 3) gave us confidence in the model that we use here to analyse the evolution of the oxygen inventory in the deep-convection area and to quantify the relative contribution of each oxygen flux in its variation: exchanges at the air–sea interface, as well as physical and biogeochemical fluxes in the ocean interior. Based on the evolution of vertical mixing and the phytoplankton growth in the study area, Kessouri et al. (2017) divided the study pe-

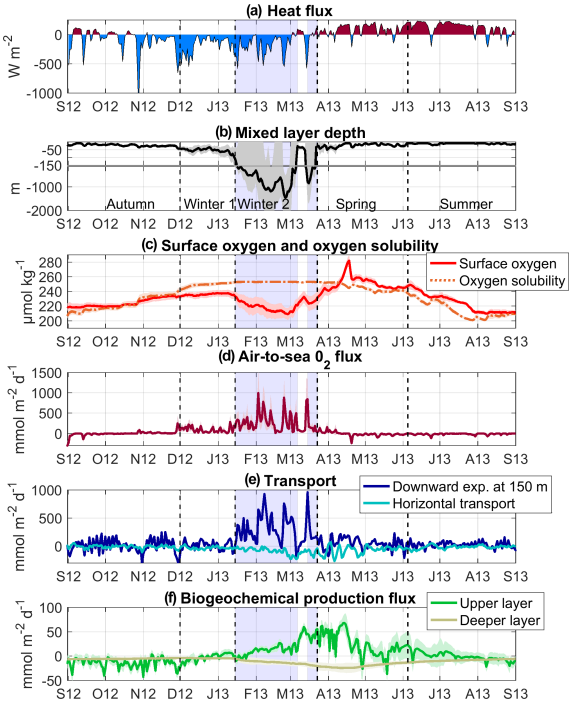

Figure 6. Time series of modelled **(a)** total heat fluxes ($W\,m^{-2}$), **(b)** mixed-layer depth (m), **(c)** surface oxygen and oxygen solubility ($\mu mol\,kg^{-1}$), **(d)** air-to-sea oxygen fluxes ($mmol\,m^{-2}\,d^{-1}$), **(e)** downward oxygen transport at 150 m (dark blue) and lateral oxygen transport towards the convection area (light blue) ($mmol\,m^{-2}\,d^{-1}$), and **(f)** biogeochemical oxygen production (see Eq. 1) ($mmol\,m^{-2}\,d^{-1}$), spatially averaged over the convection area (spatial mean in solid line and shaded area for SD). Sources: ECMWF for heat fluxes, SYMPHONIE/Eco3M-S for the other parameters and fluxes. The blue shaded area corresponds to the deep-convection period (period when spatially averaged MLD > 100 m). Note that the range of the y axis varies for the different oxygen fluxes, and due to higher values SD for vertical and lateral transport is not shown.

riod into four sub-periods. The first period from September to the end of November, which we will refer to as the autumn period, is characterised by a stratified water column (mean MLD < 50 m) and respiration dominating primary production (Kessouri et al., 2018). The second period, from the end of November to the end of March, referred to here as the winter period, is characterised by a sustained vertical mixing (mean MLD > 50 m). The third period, called spring, ran from late March to early June. It corresponds to the period of restratification of the water column (Estournel et al., 2016a) and of the peak of the phytoplankton bloom at the sea surface followed by the formation of a deep chlorophyll maximum (Kessouri et al., 2018). The last period, summer, from early June to September, is characterised by a strong stratification (mean MLD < 20 m) and the permanent presence of a deep chlorophyll maximum below 40 m depth (Kessouri et al., 2018). In the following, we will analyse the dynamics of dissolved oxygen for these four periods. The time evolution of daily oxygen budget terms is shown in Fig. 6d–f, while the time evolution of cumulative oxygen fluxes and the resulting variation in oxygen inventory for the upper (surface to 150 m) and deeper (150 m to bottom) layers is presented in Fig. 8. The biogeochemical term of the budget is defined as the sum of oxygen production through photosynthesis and of oxygen consumption through respiration by phytoplankton, zooplankton and bacteria and through oxidation of ammonium (nitrification) (see Eq. 1). The physical term is decomposed into two modes of transport: a net lateral transport due to advection (positive values correspond to an input for the deep-convection area) and a net vertical downward transport at the interface between the two layers, at 150 m depth, due to advection and turbulent mixing. Finally, the time evolution of the dissolved oxygen concentration and the oxygen saturation anomaly, ΔO_2, averaged over the convection area is shown in Fig. 9.

Autumn

From September to the end of November 2012 (91 d), depth-integrated respiration exceeded depth-integrated primary production in the upper layer (Fig. 6f). The result of biogeochemical processes in the water column was a net consumption of oxygen and a decrease of 1.8 $mol\,m^{-2}$ in oxygen inventory (Fig. 8). Lateral transport was low for autumn and yielded a slight decrease of 0.9 $mol\,m^{-2}$ in oxygen inventory (Fig. 8). The heat loss and vertical mixing caused by the northerly wind gust at the end of October 2012 led to a decrease in surface temperature and consequently to an increase in oxygen solubility (Fig. 6c). In addition, the vertical mixing reached the depth of the oxygen maximum present in the subsurface (Fig. 9). This caused its erosion and an increase in the surface oxygen concentration which was, however, lower than the oxygen solubility (Figs. 9 and 6c). From this event, the NW deep-convection area became undersaturated at the surface (Fig. 9b) and the sea began to absorb atmospheric oxygen (flux towards the ocean of 80 $mmol\,d^{-1}$ on 29 October, Fig. 6d). Over the autumnal period, the cumulative air–sea oxygen flux amounted to 0.3 $mol\,m^{-2}$ (Fig. 8a). Globally, the convection area was characterised by a decrease in oxygen inventory of 2.4 $mol\,m^{-2}$, more than two-thirds of which occurred in the upper layer.

Winter

The winter period was defined from late November 2012 to late March 2013 but can be further divided into two sub-periods based on the intensity of the vertical mixing (Kessouri et al., 2017). During the first sub-period, from the end of November to mid-January (44 d), the mixing intensified, but remained moderate: the ML averaged over

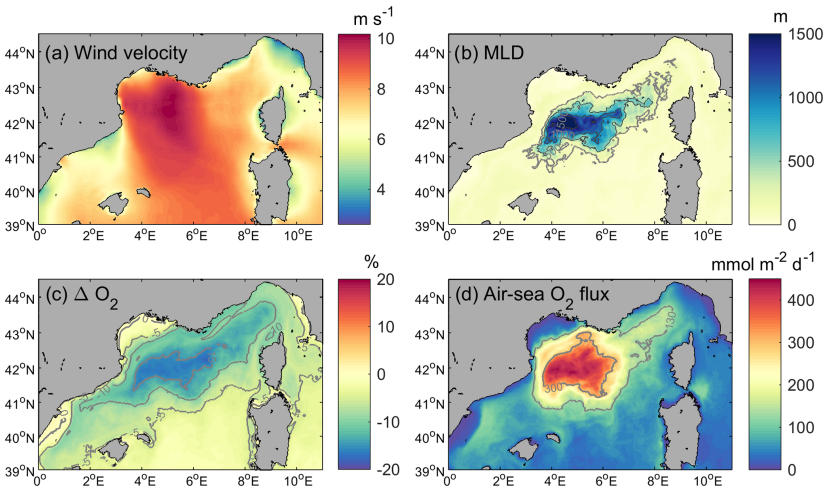

Figure 7. Modelled **(a)** wind velocity ($m\,s^{-1}$), **(b)** mixed-layer depth (m) (dark grey lines represent 500, 1000 and 1500 isocontours and light grey line the contour of the deep-convection area), **(c)** oxygen saturation anomaly (%) at the surface and **(d)** air-to-sea oxygen flux ($mmol\,m^{-2}\,d^{-1}$), averaged over the 2013 deep-convection period (15 January–8 March; 15–24 March).

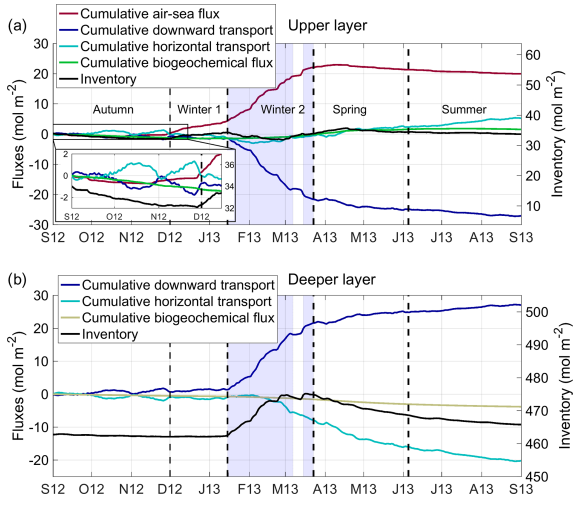

Figure 8. Time series from September 2012 to September 2013 of the oxygen inventory (black line) and cumulative air–sea flux (red line), downward transport (dark blue), lateral transport (positive values: input for the convection area, light blue), and biogeochemical flux (green line) in the **(a)** upper (surface to 150 m) and **(b)** deeper (150 m to bottom) layer. Unit: $mol\,m^{-2}$.

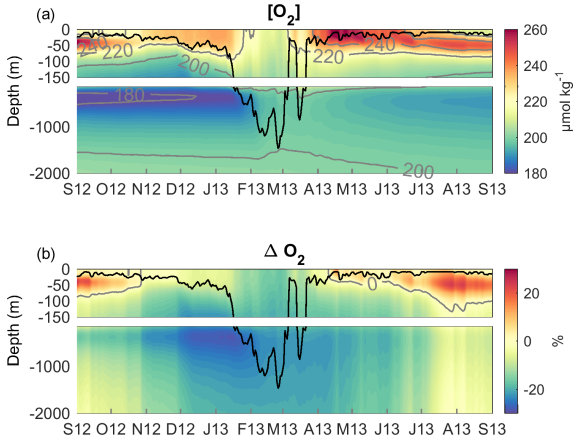

Figure 9. Time evolution of **(a)** the dissolved oxygen concentration ($\mu mol\,kg^{-1}$) and **(b)** the oxygen saturation anomaly (%), with mixed-layer depth (m) indicated by the black line, all horizontally averaged over the deep-convection area.

the deep-convection area remained above the depth of the maximum euphotic layer (150 m; see Sect. 2.1.3) (Fig. 9). The vertical mixing induced a supply of inorganic nutrients in the upper layer that supported primary production. Kessouri et al (2018) identified the beginning of this period as the beginning of a first bloom. From mid-December, the net biogeochemical production of oxygen became positive in the upper layer (Fig. 6f). However, over this sub-period, the influence of biogeochemical processes on the oxygen inventory remained low ($-0.3\,mol\,m^{-2}$, Fig. 8). Air-to-sea oxygen flux was marked by several peaks, greater than $250\,mmol\,m^{-2}\,d^{-1}$ (Fig. 6d), coinciding with cold gales from the north. Its contribution to the oxygen inventory over this sub-period amounted to $3.6\,mol\,m^{-2}$. Regarding the lateral oxygen export, it contributed to a loss of $1.3\,mol\,m^{-2}$. The sum of the contributions of the different processes in the water column and at the air–sea interface yielded an increase in O_2 inventory of $2.0\,mol\,m^{-2}$ in the water column. A total of

90 % of this increase occurred in the upper layer, from which 0.7 mol m^{-2} of O_2 was exported toward the deeper layers.

The second winter sub-period, from mid-January to late March (69 d), corresponds to the period of deep convection. From the middle to the end of January, the surface water masses previously enriched with oxygen, due to primary production and air–sea exchanges, were mixed with the intermediate water masses characterised by a minimum of oxygen (Fig. 9). From the beginning of February, the vertical mixing intensified, causing a net oxygen transport towards deeper layers (depth > 800 m, Figs. 6e, 8 and 9). O_2 concentration decreased significantly at the surface and the difference between surface oxygen concentration and oxygen solubility deepened further, with the oxygen saturation anomaly reaching −15 % until the end of the convection period (Fig. 9). Over this sub-period, the whole NW convection area was undersaturated at −10 % to −15 % (Fig. 7c). Strong undersaturation and wind intensity led to very high air–sea fluxes. Several peaks reaching 800 mmol m^{-2} d^{-1} are modelled until mid-March (Fig. 6d). The contribution of air–sea fluxes over this period amounted to 18.0 mol m^{-2} (Fig. 8a). Over the deep-convection period, air–sea oxygen exchanges are characterised by high spatial variability (Fig. 7d) with a SD of 38 %. The air-to-sea oxygen flux averaged over the deep-convection period varied between 300 and 460 mmol m^{-2} d^{-1} in the heart of the convection area and between 65 and 200 mmol m^{-2} d^{-1} in the Ligurian Sea.

With regard to biogeochemical processes, as shown in previous studies (Auger et al., 2014; Kessouri et al., 2018), zooplankton growth was largely reduced by the deep-convection process due to a dilution-induced decoupling of prey and predators. In the upper layer, oxygen production through primary production exceeded oxygen consumption processes (respiration, nitrification) (Fig. 6f). In parallel, the export of organic matter into the intermediate and deep layers during deep convection (Kessouri et al., 2018) led to an increase in remineralisation processes (Fig. 6f) and consequently a decrease in oxygen inventory in these aphotic layers. The sum of biogeochemical fluxes over the entire water column resulted in a small increase in oxygen inventory of 0.4 mol m^{-2}, negligible compared to that induced by air–sea fluxes, in consistency with the previous study of Minas and Bonin (1988).

Over this period, the lateral export of dissolved oxygen had high values, reaching 220 mmol m^{-2} d^{-1} (Fig 6e). In the upper layer, the total lateral transport over the period was low (0.5 mol m^{-2}), while it is estimated that in the deeper layers 6.7 mol m^{-2} was exported horizontally from the convection area between mid-February and the end of the convection period (Fig. 8b). The downward transport at the base of the upper layer showed strong peaks reaching 500 mmol m^{-2} d^{-1} (Fig. 6e), concomitant with the peaks of the air-to-sea fluxes and the deepening of the ML.

The model results indicate that atmospheric oxygen injected at the surface and, to a lesser extent, produced by phytoplankton or horizontally advected in the upper layer, was massively transported to the intermediate and deep layers (20.1 mol m^{-2}). It is worth noting that vertical fluxes showed high spatial variability within the convection area. Over this period, the lateral transport from the aphotic layer outside the convection area represents 33 % of the amount of downward transport. Globally, the different contributions led to an increase in the water column oxygen inventory of 12.3 mol m^{-2}.

Spring (late March to early June, 74 d)

In spring, net biogeochemical production of O_2 remained high in the upper layer until the bloom peak in mid-April; afterwards it decreased but generally remained positive until the end of that period (Fig. 6f). Oxygen consumption through heterotrophic respiration in the deeper layers also remained relatively high. The result of biogeochemical contributions was a small increase of 0.3 mol m^{-2} in the O_2 inventory of the water column.

During this period, primary production led to a sharp increase in surface oxygen concentration from 220 to 280 µmol kg^{-1} at the peak of the phytoplankton bloom (Fig. 6c), and the latter became above saturation in early April, when the convection area became a source of oxygen for the atmosphere (Fig. 6c and d). This oversaturation situation at the surface then persisted until the end of the period. The model simulates significant outgassing during the bloom peak (235 mmol m^{-2} d^{-1} on 18 April 2013, Fig. 6d) when the mean saturation anomaly reached a maximum value of 15 % (Figs. 6c and 9). Overall, the convection area released 0.8 mol m^{-2} of oxygen to the atmosphere during spring. During this restratification phase, a moderate oxygen export to the deep layers is found (3.2 mol m^{-2}, Fig. 8). Lateral export to regions surrounding the convection area continued at a high rate with a cumulative value of 5.1 mol m^{-2}. Finally, over this period, the water column in the convection area was subjected to a 5.7 mol m^{-2} decrease in its oxygen inventory, due to the lateral export of oxygen via the spreading of dense waters in the deeper layers and a slight outgassing to the atmosphere.

Summer

During the summer period (87 d), the surface oxygen concentration remained higher than the oxygen solubility (Fig. 6c). A supersaturated situation occurred in the deep chlorophyll maximum zone, due to primary production and a general stratification (Fig. 9). We estimate that the ocean released 1.4 mol O_2 m^{-2} to the atmosphere over this period (Fig. 8), mainly during moderate northerly gales. Depth-integrated oxygen-consuming biogeochemical processes exceeded depth-integrated primary production on average over this period. The result of biogeochemical fluxes was responsible for a consumption of 0.8 mol m^{-2} of oxygen.

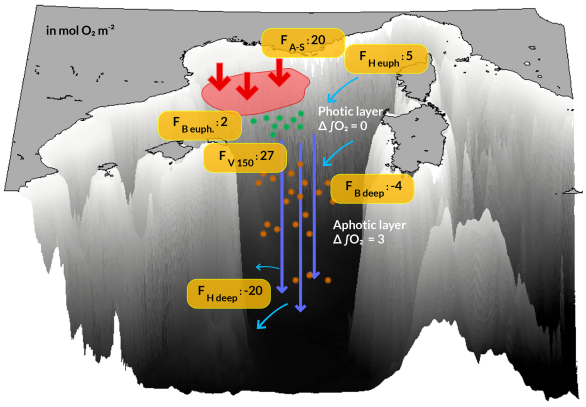

Figure 10. Schematic showing the terms of the annual oxygen budget (mol O_2 m^{-2}) for the north-western Mediterranean deep-convection area over the period from September 2012 to September 2013. F_{A-S}: air-to-sea flux; F_H: net horizontal transport; $F_{v\ 150}$: net downward transport at the base of the euphotic layer (150 m); F_B: net biogeochemical production; $\Delta \int O_2$: variation in oxygen inventory. Positive fluxes are inputs for the deep-convection zone. The terms of the budget are estimated for the upper euphotic layer (surface to 150 m) and the deeper aphotic layers (150 m to bottom).

In addition, the convection area continued to export oxygen to the adjacent zone (1.3 mol m^{-2}), but at a lower rate (15 mmol m^{-2} d^{-1}) than in the two previous periods (90 mmol m^{-2} d^{-1} over the deep-convection period and 69 mmol m^{-2} d^{-1} in spring). Finally, the oxygen inventory decreased by 3.5 mol m^{-2} in the whole water column of the deep-convection area (Fig. 8).

5.2 Annual oxygen budget

Figure 10 illustrates the oxygen budget of the NW Mediterranean convection area over the period September 2012 to September 2013. At the annual scale, the deep-convection area is a net sink of oxygen for the atmosphere, estimated at 20.0 mol O_2 m^{-2}. A total of 88 % (17.7 mol O_2 m^{-2}) of this amount was injected into the ocean interior during the period when the deep-convection process took place.

The annual net biogeochemical production of oxygen in the euphotic layer (0–150 m) is estimated at 1.6 mol O_2 m^{-2}. The net annual NCP (net community production, defined as gross primary production minus community respiration in the euphotic zone) is estimated at 3.9 mol O_2 m^{-2} yr^{-1}, yielding autotrophy in this area. In the deeper layers (150 m–bottom) an oxygen consumption of 3.8 mol O_2 m^{-2} was associated with respiration of heterotrophic organisms by 70 % and oxidation of ammonium by 30 %. This led to an annual net biogeochemical consumption of 2.2 mol O_2 m^{-2} over the whole water column.

The model indicates that 27.1 mol m^{-2} of O_2 was exported from the upper layer to deeper layers. This net transport toward the bottom occurred during 68 % of the events of deep vertical mixing of oxygen-rich surface waters with oxygen-poor underlying waters. Finally, the budget shows that the deep-convection area appears as a net source for dissolved oxygen for the rest of the western Mediterranean Sea with an annual net horizontal transport of 15.0 mol O_2 m^{-2}. This transport breaks down into an input of 5.3 mol O_2 m^{-2} in the upper layer and an export of 20.3 mol O_2 m^{-2} in the deeper layer.

At the end of the annual cycle, a negligible decrease (0.3 mol m^{-2}, i.e. 0.05 %) in the oxygen inventory of the upper euphotic layer is found, while 3.1 mol m^{-2} (i.e. 0.66 % of the inventory) was stored in the deeper water masses.

6 Discussion

6.1 Air–sea oxygen flux

Our model results indicate that the NW Mediterranean deep-convection area was a net sink for the atmospheric oxygen at a rate of 20.0 mol m^{-2} yr^{-1} between September 2012 and September 2013 and at a rate of 280 mmol m^{-2} d^{-1} (17.7 mol m^{-2} over 63 d) during the 2013 deep-convection period. Inside the area, the annual air–sea flux shows strong spatial heterogeneity, with a range extending from 2.7 mol m^{-2} yr^{-1} at the periphery to 36.0 mol m^{-2} yr^{-1} in the centre. Considering its sea surface area (61 720 km^2), the NW deep-convection zone received 1233 Gmol of oxygen from the atmosphere over the period September 2012 to September 2013, including 1090 Gmol during the winter 2013 intense vertical mixing period. We showed that the strong oxygen ingassing was essentially driven by a high undersaturation (< -10 %) and intense northerly winds during the deep-convection period.

Nevertheless, uncertainties in the net uptake rate remain. First, uncertainties are linked to errors in modelled ocean surface variables (dissolved oxygen, temperature and salinity) and wind velocity used for the calculation of the air–sea flux. The comparisons of model results with in situ high-frequency measurements at the surface during the period of maximum flux (deep-convection period) indicate a bias of less than or close to 1 % and a NRMSE smaller than 14 % for the wind velocity, surface temperature, salinity and oxygen concentration (Sect. 3.1). A second source of uncertainty is linked to the parameterisation chosen for the calculation of the gas transfer velocity. In the standard run, we used the cubic dependence with wind speed parameterisation proposed by Wanninkhof and McGillis (1999). Sensitivity analyses were performed using eight other parameterisations for the calculation of air–sea flux (Wanninkhof, 1992, 2014; Woolf, 1997; Nightingale et al., 2000; Wanninkhof et al., 2009; Stanley et al., 2009; Liang et al., 2013; Bushinsky and Emerson, 2018; see Sect. 2.1.2). Estimates of annual air–sea flux, as well as flux and amount of atmospheric oxy-

gen captured by the study area during the deep-convection period, calculated with all these parameterisations are gathered in Table 2. All estimates show a net sink for atmospheric oxygen for the study area. They range from 14.2 to 21.5 mol m^{-2} yr^{-1} at the annual scale, with a mean value of 17.7±2.8 mol m^{-2} yr^{-1}, and from 188 to 285 mmol m^{-2} d^{-1}, with a mean value of 242 ± 38 mmol m^{-2} d^{-1}, during the deep convection. Both estimates in the standard run are in the upper range of all estimates. Considering all estimates, we determine an uncertainty (SD) of 15 %–16 % for the annual and convection period air–sea flux. This uncertainty, associated with the parameterisation of the gas transfer velocity, propagates to the estimates of vertical and lateral transport of oxygen in the ocean interior. Depending on the gas transfer parameterisation used, at the annual scale, downward export below the euphotic zone ranges from 22.0 to 27.9 mol m^{-2} yr^{-1} (mean value: 25.1 ± 2.2 mol m^{-2} yr^{-1}), and lateral transport ranges from 4.8 to 6.1 mol m^{-2} yr^{-1} (mean value: 5.6 ± 0.5 mol m^{-2} yr^{-1}) in the euphotic layer and from -17.1 to -20.6 mol m^{-2} yr^{-1} (mean value: -19.0 ± 1.3 mol m^{-2} yr^{-1}) in the aphotic layer. During the deep-convection event, downward export below the euphotic zone ranges from 223 to 302 mmol m^{-2} d^{-1} (mean value: 265 ± 30 mmol m^{-2} d^{-1}). The uncertainty on the transport terms of the annual budget thus remains smaller than 12 %. The values of the NRMSE between cruise observations and modelled dissolved oxygen from sensitivity tests are found very close to the NRMSE obtained for the standard run. Slightly smaller NRMSE values (≈ 10 %) are found only for the winter DEWEX-Leg1 cruise period using the parameterisations of Wanninkhof and McGillis (1999), Woolf (1997), Stanley et al. (2009), and Liang et al. (2013), which give a higher oxygen transfer than the other parameterisations. Previous studies on oxygen air–sea flux in deep-convection zones recommended the use of parameterisations with high transfer during periods of strong wind and convection (Copin-Montégut and Bégovic, 2002; Körtzinger et al., 2008b; Koelling et al., 2017; Atamanchuk et al., 2020). Atamanchuk et al. (2020), comparing flux estimates based on several parameterisations, found that these flux estimates may vary by an order of magnitude and warned of the possibility of a strong underestimation of air–sea oxygen flux in biogeochemical models that do not include bubble-mediated terms. In our study, the range of estimates obtained with both types of parameterisations, those that are only diffusive and those that include bubble-mediated terms, is similar. Although the parameterisation of Wanninkhof and McGillis (1999) used in our standard run does not include an explicit bubble-mediated transfer term, it provides estimates of air–sea fluxes close to those obtained with the bubble-flux-inclusive one of Stanley et al (2009), preferred by Atamanchuk et al. (2020) in their Labrador Sea study. The strong undersaturation obtained in the north-western Mediterranean during the convection period, between -10 % and -20 %, may explain a greater contribution of the diffusive flux compared to the air injection by bubbles. Moreover, winter conditions are less extreme than in the Labrador Sea where strong wind speeds of more than 13.8 m s^{-1} were encountered for at least 40 d. In the NW Mediterranean Sea and in winter 2012/13, only 13 % of the convection area was characterised by a number of days with wind speeds > 13.8 m s^{-1} varying between 30 and 35 d. An experimental study of flux measurements in this region over a whole year would allow a better assessment of the contribution of air injection in the total air–sea flux and hence of the different parameterisations of gas transfer.

Previous studies based on in situ observations have proposed estimates for the air–sea oxygen flux in the study area. Our modelled seasonal cycle of air–sea oxygen flux agrees with the results of Copin-Montégut and Bégovic (2002) and Coppola et al. (2018) in the Ligurian Sea, at the DYFAMED site, who observed an annual cycle with a net ingassing from December to March and net outgassing from April to November. In the Ligurian Sea the deep-convection process does not occur each winter. When occurring, it is generally shorter and shallower than in the centre of the Gulf of Lion, the core of dense water formation. Coppola et al. (2018) using temperature, salinity and oxygen monthly profiles and the gas transfer parameterisation of Ho et al. (2006) estimated for the period 1994–2014 a monthly air-to-sea flux varying from -15.1 to 14.8 mol O_2 m^{-2} yr^{-1}, with an annual mean value of -2.6 mol O_2 m^{-2} yr^{-1}. Over this 20-year period, the authors identified one winter, winter 2005/2006, with intense vertical mixing reaching the deep layers, and four winters (1999, 2000, 2006 and 2013) with moderate vertical mixing reaching intermediate depths. From the difference in O_2 inventory between December 2005 and April 2006, they deduced that 24 mol m^{-2} of atmospheric O_2 was injected between 350 and 2000 m at a rate of 300 mmol m^{-2} d^{-1}. At the same site, Copin-Montégut and Bégovic (2002) estimated an air–sea ingassing of 5 and 2.6 mol O_2 m^{-2}, respectively, for the moderate cold winters 1999 (for 26 d, rate of 190 mmol m^{-2} d^{-1}) and 2000 (for 23 d, rate of 110 mmol m^{-2} d^{-1}), respectively, using in situ surface measurements of oxygen in winter and the formulation of gas transfer velocity from Wanninkhof and McGillis (1999). Those estimates were twice as small as their observation of variation in the oxygen content in the first 600 m of depth, namely 11 and 15 mol m^{-2} (in 1 month) for winters 1999 and 2000, respectively. Those authors suggested an underestimation in their estimates due to low-frequency measurements and an underestimation of the gas transfer coefficient. At the same location, for the study period, we found a net oxygen ingassing of 9.2 mol m^{-2} yr^{-1} at the annual scale and 135 mmol O_2 m^{-2} d^{-1} during the period of deep-convection events (63 d) (Fig. 7d). Thus our calculation of atmospheric oxygen uptake in the Ligurian Sea is close to the ones of Copin-Montégut and Bégovic (2002) for moderate convective winters. Our estimates in the centre of the Gulf of Lion, where convection reached the deep waters, with val-

Table 2. Estimates of air-to-sea oxygen flux (F_{A-S}) for the period September 2012–September 2013 and during the deep convection (15 January–8 March, 15–24 March), using different parameterisations of gas transfer velocity.

Gas exchange parameterisation	Annual F_{A-S} mol O_2 m^{-2} yr^{-1}	F_{A-S} and amount exchanged at the air–sea interface during the 2013 deep-convection event mmol O_2 m^{-2} d^{-1} – mol O_2 m^{-2}
Wanninkhof and McGillis (1999) (used in the standard run)	20	280–18
Wanninkhof et al. (1992)	18	247–16
Woolf (1997)	20	279–18
Nightingale et al. (2000)	15	207–13
Wanninkhof et al. (2009)	15	212–13
Stanley et al. (2009)	21	285–18
Liang et al. (2013)	20	270–17
Wanninkhof et al. (2014)	15	214–14
Bushinsky and Emerson (2018)	14	188–12
Mean (SD)	18 (3)	242 (38)–15 (2)

ues of 20–28 mol O_2 m^{-2} during deep convection are also close to the estimate by Coppola et al. (2018) for the intense vertical mixing winter 2005/2006 in the Ligurian Sea.

Finally, our model calculation of air–sea oxygen flux for the NW Mediterranean is in the same range found for other worldwide deep-convection areas. At the centre of the Labrador Sea, Körtzinger et al. (2008b) found an annual air–sea ingassing of 10.0 ± 3.1 mol O_2 m^{-2} yr^{-1} over the period 2004/2005, using in situ observations at the K1 mooring site and the Wanninkhof (1992) parameterisation. By quantifying the relative contribution of biogeochemical and lateral fluxes, Koelling et al. (2017) estimated an oxygen ingassing of 29.1 ± 3.8 mol m^{-2} over winter 2014/2015 at the same mooring site K1. Wolf et al (2018) derived from Argo float observations in the Labrador Sea mean air–sea fluxes with a large range of values varying from 5.7 to 22.8 mol m^{-2} yr^{-1} using various parameterisations. Using parameterisations including bubble-mediated fluxes (Liang et al., 2013; Yang et al., 2017), their estimates of atmospheric oxygen uptake ranged from 21.6 to 36.6 mol m^{-2} for the convective winter 2003/2004. Based on measurements of oxygen from a moored profiler and Argo floats and on the Stanley et al. (2009) parameterisation, Atamanchuk et al. (2020) estimated an annual air–sea flux of oxygen of 19.3 ± 3.4 mol m^{-2} yr^{-1} for the year 2016/2017. For the Irminger Sea, Maze et al. (2012) estimated an abiotic air–sea oxygen flux of 13 ± 3 mol m^{-2} yr^{-1} for the years 2002, 2004 and 2006, using an optimisation method and observations from three surveys and Word Ocean Atlas 2009.

6.2 The role of the NW deep-convection area in the ventilation of the western Mediterranean Sea

Open-sea convection and shelf dense water cascading (Canals et al., 2006; Ulses et al., 2008b) in the NW Mediterranean are the main mechanisms for the ventilation of the entire western Mediterranean Sea. Over the past decades, several observational studies reported increases in O_2 concentration in deep water masses at several sites in the western Mediterranean where deep convection did not occur and where winter vertical mixing was limited to surface or intermediate levels. Coppola et al. (2018) associated the high concentrations of O_2 observed in deep layers of the Ligurian Sea in 1994 and 2005, when convection was limited to intermediate waters, with the arrival of deep water formed in the open sea of the Gulf of Lion or formed on the Gulf of Lion shelf and cascading down to the deep basin. Using measurements from five cruises, Schroeder et al. (2008a) documented an abrupt increase in heat, salt and O_2 inventory of deep waters in an extensive area of the western Mediterranean, occurring in 2005 and 2006. The authors attributed these changes, referred to as the western Mediterranean Transient (hereafter WMT; Zunino et al., 2012), to the propagation of the new dense waters formed in the NW deep-convection area during the winters 2004/2005 and 2005/2006, when severe weather conditions caused intense dense water formation (Lopez-Jurado et al., 2005; Schroeder et al., 2006). The study of Schroeder et al. (2008a) showed the presence of these new O_2-rich deep waters in the Balearic Sea, the Ligurian Sea and in the Algerian sub-basin in June 2005 and their propagation to the whole Algerian sub-basin and the west of the Alboran Sea in October 2006. New oxygenated waters were also observed in the entire deep layers of the Algerian sub-basin in 2011 (Schneider et al., 2014; Stöven and Tanhua, 2015), 2014 (Keraghel et al., 2020), 2016 and 2018 (Li and Tanhua, 2020). Moreover, the results of Li and Tanhua (2020) showed a ventilation of the deep waters of the Tyrrhenian Sea through

an overflow of well-oxygenated water masses from the Algerian basin into the deep layer, between 2011 and 2016.

Somot et al. (2016) found that winter 2012/13 is one of the five winters over the 33-year period 1980–2013 showing high dense water formation rates (above 0.6 Sv), using the CNRM-RCSM4 model. According to their estimates, the cumulative volume of dense water formed over the winters 2011/2012 (0.45 Sv) and 2012/13 (0.7 Sv), amounting to 1.15 Sv, may be close to the volume of dense water formed in winter 2004/2005 of 1.2 Sv. As a result, these successive 2012 and 2013 deep-convection events could have been responsible for a similar ventilation as the one observed after the event of 2005 (Schroeder et al., 2008b; Schneider et al., 2004; Stoven and Tanhua, 2015), assuming similar air–sea exchanges.

Our modelling study indicates that, over the period September 2012 to September 2013, the upper layer of the NW deep-convection area captured 5.3 mol O_2 m^{-2} from the surrounding regions, in addition to the 20.0 mol m^{-2} of oxygen from the atmosphere, while the deeper layers released 20.3 mol m^{-2} toward the adjacent seas (Sect. 5.2). Considering the deep-convection surface area of 61 720 km^2, the lateral transport led to a gain in the upper layer of 330 Gmol yr^{-1} in the convection area and a loss of 1250 Gmol yr^{-1} towards the adjacent deep areas. As a result, the NW convection area appears as a source of 920 Gmol yr^{-1} of oxygen for the rest of the western basin for the period 2012/13. Lateral O_2 inputs in the upper layer occurred mainly from February to September with two peak periods, in early March, a calm period between two convective events, and in April, during restratification. These imports were mainly related to eddies produced by the baroclinic instability that was triggered at the periphery of the convection zone when strong wind ceased (Killworth, 1976; Testor et al., 2018). These inputs from the peripheral zone contributed to the vertical export of oxygen to the aphotic layer. First in the short term, the oxygen imported between two convection events was exported at depth by the following events. At longer timescales (April–September), the convection area was also fed by the peripheral zones and in turn produced a vertical export to the aphotic layer. These exchanges were of lower intensity and concerned shallower layers but are not negligible when integrated over the year. Regarding the lateral transport in the deeper layer, our model outputs show that the O_2-rich dense waters formed in the NW deep-convection area propagated towards the Balearic Sea, first at intermediate depths (150–800 m) from the beginning of the winter mixing period and then through deep layers (800 m to bottom) from mid-February (not shown). These water masses then mostly flowed towards the south of the western basin, while a smaller part was advected back in the convection area through mesoscale circulations counteracting the effect of the intrusions of low-oxygen LIW during the restratification period, in increasing the oxygen inventory of intermediate waters (not shown). A preferential pathway to the south of the basin was the one along the eastern coast of Minorca in the Algerian sub-basin, in agreement with previous observational and modelling studies that examined the spreading of waters formed in winter in the NW region (Pinot and Ganachaud, 1999; Schroeder et al 2008b; Beuvier et al., 2012). Our simulated circulation of oxygen in the western basin is also consistent with the study of Piñeiro et al. (2019), who reported the arrival of new dense water masses formed in the deep-convection area east of Minorca over the 2011–2013 period using temperature and salinity observations at the hydrographic stations RADMED. In our model outputs, the offshore Balearic Sea (bathymetry > 1000 m, surface area: 19 700 km^2) and Algerian sub-basin (bathymetry > 1000 m, surface area: 171 610 km^2) experienced an increase in their oxygen inventory, during and after the NW deep-convection events, receiving oxygen through lateral transport (271 and 1276 Gmol, respectively) while the amounts of oxygen captured at the air–sea interface during the period of intense vertical mixing were smaller in those areas than in the NW deep-convection area by a factor of 10 and 3, respectively (i.e. 104 and 385 Gmol versus 1090 Gmol for the NW deep-convection area). This suggests that an important part of the oxygen absorbed at the air–sea interface of the NW deep-convection area, exported first vertically towards its deeper layers and then horizontally towards the adjacent regions, was stored, at least temporarily, in the Algerian sub-basin.

Finally, our results demonstrate that the total oxygen supply by air–sea exchanges in the NW deep-convection region for the period 2012/13 (1233 Gmol yr^{-1}), which was then mainly released to adjacent seas in the aphotic layer, constitutes a major source of oxygen at the scale of the whole Mediterranean Sea. Indeed this supply is close to the biogeochemical oxygen consumption within the Mediterranean Sea estimated at 1545 Gmol yr^{-1} by Huertas et al. (2009) using in situ measurements at the Strait of Gibraltar over the period 2005–2007.

The present study of the period 2012/13 constitutes a first step in our analysis and quantification of the oxygen budget for the western Mediterranean Sea. Previous observational studies (Coppola et al., 2018; Mavropoulou et al., 2020) over periods of 20 years or more showed that the mean oxygen concentration in the western Mediterranean and in particular in the NW deep-convection area is subjected to a strong interannual variability, mainly in response to the variability of deep convection, the latter being influenced by transient changes such as the WMT event. A deeper analysis of the physical processes involved in the vertical and horizontal transport in the convection zone as well as of the spreading of the oxygen-enriched dense waters, formed in the NW deep-convection area, in the western basin and toward the Atlantic Ocean through the Gibraltar Strait will be conducted in further studies using a numerical simulation with extended domain and period.

6.3 Net community production

Our budget calculation shows that in this region characterised by intense vertical mixing the biogeochemical terms remained very low compared to the air–sea oxygen flux over the period 2012/13. Our modelling results indicate that the net biogeochemical production of oxygen in the euphotic layer was positive from mid-December to the end of July and negative the rest of the year. It was maximum during the spring bloom from mid-March to mid-April. We estimate a net annual NCP (in the upper layer) of 46.8 g C m^{-2} yr^{-1} (3.9 molO_2 m^{-2} yr^{-1}; see Eq. 1). This indicates a net autotrophy for the euphotic layer of the NW Mediterranean deep-convection area over the period September 2012–September 2013. If consumption of oxygen through nitrification is considered, net biogeochemical production amounted to 1.6 mol O_2 m^{-2} yr^{-1}. It is worth noting that nitrification, discussed in Kessouri et al. (2017), who estimated a nitrogen budget using the same coupled model, accounts only for 7 % of the total oxygen consumption but for 60 % of the NCP, suggesting that this process should be considered when estimating NCP from oxygen concentration.

Our value of NCP is higher than the net downward export of organic carbon at the base of the euphotic layer estimated at 35 g C m^{-2} yr^{-1} (25 g C m^{-2} yr^{-1} for particulate organic carbon and 10 g C m^{-2} yr^{-1} for dissolved organic carbon) by Kessouri et al. (2018) over the same period and using the same coupled model. Also using the same coupled model, Kessouri et al. (2017), who analysed the nitrogen cycle over the study period, obtained a new primary production varying from 65 to 77 g C m^{-2} yr^{-1} in the deep-convection zone. By analysing the carbon, nitrogen and oxygen cycles, the NW deep-convection region is always found to be an autotrophic ecosystem. The discrepancies in magnitude obtained depending on the element considered reflect different dynamics for these elements in the euphotic layer, possibly due to variable O_2 : C : N ratios in biogeochemical production and consumption processes as shown by Copin-Montégut (2000) in the Ligurian Sea using high-frequency measurements.

Our estimate of NCP is smaller than the estimate of 85.2 g C m^{-2} yr^{-1} in the Ligurian Sea at the DYFAMED site over the period 1994–2014 by Coppola et al. (2018) using monthly observations. It is close to the estimate by Ulses et al. (2016) of 42.8 g C m^{-2} yr^{-1} over the period 2003–2008 using the same numerical model and considering an area extending to the whole offshore NW Mediterranean and a 100 m thick upper layer. It is also similar to the previous estimates of new primary production by Severin et al. (2014) varying from 46 to 63 g C m^{-2} yr^{-1} over the period February–March 2011, based on in situ nutrient concentrations.

NCP is often used to estimate the strength of the biological pump and the potential capacity of a system to capture atmospheric CO_2. Although the NW deep-convection pelagic ecosystem appears as a net annual sink for atmospheric CO_2 from our modelling results and previous studies (Coppola et al., 2018; Ulses et al., 2016), the role of this region in terms of carbon sequestration remains highly uncertain. Deep convection generates a strong downward transport of organic carbon below the euphotic layer (Ulses et al., 2016; Kessouri et al., 2018). A large amount of organic carbon transferred below the euphotic zone is then consumed and demineralised after deep convection (Santinelli et al., 2010), leading to an increase in CO_2 inventory into the deeper reservoir that could be raised back in the euphotic layer during the following deep-convection events as shown in the Atlantic Ocean by Körtzinger et al. (2008a) and in the Pacific Ocean by Palevsky et al. (2016). Episodes of oversaturation of sea surface pCO_2 related to atmospheric pCO_2 were reported during short wind gusts and intense vertical mixing events in the Ligurian Sea (Copin-Montégut et al., 2004; Merlivat et al., 2018) and in the central Gulf of Lion open sea (Touratier et al., 2016). The authors explained those oversaturation episodes by the increase in CO_2 concentration at the ocean surface induced by the mixing of surface CO_2-poorer waters with deep CO_2-rich waters. Those punctual observations suggested short releases of CO_2 by the ocean induced by deep convection. On the other hand, using a 0.5° resolution array of coupled 1D hydrodynamic–biogeochemical models of the upper layer in the Mediterranean Sea over the period 1998–2004, D'Ortenzio et al. (2008) estimated that the NW region is a sink for atmospheric CO_2 in winter and at the annual scale (between 12 and 24 g C m^{-2} yr^{-1}) and found that biogeochemical processes dominate air–sea exchanges and mixing processes in this region most of the year. In another region of deep convection, the Labrador Sea, DeGrandpre et al. (2006) and Körtzinger et al. (2008b) also found an annual uptake of atmospheric CO_2 that amounted to 55.2 g C m^{-2} yr^{-1} for the period 2000–2001 and 32.4 ± 9.6 g C m^{-2} yr^{-1} for the period 2004–2005, using mooring observations (and also a 1D biogeochemical model for DeGrandpre et al., 2006).

In the study area, our results show that lateral transport dominated the budget of oxygen during the restratification period when deep dense waters spread in the western basin and LIW reintegrated the deep-convection zone. This suggests that coupled 3D biogeochemical–physical models, including a carbonate system module, could be useful tools to complete the previous 1D studies of dissolved inorganic carbon dynamics and integrate on an annual scale the exchanges at the air–sea interface by taking into account lateral transport and mesoscale structures influencing the spreading of water masses and their compounds during convection and restratification phases and impacting the budgets.

7 Conclusions

Our study is the first attempt to describe the seasonal cycle of dissolved oxygen and to estimate the oxygen budget over the whole NW Mediterranean deep-convection area, using a high-resolution coupled 3D physical–biogeochemical model. The assessment of the model results using in situ measurements from DEWEX and MOOSE-GE cruises and from Argo-O_2 floats shows the ability of the model to capture the main spatial and temporal variability of dissolved oxygen observed. From our modelling results, the following conclusions can be drawn for the period 2012/13.

- The seasonal cycle of surface dissolved oxygen in this area exhibited a winter period with strong undersaturation due to a decrease in temperature and surface dissolved oxygen concentration, induced by strong heat loss and vertical mixing of surface O_2-rich waters with the underlying low-O_2 waters. The undersaturation averaged over the whole area indeed reached -15 % during the deep-convection event. During the stratified period, an oversaturation situation occurred with a maximum surface value of 15 % during the peak of the spring bloom.

- The NW Mediterranean deep-convection area acted as a large sink for atmospheric oxygen. We estimate that the area captured 20 mol m^{-2} yr^{-1} of atmospheric oxygen at the annual timescale. An uptake of 18 mol m^{-2} of atmospheric oxygen, which equals 88 % of the annual uptake, took place during the deep-convection period. This uptake is characterised by high spatial variability, with a SD of 38 % in this area including the open sea of the Gulf of Lion and Ligurian Sea. The magnitude of the uptake is maximum inside a central zone of the Gulf of Lion where the average over the deep-convection period (63 d) reached a rate ranging between 300 and 460 mmol O_2 m^{-2} d^{-1}.

- The NW Mediterranean deep-convection area acts as a conveyor of atmospheric oxygen, as well as of oxygen produced in the upper layer, both locally and in the surrounding areas, towards the intermediate and deep layers of the western Mediterranean Sea. Based on the rate of dense water formation (Somot et al., 2016), the ventilation due to deep convection in the NW area in 2012/13 may represent half of the ventilation observed in 2004/2005 by Schroeder et al. (2008a). The magnitude of atmospheric O_2 uptake and lateral transport to the adjacent regions in the aphotic layers in 2012/13 is close to the magnitude of the oxygen consumption of the whole Mediterranean Sea estimated by Huertas et al. (2009).

- Sensitivity tests to the parameterisation of the gas transfer velocity yield an estimate of the budget term (air–sea exchanges and transport terms) uncertainty of 12 %–16 %.

- As expected for this very energetic region, the annual budget of oxygen is clearly dominated by air–sea exchanges and physical transport over convective years such as 2012/13. The net biogeochemical production in the euphotic zone is estimated to account for 10 %, i.e. 2 mol O_2 m^{-2} yr^{-1}, of the net atmospheric oxygen uptake. In deeper depths, heterotrophic organisms' respiration and nitrification resulted in an oxygen consumption of 4 mol m^{-2} yr^{-1}.

- The NW Mediterranean deep-convection area is found to be an autotrophic ecosystem with an annual NCP (in the 150 m upper layer) estimated at 47 g C m^{-2} yr^{-1}.

The high interannual variability of deep convection in the NW Mediterranean (Houpert et al., 2016; Somot et al., 2016) suggests a high variability of the oxygen budget. Further modelling at pluri-annual and multi-decadal scales is thus needed to investigate the interannual variability of the annual budget over the whole western basin, as well as the evolution of this budget under climate warming, the effects of which could have been masked for the time being by the significant impacts of climatic transient shifts such as WMT according to Mavropoulou et al. (2020).

Data availability. The Argo data are available on the Coriolis platform (https://doi.org/10.17882/42182, Argo (2020), last access: 19 May 2017), MOOSE data on SEANOE/ SISMER (https://www.ir-ilico.fr/en/Data-access/MOOSE, Testor et al., 2013, last access: 8 June 2017) and DEWEX data on the MerMex database (https://mistrals.sedoo.fr/MERMeX/, Testor, 2013 and Conan, 2013, last access: 1 February 2019). Results of simulations are available on request (caroline.ulses@legos.obs-mip.fr), Ulses et al., 2020, last access: 13 October 2020.

Author contributions. CU, FK, CE and PM developed the coupled model. CU, FK and CE designed the simulations. CU performed model simulations. LC, MF and DL provided the observational data and helped with data analyses and interpretation. CU, CE, MF and FK performed the analyses of the model outputs. CU wrote the initial version of the manuscript. All authors discussed the results and revised the manuscript.

Competing interests. The authors declare that they have no conflict of interest.

Acknowledgements. The numerical simulations were performed using the SYMPHONIE model, developed by the SIROCCO group (https://sirocco.obs-mip.fr/), and computed on the cluster of Laboratoire d'Aérologie and HPC resources from CALMIP

grants (P1325, P09115 and P1331). We acknowledge the scientists and crews of the Flotte océanographique française (https://www.flotteoceanographique.fr/), who contributed to the cruises carried out in the framework of the DEWEX project and MOOSE programme (CNRS-INSU). We thank Toste Tanhua and the two other anonymous reviewers for their constructive comments. We thank Dariia Atamanchuk for sharing with us a MATLAB code with the calculation of air–sea oxygen fluxes including bubble-mediated terms.

Financial support. This research has been supported by the international metaprogramme MISTRALS dedicated to the understanding of the Mediterranean basin environmental processes (http://www.mistrals-home.org/), in particular by the French MERMEX (Marine Ecosystem Response in the Mediterranean Experiment), HYMEX (Hydrological cycle in the Mediterranean EXperiment) and MOOSE (Mediterranean Ocean Observing System for the Environment) programmes coordinated by CNRS-INSU.

Review statement. This paper was edited by Marilaure Grégoire and reviewed by Toste Tanhua and two anonymous referees.

References

Allen, J. I., Somerfield, P., and Gilbert, F.: Quantifying uncertainty in high-resolution coupled hydrodynamic-ecosystem models, J. Mar. Syst., 64, 3–14. https://doi.org/10.1016/j.jmarsys.2006.02.010, 2007.

Andrews, O., Buitenhuis, E., Le Quéré, C., Suntharalingam, P. : Biogeochemical modelling of dissolved oxygen in a changing ocean, Phil. Trans. R. Soc. A, 37520160328, https://doi.org/10.1098/rsta.2016.0328, 2017.

Argo: Argo float data and metadata from Global Data Assembly Centre (Argo GDAC), SEANOE, available at: https://doi.org/10.17882/42182 (last access: 19 May 2017), 2020.

Atamanchuk, D., Koelling, J., Send, U., and Wallace, D. W. R.: Rapid transfer of oxygen to the deep ocean mediated by bubbles, Nat. Geosci. 13, 232–237, https://doi.org/10.1038/s41561-020-0532-2, 2020.

Auger, P. A., Diaz, F., Ulses, C., Estournel, C., Neveux, J., Joux, F., Pujo-Pay, M., and Naudin, J. J.: Functioning of the planktonic ecosystem on the Gulf of Lions shelf (NW Mediterranean) during spring and its impact on the carbon deposition: a field data and 3-D modelling combined approach, Biogeosciences, 8, 3231–3261, https://doi.org/10.5194/bg-8-3231-2011, 2011.

Auger, P., Ulses, C., Estournel, C., Stemmann, L., Somot, S., Diaz, F.: Interannual control of plankton communities by deep winter mixing and prey/predator interactions in the NW Mediterranean: Results from a 30-year 3D modeling study, Prog. Oceanogr., 124, 12–27, https://doi.org/10.1016/j.pocean.2014.04.004, 2014.

Bentsen, M., Evensen, G., Drange, H., Jenkins, A. D.: Coordinate transformation on a sphere using conformal mapping. Mon. Weather Rev., 127, 2733–2740, 1999.

Bernardello, R., Cardoso, J. G., Bahamon, N., Donis, D., Marinov, I., and Cruzado, A.: Factors controlling interannual variability of vertical organic matter export and phytoplankton bloom dynamics – a numerical case-study for the NW Mediterranean Sea, Biogeosciences, 9, 4233–4245, https://doi.org/10.5194/bg-9-4233-2012, 2012.

Béthoux, J. P., Durrieu de Madron, X., Nyffeler, F., and Tailliez, D.: Deep water in the western Mediterranean: peculiar 1999 and 2000 characteristics, shelf formation hypothesis, variability since 1970 and geochemical inferences, J. Mar. Syst., 33-34, 117–131, https://doi.org/10.1016/S0924-7963(02)00055-6, 2002.

Beuvier, J., Béranger, K., Brossier, C. L., Somot, S., Sevault, F., Drillet, Y., Lyard, F.: Spreading of the Western Mediterranean deep water after winter 2005: Time scales and deep cyclone transport, J. Geophys. Res., 117, C07022, https://doi.org/10.1029/2011JC007679, 2012.

Breitburg, D., L.A. Levin, A. Oschlies, M. Grégoire, F.P. Chavez, D.J. Conley, V. Garçon, D.Gilbert, D. Gutiérrez, K. Isensee, et al.:Declining oxygen in the global ocean and coastal waters, Science, 359, eaam7240, 2018.

Breitburg, D. L., D. W. Hondorp, L. A. Davias, R. J. Diaz: Hypoxia, nitrogen, and fisheries: Integrating effects across local and global landscapes. Annu. Rev. Mar. Sci. 1, 329–349, 21141040, 2009.

Bristow, L. A., et al.: N2 production rates limited by nitrite availability in the Bay of Bengal oxygen minimum zone, Nat. Geosci., 10, 24–29, https://doi.org/10.1038/ngeo2847, 2017.

Brodeau, L., Koenigk, T.: Extinction of the northern oceanic deep convection in an ensemble of climate model simulations of the 20th and 21st centuries, Clim. Dyn., 46, 2863–2882, https://doi.org/10.1007/s00382-015-2736-5, 2016.

Bushinsky, S. M. and Emerson, S. R.: Biological and physical controls on the oxygen cycle in the Kuroshio Extension from an array of profiling floats, Deep Sea Res. Part I Oceanogr. Res. Pap., 141, 51–70, ISSN 0967-0637, https://doi.org/10.1016/j.dsr.2018.09.005, 2018.

Bopp, L., Le Quéré, C., Heimann, M., Manning, A. C., and Monfray, P.: Climate-induced oceanic oxygen fluxes: implications for the contemporary carbon budget, Global Biogeochem. Cy., 16, 1022, https://doi.org/10.1029/2001GB001445, 2002.

Canals, M., Puig, P., de Madron, X. et al. Flushing submarine canyons, Nature 444, 354–357, https://doi.org/10.1038/nature05271, 2006.

Conan, P.: DEWEX-MERMEX 2013 LEG2 cruise, RV Le Suroît, SISMER, Brest, France, https://doi.org/10.17600/13020030, 2013.

Conan, P., Testor, P., Estournel, C., D'Ortenzio, F., Pujo-Pay, M., Durrieu de Madron, X.: Preface to the Special Section: Dense water formations in the northwestern Mediterranean: From the physical forcings to the biogeochemical consequences. J. Geophys. Res. Oceans, 123, 6983–6995, https://doi.org/10.1029/2018JC014301, 2018.

Copin-Montégut, C.: Consumption and production on scales of a few days of inorganic carbon, nitrate and oxygen by the planktonic community: results of continuous measurements at the Dyfamed Station in the northwestern Mediterranean Sea (May 1995). Deep Sea Res. Part I, 47, 447–477, https://doi.org/10.1016/S0967-0637(99)00098-9, 2000.

Copin-Montégut, C., Bégovic, M.: Distributions of carbonate properties and oxygen along the water column (0–2000 m) in the central part of the NW Mediterranean Sea (Dyfamed site): influence of winter vertical mixing on air–sea CO_2

and O_2 exchanges. Deep Sea Res. Part II, 49, 2049–2066, https://doi.org/10.1016/S0967-0645(02)00027-9, 2002.

Copin-Montégut, C., Bégovic, M., Merlivat, L.: Variability of the partial pressure of CO_2 on diel to annual time scales in the Northwestern Mediterranean Sea, Mar. Chem., 85, 3–4, 169-189, https://doi.org/10.1016/j.marchem.2003.10.005, 2004.

Coppola, L., Prieur, L., Taupier-Letage, I., Estournel, C., Testor, P., Lefevre, D., Belamari, S., LeReste, S., Taillandier, V.:. Observation of oxygen ventilation into deep waters through targeted deployment of multiple Argo-O_2 floats in the north-western Mediterranean Sea in 2013, J. Geophys. Res. Oceans, 122, 6325–6341, https://doi.org/10.1002/2016JC012594, 2017.

Coppola, L., Legendre, L., Lefevre, D., Prieur L., Taillandier V., Diamond Riquiera, E.: Seasonal and inter-annual variations of dissolved oxygen in the northwestern Mediterranean Sea (DYFAMED site). Prog. Oceanogr., 162, 187–201, https://doi.org/10.1016/j.pocean.2018.03.001, 2018.

DeGrandpre, M., Körtzinger, A., Send, U., Wallace, D.W.R., Bellerby, Richard, Uptake and sequestration of atmospheric CO_2 in the Labrador Sea deep convection region, Geophys. Res. Lett., 33, L21S03, https://doi.org/10.1029/2006GL026881, 2006.

de Lavergne, C., Palter, J., Galbraith, E. et al. Cessation of deep convection in the open Southern Ocean under anthropogenic climate change. Nature Clim Change, 4, 278–282. https://doi.org/10.1038/nclimate2132, 2014.

Diaz, R. J., Rosenberg, R.: Spreading dead zones and consequences for marine ecosystems, Science, 321, 926–929, 18703733, https://doi.org/10.1126/science.1156401, 2008.

D'Ortenzio, F., D. Antoine and S. Marullo: Satellite-driven modelling of the upper ocean mixed layer and air-sea CO_2 flux in the Mediterranean Sea, Deep-Sea Res. I, 55, 405–434, https://doi.org/10.1016/j.dsr.2007.12.008, 2008.

Dugenne, M. :Dynamique du phytoplancton en mer Méditerranée: Approches par mesures à haute fréquence, modélisation, et statistiques bayésiennes, PhD Thesis, Aix Marseille Université, available at: http://www.theses.fr/s137171 (last access: 15 April 2020), 2017.

Estournel, C., Durrieu de Madron, X., Marsaleix, P., Auclair, F., Julliand, C., and Vehil, R.: Observation and modeling of the winter coastal oceanic circulation in the Gulf of Lion under wind conditions influenced by the continental orography (FETCH experiment), J. Geophys. Res., 108, 8059, https://doi.org/10.1029/2001JC000825, C3, 2003.

Estournel, C., Testor, P., Damien, P., D'Ortenzio, F., Marsaleix, P., Conan, P., Kessouri, F., Durrieu de Madron, X., Coppola L., Lellouche, J.-M., Belamari, S., Mortier, L., Ulses, C., Bouin, M.-N., and Prieur, L.: High resolution modeling of dense water formation in the north-western Mediterranean during winter 2012–2013: Processes and budget, J. Geophys. Res. Oceans, 121, 5367–5392, https://doi.org/10.1002/2016JC011935, 2016a.

Estournel, C., P. Testor, I. Taupier-Letage, M.-N. Bouin, L. Coppola, P. Durand, P. Conan, A. Bosse, P.-E. Brilouet, L. Beguery, S. Belamari, K. Béranger, J. Beuvier, D. Bourras, G. Canut, A. Doerenbecher, X. Durrieu de Madron, F. D'Ortenzio, P. Drobinski, V. Ducrocq, N. Fourrié, H. Giordani, L. Houpert, L. Labatut, C.L. Brossier, M. Nuret, L. Prieur, O. Roussot, L. Seyfried, and S. Somot: HyMeX-SOP2: The field campaign dedicated to dense water formation in the northwestern Mediterranean. Oceanography 29(4):196–206, https://doi.org/10.5670/oceanog.2016.94, 2016b.

Estournel, C., Zervakis, V., Marsaleix, P., Papadopoulos, A., Auclair, F., Perivoliotis, L., Tragou, E.: Dense water formation and cascading in the Gulf of Thermaikos (North Aegean) from observations and modelling, Cont. Shelf Res., 25, 2366–2386, 2005.

Fröb, F., A. Olsen, K. Vage, G. W. Moore, I. Yashayaev, E. Jeansson, and B. Rajasakaren: Irminger Sea deep convection injects oxygen and anthropogenic carbon to the ocean interior, Nat. Commun., 7, 13244, https://doi.org/10.1038/ncomms13244, 2016.

Garcia, Herncin E., Gordon, Louis I.: Oxygen solubility in seawater: Better fitting equations, Limnol. Oceanogr., 37, 1307–1312, https://doi.org/10.4319/lo.1992.37.6.1307, 1992.

Gaspar, P., Y. Gregoris, and J. M. Lefevre, A simple eddy kinetic energy model for simulations of the oceanic vertical mixing: Tests at station Papa and long-term upper ocean study site, J. Geophys. Res., 95, C9, 16179-16193, 1990.

Giorgi, F.: Climate change hot-spots, Geophys. Res. Lett. 33, L08707, https://doi.org/10.1029/2006GL025734, 2006.

Grégoire, M., C. Raick, K. Soetaert: Numerical modeling of the central Black Sea ecosystem functioning during the eutrophication phase, Prog. Oceanogr., 76, 3, 286–333, ISSN 0079-6611, https://doi.org/10.1016/j.pocean.2008.01.002, 2008.

Helm, K. P., Bindoff, N. L. Church, J. A.: Observed decreases in oxygen content of the global ocean. Geophys. Res. Lett. 38, L23602, https://doi.org/10.1029/2011GL049513, 2011.

Herrmann, M., Somot, S., Sevault, F., Estournel, C., Déqué, M. : Modeling the deep convection in the Northwestern Mediterranean sea using an eddy-permitting and an eddy-resolving model: Case study of winter 1986–87. J. Geophy. Res., 113, C04011, https://doi.org/10.1029/2006JC003991, 2008.

Herrmann, M., Auger, P.-A., Ulses, C., and Estournel, C.: Long-term monitoring of ocean deep convection using multisensors altimetry and ocean color satellite data, J. Geophys. Res. Oceans, 122, 1457– 1475, https://doi.org/10.1002/2016JC011833, 2017.

Ho, D.T., Law, C.S., Smith, M.J., Schlosser, P., Harvey, M., Hill, P.: Measurements of air-sea gas exchange at high wind speeds in the Southern Ocean: implications for global parameterizations. Geophys. Res. Lett., 33, L16611, https://doi.org/10.1029/2006GL026817, 2006.

Houpert, L., et al.: Observations of open-ocean deep convection in the northwestern Mediterranean Sea: Seasonal and interannual variability of mixing and deep water masses for the 2007–2013 Period, J. Geophys. Res. Oceans, 121, 8139–8171, https://doi.org/10.1002/2016JC011857, 2016.

Huertas, I. E., Ríos, A. F., García-Lafuente, J., Makaoui, A., Rodríguez-Gálvez, S., Sánchez-Román, A., Orbi, A., Ruíz, J., and Pérez, F. F.: Anthropogenic and natural CO2 exchange through the Strait of Gibraltar, Biogeosciences, 6, 647–662, https://doi.org/10.5194/bg-6-647-2009, 2009.

Ingall, E., R. Jahnke, Evidence for enhanced phosphorus regeneration from marine sediments overlain by oxygen depleted waters. Geochim. Cosmochim. Acta 58, 2571–2575, https://doi.org/10.1016/0016-7037(94)90033-7, 1994.

Ito, T., Minobe, S., Long, M. C., and Deutsch, C.: Upper ocean O_2 trends: 1958–2015, Geophys. Res. Lett., 44, 4214–4223, https://doi.org/10.1002/2017GL073613, 2017.

Joos, F., G. K. Plattner, T. F. Stocker, A. Kortzinger, and D. W. R. Wallace: Trends in marine dissolved oxygen: Implications for

ocean circulation changes and the carbon budget, Eos Trans. AGU, 84(21), 197, https://doi.org/10.1029/2003EO210001, 2003.

Keeling, R. F., and H. Garcia: The change in oceanic O_2 inventory associated with recent global warming, Proc. Natl. Acad. Sci. USA, 99, 7848–7853, https://doi.org/10.1073/pnas.122154899, 2002.

Keeling, R. F., Körtzinger, A., and Gruber, N.: Ocean deoxygenation in a warming world, Annu. Rev. Marin. Sci., 2, 199–229, https://doi.org/10.1146/annurev.marine.010908.163855, 2010.

Keraghel M.A., Louanchi F., Zerrouki M., Aït Kaci M., Aït-Ameur N., Labaste M., Legoff H., Taillandier V., Harid R., Mortier L.: Carbonate system properties and anthropogenic carbon inventory in the Algerian Basin during SOMBA cruise (2014): Acidification estimate. Mar. Chem., 221, 103783, https://doi.org/10.1016/j.marchem.2020.103783, 2020.

Kessouri, F., Ulses, C., Estournel, C., Marsaleix, P., Severin, T., Pujo-Pay, M., et al.: Nitrogen and phosphorus budgets in the Northwestern Mediterranean deep convection region, J. Geophys. Res. Oceans, 122, 9429–9454. https://doi.org/10.1002/2016JC012665, 2017.

Kessouri, F., Ulses, C., Estournel, C., Marsaleix, P., D'Ortenzio, F., Severin, T., et al.: Vertical mixing effects on phytoplankton dynamics and organic carbon export in the western Mediterranean Sea. J. Geophys. Res. Oceans, 123, 1647–1669. https://doi.org/10.1002/2016JC012669, 2018.

Killworth, P.: The mixing and spreading phases of MEDOC. I, Prog. Oceanogr., 7, 59–90, https://doi.org/10.1016/0079-6611(76)90005-7, 1976.

Koelling, J., D. W. R. Wallace, U. Send, and J. Karstensen: Intense oceanic uptake of oxygen during 2014–2015 winter convection in the Labrador Sea, Geophys. Res. Lett., 44, 7855–7864, https://doi.org/10.1002/2017GL073933, 2017.

Körtzinger, A., Schimanski, J., Send, U., Wallace, D.: The ocean takes a deep breath, Science, 306, 1337, https://doi.org/10.1126/science.1102557, 2004.

Körtzinger, A., U. Send, R. S. Lampitt, S. Hartman, D. W. R. Wallace, J. Karstensen, M. G. Villagarcia, O. Llinaìs, and M. D. DeGrandpre: The seasonal pCO_2 cycle at 49° N/16.5° W in the northeastern Atlantic Ocean and what it tells us about biological productivity, J. Geophys. Res., 113, C04020, https://doi.org/10.1029/2007JC004347, 2008a.

Körtzinger, A., Send, U., Wallace, D. W. R., Kartensen, J., DeGrandpre, M.: Seasonal cycle of O_2 and pCO_2 in the central Labrador Sea: Atmospheric, biological, and physical implications. Global Biogeochem. Cycles, 22, GB1014. https://doi.org/10.1029/2007GB003029, 2008b.

Large, W. G., Yeager, S. G.: Diurnal to decadal global forcing for ocean and sea-ice models: The data sets and flux climatologies (NCAR Tech. Note NCAR/TN-4601STR). Boulder, CO: National Center of Atmospheric Research. https://doi.org/10.5065/D6KK98Q6, 2004.

Lavigne, H., D'Ortenzio, F., Migon, C., Claustre, H., Testor, P., Ribera d'Alcala, M., et al. : Enhancing the comprehension of mixed layer depth control on the Mediterranean phytoplankton phenology. J. Geophys. Res. Oceans, 118, 3416–3430. https://doi.org/10.1002/jgrc.20251, 2013.

Leonard, B.P. A stable and accurate convective modelling procedure based on quadratic upstream interpolation, Comput. Methods Appl. Mech. Eng., 19, 59–98, https://doi.org/10.1016/0045-7825(79)90034-3, 1979.

Lellouche, J.-M., Le Galloudec, O., Drévillon, M., Régnier, C., Greiner, E., Garric, G., Ferry, N., Desportes, C., Testut, C.-E., Bricaud, C., Bourdallé-Badie, R., Tranchant, B., Benkiran, M., Drillet, Y., Daudin, A., and De Nicola, C.: Evaluation of global monitoring and forecasting systems at Mercator Océan, Ocean Sci., 9, 57–81, https://doi.org/10.5194/os-9-57-2013, 2013.

Levin, L.: Oxygen minimum zone benthos: Adaptation and community response to hypoxia, Oceanogr. Mar. Biol. 41, 1–45, 2003.

Li, P., and Tanhua, T.: Recent Changes in Deep Ventilation of the Mediterranean Sea; Evidence From Long-Term Transient Tracer Observations, Front. Mar. Sci., 7, https://doi.org/10.3389/fmars.2020.00594, 2020.

Liang, J.-H., Deutsch, C., McWilliams, J. C., Baschek, B., Sullivan, P. P., Chiba, D.: Parameterizing bubble-mediated air-sea gas exchange and its effect on ocean ventilation. Global Biogeochem. Cycles, 27, 894–905, https://doi.org/10.1002/gbc.20080, 2013.

Lopez-Jurado, J.-L., C. Gonzalez-Pola, and P. Velez-Belchi: Observation of an abrupt disruption of the long-term warming trend at the Balearic Sea, western Mediterranean Sea, in summer 2005, Geophys. Res. Lett., 32, L24606, https://doi.org/10.1029/2005GL024430, 2005.

Ludwig, W., Bouwman, A. F., Dumont, E., Lespinas, F.: Water and nutrient fluxes from major Mediterranean and Black Sea rivers: Past and future trends and their implications for the basin-scale budgets. Global Biogeochem. Cycles, 24, GB0A13. https://doi.org/10.1029/2009GB003594, 2010.

Manca, M., Burca, M., Giorgetti, A., Coatanoan, C., Garcia, M. J., Iona, A.: Physical and biochemical averaged vertical profiles in the Mediterranean regions: An important tool to trace the climatology of water masses and to validate incoming data from operational oceanography. J. Mar. Syst., 48(1–4), 83–116, 2004.

Marsaleix P., F. Auclair, J. W. Floor, M. J. Herrmann, C. Estournel, I. Pairaud, and C. Ulses, Energy conservation issues in sigma-coordinate free-surface ocean models, Ocean Modell., 20, 61–89, 2008.

Mavropoulou, A.-M., Vervatis, V., and Sofianos, S.: Dissolved oxygen variability in the Mediterranean Sea, J. Mar. Syst., 208, https://doi.org/10.1016/j.jmarsys.2020.103348, 2020.

Maze, G., Mercier, H., Thierry, V., Memery, L., Morin, P., and Perez, F. F.: Mass, nutrient and oxygen budgets for the northeastern Atlantic Ocean, Biogeosciences, 9, 4099–4113, https://doi.org/10.5194/bg-9-4099-2012, 2012.

MEDOC-Group: Observations of formation of deep-water in the Mediterranean Sea, Nature, 227, 1037–1040, 1970.

Merlivat, L., Boutin, J., Antoine, D., Beaumont, L., Golbol, M., and Vellucci, V.: Increase of dissolved inorganic carbon and decrease in pH in near-surface waters in the Mediterranean Sea during the past two decades, Biogeosciences, 15, 5653–5662, https://doi.org/10.5194/bg-15-5653-2018, 2018.

Mertens, C. and Schott F.: Interannual variability of deep-water formation in the northwestern Mediterranean, J. Phys. Oceanogr., 28, 1410–1424, https://doi.org/10.1175/1520-0485(1998)028<1410:IVODWF>2.0.CO;2, 1998.

Minas, H.J. and Bonin, M.-C. : Oxygénation physique et biologique de la Méditerranée nord-occidentale en hiver et au printemps. Oceanol. Acta (Special Issue No. 9), 123–132, 1988.

Moutin, T., Raimbault, P., Golterman, H. L., and Coste, B.: The input of nutrients by the Rhône River into the Mediterranean Sea: Recent observations and comparison with earlier data. Hydrobiologia, 373, 237, https://doi.org/10.1023/A:1017020818701, 1998.

Naqvi, S. W. A., Bange, H. W., Farías, L., Monteiro, P. M. S., Scranton, M. I., and Zhang, J.: Marine hypoxia/anoxia as a source of CH4 and N2O, Biogeosciences, 7, 2159–2190, https://doi.org/10.5194/bg-7-2159-2010, 2010.

Nightingale PD, Malin G, Law CS, Watson AJ, Liss PS, et al.: In situ evaluation of air-sea gas exchange parameterizations using novel conservative and volatile tracers, Glob. Biogeochem. Cycles, 14, 373–387, https://doi.org/10.1029/1999GB900091, 2000.

Palevsky, H. I., Quay, P. D., Lockwood, D. E., and Nicholson, D. P.: The annual cycle of gross primary production, net community production, and export efficiency across the North Pacific Ocean, Global Biogeochem. Cycles, 30, 361–380, https://doi.org/10.1002/2015GB005318, 2016.

Pastor, L., Cathalot, C., Deflandre, B., Viollier, E., Soetaert, K., Meysman, F. J. R., Ulses, C., Metzger, E., and Rabouille, C.: Modeling biogeochemical processes in sediments from the Rhône River prodelta area (NW Mediterranean Sea), Biogeosciences, 8, 1351–1366, https://doi.org/10.5194/bg-8-1351-2011, 2011.

Piñeiro, S., González Pola, C., Fernández Díaz, J. M., and Balbin, R.: Thermohaline evolution of the Western Mediterranean deep waters since 2005: Diffusive stages and interannual renewal injections. J. Geophys. Res. Oceans, 124, 8747–8766, https://doi.org/10.1029/2019JC015094, 2019.

Pinot, J.M. and Ganachaud, A.: The role of winter intermediate waters in the spring-summer circulation of the Balearic Sea: 1. Hydrography and inverse box modeling, J. Geophys. Res., 104(C12), 29843–29864, https://doi.org/10.1029/1999JC900202, 1999.

Plattner, G.-K. and Joos, E., Stocker, T. E.: Revision of the global carbon budget due to changing air-sea oxygen fluxes, Global Biogeochem. Cycles, 16, 1096, https://doi.org/10.1029/2001GB001746, 2002.

Rhein, M.: Deep water formation in the western Mediterranean, J. Geophys. Res., 100(C4), 6943, https://doi.org/10.1029/94JC03198, 1995.

Santinelli, C., Nannicini, L., Seritti, A.: DOC dynamics in the meso and bathypelagic layers of the Mediterranean Sea, Deep Sea Res. Part II, 57, 1446–1459, 2010.

Schmidtko, S., Stramma, L., and Visbeck, M.: Decline in global oceanic oxygen content during the past five decades. Nature 542, 335–339, https://doi.org/10.1038/nature21399, 2017.

Schneider, A., Tanhua, T., Roether, W., and Steinfeldt, R.: Changes in ventilation of the Mediterranean Sea during the past 25 year, Ocean Sci., 10, 1–16, https://doi.org/10.5194/os-10-1-2014, 2014.

Scholz, F., McManus, J., Mix, A. C. , Hensen, C., Schneider, R. R.: The impact of ocean deoxygenation on iron release from continental margin sediments. Nat. Geosci. 7, 433–437, https://doi.org/10.1038/ngeo2162, 2014.

Schott F, Visbeck, M., Send, U., Fischer, J., Stramma, L., and Desaubies, Y.: Observations of deep convection in the Gulf of Lion, Northern Mediterranean, during the winter of 1991/1992, J. Phys. Oceanogr., 26, 505–524, https://doi.org/10.1175/1520-0485(1996)026<0505:OODCIT>2.0.CO;2, 1996.

Schroeder, K., Gasparini, G. P., Tangherlini, M., and Astraldi, M.: Deep and intermediate water in the western Mediterranean under the influence of the Eastern Mediterranean Transient, Geophys. Res. Lett., 33, L21607, https://doi.org/10.1029/2006GL027121, 2006.

Schroeder, K., Ribotti, A., Borghini, M., Sorgente, R., Perilli, A., Gasparini, G. P.: An extensive Mediterranean deep water renewal between 2004 and 2006. Geophys. Res. Lett., 35, L18605, https://doi.org/10.1029/2008GL035146, 2008a.

Schroeder, K., Taillandier, V., Vetrano, A., and Gasparini, G.P.: The circulation of the western Mediterranean Sea in spring 2005 as inferred from observations and from model outputs, Deep Sea Res. Part I Oceanogr. Res. Pap., 55, 8 947–965, ISSN 0967-0637, https://doi.org/10.1016/j.dsr.2008.04.003, 2008b.

Sempéré, R., Charrière, B., Van Wambeke, F., Cauwet, G.: Carbon inputs of the Rhône River to the Mediterranean Sea: Biogeochemical Implications. Global Biogeochem. Cycles, 14, 669–681, https://doi.org/10.1029/1999GB900069, 2000.

Severin, T., Conan, P., Durrieu de Madron, X., Houpert, L., Oliver, M. J., Oriola, L., et al., Impact of open-ocean convection on nutrients, phytoplankton biomass and activity. Deep Sea Res. Part I Oceanogr. Res. Pap., 94, 62–71. https://doi.org/10.1016/j.dsr.2014.07.015, 2014.

Soetaert, K., Herman, P. M. J., Middelburg, J. J., Heip, C., Smith, C. L., Tett, P., and Wild-Allen, K.: Numerical modelling of the shelf break ecosystem: Reproducing benthic and pelagic measurements, Deep Sea Res. Part II Top. Stud. Oceanogr., 48, 3141–3177, 2001.

Somot, S., Houpert, L., Sevault, F., Testor, P., Bosse, A., Taupier-Letage, I., Bouin, M.-N., Waldman, R., Cassou, C., Sanchez-Gomez, E., Durrieu de Madron, X., Adloff, F., Nabat, P., and Herrmann, M.: Characterizing, modelling and understanding the climate variability of the deep water formation in the North-Western Mediterranean Sea, Clim. Dyn., 51, 1179–1210, https://doi.org/10.1007/s00382-016-3295-0, 2016.

Soto-Navarro, J., Jordá, G., Amores, A., Cabos, W., Somot, S., Sevault, F., Macías, D., Djurdjevic, V., Sannino, G., Li, L., and Sein, D.: Evolution of Mediterranean Sea water properties under climate change scenarios in the Med-CORDEX ensemble, Clim. Dyn., 54, 2135–2165, https://doi.org/10.1007/s00382-019-05105-4, 2020.

Stanley, R. H. R., Jenkins, W. J., Lott, D. E., and Doney, S. C.: Noble gas constraints on air-sea gas exchange and bubble fluxes, J. Geophys. Res., 114, C11020, https://doi.org/10.1029/2009JC005396, 2009.

Stöven, T. and Tanhua, T.: Ventilation of the Mediterranean Sea constrained by multiple transient tracer measurements, Ocean Sci., 10, 439–457, https://doi.org/10.5194/os-10-439-2014, 2014.

Stramma, L., Schmidtko, S., Levin, L. A., Johnson, G. C.: Ocean oxygen minima expansions and their biological impacts. Deep-Sea Res. Part I, 57, 587–595, https://doi.org/10.1016/j.dsr.2010.01.005, 2010.

Tanhua, T., Hainbucher, D., Schroeder, K., Cardin, V., Álvarez, M., and Civitarese, G.: The Mediterranean Sea system: a review and an introduction to the special issue, Ocean Sci., 9, 789–803, https://doi.org/10.5194/os-9-789-2013, 2013.

Testor, P.: DEWEX-MERMEX 2013 LEG1 cruise, RV Le Suroît, SISMER, Brest, France, https://doi.org/10.17600/13020010, 2013.

Testor, P., Bosse, A., Houpert, L., Margirier, F., Mortier, L., Legoff, H., Dausse, D., Labaste, M., Karstensen, J., Hayes, D., Olita, A., Ribotti, A., Schroeder, K., Chiggiato, J., Onken, R., Heslop, E., Mourre, B., D'ortenzio, F., Mayot, N., Lavigne, H., de Fommervault O., Coppola, L., Prieur, L., Taillandier, V., Durrieu de Madron, X., Bourrin , F., Many, G., Damien, P., Estournel, C., Marsaleix, P., Taupier-Letage, I., Raimbault, P., Waldman, R., Bouin, M.N., Giordani, H., Caniaux, G., Somot, S., Ducrocq, V., and P. Conan: Multiscale observations of deep convection in the northwestern Mediterranean Sea during winter 2012–2013 using multiple platforms. J. Geophys. Res. Oceans, 123, https://doi.org/10.1002/2016JC012671, 2018.

Testor, P., Coppola, L., and Mortier, L.: MOOSE-GE 2013 cruise, RV Téthys II, SISMER, Brest, France, https://doi.org/10.17600/13450110, 2013.

Touratier, F., Goyet, C., Houpert, L., de Madron, X.D., Lefèvre, D., Stabholz, M., and Guglielmi, V.: Role of deep convection on anthropogenic CO_2 sequestration in the Gulf of Lions (northwestern Mediterranean Sea), Deep Sea Res. Part I, 113, 33–48, https://doi.org/10.1016/j.dsr.2016.04.003, 2016.

Ulses, C., Auger, P.-A., Soetaert, K., Marsaleix, P., Diaz, F., Coppola, L., Herrmann, M., Kessouri, F., and Estournel, C.: Budget of organic carbon in the North-Western Mediterranean Open Sea over the period 2004–2008 using 3D coupled physical biogeochemical modeling. J. Geophys. Res. Oceans, 121, 7026–7055, https://doi.org/10.1002/2016JC011818, 2016.

Ulses, C., Estournel, C., Fourrier, M., Coppola, L., Kessouri, F., Lefèvre, D., and Marsaleix, P.: Modelling the dissolved oxygen dynamics in the north-western Mediterranean deep-convection region during the year 2012/13, [Data set], available on request from the corresponding author, last access: 13 October 2020.

Ulses, C., C. Estournel, J. Bonnin, X. Durrieu de Madron, and P. Marsaleix: Impact of storms and dense water cascading on shelf-slope exchanges in the Gulf of Lion (NW Mediterranean), J. Geophys. Res., 113, C02010, https://doi.org/10.1029/2006JC003795, 2008a.

Ulses, C., C. Estournel, P. Puig, X. Durrieu de Madron, and P. Marsaleix: Dense shelf water cascading in the northwestern Mediterranean during the cold winter 2005. Quantification of the export through the Gulf of Lion and the Catalan margin. Geophys. Res. Lett., 35, L07610, https://doi.org/10.1029/2008GL033257, 2008b.

Wanninkhof, R.: Relationship between wind speed and gas exchange over the ocean. J. Geophys. Res., 97, 7373–7382, https://doi.org/10.1029/92JC00188, 1992.

Wanninkhof, R.: Relationship between wind speed and gas exchange over the ocean revisited, Limnol. Oceanogr. Methods, 12, https://doi.org/10.4319/lom.2014.12.351, 2014.

Wanninkhof, R., Asher, W. E., Ho, D. T., Sweeney, C., and McGillis, W. R.: Advances in quantifying air-sea gas exchange and environmental forcing, Annu. Rev. Mar. Sci., 1, 213–244, https://doi.org/10.1146/annurev.marine.010908.163742, 2009.

Wanninkhof, R. and McGillis, W. R.: A cubic relationship between gas transfer and wind speed. Geophys. Res. Lett., 26, 1889–1893, 1999.

Wolf, M. K., Hamme, R. C., Gilbert, D., Yashayaev, I., Thierry, V.: Oxygen saturation surrounding Deep Water formation events in the Labrador Sea from Argo-O_2 data, Global Biogeochem. Cycles, 32, 635–653, https://doi.org/10.1002/2017GB005829, 2018.

Woolf, D. K.: Bubbles and their role in gas exchange, in The Sea Surface and Global Change, edited by P. S. Liss and R. A. Duce, 173–206, Cambridge Univ. Press, Cambridge, U.K., https://doi.org/10.1017/CBO9780511525025.007, 1997.

Yang, B., Emerson, S. R., Bushinsky, S. M.: Annual net community production in the subtropical Pacific Ocean from in situ oxygen measurements on profiling floats, Global Biogeochem. Cycles, 31, 728–744, https://doi.org/10.1002/2016GB005545, 2017.

Zunino, P., Schroeder, K., Vargas-Yáñez, M., Gasparini, G.P., Coppola, L., García-Martínez, M.C., Moya-Ruiz, F.: Effects of the Western Mediterranean Transition on the resident water masses: Pure warming, pure freshening and pure heaving, J. Mar. Syst., 96, 15–23, https://doi.org/10.1016/j.jmarsys.2012.01.011, 2012.

Annexe 3 : Article : Seasonal and Interannual Variability of the CO_2 System in the Eastern Mediterranean Sea : A Case Study in the North Western Levantine Basin

Wimart-Rousseau, C., Wagener, T., Álvarez, M., Moutin, T., **Fourrier, M.**, Coppola, L., Niclas-Chirurgien, L., Raimbault, P., D'Ortenzio, F., Durrieu de Madron, X., Taillandier, V., Dumas, F., Conan, P., Pujo-Pay, M., and Lefèvre, D.
Frontiers in Marine Science (2021)

frontiers in Marine Science

ORIGINAL RESEARCH
published: 17 May 2021
doi: 10.3389/fmars.2021.649246

Seasonal and Interannual Variability of the CO_2 System in the Eastern Mediterranean Sea: A Case Study in the North Western Levantine Basin

Cathy Wimart-Rousseau[1], Thibaut Wagener[1], Marta Álvarez[2], Thierry Moutin[1], Marine Fourrier[3], Laurent Coppola[3,4], Laure Niclas-Chirurgien[1], Patrick Raimbault[1], Fabrizio D'Ortenzio[3], Xavier Durrieu de Madron[5], Vincent Taillandier[3], Franck Dumas[6], Pascal Conan[7], Mireille Pujo-Pay[7] and Dominique Lefèvre[1]*

[1] Aix Marseille Université, Université de Toulon, CNRS, IRD, MIO, UM 110, Marseille, France, [2] Instituto Español de Oceanografia, A Coruña, Spain, [3] Sorbonne Université, CNRS, Laboratoire d'Océanographie de Villefranche, Villefranche-sur-Mer, France, [4] Sorbonne Université, CNRS, Institut de la Mer de Villefranche, Villefranche-sur-Mer, France, [5] CEFREM, CNRS-Université de Perpignan Via Domitia, Perpignan, France, [6] Service Hydrographique et Océanographique de la Marine—Shom, Brest, France, [7] Sorbonne Université, CNRS, Laboratoire d'Océanographie Microbienne, Observatoire Océanologique, Banyuls-sur-Mer, France

OPEN ACCESS

Edited by:
Gotzon Basterretxea, Mediterranean Institute for Advanced Studies (IMEDEA), Spain

Reviewed by:
Siv Kari Lauvset, Norwegian Research Institute (NORCE), Norway
Anne Willem Omta, Massachusetts Institute of Technology, United States

***Correspondence:**
Cathy Wimart-Rousseau
cathy.wimart-rousseau@mio.osupytheas.fr

Specialty section:
This article was submitted to Marine Biogeochemistry, a section of the journal Frontiers in Marine Science

Received: *04 January 2021*
Accepted: *09 April 2021*
Published: *17 May 2021*

Citation:
Wimart-Rousseau C, Wagener T, Álvarez M, Moutin T, Fourrier M, Coppola L, Niclas-Chirurgien L, Raimbault P, D'Ortenzio F, Durrieu de Madron X, Taillandier V, Dumas F, Conan P, Pujo-Pay M and Lefèvre D (2021) Seasonal and Interannual Variability of the CO_2 System in the Eastern Mediterranean Sea: A Case Study in the North Western Levantine Basin. Front. Mar. Sci. 8:649246. doi: 10.3389/fmars.2021.649246

The seasonal variability of the carbonate system in the eastern Mediterranean Sea (EMed) was investigated based on discrete total alkalinity (A_T), total dissolved inorganic carbon (C_T), and pH measurements collected during three cruises around Crete between June 2018 and March 2019. This study presents a detailed description of this new carbonate chemistry dataset in the eastern Mediterranean Sea. We show that the North Western Levantine Basin (NWLB) is unique in terms of range of A_T variation vs. C_T variation in the upper water column over an annual cycle. The reasons for this singularity of the NWLB can be explained by the interplay between strong evaporation and the concomitant consumption of C_T by autotrophic processes. The high range of A_T variations, combined to temperature changes, has a strong impact on the variability of the seawater pCO_2 (pCO_2^{SW}). Based on Argo float data, an entire annual cycle for pCO_2^{SW} in the NWLB has been reconstructed in order to estimate the temporal sequence of the potential "source" and "sink" of atmospheric CO_2. By combining this dataset with previous observations in the NWLB, this study shows a significant ocean acidification and a decrease in the oceanic surface pH_T^{25} of -0.0024 ± 0.0004 pH_T^{25} units.a^{-1}. The changes in the carbonate system are driven by the increase of atmospheric CO_2 but also by unexplained temporal changes in the surface A_T content. If we consider that the EMed will, in the future, encounter longer, more intense and warmer summer seasons, this study proposes some perspectives on the carbonate system functioning of the "future" EMed.

Keywords: carbonate system, Mediterranean Sea, acidification, CO_2 fluxes, Levantine Sea, inorganic carbon

INTRODUCTION

Since the beginning of the industrial era, the rise in atmospheric CO_2 due to anthropogenic activities is considered to be the main factor responsible for current climate change (IPCC, 2018). The ocean plays a significant role in modulating atmospheric CO_2 as it has sequestrated *ca.* 31% of the global anthropogenic CO_2 emissions in the past few decade (Gruber et al., 2019). Between 2009 and 2018, the ocean CO_2 sink was estimated to be equal to 2.5 $\pm$ 0.6 $PgC.a^{-1}$ (Friedlingstein et al., 2019). Ocean CO_2 uptake induces an increase in hydronium ion concentration (*i.e.,* a decrease in oceanic pH) commonly referred as ocean acidification (Doney et al., 2009). This ocean acidification represents a significant threat to marine organisms (Kroeker et al., 2013) and is likely to affect marine ecosystems (Feely et al., 2004).

The marginal Mediterranean Sea (MedSea) is a singular oceanic basin in terms of carbonate chemistry and deserves specific study. Due to the relatively short residence time of its water masses, this semi-enclosed, basin is considered to be more reactive to external forcing than other oceanic areas (Durrieu de Madron et al., 2011). The warm and highly alkaline waters absorb CO_2 from the atmosphere and transport it to the interior by active overturning circulation (Schneider et al., 2010; Álvarez et al., 2014). Indeed, while representing only 0.3% of the global oceanic volume, the anthropogenic carbon content of the MedSea was estimated to represent 1.1% of the world's ocean content in 1994 (Schneider et al., 2010; Lee et al., 2011). Moreover, several studies have reported a marked decline in the pH of the MedSea over the last few decades (*e.g.,* Touratier and Goyet, 2011; Hassoun et al., 2015b; Palmiéri et al., 2015; Flecha et al., 2019).

Detailed descriptions of the circulation and water masses of the MedSea can be found in Millot and Taupier-Letage (2005), Bergamasco and Malanotte-Rizzoli (2010), and Durrieu de Madron et al. (2011). The water masses of the Eastern Mediterranean Sea (EMed) are warmer, more haline, more oxygenated and more alkaline than those in the Western Mediterranean Sea (WMed) (Álvarez et al., 2014). The EMed water column can be schematically divided into three layers: (1) The surface layer, filled with Modified Atlantic Waters (MAW) with specific regional and seasonal characteristics [*e.g.,* Levantine Surface Waters (LSW)]; (2) Intermediate waters characterised, in the presence of MAW, by a local salinity maximum and generally described by the generic name Levantine Intermediate Waters (LIW); (3) The Eastern Mediterranean Deep Waters (EMDW), mostly retained in the EMed, consisting of a mixture of Adriatic Deep Waters (AdDW) and Aegean Deep Waters (AeDW). EMDW have undergone drastic changes over the last few decades (known as the Eastern Mediterranean Transient; Roether et al., 1996).

The MedSea is already exhibiting a consistent ocean acidification trend as a direct consequence to oceanic CO_2 uptake. It is therefore important to observe carbonate chemistry over sustained time-series to understand the long-term changes in ocean chemistry. The seasonal dynamics of the carbonate system, crucial in understanding the variability in the air-sea CO_2 exchanges, also requires these important time-series observations. When compared to other oceanic areas, including the WMed, the oligotrophic EMed (Pujo-Pay et al., 2011) is characterised by low primary production rates (Moutin and Raimbault, 2002). This low productivity reduces the vertical gradients of dissolved inorganic carbon, making the detection and understanding of decadal and seasonal changes in the carbonate system particularly challenging in this area. Over the last few decades, a considerable amount of work has been devoted to the EMed (*e.g.,* Schneider et al., 2010; Álvarez et al., 2014; Hassoun et al., 2015b; Hainbucher et al., 2019), however, these cruises do not cover a full seasonal cycle leading to biased observations. Most of the time-series measurements recorded in the MedSea have been taken in the coastal (*e.g.,* De Carlo et al., 2013; Ingrosso et al., 2016; Kapsenberg et al., 2017) and oceanic WMed (Lefèvre, 2010; Coppola et al., 2018). In the EMed, time-series measurements are scarce and mostly based in the Cretan Sea (Petihakis et al., 2018) or coastal sites such as the Lebanese coast (Hassoun et al., 2019) or the Israeli coast (Sisma-Ventura et al., 2017), precluding a rigorous description of the temporal variability of the carbonate system in the open-ocean EMed. In the MedSea open-ocean, studies based on data derived from satellite observations have been conducted to decipher, over a seasonal and interannual scale, the variations in pCO_2 (D'Ortenzio et al., 2008; Taillandier et al., 2012). Nonetheless, understanding the variability in the seasonal carbonate system in the EMed is required to evaluate the effects of the increasing threats in this area, such as warming (Nykjaer, 2009) and ocean acidification.

In the frame of the PERLE project (the Pelagic Ecosystem Response to deep water formation in the Levant Experiment), an intense *in situ* survey of the Levantine area was carried out during 2018–2019 (D'Ortenzio et al., 2020). This study reports on a new oceanic inorganic carbon dataset acquired over three different periods of the year in the South Cretan area (described as the North Western Levantine Basin or NWLB hereafter) (**Figure 1**).

This study gives a detailed description of this new dataset and the oceanographical context (section "Descriptive Carbonate Chemistry in the Context of the PERLE Cruises"). In section "Atypical Drivers of the Seasonal Dynamics of the Carbonate Chemistry Within the Mixed Layer of the North Western Levantine Basin," using these new annual observations in the NWLB, the physical and biological drivers explaining the seasonal variability of the carbonate parameters in the upper water column will be investigated and the impact of the variations on air-sea CO_2 fluxes will be discussed. In section "Long Term Temporal Changes in Carbonate Chemistry in the North Western Levantine Basin," the main drivers of carbonate chemistry changes will be considered on longer timescales, based on the estimated trends in the surface carbonate chemistry of the NWLB derived from existing data over the last 20 years. Some hypotheses on the future of the carbonate system functioning of the EMed will be discussed.

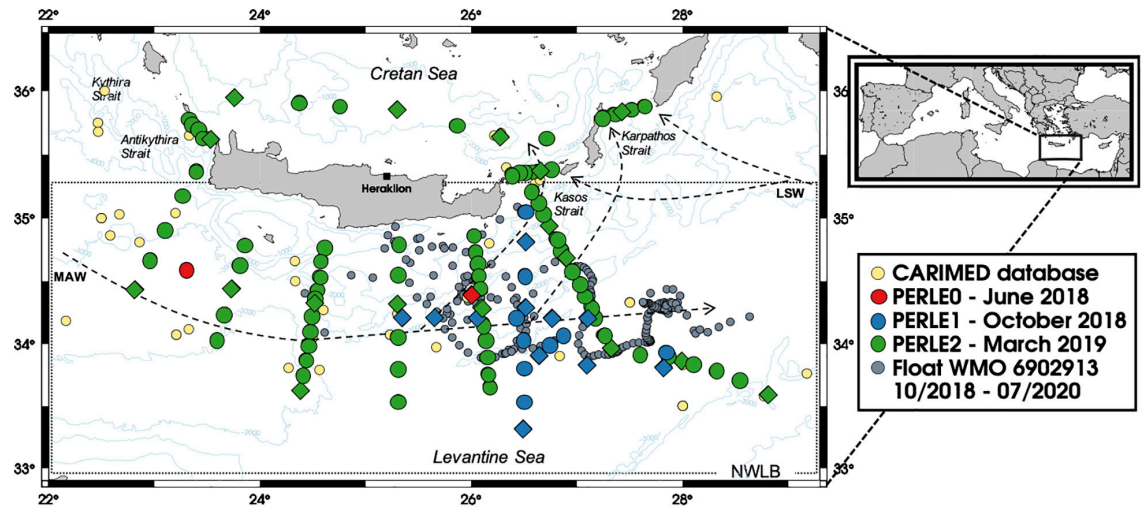

FIGURE 1 | Map of the "PERLE area." Stations visited during PERLE0 are in red, during PERLE1 in blue and during PERLE2 in green. Diamonds represent stations with carbonate chemistry. Stations from the CARIMED database with A_T and C_T measurements are shown by small yellow dots. Grey dots show the WMO 6902913 Argo profiler positions from October 2018 to July 2020. Arrows show the main surface water mass pathways (see acronyms in the text). The North Western Levantine Basin area (NWLB) is defined by the dotted insert.

MATERIALS AND METHODS

Cruise and Sampling Strategy

This study focuses on three PERLE cruises: PERLE0, PERLE1, and PERLE2 (**Figure 1**). These cruises were carried out in the EMed between 2018 and 2019. At all stations, a CTD-Rosette was deployed (1) to acquire data with sensors (Conductivity Temperature and Depth–CTD and associated parameters) along vertical profiles and (2) to collect discrete seawater samples from Niskin bottles for chemical analysis. Over the 11, 31, and 125 casts performed during the PERLE0, PERLE1, and PERLE2 cruises, seawater was sampled from 1, 12, and 17 casts, respectively, for carbonate parameter analysis (see **Supplementary Table 1** and **Supplementary Figure 1**). Details for the cruises and parameters measured during each PERLE cruise are summarised in **Table 1**.

Parameters Measured

CTD and Seawater Sampling

A SeaBird^{TM} 911+ underwater unit was used to interface a pressure sensor, an external temperature probe (SBE3plus) and an external conductivity cell (SBE4C). Sensors were calibrated by the manufacturer. Additional sensors were interfaced and data from a fluorescence (Chelsea Aqua 3) and an oxygen (SBE43) sensor are used in this study. Fluorescence and oxygen are expressed in A.U. (Arbitrary Unit) and $\mu mol.kg^{-1}$, respectively, in this study. For vertical profiles, 24 Hz data on the downcast were averaged on 1 dbar bins by the SeaBird^{TM} dedicated software. Water samples were collected from CTD-Rosette casts with a carousel equipped with 22 Niskin bottles (12 L). Water was sampled from 10 to 21 depths, from a few meters above the seafloor up to the surface (0–5 dbars). From 0 to 200 dbars, a higher sampling resolution was applied (every *ca.* 20 dbars) than below 200 dbars (every *ca.* 200 dbars).

In addition, the "Real-time" CTD data from the WMO 6902913 Argo float (Argo, 2000) deployed during the PERLE1 cruise were used in this study to complete the hydrological data. Data collected from October 2018 to July 2020 were used (**Figure 1**). Because the Argo float considered in this study is still operational, no "Delayed Mode" data were available at this stage. The Argo real-time quality control procedures have been applied by the Coriolis data centre (Wong et al., 2020). A visual comparison of the Argo CTD data with collocated PERLE cruise CTD data was carried out on two profiles to exclude major deviations in the Argo data. Salinity measurements (derived from conductivity—SBE41CP sensor, Seabird^{TM}) were recorded with an accuracy of 0.005 psu.

Total Alkalinity and Total Dissolved Inorganic Carbon

Samples for total dissolved inorganic carbon (C_T) and total alkalinity (A_T) were collected into acid-washed 500 cm^3 borosilicate glass bottles, poisoned with 200 mm^3 of a 36 $g.dm^{-3}$ $HgCl_2$, as recommended by Dickson et al. (2007) and stored in the dark at 4°C. Analyses were performed after 5 months of storage. Measurements of C_T and A_T were performed simultaneously by potentiometric acid titration using a closed cell following the methods described by Edmond (1970) and Dickson and Goyet (1994). Analyses were performed at the National Facility for Analysis of Carbonate System Parameters (SNAPO-CO2, LOCEAN, Sorbonne University—CNRS, France) with a prototype developed at LOCEAN. The average accuracy of A_T and C_T analysis (estimated from repeated measurements of Certified Reference Material provided by Prof. Dickson's laboratory from the Scripps Institution of Oceanography, San

TABLE 1 | Summary of the cruise information and the parameters measured during each PERLE cruises including availability, number of samples (n) and their associated accuracy.

		PERLE0	PERLE1	PERLE2
Cruise information	Date	8th–24th June 2018	10th–21st October 2018	27th February–16th March 2019
	Research Vessel	*Téthys II*	*L'Atalante*	*Pourquoi Pas?*
	DOI	10.17600/18000550	No DOI available	10.17600/18000865
Carbonate parameters	A_T/C_T	Parameter sampled *[n = 12]* QC test ok *[±1.8/2.1 μmol.kg^{-1}]*	Parameter sampled *[n = 164]* QC test not ok–Derived** *[±19/19 μmol.kg^{-1}]*	Parameter sampled *[n = 341]* QC test ok *[±4.6/4.7 μmol.kg^{-1}]*
	pH	Parameter not sampled Derived* *[±0.012]*	Parameter sampled *[n = 156]* QC test ok *[±0.007]*	Parameter sampled *[n = 361]* QC test ok *[±0.003]*
Ancillary data	Oxygen	Parameter sampled QC test ok	Parameter sampled QC test ok	Parameter sampled QC test ok
	Nutrients	Parameter sampled QC test ok	Parameter sampled QC test ok	Parameter sampled QC test ok

** pH_T^{25} values were calculated with the A_T/C_T couple.*
*** A_T values deduced from the A_T-S relationship proposed by Hassoun et al. (2015a,see section 3.2.2). C_T values were calculated with the A_T/pH_T^{25} couple.*
*Stations where carbonate parameters were studied are represented by diamonds on **Figure 1**. Nutrients were used at these stations to calculate the derived carbonate parameters. Errors for the derived carbonate parameters have been computed by propagating the standard uncertainties of the thermodynamic constants and associated errors of the environmental variables (Orr et al., 2018).*

Diego) was 1.8 and 2.1 μmol.kg^{-1}, respectively, for PERLE0 and 4.6 and 4.7 μmol.kg^{-1}, respectively, for PERLE2. Although A_T and C_T measurements were carried out during the PERLE1 cruise, the accuracy of the dataset did not conform to the quality control procedure (see section "Primary Quality Control of the Measured Data") therefore the measured PERLE1 A_T/C_T dataset was not used in this study. However, A_T values were reconstructed for PERLE1 based on a published A_T-S relationship (see section "Derived Parameters").

pH

The pH was measured directly on board. Samples for pH measurements were collected in cylindrical optical glass vials and analyses were performed manually using purified m-Cresol Purple (mCP) following the spectrophotometric protocol (at 25°C) described by Clayton and Byrne (1993) (see details in **Supplementary Material**). This method is based on the dissociation of the pH-sensitive mCP dye (provided by Prof. Byrne, University of Southern Florida) in the water sample. pH is reported on the total scale at 25°C (pH_T^{25}) using the equation by Liu et al. (2011). The reproducibility of measurements was estimated to be ± 0.0009 by measuring replicates from the same Niskin bottle. The accuracy was determined to range within ± 0.007 for PERLE1 and ± 0.003 for PERLE2 by analysing replicates of TRIS solution (provided by Prof. Dickson, Scripps Institution of Oceanography, San Diego). No direct pH measurements were carried out during the PERLE0 cruise. The effect of the addition of the indicator on the seawater pH was evaluated and corrected (see details in the **Supplementary Material**).

Oxygen

For all three PERLE cruises, dissolved oxygen concentrations ($[O_2]_{mes}$) were analysed on board following the Winkler method (Winkler, 1888; modified Carritt and Carpenter, 1966) using photometric endpoint detection (Williams and Jenkinson, 1982). The recommendations of Langdon (2010) were followed for sampling, reagent preparation and sample analysis. The thiosulfate solution was calibrated by titrating it against a potassium iodate certified standard solution of 0.0100 N (CSK standard solution—WAKO). The reproducibility of measurements, calculated by measuring replicates from the same Niskin bottle, was estimated to be ± 0.86 μmol.kg^{-1} (n = 42, PERLE2).

Oxygen measurements from the SBE43 sensor from the CTD rosette were systematically adjusted for all cruises with the "Winkler" values on the whole water column. Based on the raw data processing algorithm (Owens and Millard, 1985), 3 calibration coefficients were adjusted (the oxygen signal slope, the voltage at zero oxygen signal and the pressure correction factor) by minimising the sum of the square of the difference between the Winkler oxygen values and oxygen derived from the sensor signal. The accuracy of the SBE43 adjusted values is around ± 2 μmol.kg^{-1}.

Nutrients

Samples for dissolved inorganic nutrients were collected from Niskin bottles in 20 mL polyethylene bottles. Samples were analysed directly on board during PERLE2 and frozen before analysis on land for PERLE0 and PERLE1. Analyses were performed after less than a month of storage. All nutrient samples were analysed by a standard colorimetric method on a segmented flow analyser (Autoanalyser II Seal Bran& Luebbe®) following Aminot and Kerouel (2007). The relative precision of these analyses ranged from 5 to 10% (Aminot and Kerouel, 2007).

Primary Quality Control of the Measured Data

Systematic primary quality control of the measured data was performed on each PERLE dataset. No significant problems have been detected for Winkler oxygen and pH measurements. During PERLE1, for a few casts, a CTD pump dysfunction

significantly altered the quality of the CTD oxygen: oxygen measurements from these casts were disregarded. A systematic quality control procedure for A_T and C_T was conducted based on internal consistency tests between A_T, C_T and pH_T (see details in the **Supplementary Material**). Following these steps, only 15 PERLE2 casts were validated, leading to the loss of *ca.* 60% of the PERLE2 A_T/C_T dataset. All the A_T/C_T PERLE1 dataset was lost. A comparison of the quality controlled PERLE dataset with previously collected data does not reveal systematic biases for A_T, C_T, or $pH_T{}^{25}$ (**Figure 2A–C**).

Statistical Tests on the Linear Model

Relationships between years and carbonate parameters (A_T, C_T, and $pH_T{}^{25}$) and between A_T and salinity were computed using a linear regression model. Linear regression statistics, including the standard error of the slope (*i.e.,* the error of the estimated trend), the coefficient of determination (r^2) and the significance of the trend (*p*-value) were calculated using the R software. Linear relationships have been tested using the Pearson coefficient for parametric test (Sokal and Rohlf, 1969) with a significance level of 95%.

Parameters derived from the A_T-S linear relationship were tested against previously published A_T-S relationships in the area using a Student's *t*-test for the slope and intercept. The null hypothesis, H_0, was that our observations were not significantly different from these linear models.

Derived Parameters

Absolute salinity (S_A), conservative temperature (Θ) and potential density (σ_θ) were derived from practical salinity, temperature and pressure and the geographic position based on the TEOS-10 (The International Thermodynamic Equation of Seawater-2010). In this study, following the recommendations of the Intergovernmental Oceanographic Commission (Valladares et al., 2011), S_A and Θ were used to study the hydrological context ($\Theta - S_A$ diagrams). Calculations were made with the "oce" R package (Kelley et al., 2017). Note that practical salinity (labelled Salinity) and *in situ* temperature (labelled Temperature) were used in this study to facilitate comparisons with previous studies in particular, for A_T-S relationships.

Apparent Oxygen Utilisation (AOU–$\mu mol.kg^{-1}$) was calculated from the difference between oxygen solubility concentration (at P = 0 dbar) estimated with the "Benson and Krause coefficients" (Garcia and Gordon, 1992) and *in situ* $[O_2]_{mes}$.

A density threshold of 0.03 $kg.m^{-3}$ with a reference depth of 10 dbars was used to compute the Mixed Layer Depth (MLD) (D'Ortenzio et al., 2005).

Salinity data were used to reconstruct an A_T time-series using the sub-surface A_T-S relationship proposed by Hassoun et al. (2015a) (see discussion in section "Total Alkalinity and Salinity Relationships Within the Mixed Layer"). In this study, the PERLE1 and the Argo float A_T datasets were reconstructed following this A_T-S relationship. Considering the standard deviation of the A_T-S relationship proposed by Hassoun et al. (2015a), the accuracy of the calculated A_T values is ± 19 $\mu mol.kg^{-1}$.

Salinity-normalised changes in A_T ($NA_T{}^{39.3}$) and C_T ($NC_T{}^{39.3}$) were calculated dividing by *in situ* salinity and multiplying by 39.3 (*i.e.,* the mean PERLE salinity above 200 dbars).

Seawater carbonate system parameters were derived from A_T and C_T values. Calculations were made with the software program CO2SYS-MATLAB (van Heuven et al., 2011) using silicate and phosphate concentrations. When nutrient data was not available, silicate and phosphate mean concentrations for each depth were used. As recommended for the MedSea by Álvarez et al. (2014), the carbonic acid dissociation constants K_1 and K_2 from Mehrbach et al. (1973) as refitted by Dickson and Millero (1987) and the dissociation constant for HSO_4^- from Dickson (1990) were used. Uppström (1974) was used to calculate the ratio of total boron to salinity and Dickson and Riley (1979) to calculate the hydrogen fluoride constant K_F.

The buffer factors γA_T (γC_T), βA_T (βC_T) and ωA_T (ωC_T) provide an estimation of the seawater's ability to buffer changes in the aqueous CO_2 [CO_2], protons [H^+] and the carbonate saturation state (Ω) when A_T (C_T) changes at constant C_T (A_T) (Egleston et al., 2010). The calculations were performed following the formula proposed by Álvarez et al. (2014).

Quantification of Biological Processes

Net Ecosystem Production (NEP) is defined as the sum of biotic and abiotic carbon fluxes in the ecosystem (Borges et al., 2008). Net Ecosystem Calcification (NEC) is a measure of the balance between $CaCO_3$ formation (calcification) and dissolution (Smith and Kinsey, 1978). Based on the $NA_T{}^{39.3}$ and $NC_T{}^{39.3}$ plot, the reaction path can take on variable slopes depending on the ratio of different processes, such as photosynthesis/respiration, carbonate dissolution/formation and CO_2 release/invasion (Zeebe, 2012). Temporal changes in $NA_T{}^{39.3}$ ($\Delta NA_T{}^{39.3}$) and $NC_T{}^{39.3}$ ($\Delta NC_T{}^{39.3}$) between each PERLE cruise can be calculated according to NEP and NEC processes as:

$$\triangle NC_T^{39.3} = -0.15 * NEP + 0.9 * NEC \quad (1)$$

$$\triangle NA_T^{39.3} = 0.02 * NEP + 1.8 * NEC \quad (2)$$

Following equation (2), NEP can be expressed according to NEC as:

$$NEP = \frac{\Delta NA_T^{39.3} - 1.8 * NEC}{0.02} \quad (3)$$

Then, by replacing the NEP term in equation (1) by equation (3), NEC can be calculated as:

$$NEC = \frac{\Delta NC_T^{39.3} + \frac{(0.15 * \Delta NA_T^{39.3})}{0.02}}{14.4} \quad (4)$$

NEC and NEP are expressed in $\mu molC.kg^{-1}.d^{-1}$. Salinity-normalised A_T and C_T values "exclude" the "precipitation-evaporation" influence in the layer where biological activity is at a maximum. It is assumed that the layers considered (MLD-200 dbars) to estimate the NEP and NEC processes are not influenced by air-sea CO_2 fluxes, which were therefore not considered.

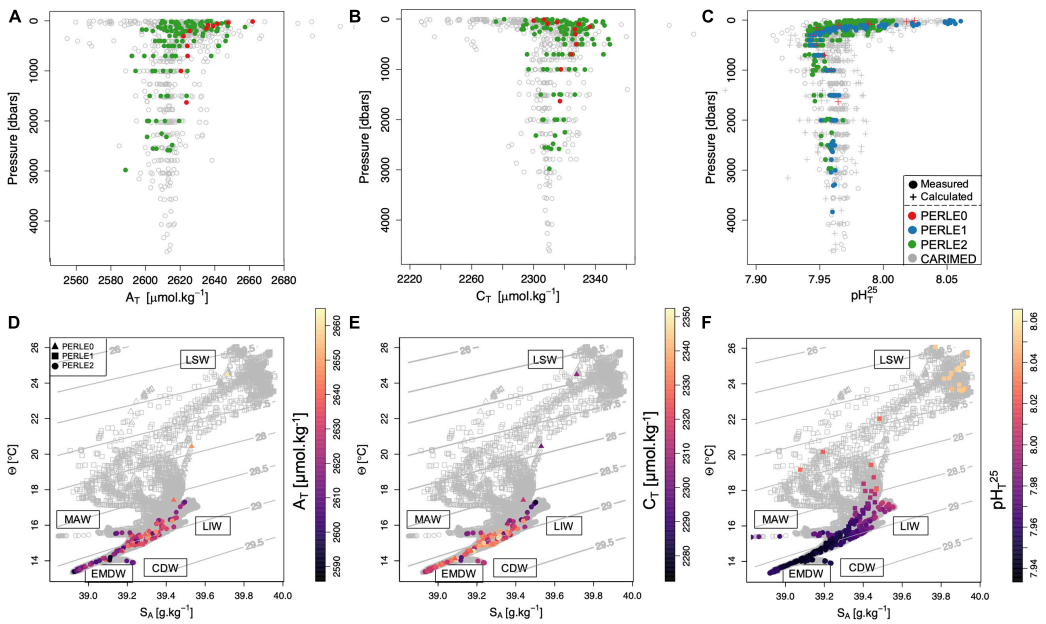

FIGURE 2 | Upper panel: Vertical profiles of total alkalinity (A_T–µmol.kg^{-1}; **A**), total dissolved inorganic carbon (C_θ–µmol.kg^{-1}; **B**) and pH (measured and calculated) in total scale at 25°C (pH_T^{25}; **C**) for the three PERLE cruises superimposed on the CARIMED data corresponding to the PERLE area (22°–29°E, 33°–36.5°N; grey dots). Lower panel: Θ–S_A diagrams for the three PERLE cruises with the name of the main water mass end members for the entire water column. Colored points correspond to A_T on **(D)**, to C_T on **(E)** and to pH_T^{25}on **(F)**. Isopycnal horizons based on potential density referenced to a pressure of 0 dbar (σ_θ) are represented by grey contour lines. On **(D–F)**, different dots have been used for each PERLE cruise. Because no A_T and C_T data were available for PERLE1 cruise, only pH_T^{25} data have been represented **(C,F)**.

CARIMED Database

CARIMED (CARbon, tracer and ancillary data In the MEDsea) aims to be an internally consistent database containing inorganic carbon data relevant for this basin (Álvarez et al., in preparation). Ancillary (hydrographic, inorganic nutrients and dissolved oxygen), CO_2 (pH, A_T, and C_T) and transient tracer (CFC-11 and 12, Tritium, SF_6, Neon, CCl_4, and ΔHe^3) data from several cruises in the MedSea from 1976 until 2018 were assembled. Primary and secondary quality control procedures following the GLODAP (Global Ocean Data Analysis Project) philosophy (Tanhua et al., 2010) are locally adapted to this marginal sea. This work only uses data collected in the Levantine basin (**Supplementary Table 2**).

DESCRIPTIVE CARBONATE CHEMISTRY IN THE CONTEXT OF THE PERLE CRUISES

Carbonate Chemistry Along the Water Column Below the Surface Layer

All vertical profiles for A_T, C_T and pH_T^{25} measured during the PERLE cruises are presented in **Figures 2A–C**, respectively. All the A_T profiles presented maximum values in the surface, minimum values between 500 and 700 dbars and remained almost constant (or slightly decreasing) below 1000 dbars. Most of the C_T vertical profiles presented the lowest values in surface waters, reaching maximum values between 500 and 700 dbars and then remaining relatively invariable below 1000 dbars. pH_T^{25} presented maximum values at the surface (with values around 8.060 measured during PERLE1 cruise), minimum values close to 700 dbars and nearly constant values under 1000 dbars (**Figure 2C**). The main water masses are identified in **Figures 2D–F** and detailed in **Supplementary Figure 1**.

Intermediate waters (mostly LIW) were located around the 29.0 kg.m^{-3} isopycnal layer (Lascaratos and Nittis, 1998; see **Supplementary Figure 1**) and were characterised by an A_T maximum evolving from 2,600 to 2,640 µmol.kg^{-1} (**Figures 2A,D**). As observed by Álvarez et al. (2014), the LIW was located above the layer of maximum organic matter mineralisation in the EMed and was associated with low C_T concentrations (*ca.* 2,290 µmol.kg^{-1}) and high pH_T^{25} values (*ca.* 8.000) in contrast to the deepest water masses. It can be observed that slightly colder, more haline and denser Cretan Intermediate Waters (Velaoras et al., 2019) were detected during PERLE2 in the western part of the Cretan Sea with the highest A_T value for PERLE2 cruise (*ca.* 2,660 µmol.kg^{-1}, **Figure 2A**).

In the deep-water layer (*i.e.,* EMDW), both AeDW and AdDW presented similar C_T values (**Figure 2E**) while slightly higher pH_T^{25} (**Figure 2F**) and A_T (**Figure 2D**) values were measured in the AeDW (see **Supplementary Figure 2**). On the Cretan

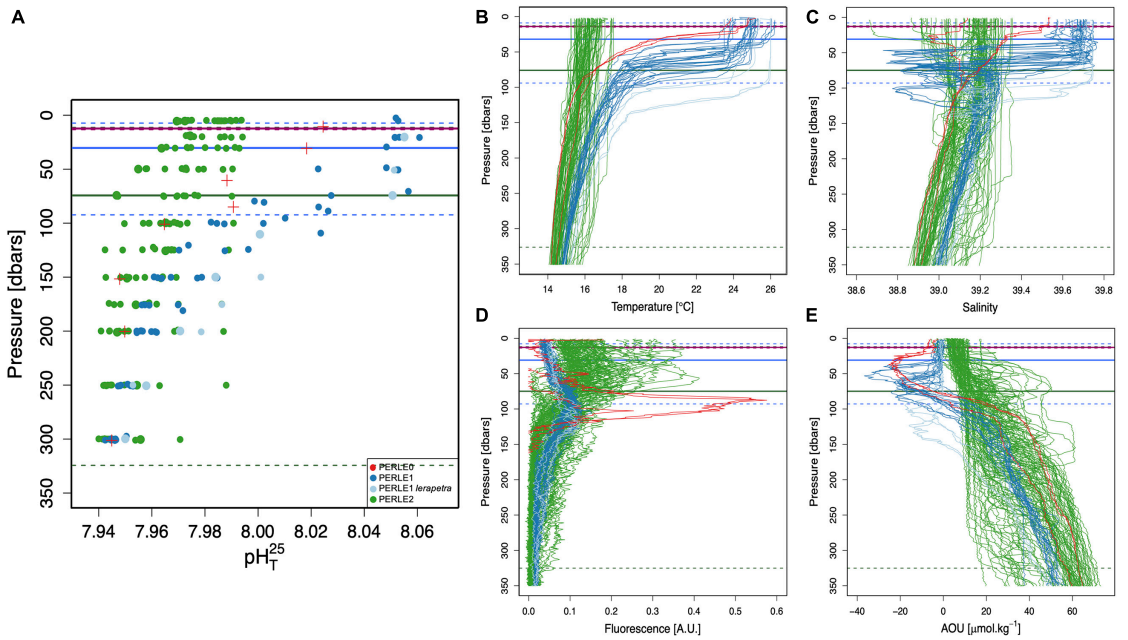

FIGURE 3 | Vertical profiles of pH in total scale at 25°C (pH_T^{25}, **A**), temperature (°C, **B**), salinity **(C)**, fluorescence (A.U., **D**) and AOU concentrations ($O_2^{sol} - O_2^{mes}$; µmol.kg^{-1}, **E**) above 350 dbars for all stations in the North Western Levantine Basin during the three PERLE cruises. Horizontal full lines represent the mean Mixed Layer Depth (MLD; dbars). Dotted lines represent the minimum and maximum MLD values, respectively. For PERLE1, a distinction is made between inside (light blue lines) and outside (dark blue lines) the lerapetra gyre.

shelf, deep waters were comprised of dense EMDW with high A_T (≈ 2,650 µmol.kg^{-1}) and C_T values (≈ 2,350 µmol.kg^{-1}). Deep waters of the Cretan Sea were filled with CDW with low pH_T^{25} (≈ 7.950) values resulting from relatively low A_T and high C_T content (**Figures 2D–F**).

This description of the carbonate chemistry in the deep and intermediate water masses in the PERLE area is in good agreement with previous studies (Schneider et al., 2010; Álvarez et al., 2014). However, the PERLE strategy based on an intense observation period over a year is not appropriate to describe changes in deep-water masses. For the rest of this study, in order to tackle the seasonal dynamics of the surface waters, only data in the NWLB (**Figure 1**) where all three PERLE cruises were conducted, will be discussed further.

Seasonal Variability in the Upper Water Column

The highest spatial and temporal variability in carbonate chemistry parameters was encountered in the upper water layer which has been defined to be approximately the first 200 dbars. Discrete pH_T^{25} values (measured and calculated), taken from the southern part of the PERLE sampling area (the NWLB) illustrate the seasonal variability of the carbonate chemistry in the upper layer (**Figure 3A**). The pH_T^{25} was the most measured carbonate parameter in this study and, when normalised to 25°C, can be considered as an indicator of the carbonate chemistry status by including the changes in A_T and C_T. An overview of the upper layer seasonal dynamics is also presented for temperature, salinity, fluorescence, and AOU profiles in **Figures 3B–E**, respectively.

The lowest pH_T^{25} values were encountered in March 2019 during the PERLE2 cruise and correspond to the relatively higher C_T values and lower A_T values. During this cruise, a significant range in the MLD was encountered with the deepest values observed. This cruise coincided with the abrupt stratification observed in the EMed after the deepening of the MLD from November to February-March (D'Ortenzio et al., 2005). Increased fluorescence values were observed in shallow waters at the end of the cruise (in the eastern part of the area) in comparison to the beginning of the cruise (in the western part).

Intermediate pH_T^{25} values were measured in June 2018 during the PERLE0 cruise corresponding to increased surface alkalinity and a moderate depletion in inorganic carbon. The PERLE0 cruise is an early summer cruise characterised by a shallow MLD. The highest fluorescence values were recorded during this cruise well below the MLD (*ca.* 90 dbars) and light oxygen supersaturation (AOU ≈ −20 µmol.kg^{-1}) just beneath the MLD.

Finally, high pH_T^{25} values (>8.000) were measured up to 100 dbars during the PERLE1 cruise, probably in association with a high A_T content due to evaporation. During this late summer cruise, the deepest Deep Chlorophyll Maximum (DCM)

with the lowest fluorescence values but also the deepest negative AOU concentrations were encountered. Moreover, during this cruise, the mesoscale Ierapetra Eddy (IE) was crossed (see **Supplementary Figure 3** and Ioannou et al., 2019). The core of this warm and salty eddy (**Figures 3B,C**) was characterised by a deepening of the MLD associated with a deep DCM and negative AOU values. Nonetheless, no clear IE signal was observed on the pH_T^{25} values (**Figure 3A**).

In the EMed, spring and autumn seasons need to be considered as short transition periods between the summer and winter, which come later than on the continent (Özsoy et al., 1989). Moreover, in the EMed, summer is characterised by maximum heat in the surface layer that can remain up until November, whereas winter is identified with minimal heat that can occur until April. Considering each cruise as representative of a period within the annual cycle, the PERLE0 cruise (June 2018) associated with intermediate pH_T^{25} values corresponds to the early summer period with decreasing biological activity associated with the strengthening of stratification. PERLE1 (October 2018) is associated with the highest pH_T^{25} values and corresponds to the end of the summer period characterised by a warm and stratified water column with deep and low fluorescence maximum. PERLE2 (March 2019), associated with the lowest pH_T^{25} values and shallow fluorescence maximum, corresponds to the end of the winter period, with the beginning of the seasonal stratification of the water column in the eastern part. These features agree with the analysis of the seasonal patterns of surface chlorophyll *a* concentration (Chl *a*) (based on remote sensing). The lowest values of surface Chl *a* were observed during the summer period, whereas an increase in surface Chl *a* was observed in winter, concomitantly to the deepening of MLD (Bosc et al., 2004; D'Ortenzio and Ribera d'Alcalà, 2009).

Total Alkalinity and Salinity Relationships Within the Mixed Layer

When no A_T values were available (see section "Primary Quality Control of the Measured Data"), A_T can be estimated based on an A_T-S relationship. In the MedSea, several linear relationships between A_T and salinity in the surface waters have been proposed for different sub-basins (*e.g.,* Schneider et al., 2007; Cossarini et al., 2015; Hassoun et al., 2015a; Gonzaìlez-Daìvila et al., 2016).

During the PERLE cruises, in the NWLB, AT was significantly (n = 14, p-value = 0.014, r^2 = 0.36) influenced by salinity variations within the mixed layer (**Figure 4**). **Figure 4** also displays the A_T-S distribution in the Cretan Sea (grey dots on **Figure 4**). The mixing of high alkalinity Black Sea waters (values of *ca.* 2,967 $\mu mol.kg^{-1}$; Hiscock and Millero, 2006) in the Cretan Sea shifts the A_T-S characteristics of surface waters in agreement with Schneider et al. (2007) who demonstrated that freshwater and Black Sea inputs affect the A_T-S relationship. More pronounced deviations from the expected linear A_T-S relationship are observed for stations with deeper mixed layers (**Figure 4**). This might be the result of the mixing of water masses with different A_T-S relationships during winter mixing. As A_T values were available only for PERLE0 and PERLE2 cruises, the A_T-S relationship derived for the PERLE cruises in the mixed layer (and in the NWLB) have been based on a very limited number of data. The PERLE A_T-S linear relationship was tested against the Hassoun A_T-S linear model (Hassoun et al., 2015a). No significant differences were found on either the slope (t-test = 1.86, n = 14, $p < 0.05$) or the intercept (t-test = 0.27, n = 14, $p < 0.05$). Therefore, the annual time-series were reconstructed based on the A_T-S linear relationship measured by Hassoun et al. (2015a) in the surface waters (0–25 m) of the eastern Mediterranean sub-basin, and A_T has been estimated based on this relationship.

ATYPICAL DRIVERS OF THE SEASONAL DYNAMICS OF THE CARBONATE CHEMISTRY WITHIN THE MIXED LAYER OF THE NORTH WESTERN LEVANTINE BASIN

Seasonal Variations in Total Alkalinity and Total Inorganic Carbon

During the PERLE cruises, the NWLB exhibited a greater range in A_T than C_T values within the mixed layer (see section "Total alkalinity control on the seasonal air-sea CO_2 exchanges"). A_T ranged between 2,610 and 2,693 $\mu mol.kg^{-1}$ whereas C_T ranged between 2,292 and 2,332 $\mu mol.kg^{-1}$. Over an annual scale, the ratio of the range in A_T variations to the range in C_T variations ($\Delta A_T/\Delta C_T$) can be used to infer the sensitivity to A_T and C_T changes in the upper ocean. Over the period studied, in the NWLB, the ratio $\Delta A_T/\Delta C_T$ is equal to 2.1. In the global ocean, long-term time-series $\Delta A_T/\Delta C_T$ ratios are lower than 1.0 (**Table 2**).

The reasons for these apparent and rather unique ranges of A_T and C_T over the year in the NWLB can be attributed to several factors: (1) The main drivers of the C_T gradient in the water column are, primary production transforming the C_T into organic carbon in the photic layer, and respiration transforming the organic carbon into C_T. As the EMed is an area of low productivity (Moutin and Raimbault, 2002), the vertical C_T gradient is lower than in other oceanic areas. Consequently, the C_T range in surface waters, driven by C_T consumption during the stratified period and replenishment via vertical mixing with sub-surface waters enriched in C_T, is greatly reduced. (2) The high levels of evaporation that affect the MAW in the EMed during the summer season increases salinity by nearly 1 $g.kg^{-1}$ (**Figure 2**) between the end of winter (PERLE2) and the end of summer (PERLE1). The A_T and C_T parameters should be equally affected by evaporation in a closed system. However, when reported on a A_T/C_T diagram (with normalised axes—see **Figure 5**), a higher range of A_T variation compared to C_T is observed. This indicates that when salinity increases in surface waters, a concomitant consumption of C_T must occur to compensate for the C_T increase due to evaporation to maintain an apparent stability in C_T concentrations. The biological consumption of C_T

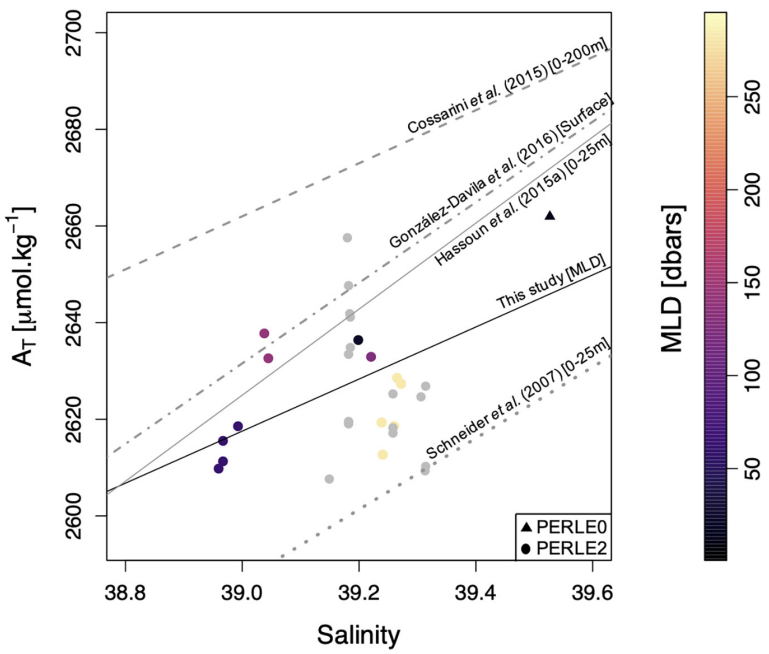

FIGURE 4 | A_T vs. Salinity during PERLE0 and PERLE2 cruises within the mixed layer for all stations situated in the North Western Levantine Basin. The colour scale corresponds to the mixed layer depth (MLD–dbars). The black line corresponds to the significant linear regression (in the NWLB). The different grey lines correspond to the linear regressions between A_T and salinity in the surface EMed reported by Schneider et al. (2007), Cossarini et al. (2015), Hassoun et al. (2015a), and Gonzaìlez-Daìvila et al. (2016). The grey dots correspond to data in the Cretan Sea (not used in the linear regression).

TABLE 2 | Ratios ($\Delta A_T/\Delta C_T$) of the range in A_T variations (maximum value minus minimum value) to the range in C_T variations (maximum value minus minimum value) in the upper ocean for the different time-series.

	NWLB	ANTARES Time-series	DYFAMED Time-series	BATS (Bermuda Atlantic Time-series Study)	HOT (Hawaii Ocean Time-series)	ESTOC (European station for Time-series in the ocean Canary islands)	Iceland sea
Localisation	EMed	WMed	WMed	North western Atlantic	North Pacific	North eastern Atlantic	Iceland sea
Depth	MLD	0–30 dbars	0–30 dbars	0–30 dbars	0–30 dbars	Surface	0–30 dbars
Period	2018–2019	2009–2019	1994–2018	1988–2019	1988–2018	1996–2004	2014–2019
$\Delta A_T/\Delta C_T$	2.1	0.6	0.9	0.2	0.9	0.8	0.5
References	This study	Lefèvre, 2010	Coppola et al., 2020	Bates et al., 1996	Dore et al., 2009	Santana-Casiano and González-Dávila, 2010	Olafsson et al., 2009

will be discussed in the next section as a possible mechanism to explain this low C_T variability.

Impact of Biological Processes on Variations in Seasonal Carbonate Parameters

To understand the overall impact of biological processes on the seasonal variations in the carbonate system in the NWLB, changes in A_T and C_T need to be considered independently from the changes induced by dilution and evaporation. For this purpose, salinity-normalised changes of A_T and C_T in the upper 200 dbars are plotted in **Figure 5**. To differentiate waters affected by air-sea exchanges from sub-surface waters, the upper 200 dbars of water column has been divided into two layers: within and below the mixed layer (0 dbars—MLD and MLD—200 dbars). The barycentre of all observational points, defined as the coordinate of the mean A_T and C_T values during each cruise, is reported and considered to be representative of the "season" sampled.

The barycentres are spread along the photosynthesis-respiration line between the three cruises, reflecting the effects of biological processes on the carbonate system over the year. From the early summer period (PERLE0—red dots on **Figure 5**) to the end of the summer period (PERLE1—blue dots on **Figure 5**), for both layers, the barycentre shift was a signature for increased photosynthetic processes compared

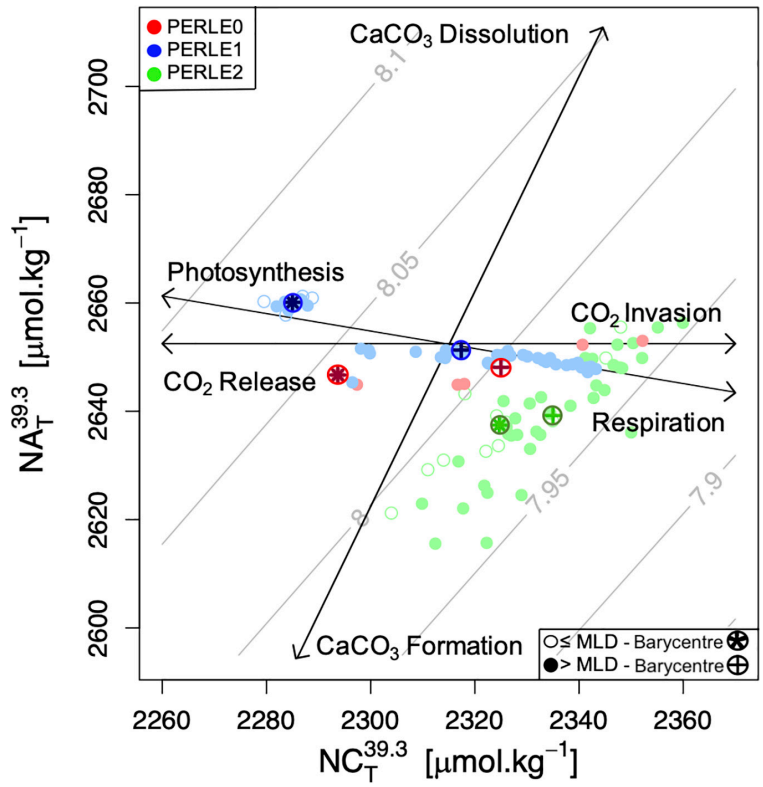

FIGURE 5 | Salinity-normalised A_T ($NA_T^{39.3}$) vs. salinity-normalised C_T ($NC_T^{39.3}$) during the three PERLE cruise in the upper 200 dbars for all stations situated in the North Western Levantine Basin. The layer of 0-200 dbars has been chosen as having the highest AOU variability because of the biological signal. Salinity-normalised values have been calculated with the mean PERLE salinity above 200 dbars (*i.e.,* 39.3). Empty and full dots represent data within and below the mixed layer, respectively. Circled crosses and circled stars represent the barycentre of data below and within the mixed layer, respectively. Black vectors reflect theoretical impacts of various processes (photosynthesis/respiration, carbonate dissolution/formation and CO_2 release/invasion) on A_T and C_T. Grey isolines indicate levels of constant pH_T^{25} as a function of A_T and C_T.

to respiration processes. The deepening of the DCM observed between the PERLE0 and PERLE1 cruises and the negative AOU values recorded during these cruises supported this observation. The deepening of the DCM is a signature to the downward displacement of primary producers related to surface nutrient depletion (Sigman and Hain, 2012), and negative AOU values reflect oxygen production. All these elements indicate that autotrophic processes dominate the upper water column between early and late summer. Based on these assumptions, between the end of the summer period (PERLE1) and the end of the winter period (PERLE2—green dots on **Figure 5**), the barycentre shift indicates that heterotrophic processes were dominant in the upper water column. Whilst observations cannot be time related, it can be assumed that between the late winter period of PERLE2 and the early summer period of PERLE0, the "theoretical" shift of the barycentre indicates a balance in favor of autotrophic processes during this period. When considered together, these seasonal changes in normalised A_T and C_T confirm that during periods of high evaporation, autotrophic processes are consuming C_T and increasing A_T. This can explain the apparent C_T stability and the important change in A_T over an annual cycle.

Based on the assumption that, below the mixed layer, the PERLE sampling area is a closed system (unimpacted by air-sea CO_2 fluxes), the temporal evolution in $NA_T^{39.3}$ and $NC_T^{39.3}$ was used to calculate NEP and NEC fluxes. From the end of the bloom period (PERLE0) to the end of the summer period (PERLE1), daily NEP and NEC values of 0.53 and 0.01 $\mu molC.kg^{-1}.d^{-1}$, respectively, were estimated whereas from the end of the summer period (PERLE1) to the start of the bloom period (PERLE2), negative daily NEP and NEC values of −1.02 and −0.04 $\mu molC.kg^{-1}.d^{-1}$, respectively, were estimated. In the MedSea, the MLD seasonal variability is characterised by a deepening from November to February-March (D'Ortenzio et al., 2005). Therefore, it can be assumed that the water masses below the mixed layer remain isolated from surface CO_2 inputs between the PERLE0 and PERLE1 cruises. However, due to the late winter deepening of the MLD (**Figure 3**), between the end of the summer period (PERLE1) and the late winter period (PERLE2), NEC and NEP could be biased by air-sea exchanges.

The seasonal NEP values estimated in this study confirm previous estimations based on oxygen concentration changes monitored with short-time incubations during the stratified period. In June 2006, Regaudie-de-Gioux et al. (2009) reported a positive NEP value of 0.22 ± 1.30 mmol $O_2.m^{-3}d^{-1}$ in waters above 100 meters in the EMed and in summer 2008, Christaki et al. (2011) reported positive NEP values of 4 ± 14 mmol $O_2.m^{-2}d^{-1}$. As previously observed by Schneider et al. (2007), the contribution of calcification and dissolution processes to variations in the carbonate system could be assumed to have a minor role in the MedSea. The NEC values calculated in the NWLB confirm this. The spreading of PERLE2 data points along the $CaCO_3$ formation/dissolution line in **Figure 5** (green dots) might be associated to the spatial changes in alkalinity content across the geographical distribution of sampling sites during this cruise rather than to calcification and dissolution processes.

Total Alkalinity Control on the Seasonal Air-Sea CO_2 Exchanges

To address the question of the control of A_T and C_T changes on the "source" ($pCO_2^{SW} > pCO_2^{ATM}$) or "sink" ($pCO_2^{SW} < pCO_2^{ATM}$) of CO_2 in the NWLB, PERLE's A_T and C_T values are reported in **Figure 6**. The temperature range in the area has been used to draw the red and blue "iso pCO_2^{SW}-lines" as representative of the pCO_2^{SW} values encountered during the winter and summer PERLE cruises. Considering a mean atmospheric partial pressure (pCO_2^{ATM}) value of 403 µatm (recorded at Lampedusa site from October 2018 to December 2019; Dlugokencky et al., 2021), the upper seawaters encountered at the warm end of summer with high alkalinity (PERLE1) were a "source" of CO_2. In contrast, the cold and low alkalinity end of winter (PERLE2) surface waters were a "sink" of CO_2 with pCO_2^{SW}.

Although the C_T content remained almost stable between the PERLE cruises, the A_T variability was noticeable with the lowest A_T values measured at the end of the winter period (PERLE2) and the highest A_T values estimated during PERLE1, at the end of the summer period. When considering the large pCO_2^{SW} variations due to the temperature variability represented by the shift between the red and blue isolines, the high alkalinity seawater at the end of summer (PERLE1–blue dots on **Figure 6**) induces low pCO_2^{SW} values when seawater starts to cool and therefore highlights the potential for surface waters to absorb atmospheric CO_2. In the NWLB, the variability of the A_T content of the surface waters over an annual cycle impacts the air-sea CO_2 exchanges. The "classical" vision that the pCO_2^{SW} variability is not driven by temperature change but by the biological control on C_T, must be largely revisited in light of the important effect that variations in A_T have on the pCO_2^{SW} regulation capability in the EMed.

In order to estimate the effect of the A_T variability on the pCO_2^{SW} over an annual cycle, alkalinity was derived from salinity data from an Argo float that cycled in the NWLB for over a year. The temperature and total alkalinity (derived from salinity) values recorded by the float in the upper 20 dbars of the water column representative of the surface mixed layer affected by air-sea exchanges are presented in **Figure 7**. The cruise data within the mixed layer are also reported. In **Figure 7**, the red "iso pCO_2^{SW}-line" indicates the pCO_2 equilibrium between the ocean and the atmosphere. This isoline was derived at constant C_T, based on the assumption that the pCO_2^{SW} is, apart from temperature, controlled by A_T rather than by C_T in the NWLB. The distribution of data above and below this line highlights the "source" or "sink" status of the NWLB for atmospheric CO_2, respectively.

The float derived data agreed with data measured during the PERLE cruises and indicate a penetration of atmospheric CO_2 into the EMed from December to April, and a release of CO_2 into the atmosphere from May to November. It must be noted that these estimates are sensitive to the C_T value used. Indeed, by considering a high C_T content (grey isoline labelled "C_T max" in **Figure 7**), the period of CO_2 "sink" for the atmosphere will be shorter (from February to April). Conversely, if the lowest C_T mean value is considered (black isoline labelled "C_T min" in **Figure 7**), the area will act as a "sink" from December to May. The observed "iso pCO_2^{SW}-lines" shift (grey and black isolines in **Figure 7**) from the "iso pCO_2^{SW}-line" at mean C_T (red isoline in **Figure 7**) due to the C_T variability over a year induces a temporal change in the status of "source" or "sink" of the upper water masses.

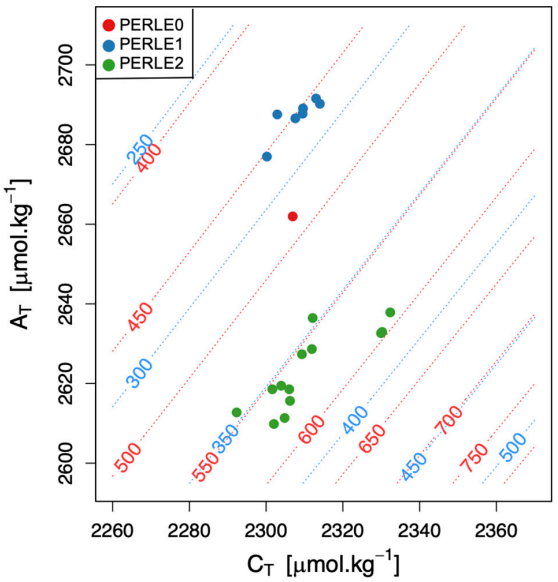

FIGURE 6 | Total alkalinity (A_T) vs. total dissolved inorganic carbon (C_T) within the MLD for all stations situated in the North Western Levantine Basin during the three PERLE cruises. Red and blue isolines indicate levels of constant pCO_2^{SW} as a function of A_T and C_T at 26°C and 15°C, respectively.

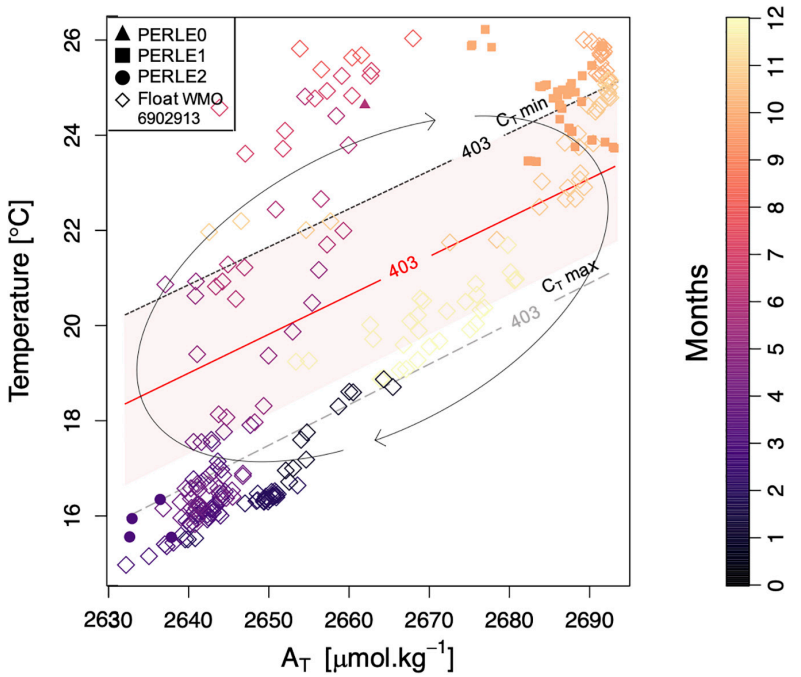

FIGURE 7 | Total alkalinity (A_T) vs. temperature in the upper 20 dbars during the three PERLE cruises and for the WMO 6902913 float data from October 2018 to July 2020 [A_T values have been estimated from the float salinity following the A_T-S sub-surface relationship proposed by Hassoun et al. (2015a)]. The colour bar corresponds to the "month of the year." The red "iso pCO_2^{SW}-line" corresponds to the mean pCO_2^{ATM} value at Lampedusa site (estimated from the mean mole fraction of CO_2 in ppm) calculated with the mean C_T values for all PERLE cruises (= 403 µatm). The two others grey isolines correspond to the same constant pCO_2^{SW} with the minimum and maximum C_T values (from PERLE cruises) (2,292 and 2,332 µmol.kg^{-1}, respectively). Arrows reflect the theoretical changes in A_T and temperature throughout the year. The coloured area represents the error associated to the red "iso pCO_2^{SW}-line" deduced by combining the uncertainty associated to the A_T values (*i.e.,* ± 19 µmol.kg^{-1}) with the default standard uncertainties from the constants (Orr et al., 2018).

Moreover, by considering the accuracy of ± 19 µmol.kg^{-1} associated to the A_T estimation (according to Hassoun et al., 2015a), the uncertainty of the estimated pCO_2^{SW} has been calculated (Orr et al., 2018) and ranged between the two "iso pCO_2^{SW}-lines" deduced from the maximum and minimum C_T values (red area on **Figure 7**). Although the displacement of the air-sea pCO_2 equilibrium might shift considering the A_T uncertainty, the temporal succession of the "sink" or "source" status for atmospheric CO_2 throughout a year in the NWLB is evidenced. It confirms that the A_T content of the surface waters is a significant driver of the air-sea CO_2 fluxes in the NWLB.

These are, to the best of our knowledge, the first estimates of the succession of the "sink" and "source" status in the NWLB based on *in situ* data. Previous estimates based on satellite observations of sea surface properties, and on a model characterising the evolution of the mixed layer pCO_2^{SW} (D'Ortenzio et al., 2008; Taillandier et al., 2012) are confirmed by this study. Moreover, coastal observations in the South eastern Levantine basin close to the Israeli shelf have also reported a CO_2 source for the atmosphere in summer (from May to December) and a sink of atmospheric CO_2 in winter (from January to April) (Sisma-Ventura et al., 2017).

LONG TERM TEMPORAL CHANGES IN CARBONATE CHEMISTRY IN THE NORTH WESTERN LEVANTINE BASIN

Decadal Carbonate Chemistry Trends in Surface Waters in the NWLB

Based on historical observations from the CARIMED dataset and observations from the PERLE cruises, temporal changes in carbonate chemistry between 2001 and 2019 in the surface NWLB have been assessed to study the mechanisms that could explain the carbonate system changes over the last twenty years (**Figure 8**). The surface layer has been defined to a depth of 50 dbars to include sufficient data. Due to the seasonal changes in surface salinity in the EMed (Grodsky et al., 2019), salinity-normalised A_T ($NA_T^{39.3}$) and C_T ($NC_T^{39.3}$) were used to facilitate the comparison between the different datasets across space and time. Indeed, due to the strong salinity dependency of alkalinity, by normalising by salinity, a significant part of the seasonal signal for alkalinity is removed.

While being higher (even when salinity-normalised) than the trends observed in the North Western MedSea (*i.e.,* 1.40 ± 0.15 µmol.kg^{-1}.a^{-1}; Merlivat et al., 2018), the temporal C_T increase

in the NWLB surface waters (**Figure 8A**) is consistent with other trends measured in the eastern Levantine basin (*i.e.,* 5 ± 2 µmol.kg^{-1}.a^{-1}; Hassoun et al., 2019). However, when compared to other time-series over the global ocean, the trends measured in the surface NWLB waters are 3.7–1.5 times higher (if the $NC_T^{39.3}$ trend is considered) than the global ocean range which lies between 0.78 µmol.kg^{-1}.a^{-1} (Munida South Pacific time-series) and 1.89 µmol.kg^{-1}.a^{-1} (CARIOCA time-series; Bates et al., 2014). This suggests that distinct mechanisms explaining the increasing C_T trend exist in the NWLB.

While A_T is considered insensitive to atmospheric CO_2 penetration (Zeebe, 2012), positive trends in C_T and negative trends in pH_T^{25} (**Figures 8A,E**) can be explained, at least partially, by the increase in atmospheric CO_2. Indeed, between 2006 and 2018, a mean annual increase of 2.2 ± 0.08 ppm.a^{-1} in xCO_2^{ATM} (mole fraction of CO_2) was recorded at the Lampedusa site (equivalent to the trend recorded on a global scale; Dlugokencky et al., 2021). To estimate the sensitivity of the estimated trends to the increase in atmospheric CO_2, the increase in xCO_2^{ATM} was assumed to be equivalent to a surface ocean increase in pCO_2^{SW}. Based on the estimated trends in pCO_2^{SW}, $NA_T^{39.3}$, and $NC_T^{39.3}$, annual changes in carbonate chemistry pCO_2^{SW} have been calculated by solving thermodynamic equations (**Table 3**). The observed annual decrease in pH_T^{25} (**Figure 8E**) and increase in C_T (**Figure 8A**) lies between the values estimated with and without an A_T increase. This suggests that an A_T increase must exist to compensate for the decrease in pH and the increase in C_T or, in other words, that the high observed C_T trend is the consequence of the observed A_T increase. Although a positive A_T trend has been observed elsewhere in a coastal site of the MedSea (Kapsenberg et al., 2017), it remains unexplained. These changes could be related to changes in riverine inputs or changes in Black Sea water inputs (Schneider et al., 2007).

It is worth noting that the CARIMED database, by merging data measured over the past 20 years, has a large over-representation of the spring season (**Supplementary Figure 1** and **Supplementary Table 2**). Moreover, the spatial distribution of the sampled stations was different for each cruise. The

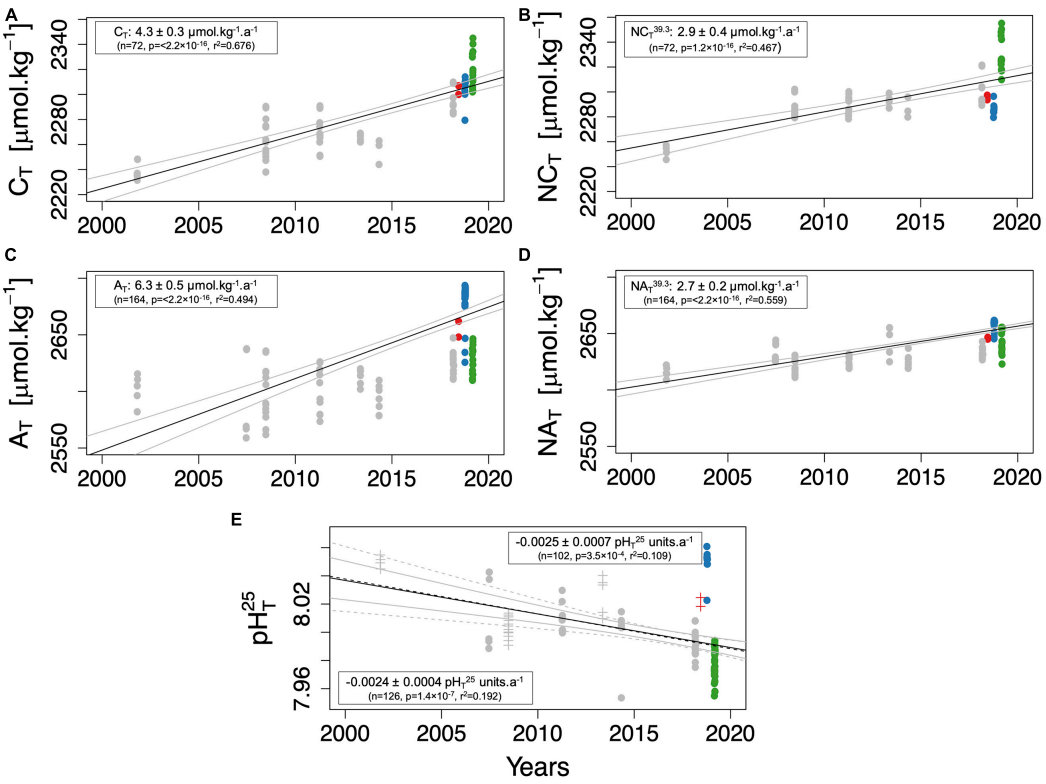

FIGURE 8 | Temporal evolution in the North Western Levantine Basin of total dissolved inorganic carbon (C_T–µmol.kg^{-1}; **A**) and salinity-normalised C_T ($NC_T^{39.3}$–µmol.kg^{-1}; **B**), total alkalinity (A_T–µmol.kg^{-1}; **C**) and salinity-normalised A_T ($NA_T^{39.3}$–µmol.kg^{-1}; **D**) and pH_T^{25} **(E)** based on the CARIMED dataset (grey dots) and PERLE cruises. The colour code for the dots is the same as in **Figure 1**. Only data above 50 dbars are used. In **(E)**, full line and dashed lines correspond to the temporal trends calculated according to all pH_T^{25} data [measured (full dots—trend framed in full lines) and calculated (crosses—trend framed in dotted lines)]. Estimated trends are obtained from slope values of a linear regression between the studied parameters and time. The confident interval has been added for each trend with the coefficient of determination (r^2), the number of values used (n) and the significance of the trend (*p*-value).

TABLE 3 | Projection of annual changes on the carbonate parameters. Considering the temporal trends calculated in section "Decadal carbonate chemistry Trends in Surface Waters in the NWLB," changes were calculated by adding the trend values to the mean values estimated for the surface layer (0–50 dbars) of the PERLE area.

Trends presented in this study		Projection of annual changes			
		pCO_2^{SW} *increase* (A_T constant)	$NC_T^{39.3}$ *increase* (A_T constant)	$NC_T^{39.3}$ *and* $NA_T^{39.3}$ *increases*	$NA_T^{39.3}$ *and* pCO_2^{SW} *increases*
**Annual* pCO_2^{SW} *changes* (μatm.a^{-1})	+2.2	+2.2	+ 4.7	+1.2	+2.2
Annual pH_T^{25} *changes* (pH_T^{25} units.a^{-1})	−0.0024	−0.0020	−0.0042	−0.0007	−0.0016
Annual $NC_T^{39.3}$ *changes* (μmol.kg^{-1}.a^{-1})	+2.9	+1.4	+ 2.9	+2.9	+3.6
Annual $NA_T^{39.3}$ *changes* (μmol.kg^{-1}.a^{-1})	+2.7	/	/	+2.7	+2.7

**Assuming that the increase in* pCO_2^{SW} *in the surface ocean is equal to the increase in* xCO_2^{ATM}.

scarcity of observations in the NWLB precludes the estimation of the seasonal variability on the observed trends. Due to the observed influence of seasonal conditions on the carbonate parameters during the PERLE cruises, time-series that would include observations of the peculiar conditions observed in the late summer (high surface pH_T^{25} associated with high A_T values during PERLE1—**Figure 2C**) or winter could modulate the observed temporal trends. Nonetheless, when data collected during "not spring" cruises are not considered to estimate the trends, despite shifting the temporal trend values, tendencies remain significant for each parameter. Thus, the conclusion that a decadal A_T increase must exist to counterbalance the pH decrease associated to the C_T increase remains coherent and valid.

Perspectives on the Future Functioning of the Eastern Mediterranean Carbonate System

In the projected warmer MedSea (Nykjaer, 2009), increased stratification but also reduced nutrient inputs from river discharge caused by more frequent drought periods could increase the oligotrophy of the MedSea (*e.g.*, Moon et al., 2016; Pagès et al., 2019, 2020). As this study suggests that the magnitude of the annual C_T variation in surface waters is reduced in the EMed due to the low C_T vertical gradients, all processes that could decrease primary production in the future could reduce the C_T contribution to the air-sea exchanges.

Even if internal thermohaline oscillation needs to be considered to draw solid conclusions about salinity trends, over the past 30 years, a positive long-term trend in salinity for the LSW and LIW has been recorded (Ozer et al., 2017). Because of the salinity impact on alkalinity concentrations (**Figure 4**) and of the A_T impact on the air-sea CO_2 fluxes (**Figure 7**), if the PERLE1 conditions are exacerbated in the future with marine heatwaves extending over longer periods of the year, even more alkaline waters can be expected at the end of the summer. An even greater potential pCO_2^{ATM} sink will result when surface seawaters cool. The gyres (such as the IE), which have a higher A_T content due to their saltier waters, might be even more efficient at catching atmospheric CO_2 when seawater cools. The control of air-sea CO_2 exchange by alkalinity that is suggested in this study could be enhanced in a future warmer and less productive EMed. However, as C_T and A_T are equally affected by evaporation and as, in the future less productive EMed, the C_T biological consumption will be less efficient, the mechanisms leading to stable inorganic carbon content described in this study might be altered.

In an attempt to quantify the sensitivity of the carbonate system to future C_T and A_T changes, estimated buffer factors within the MLD for each PERLE cruise are presented in **Table 4**. At a comparable period of the year (March–April for PERLE2 cruise), the estimated buffer factors are in good agreement with former estimates (Álvarez et al., 2014) whereas the estimated buffer factors for PERLE0 and PERLE1 cruises during summer are significantly higher. Higher absolute buffer values imply higher buffering capacity and lower changes in $[CO_2]$, pH or Ω for a given change in A_T or C_T. Assuming that the PERLE1 conditions will be exacerbated in the future (Darmaraki et al., 2019), the EMed surface water is moving toward an overall increase in its buffering capacity (relative to changes in A_T and C_T).

It is worth noting that, when atmospheric CO_2 dissolves in seawater, the CO_2 concentration in solution changes due to the carbonate ion buffering effect. The future effects of the decadal trends measured in the NWLB on the buffering capacities of the carbonate ion can be discussed using three different perspectives: (1) By considering the observed decrease in pH_T^{25}, the carbonate ion availability will decrease accordingly, reducing the atmospheric CO_2 uptake by the MedSea. (2) The greater increase in C_T in comparison to the increase in A_T will reduce the carbonate ion availability, but, nevertheless, will compensate

TABLE 4 | Mean values and standard deviations of buffer factors (in mmol.kg^{-1}) during PERLE cruises.

Cruise	Season	γ_{CT}	β_{CT}	ω_{CT}	γ_{AT}	β_{AT}	ω_{AT}
PERLE0	Early summer period	0.26 ± NA	0.33 ± NA	−0.44 ± NA	−0.33 ± NA	−0.36 ± NA	0.41 ± NA
PERLE1	End of summer period	0.27 ± 0.00	0.34 ± 0.00	−0.46 ± 0.00	−0.34 ± 0.00	−0.38 ± 0.00	0.43 ± 0.00
PERLE2	End of winter period	0.24 ± 0.00	0.30 ± 0.00	−0.38 ± 0.00	−0.30 ± 0.00	−0.32 ± 0.01	0.35 ± 0.01

for the impact of a pH decrease on the carbonate ion content, so allowing the CO_2 uptake into the atmosphere. (3) The positive trend in A_T, and its impact on the CO_2 atmospheric uptake and on mitigating the decreasing pH trend, may indirectly increase the C_T.

CONCLUSION

Based on data collected in the EMed over three different seasons of the year, this study provides for the first time, an annual overview of the seasonal dynamics of the carbonate chemistry in the NWLB. In this area, an atypical seasonal range in A_T variations compared to the range in C_T variations results from the combination of high rates of evaporation and biological processes.

The high A_T content at the "end of summer" period has a strong impact on the air-sea exchanges of CO_2. In the NWLB, the status of "source" or "sink" for atmospheric CO_2 is adjusted by the A_T variability more than the C_T variability. Over longer time scales, and by compiling historical data, the reported increasing trends in A_T and C_T impact with divergent effects the observed acidification. These "end of summer" conditions will occur more frequently and lasting longer in the future. This ocean warming up will result in an increased buffer capacity that could mitigate the ocean acidification of the EMed.

DATA AVAILABILITY STATEMENT

The datasets presented in this study can be found in online repositories. The names of the repository/repositories and accession number(s) can be found below: https://mistrals.sedoo.fr/MERMeX/ and http://www.coriolis.eu.org.

AUTHOR CONTRIBUTIONS

CW-R, TW, and DL initiated and design the study. MÁ provided the CARIMED database and contributed to carbonate chemistry interpretation. PR helped supervising the study. MP-P and PC provided the nutrients database. MF, LC, TM, LN-C, CW-R, and TW performed on board carbonate parameters and oxygen analytical measurements. VT and FD'O provided CTD and ARGO dataset. FD'O, XD, and PC planned and designed the PERLE Research cruises. CW-R, TW, and DL wrote the first draft of the manuscript. All authors contributed to manuscript revision, read, and approved the submitted version.

FUNDING

This study takes part of the PERLE (Pelagic Ecosystem Response to the Levantine Experiment) of the MISTRALS-MERMEX project. The project leading to this publication has received funding from European FEDER Fund under project 1166-39417. The SNAPO-CO2 service at LOCEAN was supported by the CNRS-INSU and OSU Ecce-Terra.

ACKNOWLEDGMENTS

We wish to thank the crew members of the R/V "Téthys II" operated by the DT-INSU, for making the PERLE0 (BIO-ARGO-MED2018) cruise possible. We gratefully acknowledge the Délégation Générale de l'Armement which funded the program Protevs II into which the PROTEVS-PERLE1 campaign was scheduled, the French Naval Hydrologic and Oceanographic Service (SHOM) and the crew of the R/V "L'Atalante" (IFREMER) for their contribution to the PROTEVS-PERLE1 campaign. We acknowledge "Flotte Oceanographique Française", FOF, and the crew of the R/V "Pourquoi Pas?" (IFREMER) for their help in the PERLE2 sampling. The many researchers responsible for the collection of data and quality control are thanked for their contribution. For seawater sample analyses, we also thank the SNAPO-CO2 at LOCEAN, Paris, and in particular J. Fin and N. Metzl. Argo data were collected and made freely available by the Coriolis project and contributing programmes (http://www.coriolis.eu.org). The Argo Program is part of the Global Ocean Observing System. We thank Tracy Lynne Bentley for language editing. The two referees are thanked for helping improve this work.

SUPPLEMENTARY MATERIAL

The Supplementary Material for this article can be found online at: https://www.frontiersin.org/articles/10.3389/fmars.2021.649246/full#supplementary-material

REFERENCES

Álvarez, M., Sanleón-Bartolomé, H., Tanhua, T., Mintrop, L., Luchetta, A., Cantoni, C., et al. (2014). The CO_2 system in the mediterranean sea: a basin wide perspective. *Ocean Sci.* 10:6992. doi: 10.5194/os-10-69-2014

Aminot, A., and Kerouel, R. (2007). *Dosage Automatique des Nutriments Dans les Eaux Marines Methodes en Flux Continued*. Versailles-Cedex: Ed Ifremer-Quae, 188.

Argo (2000). Argo float data and metadata from global data assembly centre (argo GDAC). *SEANOE*. doi: 10.17882/42182

Bates, N. R., Astor, Y. M., Church, M. J., Currie, K., Dore, J. E., González-Dávila, M., et al. (2014). A time-series view of changing ocean chemistry due to ocean uptake of anthropogenic CO_2 and ocean acidification. *Oceanography* 27, 126–141. doi: 10.5670/oceanog.2014.16

Bates, N. R., Michaels, A. F., and Knap, A. H. (1996). Seasonal and interannual variability of oceanic carbon dioxide species at the U.S. JGOFS Bermuda Atlantic Time-series Study (BATS) site. *Deep Sea Res. Part II Top. Stud. Oceanogr.* 43, 347–383. doi: 10.1016/0967-0645(95)00093-3

Bergamasco, A., and Malanotte-Rizzoli, P. (2010). The circulation of the mediterranean sea: a historical review of experimental investigations. *Adv. Oceanogr. Limnol.* 1:1128. doi: 10.1080/19475721.2010.491656

Borges, A. V., Ruddick, K., Schiettecatte, L.-S., and Delille, B. (2008). Net ecosystem production and carbon dioxide fluxes in the Scheldt estuarine plume. *BMC Ecol.* 8:15.

Bosc, E., Bricaud, A., and Antoine, D. (2004). Seasonal and interannual variability in algal biomass and primary production in the mediterranean sea, as derived from 4 years of SeaWiFS observations: mediterranean sea biomass and production. *Glob. Biogeochem. Cycl.* 18:GB1005. doi: 10.1029/2003GB002034

Carritt, D. E., and Carpenter, J. H. (1966). Comparison and evaluation of currently employed modifications of the winkler method for determining dissolved oxygen in seawater; a NASCO report. *J. Mar. Res.* 24, 286–318.

Christaki, U., Van Wambeke, F., Lefevre, D., Lagaria, A., Prieur, L., Pujo-Pay, M., et al. (2011). Microbial food webs and metabolic state across oligotrophic waters of the Mediterranean Sea during summer. *Biogeosciences* 8, 1839–1852. doi: 10.5194/bg-8-1839-2011

Clayton, T. D., and Byrne, R. H. (1993). Spectrophotometric seawater pH measurements: total hydrogen ion concentration scale calibration of m-Cresol purple and at-Sea results. *Deep Sea Res. Part I Oceanogr. Res. Pap.* 40:211529. doi: 10.1016/0967-0637(93)90048-8

Coppola, L., Boutin, J., Gattuso, J.-P., Lefèvre, D., and Metzl, N. (2020). "The carbonate system in the Ligurian Sea," in *The Mediterranean Sea in the Era of Global Change (Volume 1),- Evidence From 30 Years of Multidisciplinary Study of the Ligurian Sea*, eds C. Migon, A. Sciandra, and P. Nival (London: ISTE Science Publication LTD), 49–78. doi: 10.1002/9781119706960.ch4

Coppola, L., Diamond Riquier, E., and Carval, T. (2018). *Dyfamed Observatory Data*. SEANOE. doi: 10.17882/43749

Cossarini, G., Lazzari, P., and Solidoro, C. (2015). Spatiotemporal variability of alkalinity in the Mediterranean Sea. *Biogeosciences* 12, 1647–1658. doi: 10.5194/bg-12-1647-2015

D'Ortenzio, F., and Ribera d'Alcalà, M. (2009). On the trophic regimes of the Mediterranean Sea: a satellite analysis. *Biogeosciences* 6, 139–148. doi: 10.5194/bg-6-139-2009

D'Ortenzio, F., Antoine, D., and Marullo, S. (2008). Satellite-driven modelling of the upper ocean mixed layer and air-sea CO_2 flux in the Mediterranean Sea. *Deep Sea Res. Pt. I* 55, 405–434. doi: 10.1016/j.dsr.2007.12.008

D'Ortenzio, F., Iudicone, D., De, C., de Boyer Montégut, C., Testor, P., Antoine, D., et al. (2005). Seasonal variability of the mixed layer depth in the Mediterranean Sea as derived from in situ profiles. *Geophys. Res. Lett.* 32, 1–4. doi: 10.1029/2005GL022463

D'Ortenzio, F., Taillandier, V., Claustre, H., Coppola, L., Conan, P., Dumas, F., et al. (2020). BGC?Argo floats observe nitrate injection and spring phytoplankton increase in the surface layer of Levantine Sea (Eastern Mediterranean). *Geophys. Res. Lett.* 48:e2020GL091649. doi: 10.1029/2020GL091649

Darmaraki, S., Somot, S., Sevault, F., Nabat, P., Cabos Narvaez, W. D., Cavicchia, L., et al. (2019). Future evolution of Marine Heatwaves in the Mediterranean Sea. *Clim. Dynam.* 53, 1371–1392. doi: 10.1007/s00382-019-04661-z

De Carlo, E. H., Mousseau, L., Passafiume, O., Drupp, P. S., and Gattuso, J.-P. (2013). Carbonate chemistry and air–sea CO_2 flux in a NW Mediterranean Bay over a four-year period: 2007–2011. *Aquat. Geochem.* 19, 399–442. doi: 10.1007/s10498-013-9217-4

Dickson, A. G. (1990). Standard potential of the reaction: AgCl(s) + 1/2 H_2(g) = Ag(s) + HCl(aq), and the standard acidity constant of the ion HSO_4^- in synthetic sea water from 273.15 to 318.15 K. *J. Chem. Thermodynam.* 22:11327. doi: 10.1016/0021-9614(90)90074-Z

Dickson, A. G., and Goyet, C. (1994). *ORNL/CDIAC-74 (Ed.), Handbook of Methods for the Analysis of the Various Parameters of the Carbon Dioxide System in Sea Water. Version 2, no 74*. Washington, DC: US Department of Energy.

Dickson, A. G., and Millero, F. (1987). A comparison of the equilibrium constants for the dissociation of carbonic acid in seawater media. *Deep Sea Res.* 34, 1733–1743. doi: 10.1016/0198-0149(87)90021-5

Dickson, A. G., and Riley, J. P. (1979). The estimation of acid dissociation constants in seawater media from potentiometric titrations with strong base, I. The ionic product of water – KW. *Mar. Chem.* 7, 89–99. doi: 10.1016/0304-4203(79)90001-X

Dickson, A. G., Sabine, C. L., and Christian, J. R. (eds) (2007). *Guide to best practices for Ocean CO_2 Measurements. PICES Special Publication*, Vol. 3. Sidney, BC: North Pacific Marine Science Organisation, 191.

Dlugokencky, E. J., Mund, J. W., Crotwell, A. M., Crotwell, M. J., and Thoning, K. W. (2021). *Atmospheric Carbon Dioxide Dry Air Mole Fractions from the NOAA GML Carbon Cycle Cooperative Global Air Sampling Network, 1968-2019, Version: 2021-02*. doi: 10.15138/wkgj-f215

Doney, S. C., Fabry, V. J., Feely, R. A., and Kleypas, J. A. (2009). Ocean acidification: the other CO_2 problem. *Annu. Rev. Mar. Sci.* 1, 169–192. doi: 10.1146/annurev.marine.010908.163834

Dore, J. E., Lukas, R., Sadler, D. W., Church, M. J., and Karl, D. M. (2009). Physical and biogeochemical modulation of ocean acidification in the central North Pacific. *Proc. Natl. Acad. Sci. U.S.A.* 106, 12235–12240. doi: 10.1073/pnas.0906044106

Durrieu de Madron, X., Guieu, C., Sempéré, R., Conan, P., Cossa, D., D'Ortenzio, F., et al. (2011). Marine ecosystems' responses to climatic and anthropogenic forcings in the Mediterranean. *Progr. Oceanogr.* 91, 97–166. doi: 10.1016/j.pocean.2011.02.003

Edmond, J. M. (1970). High precision determination of titration alkalinity and total carbon dioxide content of sea water by potentiometric titration. *Deep Sea Res. Oceanogr. Abstract.* 17:73750. doi: 10.1016/0011-7471(70)90038-0

Egleston, E. S., Sabine, C. L., and Morel, F. M. M. (2010). Revelle revisited: Buffer factors that quantify the response of ocean chemistry to changes in DIC and alkalinity. *Glob. Biogeochem. Cycles* 24:GB1002. doi: 10.1029/2008GB003407

Feely, R. A., Sabine, C. L., Lee, K., Berelson, W., Kleypas, J., Fabry, V. J., et al. (2004). Impact of anthropogenic CO_2 on the $CaCO_3$ system in the oceans. *Science* 305, 362–366. doi: 10.1126/science.1097329

Flecha, S., Pérez, F. F., Murata, A., Makaoui, A., and Huertas, I. E. (2019). Decadal acidification in Atlantic and mediterranean water masses exchanging at the strait of gibraltar. *Sci. Rep.* 9:52084. doi: 10.1038/s41598-019-52084-x

Friedlingstein, P., Jones, M. W., O'Sullivan, M., Andrew, R. M., Hauck, J., Peters, G. P., et al. (2019). Global carbon budget 2019. *Earth Syst. Sci. Data* 11, 1783–1838. doi: 10.5194/essd-11-1783-2019

Garcia, H. E., and Gordon, L. I. (1992). Oxygen solubility in seawater: better fitting equations. *Limnol. Oceanogr.* 37, 1307–1312. doi: 10.4319/lo.1992.37.6.1307

Gonzaìlez-Daìvila, M., Santana-Casiano, J. M., Petihakis, G., Ntoumas, M., Suárez de Tangil, M., and Krasakopoulou, E. (2016). Seasonal pH variability in the Saronikos Gulf: a year-study using a new photometric pH sensor. *J. Mar. Syst.* 162, 37–46. doi: 10.1016/j.jmarsys.2016.03.007

Grodsky, S. A., Reul, N., Bentamy, A., Vandemark, D., and Guimbard, S. (2019). Eastern Mediterranean salinification observed in satellite salinity from SMAP mission. *J. Mar. Syst.* 198:103190. doi: 10.1016/j.jmarsys.2019.103190

Gruber, N., Clement, D., Carter, B. R., Feely, R. A., Van Heuven, S., Hoppema, M., et al. (2019). The oceanic sink for anthropogenic CO_2 from 1994 to 2007. *Science* 363, 1193–1199. doi: 10.1126/science.aau5153

Hainbucher, D., Álvarez, M., Astray, B., Bachi, G., Cardin, V., Celentano, P., et al. (2019). *Variability and Trends in Physicial and Biogeochemical Parameters of the Mediterranean Sea, Cruise No. MSM72, March 02, 2018 – April 03, 2019, Iraklion (Greece) – Cádiz (Spain), MED-SHIP2*. Bremen: Gutachterpanel Forschungsschiffe, 61. doi: 10.2312/cr_msm72

Hassoun, A. E. R., Fakhri, M., Raad, N., Saab, M. A.-A., Gemayel, E., and De Carlo, E. H. (2019). The carbonate system of the eastern-most mediterranean sea, levantine sub-basin: variations and drivers. *Deep Sea Res. Part II Top. Stud. Oceanogr.* 164, 54–73. doi: 10.1016/j.dsr2.2019.03.008

Hassoun, A. E. R., Gemayel, E., Krasakopoulou, E., Goyet, C., Saab, M. A.-A., Ziveri, P., et al. (2015a). Modelling of the total alkalinity and the total inorganic carbon in the Mediterranean Sea. *J. Water Resourc. Ocean Sci.* 4:24. doi: 10.11648/j.wros.20150401.14

Hassoun, A. E. R., Gemayel, E., Krasakopoulou, E., Goyet, C., Saab, M. A.-A., Guglielmi, V., et al. (2015b). Acidification of the Mediterranean Sea from anthropogenic carbon penetration. *Deep Sea Res. Pt. I Oceanogr. Res. Pap.* 102:115. doi: 10.1016/j.dsr.2015.04.005

Hiscock, W. T., and Millero, F. J. (2006). Alkalinity of the anoxic waters in the western Black Sea. *Deep Sea Res. Pt. II* 53, 1787–1801. doi: 10.1016/j.dsr2.2006.05.020

Ingrosso, G., Giani, M., Comici, C., Kralj, M., Piacentino, S., De Vittor, C., et al. (2016). Drivers of the carbonate system seasonal variations in a Mediterranean gulf. *Estuar. Coast. Shelf Sci.* 168, 58–70. doi: 10.1016/j.ecss.2015.11.001

Ioannou, A., Stegner, A., Tuel, A., LeVu, B., Dumas, F., and Speich, S. (2019). Cyclostrophic corrections of AVISO/DUACS surface velocities and its application to mesoscale eddies in the Mediterranean Sea. *J. Geophys. Res. Oceans* 124, 8913–8932. doi: 10.1029/2019JC015031

IPCC (2018). "Summary for Policymakers," in *Global Warming of 1.5°C. An IPCC Special Report on the Impacts of Global Warming of 1.5°C Above Pre-Industrial levels And Related Global Greenhouse Gas Emission Pathways, In The Context Of Strengthening The Global Response To The Threat Of Climate Change, Sustainable Development, And Efforts To Eradicate Poverty*, eds V. Masson-Delmotte, P. Zhai, H.-O. Pörtner, D. Roberts, J. Skea, P. R. Shukla, et al. (Geneva: World Meteorological Organization), 32.

Kapsenberg, L., Alliouane, S., Gazeau, F., Mousseau, L., and Gattuso, J.-P. (2017). Coastal ocean acidification and increasing total alkalinity in the Northwestern Mediterranean Sea. *Ocean Sci.* 13:41126. doi: 10.5194/os-13-411-2017

Kelley, D., Richards, C., and WG127 SCOR/IAPSO (2017). *gsw: Gibbs Sea Water Functions*. R package version 1.0-5.

Kroeker, K. J., Kordas, R. L., Crim, R., Hendriks, I. E., Ramajo, L., Singh, G. S., et al. (2013). Impacts of ocean acidification on marine organisms: quantifying sensitivities and interaction with warming. *Glob. Change Biol.* 19, 1884–1896. doi: 10.1111/gcb.12179

Langdon, C. (2010). *Determination of Dissolved Oxygen in Seawater by Winkler Titration Using the Amperometric Technique, no. 14 in IOCCP Report, ICPO Publication*. Available online at: www.go-ship.org/HydroMan.html (accessed February 25, 2020).

Lascaratos, A., and Nittis, K. (1998). A high-resolution three-dimensional numerical study of intermediate water formation in the Levantine Sea. *J. Geophys. Res.* 103, 497–511. doi: 10.1029/98JC01196

Lee, K., Sabine, C. L., Tanhua, T., Kim, T.-W., Feely, R. A., and Kim, H.-C. (2011). Roles of marginal seas in absorbing and storing fossil fuel CO_2. *Ener. Environ. Sci.* 4, 1133–1146. doi: 10.1039/C0EE00663G

Lefèvre, D. (2010). *MOOSE (ANTARES)*. Available online at: https://campagnes.flotteoceanographique.fr/series/233/

Liu, X., Patsavas, M. C., Robert, H., and Byrne, R. H. (2011). Purification and characterisation of meta-cresol purple for spectrophotometric seawater pH measurements. *Environ. Sci. Technol.* 45, 4862–4868. doi: 10.1021/es200665

Mehrbach, C., Culberson, C. H., Hawley, J. E., and Pytkowicz, R. M. (1973). Measurement of the apparent dissociation constants of carbonic acid in seawater at atmospheric pressure. *Limnol. Oceanogr.* 18, 897–907. doi: 10.4319/lo.1973.18.6.0897

Merlivat, L., Boutin, J., Antoine, D., Beaumont, L., Melek Golbol, M., and Vellucci, V. (2018). Increase of dissolved inorganic carbon and decrease in pH in near-surface waters in the Mediterranean Sea during the past two decades. *Biogeosciences* 15, 5653–5662. doi: 10.5194/bg-15-5653-2018

Millot, C., and Taupier-Letage, I. (2005). *Circulation in the Mediterranean Sea, in The Handbook of Environmental Chemistry, Vol. 5: Water Pollution, Part K*. Berlin: Springer-Verlag, 29–66. doi: 10.1007/b107143

Moon, J.-Y., Lee, K., Tanhua, T., Kress, N., and Kim, I.-N. (2016). Temporal nutrient dynamics in the Mediterranean Sea in response to anthropogenic inputs. *Geophys. Res. Lett.* 43, 5243–5251. doi: 10.1002/2016GL068788

Moutin, T., and Raimbault, P. (2002). Primary production, carbon export and nutrients availability in western and eastern Mediterranean Sea in early summer 1996 (MINOS cruise). *J. Mar. Syst.* 3, 273–288. doi: 10.1016/S0924-7963(02)00062-3

Nykjaer, L. (2009). Mediterranean Sea surface warming 1985-2006. *Clim. Res.* 39, 11–17. doi: 10.3354/cr00794

Olafsson, J., Olafsdottir, S. R., Benoit-Cattin, A., Danielsen, M., Arnarson, T. S., and Takahashi, T. (2009). Rate of Iceland Sea acidification from time series measurements. *Biogeosciences* 6, 2661–2668. doi: 10.5194/bg-6-2661-2009

Orr, J., Epitalon, J.-M., Dickson, A. G., and Gattuso, J.-P. (2018). Routine uncertainty propagation for the marine carbon dioxide system. *Mar. Chem.* 207, 84–107. doi: 10.1016/j.marchem.2018.10.006

Owens, W. B., and Millard, R. C. (1985). A New Algorithm for CTD Oxygen Calibration. *J. Phys. Oceanogr.* 15, 621–631.

Ozer, T., Gertman, I., Kress, N., Silverman, J., and Herut, B. (2017). Interannual thermohaline (1979–2014) and nutrient (2002–2014) dynamics in the Levantine surface and intermediate water masses, SE Mediterranean Sea. *Glob. Planet. Change* 151, 60–67. doi: 10.1016/j.gloplacha.2016.04.001

Özsoy, E., Hecht, A., and Ünlüata, Ü (1989). Circulation and hydrography of the levantine basin. Results of POEM coordinated experiments 1985–1986. *Progr. Oceanogr.* 22, 12570. doi: 10.1016/0079-6611(89)90004-9

Pagès, R., Baklouti, M., Barrier, N., Ayache, M., Sevault, F., and Moutin, T. (2020). Projected effects of climate-induced changes in hydrodynamics on the biogeochemistry of the mediterranean sea under the RCP 8.5 regional climate scenario. *Front. Marine Sci.* 7:957. doi: 10.3389/fmars.2020.563615

Pagès, R., Baklouti, M., Barrier, N., Richon, C., Dutay, J.-C., and Moutin, T. (2019). Changes in rivers inputs during the last decades significantly impacted the biogeochemistry of the eastern Mediterranean basin: a modelling study. *Progr. Oceanogr.* 181:102242. doi: 10.1016/j.pocean.2019.102242

Palmiéri, J., Orr, J. C., Dutay, J.-C., Béranger, K., Schneider, A., Beuvier, J., et al. (2015). Simulated Anthropogenic CO_2 Storage and Acidification of the Mediterranean Sea. *Biogeosciences* 12:781802. doi: 10.5194/bg-12-781-2015

Petihakis, G., Perivoliotis, L., Korres, G., Ballas, D., Frangoulis, C., Pagonis, P., et al. (2018). An integrated open-coastal biogeochemistry, ecosystem and biodiversity observatory of the eastern Mediterranean – the Cretan Sea component of the POSEIDON system. *Ocean Sci.* 14, 1223–1245. doi: 10.5194/os-14-1223-2018

Pujo-Pay, M., Conan, P., Oriol, L., Cornet-Barthaux, V., Falco, C., Ghiglione, J.-F., et al. (2011). Integrated survey of elemental stoichiometry (C, N, P) from the western to eastern Mediterranean Sea. *Biogeosciences* 8, 883–899. doi: 10.5194/bg-8-883-2011

Regaudie-de-Gioux, A., Vaquer-Sunyer, R., and Duarte, C. M. (2009). Patterns in planktonic metabolism in the Mediterranean Sea. *Biogeosciences* 6, 3081–3089. doi: 10.5194/bg-6-3081-2009

Rivaro, P., Messa, R., Massolo, S., and Frache, R. (2010). Distributions of carbonate properties along the water column in the Mediterranean Sea: spatial and temporal variations. *Mar. Chem.* 121, 236–254. doi: 10.1016/j.marchem.2010.05.003

Roether, W., Manca, B. B., Klein, B., Bregant, D., Georgopoulos, D., Beitzel, V., et al. (1996). Recent changes in Eastern Mediterranean Deep Waters. *Science* 271, 333–335. doi: 10.1126/science.271.5247.333

Santana-Casiano, J., and González-Dávila, M. (2010). "pH decrease and effects on the chemistry of seawater (Chapter 5)," in *Oceans and the Atmospheric Carbon Content*, ed. D. J. M. Santana-Casiano (Berlin: Springer). doi: 10.1007/978-90-481-9821-4_5

Schneider, A., Tanhua, T., Körtzinger, A., and Wallace, D. W. R. (2010). High anthropogenic carbon content in the Eastern Mediterranean. *J. Geophys. Res.* 115:C12. doi: 10.1029/2010JC006171

Schneider, A., Wallace, D. W. R., and Körtzinger, A. (2007). Alkalinity of the Mediterranean Sea: alkalinity of the Mediterranean Sea. *Geophys. Res. Lett.* 34:L15608. doi: 10.1029/2006GL028842

Sigman, D. M., and Hain, M. P. (2012). The biological productivity of the Ocean. *Nat. Educ. Knowl.* 3:21.

Sisma-Ventura, G., Or, B. M., Yam, R., Herut, B., and Silverman, J. (2017). pCO_2 variability in the surface waters of the ultra-oligotrophic Levantine Sea: exploring the air-sea CO_2 fluxes in a fast warming region. *Mar. Chem.* 196, 13–23. doi: 10.1016/j.marchem.2017.06.006

Smith, S. V., and Kinsey, D. W. (1978). "Calcification and organic carbon metabolism as indicated by carbon dioxide," in *Coral Reefs: Research Methods: Monographs on Oceanographic Methodology*, ed. D. R. Stoddart (Paris: UNESCO), 469–484.

Sokal, R. R., and Rohlf, F. J. (1969). *Biometry. The Principles and Practices of Statistics in Biological Research*, 2nd Edn. San Francisco, CA: W.H. Freeman.

Taillandier, V., D'Ortenzio, F., and Antoine, D. (2012). Carbon fluxes in the mixed layer of the Mediterranea Sea in the 1980s and the 2000s. *Deep Sea Res. I* 65, 73–84. doi: 10.1016/j.dsr.2012.03.004

Tanhua, T., van Heuven, S., Key, R. M., Velo, A., Olsen, A., and Schirnick, C. (2010). Quality control procedures and methods of the CARINA database. *Earth Syst. Sci. Data* 2, 35–49. doi: 10.5194/essd-2-35-2010

Touratier, F., and Goyet, C. (2011). Impact of the Eastern Mediterranean Transient on the Distribution of Anthropogenic CO_2 and First Estimate of Acidification for the Mediterranean Sea. *Deep Sea Res. Pt. I Oceanogr. Res. Pap.* 58:115. doi: 10.1016/j.dsr.2010.10.002

Touratier, F., Guglielmi, V., Goyet, C., Prieur, L., Pujo-Pay, M., Conan, P., et al. (2012). Distributions of the carbonate system properties, anthropogenic CO_2, and acidification during the 2008 BOUM cruise (Mediterranean Sea). *Biogeosci. Discuss.* 9, 2709–2753. doi: 10.5194/bgd-9-2709-2012

Uppström, L. R. (1974). The boron/chlorinity ratio of deep-sea water from the Pacific Ocean. *Deep Sea Res.* 21, 161–162. doi: 10.1016/0011-7471(74)90074-6

Valladares, J., Fennel, W. I., and Morozov, E. G. (2011). Replacement of EOS-80 with the international thermodynamic equation of seawater-2010 (TEOS-10). *Deep Sea Res.* 58, 978.

van Heuven, S., Pierrot, D., Rae, J., Lewis, E., and Wallace, D. W. R. (2011). *CO2SYS v 1.1, MATLAB Program Developed for CO2 System Calculations. ORNL/CDIAC-105b*. Oak Ridge, TN: Oak Ridge National Laboratory.

Velaoras, D., Papadopoulos, V. P., Kontoyiannis, H., Cardin, V., and Civitarese, G. (2019). Water masses and hydrography during April and June 2016 in the cretan sea and cretan passage (Eastern Mediterranean Sea). *Deep Sea Res. Pt II Top. Stud. Oceanogr.* 164, 25–40. doi: 10.1016/j.dsr2.2018.09.005

Williams, P. J., and Jenkinson, N. W. (1982). A transportable microprocessor-controlled precise winkler titration suitable for field station and shipboard Use1. *Limnol. Oceanogr.* 27:57684. doi: 10.4319/lo.1982.27.3.0576

Winkler, L. W. (1888). Die bestimmung des im wasser gelösten sauerstoffes. *Ber. Dtsch. Chem. Ges.* 21, 2843–2854. doi: 10.1002/cber.188802102122

Wong, A., Keeley, R., Carval, T., and The Argo Data Management Team (2020). *Argo Quality Control Manual for CTD and Trajectory Data*. Available online at: https://archimer.ifremer.fr/doc/00228/33951/

Zeebe, R. E. (2012). History of seawater carbonate chemistry, atmospheric CO_2, and Ocean acidification. *Annu. Rev. Earth Planet. Sci.* 40, 141–165. doi: 10.1146/annurev-earth-042711-105521

Conflict of Interest: The authors declare that the research was conducted in the absence of any commercial or financial relationships that could be construed as a potential conflict of interest.

Annexe 4 : Article : BGC-Argo Floats Observe Nitrate Injection and Spring Phytoplankton Increase in the Surface Layer of Levantine Sea (Eastern Mediterranean)

D'Ortenzio, F., Taillandier, V., Claustre, H., Coppola, L., Conan, P., Dumas, F., Durrieu de Madron X., **Fourrier, M.**, Gogou A., Karageorgis, A., Lefevre, D., Lymarie, E., Oviedo, A., Pavlidou, A., Poteau, A., Poulain, P. M., Prieur, L., Psarra, S, Pujo-Pay, M., Ribera d'Alcalà, M., Schmechtig, C., Terrats, L., Velaoras, D., Wagener, T., and Wimart-Rousseau, C.
Geophysical Research Letters (2021)

AGU ADVANCING EARTH AND SPACE SCIENCE

Geophysical Research Letters

RESEARCH LETTER
10.1029/2020GL091649

Key Points:

- BGC-Argo floats observe nitrate injections in surface Mediterranean waters
- Mixed-layer dynamics sustain phytoplankton persistence all over winter-very early spring
- The Mediterranean BGC-Argo network provides unique observations that complement ship-based sampling and satellite monitoring

Supporting Information:

Supporting Information may be found in the online version of this article.

Correspondence to:

F. D'Ortenzio,
dortenzio@obs-vflr.fr

Citation:

D'Ortenzio, F., Taillandier, V., Claustre, H., Coppola, L., Conan, P., Dumas, F., et al. (2021). BGC-Argo floats observe nitrate injection and spring phytoplankton increase in the surface layer of Levantine Sea (Eastern Mediterranean). *Geophysical Research Letters*, *48*, e2020GL091649. https://doi.org/10.1029/2020GL091649

Received 12 NOV 2020
Accepted 5 MAR 2021

BGC-Argo Floats Observe Nitrate Injection and Spring Phytoplankton Increase in the Surface Layer of Levantine Sea (Eastern Mediterranean)

F. D'Ortenzio[1], V. Taillandier[1], H. Claustre[1], L. Coppola[2], P. Conan[3], F. Dumas[4], X. Durrieu du Madron[5], M. Fourrier[1], A. Gogou[6], A. Karageorgis[6], D. Lefevre[7], E. Leymarie[1], A. Oviedo[8], A. Pavlidou[6], A. Poteau[1], P. M. Poulain[9], L. Prieur[1], S. Psarra[6], M. Puyo-Pay[3], M. Ribera d'Alcalà[10], C. Schmechtig[11], L. Terrats[1,12], D. Velaoras[6], T. Wagener[7], and C. Wimart-Rousseau[7]

[1]Laboratoire d'Océanographie de Villefranche, CNRS, Sorbonne Université, Villefranche-sur-Mer, France, [2]Institut de la Mer de Villefranche, CNRS, Sorbonne Université, Villefranche-sur-Mer, France, [3]Laboratoire d'Océanographie Microbienne, Observatoire Océanologique de Banyuls, CNRS, Sorbonne Université, Banyuls-sur-Mer, France, [4]Service Hydrographique et Océanographique de la Marine – SHOM, Brest, France, [5]CEFREM, CNRS-Université de Perpignan Via Domitia, Perpignan, France, [6]HCMR, Institute of Oceanography, Anavyssos, Greece, [7]CNRS, IRD, MIO, Aix Marseille Université, Université de Toulon, Marseille, France, [8]Independent Researcher, Villefranche-sur-Mer, France, [9]National Institute of Oceanography and Applied Geophysics - OGS, Sgonico (TS), Italy, [10]Stazione Zoologica Anton Dohrn, SZN, Napoli, Italy, [11]OSU Ecce Terra, UMS 3455, CNRS, Université Pierre et Marie Curie, Paris, France, [12]ACRI-ST, Sophia Antipolis, France

Abstract In the eastern Mediterranean Sea, satellites have observed events of spring surface-chlorophyll increase in the Rhodes Gyre region recurring intermittently. Few in situ biogeochemical data, however, exist to confirm their consistency, elucidate their seasonal characteristics, or discriminate among the possible drivers. During the year 2018, an array of BGC-Argo floats was deployed in the region, collecting the first-ever annual time series of in situ profiles of biogeochemical parameters in this area. Their observations demonstrated that nitrates, driven by mixed-layer dynamics, were available at surface from December 2018 onwards and could have sustained phytoplankton growth. Phytoplankton accumulation at the surface was observed by satellite only in March 2019 when the mixed-layer depth shoaled. These findings confirm that blooms occurring before the start of seasonal stratification are not easily recorded by satellite observations and reaffirm the need to consolidate the BGC-Argo network to establish time series of the evolution of biogeochemical processes.

Plain Language Summary The Levantine Sea, the easternmost area of Mediterranean Sea, is considered one of the poorest oceans on the Earth in terms of abundance of phytoplankton, the microscopic organisms that fuel the marine food web. However, historical data and satellite maps of chlorophyll (the pigment that reveals phytoplankton presence in the water) show episodic increases in the concentration of this pigment in the area near the island of Rhodes. To elucidate the characteristics of these events, a set of six robotic instruments (*i.e.* the BGC-Argo floats) was deployed in the Levantine Sea in 2018. A BGC-Argo float is an autonomous, free-floating instrument that makes oceanic observations over the first 2,000 m of the water column on a regular basis. This article presents an analysis of the data collected by these six robots. They provided the very first annual time series of biogeochemical observations in area, including during winter, when ship and satellite data are hard to collect. Our results reveal the increase in phytoplankton occurring before the start of seasonal stratification, increase that is not easily recorded by satellite observations and reaffirm the need to consolidate the BGC-Argo network to establish time series of the evolution of biogeochemical processes.

1. Introduction

The Levantine Sea, the Mediterranean Sea's easternmost area, is considered as one of the most oligotrophic regions of the global ocean (Krom, Groom, & Zohary, 2003; Siokou-Frangou, Christaki, et al., 2010). In the Levantine, low-to-very-low values of phytoplankton primary production and chlorophyll-a (CHL) concentration have been obtained from both satellite (Bosc et al., 2004) and in situ (Manca et al., 2004)

Geophysical Research Letters 10.1029/2020GL091649

observations. Surface nutrient availability in the region is generally deemed insufficient to sustain significant phytoplankton biomass (Siokou-Frangou, Christaki, et al., 2010). However, biogeographical analysis of time series of available Mediterranean ocean-color observations (D'Ortenzio & Ribera d'Alcalà, 2009; Mayot et al., 2016) slightly moderates this picture of a highly oligotrophic Levantine Sea. It has been shown that episodic but recurrent events of surface CHL increase occur during the winter-to-spring transition period in an area of the Levantine Sea located southeast of Rhodes Island known as the Rhodes region, as already mentioned by Antoine et al. (1995), using satellite data and by Vidussi et al. (2001), using in situ observations. Nevertheless, these events of increased surface phytoplankton biomass in the Rhodes region are generally considered as having a feeble impact on the basin's widespread oligotrophic nature: Not only are they sporadic (out of the 16 years analyzed, they were observed 7 times, Mayot et al. [2016]), their absolute maximum concentrations also rarely exceed 1 mg m^{-3}. Occasionally (as in D'Ortenzio, Ragni, et al. [2003], Mayot et al. [2016], and in 2012, Pedrosa-Pàmies et al. [2016]), they are observed over a large surface area but they are generally short-lived. The accepted explanation for these events pertains to the prevailing physical conditions, characterized by a large-scale permanent cyclonic feature, generally referred to as the Rhodes Gyre (RG; Robinson et al., 2001). In the RG, nutrient stocks are permanently uplifted at shallow depths, and under cold and windy conditions, winter convection induces significant injection of nutrients in the sunlit layers, which, in turn, sustains moderate phytoplankton growth (Ediger & Yilmaz, 1996; Salihoğlu et al., 1990; Souvermezoglou & Krasakopoulou, 1999). Accordingly, Ediger et al. (2005) showed that the upper layer of the RG and its peripheries reveal great temporal variations in both the abundance and composition of particulate matter, more plentiful during late winter–early spring when it reaches values comparable to those of the more productive NW Mediterranean basin. Similarly, Karageorgis et al. (2008) reported elevated values of beam attenuation coefficient due to particles (c_p up to 0.5 m^{-1}) during spring in this sector of the Levantine Sea, pinpointing relatively enhanced particle concentrations presumably related to higher productivity and abundance of biogenic particles in the upper water column. Overall, then, the RG area seems to be the unique “oasis” within the desert-like Levantine area of the Eastern Mediterranean (Siokou-Frangou, Gotsis-Skreta, et al., 1999).

Although the RG is a privileged area for dense water formation events (Malanotte-Rizzoli, Manca, d'Alcala, et al., 1999), in particular by producing the Levantine Intermediate Water, a key water mass for the general circulation of the Mediterranean Sea (Robinson et al., 2001), the vertical distribution and the temporal evolution of nutrient stocks are predominantly driven by the mixed layer depth (MLD; Lascaratos et al., 1993). The MLD dynamics are therefore likely to be the primary factor in controlling the uptake and the availability of nutrients in the upper layers, and then, ultimately, of phytoplankton growth (Napolitano et al., 2000; Pedrosa-Pàmies et al., 2016; Varkitzi et al., 2020).

This overall picture, which emerged from a series of intense in situ surveys of the area performed in the 1990s (Malanotte-Rizzoli, Manca, Marullo, et al., 2003 and references therein), is, however, still not completely satisfactory. First, the MLD evolution, its interplay with the subsurface nutrient stock and the resulting phytoplankton response, are still not fully characterized, mainly because high-frequency and spatially resolved in situ data are largely insufficient. In particular, in situ data of CHL and nutrient concentrations are dramatically scarce in the RG and practically non-existent during the winter-to-spring period when CHL increase events are episodically recorded by satellite. Second, the generally rapid and intermittent nature of these CHL increase events (Mayot et al., 2016) is still largely unresolved. Furthermore, ocean-color observations are subject to several limitations (*e.g.* cloud cover, atmospheric correction and chlorophyll algorithm failures), especially in the Mediterranean Sea (Volpe et al., 2007), hence raising the question of the capability of remote sensing to satisfactorily gauge phytoplankton increase.

For these reasons, the available observations are, as a whole, presently inadequate for confirming the presumed biogeochemical dynamics of the RG. Specifically, the lack of comprehensive year-long in situ monitoring of the area has hindered the establishing of a full understanding of the physical/biogeochemical interplay.

To mitigate this chronic scarcity of data, and with the explicit objective of better characterizing the biogeochemical dynamics of the area and its main forcing factors, an array of BGC-Argo floats was deployed widely during the 2018–2019 period. Floats operations were carried out within the broader framework of an intense in situ survey of the Levantine Sea, the Pelagic Ecosystem Response to deep water formation in

Geophysical Research Letters 10.1029/2020GL091649

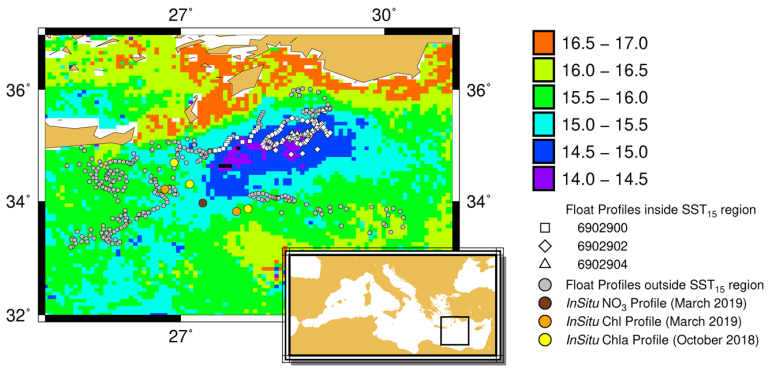

Figure 1. Map of sea surface temperature (SST) annual absolute minima, with the locations of all BGC-Argo profiles (each point represents a profile). White marks indicate the location of BGC-Argo profiles within the SST_{15} region (squares for float 6902900, diamonds for float 6902902, triangles for float 6902904), whereas gray dots indicate the location of profiles outside the SST_{15} region, independently of the float. The locations of ship-based profiles of VAL stations used for qualitative comparison with floats are also plotted: CHL profiles in October 2018 (yellow dots), CHL profiles in March 2019 (orange dots), NO_3 profiles in October 2019 (dark-brown dots).

the Levantine Experiment (PERLE): Six BGC-Argo floats (Leymarie et al., 2013) from French Novel Argo Ocean observing System (NAOS; D'Ortenzio, Taillandier, et al., 2020) and from Argo-Italy projects were deployed.

Among the main macronutrients relevant for phytoplankton growth, BGC-Argo floats can presently measure only nitrate (NO_3) concentration. In particular, floats are not able to measure phosphates, which are considered the main limiting macronutrient in the Eastern Mediterranean (Krom, Emeis, & Van Cappellen, 2010 and references therein). The recurrent observation of phytoplankton growth in the RG, however, indicates that phosphorus limitation is episodically mitigated and that environmental abiotic conditions temporally change to induce phytoplankton growth. Taking into account the observational limits of BGC-Argo, we hence focus this study on analysis of the interplay between MLD and NO_3 distribution, with the ultimate goal of evaluating their influence on phytoplankton growth. Further analyses dedicated to biogeochemical processes and based on the PERLE cruise strategy are ongoing and will not be presented here.

This study consequently presents an analysis of the BGC-Argo float observations, combined with the available satellite data (sea surface temperature and ocean color). In situ data of PERLE surveys are also referred to, in particular for the calibration of the floats' bio-optical sensors to support the autonomously obtained data.

2. Data and Methods

2.1. PERLE Cruises

Three large-scale cruises were conducted in the Levantine Sea during the period 2018–2019: PERLE-0 (May 2018), PERLE-1 (October 2018) and PERLE-2 (March to April 2019). CTD (conductivity, temperature, depth) casts were performed at all the stations. NO_3 concentrations were also evaluated at every station by sampling water at fixed depths and further analyzing with a colorimetric method using an Auto-Analyzer continuous flow analysis system (Aminot & Kérouel, 2007). Water-column CHL (through High Performance Liquid Chromatography (HPLC) analysis, Ras et al., 2008) was assessed through discrete sampling at approximately one-third of the PERLE stations. Two groups of PERLE stations are used here: A first group (referred in the next as CAL *in situ* stations), which is composed of the stations of deployment and recovery of floats, is used for sensor calibration (for NO_3) and data quality control (for both NO_3 and CHL) of the BGC-Argo sensors; a second group (referred in the next as VAL *in situ* stations) is used to qualitatively assess the BGC-Argo and satellite observations in the area (the positions of the two groups of stations are shown in Figure S1; Figure 1 shows the positions of the VAL stations).

Geophysical Research Letters 10.1029/2020GL091649

2.2. BGC-Argo Floats

Six BGC-Argo floats were deployed in the Levantine basin (see Figure S1 map of BGC-Argo deployment points) over the 2018–2019 period. All the floats were equipped with temperature, salinity and PAR (Photosynthetically Active Radiation) sensors, a fluorometer for CHL and a backscattering sensor used to measure the volume scattering coefficient measured at an angle of 124° at 700 nm and subsequently converted to a particulate backscattering coefficient (b_{bp}, in m^{-1}, following Schmechtig, Poteau, Claustre, D'Ortenzio, Dall'Olmo, and Boss [2018]), which is considered a proxy for particulate organic carbon concentration (Boss & Pegau, 2001). Four floats were additionally equipped with NO_3 concentration sensors (Suna™ Satlantic). Two floats have been recovered and four were still operational in October 2020. BGC-Argo data were obtained from the Coriolis Data Assembly Center. Considering that some floats are not yet validated in Delayed Mode as they are still operational at the time of writing (October 2020), values for CHL, b_{bp}, and NO_3 were derived from the available raw data. We followed precisely the standard BGC-Argo algorithms as indicated by Johnson et al. (2018) and by Schmechtig, Poteau, Claustre, D'Ortenzio, and Boss (2015) and Schmechtig, Poteau, Claustre, D'Ortenzio, Dall'Olmo, and Boss (2018). For NO_3 data, an additional adjustment of the standard calibration was performed, by using ancillary measurements obtained on the CAL *in situ* stations. Details of the processing of NO_3 and CHL profiles are presented in the supporting information (Text S1, Figures S2 and S3).

2.3. Satellite Observations

Sea surface temperature (SST) and ocean-color surface CHL observations were provided by the Copernicus Marine Service and CNR-ISAC Rome, respectively. Mediterranean daily products at 1/6° spatial resolution for SST and at 1 km for surface CHL were downloaded and remapped on the Levantine region. For each pixel in the interest area, a time series of SST values was extracted for the fall 2018-summer 2019 period. For each time series, the annual absolute minimum value was identified (*i.e.* the lowest SST values during the period fall 2018-summer 2019). The obtained values were then mapped (Figure 1). Almost all the SST minima values were recorded in February 2019 (data not shown).

2.4. Selection of Float Profiles and Reconstruction of Time Series

The positions of the BGC-Argo profiles in the Levantine area for the period from October 2018 to May 2019 are indicated in Figure 1, superimposed on the map of the annual satellite SST minima. From the SST minima map, all pixels having values lower than 15°C were further used to identify the region where the mixed layer cooled the most (Marullo et al., 2003). The resulting region (hereafter referred to as SST_{15}) marks a large area south of Rhodes and east of Crete (Figure 1), which comprises the coldest SST of the Levantine Sea. We considered that these values delineate the area where mixing was likely to have occurred and where nutrient injection may have been subsequently favored (Marullo et al., 2003; Napolitano et al., 2000; Vidussi et al., 2001).

Choosing to focus on the BGC-Argo profiles within the SST_{15} area (white marks in Figure 1), we reconstructed time series over the period October 2018–May 2019 (Figure 2, panel a) for MLD (using the density threshold value of 0.03 kg m^{-3} as in D'Ortenzio, Iudicone, et al. [2005]), for the depth of the lower limit of the nitrate depleted layer (NDL; Omand & Mahadevan, 2015), the depth of the isoline 5 μmol L^{-1} of nitrate (used as an indicator of the deep stock of nitrate) and the depth of the isoline 0.415 mole photons m^{-2} day^{-1} (indicating the minimum light level above which phytoplankton growth potentially occurs, Mignot, Claustre, et al., 2014). For each profile, NDL depth is computed as following: if the nitrate concentration is not null in the mixed layer, the NDL depth is set to the surface (0 m). If not, the NDL depth is estimated by the depth of the nitrate depletion density, which is the deepest isopycnal at which nitrate concentration is zero (Omand & Mahadevan, 2015). The nitrate depletion density is estimated by the intercept of the regression line reported in a nitrate-density diagram. From the same subset of profiles, surface time series were generated for NO_3 concentrations averaged over the mixed layer (NO_{3MLD}), and for CHL and b_{bp} averaged over the first 10 m, if at least 9 records at 1 m resolution were available (Figure 2, panels b–d, respectively).

The time series inside the SST_{15} region were generated by the sampling of the three floats 6902900, 6902902, and 690904. The time series outside the SST_{15} region (sampled by all the floats) is shown in Figure 2 for

Geophysical Research Letters 10.1029/2020GL091649

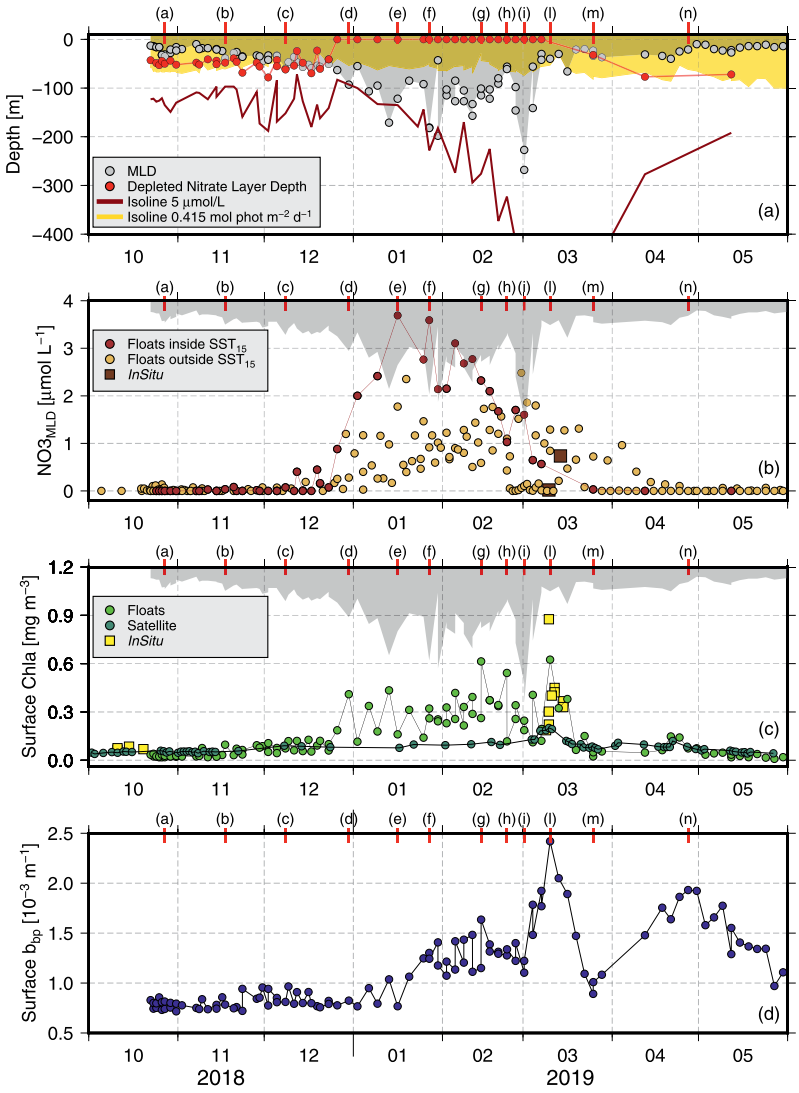

Figure 2. Time series derived from subsets of BGC-Argo floats. Panel (a) MLD (gray dots and area), NDL depth (red dots and line), depth of the NO_3 isoline of 5 µmol L^{-1} (brown line), depth of the isoline 0.415 mole photons m^{-2} day^{-1} (base of yellow area). Note that NDL values equal to zero indicate that the NDL is non-existent (*i.e.* the NO_3 concentrations present at the surface are greater than the detection limit). Dots are maintained in the plot to indicate that profiles are available. Panel (b) time series of depth averaged NO_{3MLD} concentration from BGC-Argo floats (brown dots and line for profiles inside the SST_{15} region; mustard yellow points for profiles outside the SST_{15} region) and from discrete ship-based samples from VAL stations (brown squares). Panel (c**)** surface chlorophyll concentration: from BGC-Argo floats (light-green dots), from satellite ocean color (dark-green dots), from in situ HPLC of VAL stations (yellow squares). Panel (d) BGC-Argo floats' surface b_{bp}. Letters on the top of the panels refer to the vertical profiles shown in Figure S6.

NO_{3MLD} and in Figure S4 for the other parameters. Finally, a time series of daily satellite surface CHL concentration was also derived, by averaging all available satellite ocean-color pixels over the region SST_{15}.

Surface CHL and NO_{3MLD} were also calculated from discrete *in situ* profiles collected at VAL stations during the PERLE-1 and the PERLE-2 surveys. We used the in situ samples collected in the 0–10 m layer (only one observation per profile available). The VAL stations selected were those most adjacent to the SST_{15} region

Geophysical Research Letters 10.1029/2020GL091649

(this area was not sampled during the PERLE cruises due to geopolitical issues) and they are all positioned west of the SST_{15} zone (Figure 1). These stations are only used in the next to qualitatively assess the CHL and NO_3 concentrations retrieved from floats.

3. Results and Discussion

The SST_{15} region attests to intense cooling of the surface water, suggesting that it is an area where the MLD deepens and the upper water column undergoes mixing (Marullo et al., 2003). Compared with the surrounding regions (Figure S4, panel b), the SST_{15} area shows the deepest MLD winter values, confirming the specific physical characteristics of the SST_{15} region. In this area, the MLD time series from float data confirms that the maximum deepening of the MLD was at a depth of 250 m in late February/early March 2019, while also revealing that the deepening began in December 2018 then further accelerated in January 2019. Before this period (*i.e.* October to December 2018), the MLD was shallow and never exceeded 50 m in depth. The NDL depth was observed as being close to the MLD for most of fall 2018. Over the same period, the deep stock of NO_3 in the SST_{15} area (*i.e.* isoline of 5 μmol L^{-1}) fluctuates between 100 and 200 m in depth. In the surrounding areas, NO_3 stock and DNL are generally deeper than in the SST_{15} area (Figure S4, panels b and c). The cyclonic circulation of the RG, which is particularly intense in the fall-winter seasons (Malanotte-Rizzoli, Manca, Marullo, et al., 2003) likely induces a localized (*i.e.* centered in the SST_{15} area) uplift of NO_3 stock.

In the SST_{15} area, the deepening of the MLD observed from late December 2019 onwards induced a consistent injection of NO_3 into the upper layers, resulting in the presence of NO_3 concentrations typical of deep stock close to the surface. Moreover, the NDL disappeared, indicating the surface water column was NO_3 replenished. Although maxima were observed in January 2019, NO_3 values in the MLD remained persistently elevated (always greater than 1 μmol L^{-1}) throughout the period from January to early March 2019 (Figure 2, panel b), revealing that the MLD deepening and the associated mixing continuously redistributed NO_3 from the deep stock into the surface layer. The NO_{3MLD} started to progressively decrease in February 2019, before definitively vanishing in late March 2019, when the observed values were below the detection limit.

Concomitant in situ data to confirm the NO_3 evolution assessed by floats, in particular the high NO_{3MLD} values observed in January/February, are unavailable. However, the analysis of NO_3 profiles of VAL stations measured during the PERLE-2 survey (March 2019) reveals that at one station at least, NO_{3MLD} was not completely exhausted (brown squares in Figure 2, panel b). Although the spatiotemporal matching of VAL stations with float data is not perfect (as the former were obtained from outside the SST_{15} region and outside the temporal window when the NO_3 increase was most observed by floats), the in situ data still provide confirmation of the BGC-Argo observations.

NO_3 augmentation in the mixed layer is also indirectly confirmed by the parallel increase of biomass at the surface (as assessed by the simultaneous analysis of surface CHL and b_{bp} time series). Showing very low values in October to November 2018, surface CHL started to increase slightly from December 2019, when the MLD deepened marginally. This augmentation could likely be ascribed to a redistribution of the biomass associated to the Deep Chlorophyll Maxima (DCM), directly related to the MLD deepening. During this period, the depths of DCM and of mixed layer are nearly coincident (see Figure S5 for a time series of DCM and mixed layer depths, and also some examples of vertical profiles during this phase in Figure S6, panel a–c). Additionally, since the increase in CHL was not accompanied by a respective increase in b_{bp}, it may be related to an increase in CHL per cell content as described in Bellacicco et al. (2016), resulting from a decrease in light availability rather an increase of biomass (as confirmed by the low values of the ratio b_{bp}/CHL during this phase, see Figure S5, lower panel). A phosphorus limitation could also explain the relatively low values of biomass, even in the presence of NO_3 availability. In December 2018–January 2019, however, surface biomass increased unequivocally, as concomitantly indicated by an increase in the surface CHL and b_{bp} values observed by BGC-Argo. During February 2019, biomass, although fluctuating, remained relatively constant, with CHL and b_{bp} largely higher than the fall values. In early March 2019, surface CHL concentrations and b_{bp} values reached their maxima, before further decreasing in late March.

From December 2018, the evolution of phytoplankton biomass can be directly correlated to the MLD/NO_3 interplay:

Geophysical Research Letters 10.1029/2020GL091649

1. The acceleration of MLD deepening in December/January 2019 generated a dramatic increase in NO_3 in the mixed layer; during this phase, surface CHL and b_{bp} were not synced, the former generally increasing, while the latter still showed fall values (Figure S6, panels d–e).
2. The MLD deepening stopped temporarily in mid-January, maintaining stable mean values for most of February 2019; concurrently, an abrupt decrease in NO_{3MLD} concentrations was observed, likely indicating nutrient consumption and the end (or substantial diminution) of NO_3 injection at the surface; the biomass of phytoplankton, exploiting favorable conditions, started to grow, as attested by the surface increase in b_{bp}, now synced to CHL increase (Figure S6, panels f–g).
3. In late February-early March 2019, an additional deepening of the MLD (showing the maximum MLD values of the time series, ~250 m) induced a temporary decrease in surface CHL concentration, concomitant to a significant increase in NO_{3MLD} (Figure S6, panels h–i).
4. The following and thereafter permanent shallowing of MLD induced, in early March 2019, a biomass peak, as indicated by the absolute maxima of the CHL and b_{bp} series; in situ HPLC data from VAL stations (yellow squares in Figure 2, panel c) confirmed the phytoplankton peak, which persisted for ~2 weeks (Figure S6, panel l).
5. After this last episode, the MLD remained permanently shallow, the NO_{3MLD} rapidly vanished, and surface CHL and b_{bp} decreased back to low fall values (Figure S6, panel m).
6. In April 2019, a second peak of surface b_{bp} was observed while the other parameters showed no relevant anomalies (Figure S6, panel n).

The succession of events recorded by the BGC-Argo floats is completely consistent with the dynamics of phytoplankton growth primarily driven by MLD dynamics and controlled by nutrient availability. Since December, the NO_3 availability induces an increase of surface CHL, maintaining elevated the biomass during the winter months. The spring CHL peak, occurring at the definitive stratification of the water column, concludes the biomass accumulation period, which protracted for most of the winter. The influence of light availability appears less critical than the impact of NO_3 on biomass dynamics. However, it partially explains the stable conditions observed in February 2019 when, although NO_3 was available at the surface, biomass stagnated. During this period, the isoline of 0.415 mole photons m^{-2} day^{-1} was permanently shallower than the MLD, suggesting that mixing removes phytoplankton cells from the sunlit layers, causing a slowdown of, or temporarily stop in biomass growth (Williams et al., 2000). We also considered as driver the dilution-recoupling hypothesis (Behrenfeld, 2010; Boss & Behrenfeld, 2010). Indeed, it may have favored the mid-January bloom, when there was a deepening of the mixed layer by ~50 m but (1) for the rest of winter the MLD was quite stable around 100 m and (2) the impact of the other convective event at the end of February was more in diluting the existing biomass than in favoring the accumulation of new biomass. The large scale cyclonic circulation of the RG is also an important factor driving the NO_3 dynamic (Robinson et al., 2001). The shallow values of isoline 5 μmol L^{-1} and of NDL in the SST_{15} area, compared to those observed in the surrounding regions (Figure S4, panels a and c), suggest that the fall-winter large scale circulation induces favorable conditions for NO_3 injections in the central RG.

The second surface b_{bp} peak observed in April could likely be related to the presence of detached coccoliths (Terrats et al., 2020), released by coccolithophores, a dominant group in the region (Oviedo et al., 2015; Vidussi et al., 2001), observed to thrive during late winter and spring in the Levantine basin (Knappertsbusch, 1993; Ziveri et al., 2000). During March 2019 (PERLE-2), coccolithophores were present at relatively high densities (up to 7.6×10^4 cells L^{-1}, partial results from microscopical cell counts). Alternatively, the surface b_{bp} peak could be associated with Saharan dust inputs, which are frequent in the region during this time of the year (Guerzoni et al., 1999).

Although NO_3 and CHL float data may still be affected by uncertainties (D'Ortenzio, Taillandier, et al., 2020), the rise in NO_{3MLD} concentration, followed by a significant surface CHL increase, are unequivocal. The NO_3 and CHL increases are larger than the estimated errors of float data, which, in the Mediterranean, are estimated at about 1 μmol L^{-1} and 0.2 mg m^{-3}, respectively (Mignot, D'Ortenzio, et al., 2019). Finally, although in situ ship data are used here only to corroborate floats observations, they indicate that NO_3 and CHL increases are effective, supporting the float-derived results.

The hypothesis of significant phytoplankton increase in the area, as a consequence of MLD and nutrient dynamics related to winter overturning mixing, has already been formulated in the past (Denis et al., 2010;

Geophysical Research Letters 10.1029/2020GL091649

Ediger & Yilmaz, 1996; Malanotte-Rizzoli, Manca, Marullo, et al., 2003; Souvermezoglou & Krasakopoulou, 1999; Vidussi et al., 2001). These previous studies, however, were based on a very limited set of in situ observations largely collected in late 1990s, and therefore they could not assess or predict the duration of such events. An observational gap over the following 20 years precluded further validation, resulting in the bulk of subsequent analysis being based on satellite ocean-color observations.

While satellite surface CHL concentrations match the float observations from fall 2018 and late spring 2019, they completely overlook the CHL dynamics observed in late winter and also under-evaluate the observed concentrations in March 2019 (as indicated when in situ HPLC data are compared with float and satellite observations). Cloud coverage may primarily explain the lack of ocean-color observations, while the correction of white caps (due to the intense winds recurrently observed in the area) may strongly reduce the number of available ocean-color pixels and thus available match-ups in the Levantine Sea.

The combined approach of BGC-Argo floats and satellite observations proposed here is still improvable. One such point is the selection of BGC-Argo profiles to generate time series on the basis of the annual minima of SST obtained by satellite, here considered as permanent and not temporally variable. In this respect, this approach misrepresents the very high frequency of mixing events and the patchy nature of spatial phytoplankton patterns. In addition, mesoscale and sub-mesoscale processes influence NO_3, b_{bp}, and CHL distributions, inducing additional variability for time series. The effect of these processes is evident in the oscillation of the time series, in particular during the transition periods (*i.e.* stratification/destratification). Another point is the lack of observations by BGC-Argo floats of macronutrients other than NO_3, in particular phosphorus, which is considered the main limiting nutrient in the area. The picture proposed here, based on the MLD/NO_3 interplay, appears nevertheless coherent with the existing hypothesis on the RG biogeochemical functioning. It also provides, for the first time, a description of the seasonal biogeochemical evolution of the region, providing a conceptual framework (based on in situ observations) to improve our comprehension of the functioning of the whole Levantine region. PERLE survey data (presently under analysis), including phosphorus observations, will certainly allow refining this understanding, by introducing and modulating the findings obtained in this study. Also, the analysis of biogeochemical variables related to the ecosystem dynamics should provide complementary information on this ecosystem functioning by indicating the distribution of their bulk properties.

Overall, however, and despite these limitations, the proposed approach provides the first continuous annual survey of water-column distribution of NO_3, b_{bp}, and CHL in the RG and surrounding regions. It also offers a comprehensive view of the seasonal evolution in the area, which largely confirms and also enhances previous explanations of its biogeochemical functioning.

4. Conclusions

An unprecedented BGC-Argo observation system was implemented in the Levantine area of the Mediterranean Sea in 2018–2019. It was supported by an equivalent and concomitant ship-based effort (3 seasonal surveys from May 2018 to March 2019) to elucidate the impact of physical forcing on the biogeochemical dynamics of the basin. The analysis of the floats data presented here unequivocally confirms phytoplankton response to the successive mixing events from December to March. This response was first hypothesized and observed in the 1990s, but, later on, substantiated only indirectly through models or satellite observations, which could fail in fully assessing the biogeochemical dynamic of the area (as suggested by the presented results). In the area where the lowest SSTs were recorded, BGC-Argo floats unambiguously observed significant NO_3 availability in the sunlit layer, followed by rapid accumulation of biomass on the surface. Phytoplankton growth appears to be primarily driven by MLD dynamics as shown by the temporal match between MLD stratification and destratification events and CHL fluctuations in the upper layers. As hypothesized in previous studies, MLD deepening drives surface NO_3 availability, as observed by floats in the RG from January 2019 onwards. Floats data also revealed that the upper limit of the deep stock of NO_3 was closer to the surface (between 100 and 170 m) than in the surrounding regions and that an uplift of nutrients occurred at the end of the year (*i.e.* December 2018). Our results confirm that large-scale cyclonic circulation, uplifting density isolines, is likely to be the principal preconditioning cause of subsurface NO_3 increase in the RG region. Moreover, our results indicate that phytoplankton accumulation, as well as the

AGU ADVANCING EARTH AND SPACE SCIENCE

Geophysical Research Letters 10.1029/2020GL091649

environmental conditions that induce it, occur permanently during winter. In other words, the spring event (observed here in March) delimits the end of the productive period, instead of starting it as in other temperate areas (*e.g.* the North Western Mediterranean Sea; Kessouri et al., 2018).

BGC-Argo data accuracy is still not equivalent to that of classic ship-based observations, in particular for NO_3 and CHL. The results obtained here, however, are directly and indirectly confirmed by ancillary high-quality measurements. Moreover, the variations observed by the float data are sufficiently large in relation to the estimated errors to confirm the reliability of the general picture described above. On the whole, the BGC-Argo network has provided the first observational evidence of the evolution of NO_3 concentration in the surface layer of the RG region, showing the direct influence of MLD dynamics on this evolution. The response of phytoplankton to the NO_3/MLD interplay was also documented in an unprecedented fashion, confirming existing understanding about the region's phytoplankton dynamics, providing more insight in the underlying mechanisms controlling the physical-biogeochemical interactions.

The results presented here fine-tune the existing picture of the sporadic and intermittent nature of the RG CHL increase, mainly obtained from ocean-color satellite observations. In the 2018–2019 period specifically analyzed here, satellite ocean-color observations partially failed to detect the area's increase in biomass. Considering that the region's biogeochemical budgets are primarily estimated on the basis of remote-sensing data, our evidence on the observational limits of satellites indicates then that these budgets could accordingly be biased. In this context, the massive use of BGC-Argo floats, in support of and as a supplement to space and ship-based observation, is one of the potentialities of an expanded BGC-Argo network. To fully exploit these potentialities, more investigations are required to improve integration of the different sources of biogeochemical data and to enhance the use of coupled models assimilating both BGC-Argo and satellite observations (as in Cossarini et al. [2019]). Our analysis also demonstrates that BGC-Argo floats are a powerful tool for elucidating complex interactions between physical and biogeochemical dynamics, although they should be integrated, as far as possible, to "classic" observational systems such as ship surveys, moorings and satellites (see relevant discussion in D'Ortenzio, Taillandier, et al. [2020] and in Taillandier et al. [2018]).

Acknowledgments
This study represents a contribution to the following research projects: NAOS (funded by the Agence Nationale de la Recherche in the framework of the French "Equipement d'avenir" program grant ANR J11R107-F), MISTRALS-MERMEX (CNRS, INSU), REFINE (European Research Council, Grant agreement 834177), Bio-Argo-France (TOSCA CNES), PROTEVS (funded by the French DGA) and Argo-Italy (funded by the Italian Ministry of Research). HCMR scientists acknowledge financial support by "CLIMPACT" (funded by the Public Investment Program of Greece, GSRT, Ministry of Development and Investments) and "MARRE" (Greek Ministry of Economy and Development & EU Regional Development Fund) projects. Thanks also go to the captains and crew of R/V Le Tethys II (CNRS/INSU), Pourquoi Pas? (IFREMER) and L'Atalante (IFREMER), who participated in the deployment of autonomous platforms, and of the three PERLE cruises. A special thanks to captain Gilles Ferrand, who conducted the deployements of most of the floats used in this paper. A specific and warm thanks to the whole of the "BAM Team" (in particular Loic), to the administrative staff of the LOV (Linda Féré, Corinne Poutier, Isabelle Courtois) and to the staff of the "Baleine Joyeuse". Nothing was possible without them. Finally, we would also like to thank the two referrees (Dr. Raquel Somavilla and the anonymous one) : their suggestions and comments strongly improved the final version of the paper.

Data Availability Statement

The BGC-Argo data presented here are freely available at https://doi.org/10.17882/42182#71394 or ftp://ftp.ifremer.fr/ifremer/argo/dac/. These data were collected and made freely available by the International Argo Program and the national programs that contribute to it (http://www.argo.ucsd.edu, http://argo.jcommops.org). The PERLE data are available at SISMER (https://doi.org/10.17600/18000865) and SEDOO (https://mistrals.sedoo.fr/MERMeX/). Satellite data were provided by the Copernicus Marine Service and CNR-ISAC Rome, and are available from the Copernicus Marine Service website: https://marine.copernicus.eu.

References

Aminot, A., & Kérouel, R. (2007). *Dosage automatique des nutriments dans les eaux marines: Méthodes en flux continu*. Editions Quae.

Antoine, D., Morel, A., & André, J.-M. (1995). Algal pigment distribution and primary production in the eastern Mediterranean as derived from coastal zone color scanner observations. *Journal of Geophysical Research*, *100*(C8), 16193–16210. https://doi.org/10.1029/95jc00466

Behrenfeld, M. J. (2010). Abandoning Sverdrup's critical depth hypothesis on phytoplankton blooms. *Ecology*, *91*(4), 977–989. https://doi.org/10.1890/09-1207.1

Bellacicco, M., Volpe, G., Colella, S., Pitarch, J., & Santoleri, R. (2016). Influence of photoacclimation on the phytoplankton seasonal cycle in the Mediterranean Sea as seen by satellite. *Remote Sensing of Environment*, *184*, 595–604. https://doi.org/10.1016/j.rse.2016.08.004

Bosc, E., Bricaud, A., & Antoine, D. (2004). Seasonal and interannual variability in algal biomass and primary production in the Mediterranean Sea, as derived from 4 years of SeaWiFS observations. *Global Biogeochemical Cycles*, *18*(1). https://doi.org/10.1029/2003GB002034

Boss, E., & Behrenfeld, M. (2010). In situ evaluation of the initiation of the North Atlantic phytoplankton bloom. *Geophysical Research Letters*, *37*(18), L18603. https://doi.org/10.1029/2010gl044174

Boss, E., & Pegau, W. S. (2001). Relationship of light scattering at an angle in the backward direction to the backscattering coefficient. *Applied Optics*, *40*(30), 5503. https://doi.org/10.1364/ao.40.005503

Cossarini, G., Mariotti, L., Feudale, L., Mignot, A., Salon, S., Taillandier, V., et al. (2019). Towards operational 3D-Var assimilation of chlorophyll Biogeochemical-Argo float data into a biogeochemical model of the Mediterranean Sea. *Ocean Modelling*, *133*, 112–128. https://doi.org/10.1016/j.ocemod.2018.11.005

Denis, M., Thyssen, M., Martin, V., Manca, B., & Vidussi, F. (2010). Ultraphytoplankton basin-scale distribution in the eastern Mediterranean Sea in winter: Link to hydrodynamism and nutrients. *Biogeosciences*, *7*(7), 2227–2244. https://doi.org/10.5194/bg-7-2227-2010

AGU ADVANCING EARTH AND SPACE SCIENCE

Geophysical Research Letters 10.1029/2020GL091649

D'Ortenzio, F., Iudicone, D., Montegut, C. D., Testor, P., Antoine, D., Marullo, S., et al. (2005). Seasonal variability of the mixed layer depth in the Mediterranean Sea as derived from in situ profiles. *Geophysical Research Letters*, *32*(12). L12605. https://doi.org/10.1029/2005gl022463

D'Ortenzio, F., Ragni, M., Marullo, S., & d'Alcalà, M. R. (2003). Did biological activity in the Ionian Sea change after the Eastern Mediterranean Transient? Results from the analysis of remote sensing observations. *Journal of Geophysical Research*, *108*(C9), 8113. https://doi.org/10.1029/2002jc001556

D'Ortenzio, F., & Ribera d'Alcalà, M. (2009). On the trophic regimes of the Mediterranean Sea: A satellite analysis. *Biogeosciences*, *6*(2), 139–148. https://doi.org/10.5194/bg-6-139-2009

D'Ortenzio, F., Taillandier, V., Claustre, H., Prieur, L. M., Leymarie, E., Mignot, A., et al. (2020). Biogeochemical Argo: The test case of the NAOS Mediterranean array. *Frontiers in Marine Science*, *7*, 120. https://doi.org/10.3389/fmars.2020.00120

Ediger, D., Tuğrul, S., & Yılmaz, A. (2005). Vertical profiles of particulate organic matter and its relationship with chlorophyll-a in the upper layer of the NE Mediterranean Sea. *Journal of Marine Systems*, *55*(3–4), 311–326. https://doi.org/10.1016/j.jmarsys.2004.09.003

Ediger, D., & Yilmaz, A. (1996). Characteristics of deep chlorophyll maximum in the Northeastern Mediterranean with respect to environmental conditions. *Journal of Marine Systems*, *9*(3–4), 291–303. https://doi.org/10.1016/s0924-7963(96)00044-9

Guerzoni, S., Chester, R., Dulac, F., Herut, B., Loÿe-Pilot, M. D., Measures, C., et al. (1999). The role of atmospheric deposition in the biogeochemistry of the Mediterranean Sea. *Progress in Oceanography*, *44*(1–3), 147–190.

Johnson, K., Pasqueron De Fommervault, O., Serra, R., D'Ortenzio, F., Schmechtig, C., Claustre, H., & Poteau, A. (2018). *Processing Bio-Argo nitrate concentration at the DAC level* (p. 22). Argo data management. https://doi.org/10.13155/46121

Karageorgis, A. P., Gardner, W. D., Georgopoulos, D., Mishonov, A. V., Krasakopoulou, E., & Anagnostou, C. (2008). Particle dynamics in the Eastern Mediterranean Sea: A synthesis based on light transmission, PMC, and POC archives (1991–2001). *Deep Sea Research Part I: Oceanographic Research Papers*, *55*(2), 177–202. https://doi.org/10.1016/j.dsr.2007.11.002

Kessouri, F., Ulses, C., Estournel, C., Marsaleix, P., D'Ortenzio, F., Severin, T., et al. (2018). Vertical mixing effects on phytoplankton dynamics and organic carbon export in the western Mediterranean Sea. *Journal of Geophysical Research: Oceans*, *123*(3), 1647–1669. https://doi.org/10.1002/2016jc012669

Knappertsbusch, M. (1993). Geographic distribution of living and Holocene coccolithophores in the Mediterranean Sea. *Marine Micropaleontology*, *21*(1–3), 219–247. https://doi.org/10.1016/0377-8398(93)90016-q

Krom, M. D., Emeis, K. C., & Van Cappellen, P. (2010). Why is the Eastern Mediterranean phosphorus limited? *Progress in Oceanography*, *85*(3–4), 236–244. https://doi.org/10.1016/j.pocean.2010.03.003

Krom, M. D., Groom, S., & Zohary, T. (2003). The Eastern Mediterranean. In K. D. Black, & G. B. Shimmield (Eds.), *The Biogeochemistry of Marine Systems* (pp. 91–126). Oxford: Blackwell.

Lascaratos, A., WIlliams, R. G., & Tragou, E. (1993). A mixed-layer study of the formation of Levantine intermediate water. *Journal of Geophysical Research*, *98*(C8), 14739–14749. https://doi.org/10.1029/93jc00912

Leymarie, E., Poteau, A., André, X., Besson, F., Brault, P., Claustre, H., et al. (2013). Development and validation of the new ProvBioII float. *Mercator Ocean—Coriolis Quarterly Newsletter*, *48*, 26–30.

Malanotte-Rizzoli, P., Manca, B., Marullo, S., Ribera d'Alcalà', M., Roether, W., Theocharis, A., et al. (2003). The Levantine intermediate water experiment (LIWEX) group: Levantine basin—a laboratory for multiple water mass formation processes. *Journal of Geophysical Research: Oceans*, *108*(C9), 8101. https://doi.org/10.1029/2002JC001643

Malanotte-Rizzoli, P., Manca, B. B., d'Alcala, M. R., Theocharis, A., Brenner, S., Budillon, G., & Ozsoy, E. (1999). The Eastern Mediterranean in the 80s and in the 90s: The big transition in the intermediate and deep circulations. *Dynamics of Atmospheres and Oceans*, *29*(2–4), 365–395. https://doi.org/10.1016/s0377-0265(99)00011-1

Manca, B., Burca, M., Giorgetti, A., Coatanoan, C., Garcia, M.-J., & Iona, A. (2004). Physical and biochemical averaged vertical profiles in the Mediterranean regions: An important tool to trace the climatology of water masses and to validate incoming data from operational oceanography. *Journal of Marine Systems*, *48*(1–4), 83–116. https://doi.org/10.1016/j.jmarsys.2003.11.025

Marullo, S., Napolitano, E., Santoleri, R., Manca, B., & Evans, R. (2003). Variability of rhodes and Ierapetra gyres during Levantine intermediate water experiment: Observations and model results. *Journal of Geophysical Research: Oceans*, *108*(C9), 8119. https://doi.org/10.1029/2002jc001393

Mayot, N., D'Ortenzio, F., Ribera d'Alcalà, M., Lavigne, H., & Claustre, H. (2016). Interannual variability of the Mediterranean trophic regimes from ocean color satellites. *Biogeosciences*, *13*(6), 1901–1917. https://doi.org/10.5194/bg-13-1901-2016

Mignot, A., Claustre, H., Uitz, J., Poteau, A., D'Ortenzio, F., & Xing, X. (2014). Understanding the seasonal dynamics of phytoplankton biomass and the deep chlorophyll maximum in oligotrophic environments: A Bio-Argo float investigation. *Global Biogeochemical Cycles*, *28*(8), 856–876. https://doi.org/10.1002/2013gb004781

Mignot, A., D'Ortenzio, F., Taillandier, V., Cossarini, G., & Salon, S. (2019). Quantifying observational errors in Biogeochemical-Argo oxygen, nitrate, and chlorophyll a concentrations. *Geophysical Research Letters*, *46*(8), 4330–4337. https://doi.org/10.1029/2018gl080541

Napolitano, E., Oguz, T., Malanotte-Rizzoli, P., Yilmaz, A., & Sansone, E. (2000). Simulations of biological production in the Rhodes and Ionian basins of the eastern Mediterranean. *Journal of Marine Systems*, *24*(3–4), 277–298. https://doi.org/10.1016/s0924-7963(99)00090-1

Omand, M. M., & Mahadevan, A. (2015). The shape of the oceanic nitracline. *Biogeosciences*, *12*(11), 3273–3287. https://doi.org/10.5194/bg-12-3273-2015

Oviedo, A., Ziveri, P., Álvarez, M., & Tanhua, T. (2015). Is coccolithophore distribution in the Mediterranean Sea related to seawater carbonate chemistry? *Ocean Science*, *11*(1), 13–32. https://doi.org/10.5194/os-11-13-2015

Pedrosa-Pàmies, R., Sanchez-Vidal, A., Canals, M., Lampadariou, N., Velaoras, D., Gogou, A., et al. (2016). Enhanced carbon export to the abyssal depths driven by atmosphere dynamics. *Geophysical Research Letters*, *43*(16), 8626–8636. https://doi.org/10.1002/2016GL069781

Ras, J., Claustre, H., & Uitz, J. (2008). Spatial variability of phytoplankton pigment distributions in the Subtropical South Pacific Ocean: Comparison between in situ and predicted data. *Biogeosciences*, *5*(2), 353–369. https://doi.org/10.5194/bg-5-353-2008

Robinson, A. R., Leslie, W. G., Theocharis, A., & Lascaratos, A. (2001). *Mediterranean Sea circulation*. Academic Press, Harcourt Science & Technology. Retrieved from http://www.academicpress.com

Saliho□lu, İ., Saydam, C., Baştürk, Ö., Yilmaz, K., Göçmen, D., Hatipo□lu, E., & Yilmaz, A. (1990). Transport and distribution of nutrients and chlorophyll-a by mesoscale eddies in the Northeastern Mediterranean. *Marine Chemistry*, *29*, 375–390.

Schmechtig, C., Poteau, A., Claustre, H., D'Ortenzio, F., & Boss, E. (2015). *Processing Bio-Argo chlorophyll-a concentration at the DAC level* (p. 12). Argo Data Management. http://doi.org/10.13155/39468

Schmechtig, C., Poteau, A., Claustre, H., D'Ortenzio, F., Dall'Olmo, G., & Boss, E. (2018). *Processing Bio-Argo particle backscattering at the DAC level*. Argo data management. https://doi.org/10.13155/39459

Geophysical Research Letters 10.1029/2020GL091649

Siokou-Frangou, I., Christaki, U., Mazzocchi, M. G., Montresor, M., Ribera d'Alcalá, M., Vaqué, D., & Zingone, A. (2010). Plankton in the open Mediterranean Sea: A review. *Biogeosciences*, *7*(5), 1543–1586. https://doi.org/10.5194/bg-7-1543-2010

Siokou-Frangou, I., Gotsis-Skreta, O., Christou, E., & Pagou, K. (1999). Plankton characteristics in the Aegean, Ionian and NW Levantine seas. In P. Malanotte-Rizzoli, & V. Eremeev (Eds.), *The Eastern Mediterranean as a laboratory basin for the assessment of contrasting ecosystems* (pp. 205–223). Dordrecht: Kluwer Academic Publishers.

Souvermezoglou, E., & Krasakopoulou, E. (1999). The effect of physical processes on the distribution of nutrients and oxygen in the NW Levantine Sea. *The Eastern Mediterranean as a Laboratory Basin for the Assessment of Contrasting Ecosystems* (pp. 225–240). Springer.

Taillandier, V., Wagener, T., D'Ortenzio, F., Mayot, N., Legoff, H., Ras, J., et al. (2018). Hydrography and biogeochemistry dedicated to the Mediterranean BGC-Argo network during a cruise with RV Tethys 2 in May 2015. *Earth System Science Data*, *10*(1), 627–641. https://doi.org/10.5194/essd-10-627-2018

Terrats, L., Claustre, H., Cornec, M., Mangin, A., & Neukermans, G. (2020). Detection of coccolithophore blooms with BioGeoChemical-Argo Floats. *Geophysical Research Letters*, *47*(23), e2020GL090559. https://doi.org/10.1029/2020gl090559

Varkitzi, I., Psarra, S., Assimakopoulou, G., Pavlidou, A., Krasakopoulou, E., Velaoras, D., et al. (2020). Phytoplankton dynamics and bloom formation in the oligotrophic Eastern Mediterranean: Field studies in the Aegean, Levantine and Ionian seas. *Deep-Sea Research Part II: Topical Studies in Oceanography*, *171*, 104662. https://doi.org/10.1016/j.dsr2.2019.104662

Vidussi, F., Claustre, H., Manca, B. B., Luchetta, A., & Marty, J.-C. (2001). Phytoplankton pigment distribution in relation to upper thermocline circulation in the eastern Mediterranean Sea during winter. *Journal of Geophysical Research*, *106*(C9), 19939–19956. https://doi.org/10.1029/1999jc000308

Volpe, G., Santoleri, R., Vellucci, V., Ribera d'Alcalà, M., Marullo, S., & D'Ortenzio, F. (2007). The colour of the Mediterranean Sea: Global versus regional bio-optical algorithms evaluation and implication for satellite chlorophyll estimates. *Remote Sensing of Environment*, *107*(4), 625–638. https://doi.org/10.1016/j.rse.2006.10.017

Williams, R. G., McLaren, A. J., & Follows, M. J. (2000). Estimating the convective supply of nitrate and implied variability in export production over the North Atlantic. *Global Biogeochemical Cycles*, *14*(4), 1299–1313. https://doi.org/10.1029/2000gb001260

Ziveri, P., Rutten, A., de Lange, G. J., Thomson, J., & Corselli, C. (2000). Present-day coccolith fluxes recorded in central eastern Mediterranean sediment traps and surface sediments. *Palaeogeography, Palaeoclimatology, Palaeoecology*, *158*(3–4), 175–195. https://doi.org/10.1016/s0031-0182(00)00049-3

References From the Supporting Information

Bittig, H. C., Maurer, T. L., Plant, J. N., Wong, A. P., Schmechtig, C., Claustre, H., et al. (2019). A BGC-Argo guide: Planning, deployment, data handling and usage. *Frontiers in Marine Science*, *6*, 502. https://doi.org/10.3389/fmars.2019.00502

Johnson, K. S., & Coletti, L. J. (2002). In situ ultraviolet spectrophotometry for high resolution and long-term monitoring of nitrate, bromide and bisulfide in the ocean. *Deep Sea Research Part I: Oceanographic Research Papers*, *49*(7), 1291–1305. https://doi.org/10.1016/s0967-0637(02)00020-1

Johnson, K. S., Coletti, L. J., Jannasch, H. W., Sakamoto, C. M., Swift, D. D., & Riser, S. C. (2013). Long-term nitrate measurements in the ocean using the In Situ Ultraviolet Spectrophotometer: Sensor integration into the Apex profiling float. *Journal of Atmospheric and Oceanic Technology*, *30*(8), 1854–1866. https://doi.org/10.1175/jtech-d-12-00221.1

Pasqueron de Fommervault, O., D'Ortenzio, F., Mangin, A., Serra, R., Migon, C., Claustre, H., et al. (2015). Seasonal variability of nutrient concentrations in the Mediterranean Sea: Contribution of Bio-Argo floats. *Journal of Geophysical Research: Oceans*, *120*(12), 8528–8550. https://doi.org/10.1002/2015JC011103

Sakamoto, C. M., Johnson, K. S., & Coletti, L. J. (2009). Improved algorithm for the computation of nitrate concentrations in seawater using an in situ ultraviolet spectrophotometer. *Limnology and Oceanography: Methods*, *7*(1), 132–143. https://doi.org/10.4319/lom.2009.7.132

Impact des forçages physiques sur la dynamique des éléments biogéochimiques en mer Méditerranée
Approche couplée observations *in situ* et réseaux de neurones

Résumé

La mer Méditerranée est caractérisée par une circulation rapide des masses d'eau, des concentrations faibles en nutriments avec un fort gradient d'oligotrophie, et une acidification plus rapide que pour l'océan global. Les Eaux Levantines Intermédiaires (LIW) reliant les deux bassins sont marquées par un minimum d'oxygène (O_2). Les variabilités du contenu en O_2, des nutriments et du carbone inorganique restent méconnues du fait de leur faible densité d'observation. Le développement et la validation d'une méthode neuronale CANYON-MED, spécifiquement conçue pour la Méditerranée, ont permis de dériver nutriments (nitrates, phosphates, silicates) et variables du système des carbonates (alcalinité totale, carbone total et pH) à partir de variables systématiquement mesurées (pression, température, salinité et O_2, position spatio-temporelle). La dynamique du minimum d'O2 dans la LIW face à la variabilité des processus de ventilation des eaux intermédiaires en Méditerranée nord-occidentale a été étudiée sur la période 2012-2020. L'application de CANYON-MED a permis la description des tendances en nutriments et carbonates dans cette zone, face au phénomène intermittent de convection profonde. L'importance de la convection sur la ventilation des masses d'eau, et sur les tendances des nutriments et d'acidification sont mises en évidence, dans un contexte de stratification accrue par le changement climatique. Enfin, la ventilation de la LIW a été explorée dans sa zone de formation (le bassin Levantin) à l'aide de flotteurs Argo sur la période 2018-2019, nuançant l'injection d'O_2 dans le patch de mélange.

Mots clés : réseaux de neurones, mer Méditerranée, nutriments, système des carbonates, oxygène dissous, flotteurs Argo

---

Abstract

The Mediterranean Sea is characterized by rapid circulation of its water masses, low nutrient concentrations with a strong oligotrophy gradient, and a more rapid acidification than the global ocean. The Levantine Intermediate Waters (LIW) that connect the two basins are marked by a minimum of oxygen (O_2). Variability in O_2 content, nutrients, and inorganic carbon remain poorly understood given their low density of observation. The development and validation of a neural method CANYON-MED, specifically designed for the Mediterranean Sea, allowed to derive nutrients (nitrates, phosphates, silicates) and carbonate system variables (total alkalinity, total carbon and pH) from systematically measured variables (pressure, temperature, salinity and oxygen, position in time and space). The dynamics of the O_2 minimum in the LIW in the face of variability in intermediate water ventilation processes in the northwestern Mediterranean was studied over the period 2012-2020. The application of CANYON-MED allowed the description of nutrients and carbonate trends in this area, in response to the intermittent deep convection phenomenon. The importance of convection on the ventilation of water masses, as well as on nutrient and acidification trends are thus highlighted, in a context of increased stratification by climate change. Finally, the ventilation of the LIW has been explored in its formation area (Levantine basin) using Argo floats over the period 2018-2019, nuancing the injection of O_2 in the mixing patch.

Keywords: neural networks, Mediterranean sea, nutrients, carbonate system, dissolved oxygen, Argo floats

---

Laboratoire d'Océanographie
de Villefranche
Sorbonne Université – 181 chemin du Lazaret – 06230 Villefranche-sur-Mer – France